



Strathclyde Institute of Pharmacy and Biomedical Sciences

Chemical Profiling and Biotechnological

Potential of Marine Microalgae in

Response to Light and Abiotic Stress

Alison Hannah Hughes

Thesis presented in fulfilment of the requirement for the degree


of Doctor of Philosophy.

September 2021

## Declaration

This thesis is the result of the author's original research. It has been composed by the author and has not been previously submitted for examination which has led to the award of a degree. The copyright of this thesis belongs to the author under the terms of the United Kingdom Copyright Acts as qualified by University of Strathclyde Regulation 3.50. Due acknowledgement must always be made of the use of any material contained in, or derived from, this thesis.

The experimental work pertaining to Chapter 3, section 3.2.3 was not completed by the author. However, all data analysis was completed by the author, and they are first author of the resultant publication "Exploring the Chemical Space of Macro- and Micro-algae Using Comparative Metabolomics", *Microorganisms*, 2021, 9(2); 311.

Signed: 

Date: 07/03/2022

## Publications

Some results in *Chapter 3* and excerpts from the introduction of this thesis have been published in the following research article:

**Hughes, A.H.**, Magot, F., Tawfike A.F., Rad-Menéndez, C., Thomas, N., Young L.C., Stucchi, L., Caretoni, D., Stanley, M.S., Edrada-Ebel, R., Duncan, K.R. Exploring the Chemical Space of Macro- and Micro-algae Using Comparative Metabolomics, *Microorganisms*, 2021, 9(2); 113.

DOI: 10.3390/microorganisms9020311

Other publications:

The Natural Products Atlas: An Open Access Knowledge Base for Microbial Natural Products Discovery. Jeffrey A. van Santen, Grégoire Jacob, ... **Alison H. Hughes** ... Roger G. Linington. *ACS Cent. Sci.* 2019, 5, 11, 1824-1833.

DOI: 10.1021/acscentsci.9b00806

Comparative Metabologenomics Analysis of Polar Actinomycetes. Sylvia Soldatou, Grímur Hjörleifsson Eldjárn...**Alison H. Hughes**...Katherine R. Duncan. *Marine Drugs*, 2021, 19(2), 103.

DOI: 10.3390/md19020103

The Natural Products Atlas 2.0: A Database of Microbially-derived Natural Products. Jeffrey A. van Santen, Ella F. Poynton, ... **Alison H. Hughes** ... Roger G. Linington. *Nucleic Acids Research* 2022, 50 (D1), D1317-1323.

DOI: 10.1093/nar/gkab941

## Acknowledgements

*'Is ar scáth a chéile a mhaireann na daoine' - we live in each other's shadow and in each other's shelter.*

4 years, 2 cities, 5 moves, 3 weddings (and one missed), 3 deaths, 3 births, and countless memories, this experience has been a rollercoaster. This is going to be very long so get the box of tissues ready.

To Kate, thank you letting me carve my own path. Your encouragement over the last few months has prevented me from yeeting my laptop out the window on several occasions. To all the Duncan lab members I have crossed paths with; Silvia, Laia, Parra, Alejandro, Darren, Lily, Brandon, Heather, Florent, Salma, Cailin, Hannah, Calum, Shahad, Diana, Robyn, Aimee, Grace, Robbie, Conor, Kirsten, Eve, Ellen, Connie - thank you for all your help, group meeting discussions, and Petri dish crafts! To Iain Hunter, Paul Hoskisson, Paul Herron, Nick Tucker, Arnaud Javelle, Leighton Pritchard, Morgan Feeney - thank you for the questions and advice, and all the great pub conversations. Thanks to Christine, Allison, Richie, and Craig - we literally wouldn't function without you all and you were always about for a good natter when I wanted to avoid doing work. Thank you, Marie Boyd, for being my assessor and a great encouragement at every stage. To Dougie, Sebastien, and Laurence - thanks for letting me take over the Xanthella lab, get involved in projects, and the great advice. Particular thanks to Seb for providing feedback on chapters of this thesis. Thanks to Ian Archer, Rachel Moir, Rachel Clarke, Gill McGill, Elba Becerra, and Kirsty Robb at IBioIC and the 2017 IBioIC-CTP cohort for making training events enjoyable (and more difficult to wake up for thanks to all the wine). I'd also like to thank Prof. Paul Murphy at NUIG and Prof. Pierre Schembri-Wismayer at L'Universtà ta'Malta for giving me that first taste of research in the summer of 2014 that set me down this path.

Thank you to Mads for letting me join the Women in Ocean Science team. To all the women I've worked with and interviewed over the last couple of years, thank you. Your passion is an incredible source of inspiration and I'm so proud to be just a tiny part of this amazingly supportive community. To the Virtual Writing Retreat and everyone I've met through that, your constant unwavering support has been so

comforting, particularly through this pandemic. Thanks to MicroSoc, FEMS, Phyconet, Algae UK, SfAM, British Phycological Society, ECMNP & MaNaPro, IBioIC, ASP, and The Global Science Show for giving me the opportunity to share my research with your communities and funding some of the highlights of my PhD. Thank you to Ali, and everyone at SULSA, Breaking Barriers in STEM is one of my proudest achievements and I can't wait to join the team in October.

I am so grateful to everyone in the SIPBS micro group and level 6 for making it such a brilliant place to work. To everyone that's listened to me rant on HW601, thank you for making it the best work environment (even through all the stress of the last year). I am terrified to list you all in case I forget anyone but here it goes; Gordon, Gaetan, Adriana, Ainsley, Charlie, Eilidh, Tom, Jana, Leena, Lis, Gillian, Dave, Elmira, John, Kirsty, Sarah, Becca, Anna, Liam, Robyn, Emily, Catherine, Molly, Stuart, Jonny, Alemão, Logan. From nights out in Polo, Halloween parties, subcrawls, Christmas parties, Birmingham, Belfast, and THAT research day, there's never been a group that executed the work hard, play hard mantra better. Special mention to the OG Gyros Gang, the Yippon Yippies, and the Snacktime Stalwarts - the greatest rewards at the end (or middle) of a hard week.

Now for the serious stuff! Gordon - my bay buddy and my rock (literally and figuratively). I still haven't forgiven you for Leedsing me and I've missed you so much these past few months. You've always been the one to calm me down, talk through the problem, and then crack a cringey pun to put a smile back on my face. Parra, thank you for the philosophical debates, deep discussions, and for being an amazing tour guide when I went to Costa Rica. Becca, you've been one hell of a support this past year. Thank you so much for being there for me. To Lis, my first friend in the lab, always there to offer adorable fluffy Instagram pics and crochet inspiration. Emily – it's been a bit of a wild one. Thank you for coaching me through each breakdown and checking in on me. Darren, I feel like I've shared a lot of this journey with you, you've been here for so long and you're so old now. To Lily (and Sal and Diego) for the agony aunt sessions, baked goods, and dog walks. Stuart, our mutual distaste at Gordon's abandonment brought us closer together and I hope this isn't the last I see of your

grumpy face. Dave, for always being there to say "fuck it, let's go to the pub" when things got too much. Thanks for being my writing buddy these past few months. My Oban fam, Jess, Laurence, Estelle, Jack, Daniela, Fengjia - I miss movie nights, and the dinners, the walks in the rain, and cans on the beach. Christ on a bike, that was the most wholesome time of my life!

Eimear, I think we must win an award for the number of tears we've shared together over the years, both happy and sad. You have always been the most astounding friend, and I'm so grateful for every text, email, note, letter, voice note, Skype, and real-life cup of tea. It's very comforting having a place to call home here in Glasgow. Silvia, it's been a journey, eh?! Literally! From the terrified little undergrad in Galway, to roomies in Florida, and best pals ever since, I can't thank you enough for not just being my friend but also my mentor. Endless bitching sessions, a few breakdowns, and a thousand difficult times and decisions. But you've been by my side every step and I'm so excited for our next adventures. Eoin, my babah, my Jai Ho. It still breaks my heart that COVID robbed me from being by your side on your wedding day. I'm so proud of the man you have become and can't wait to tell mini-munch (aka Jamie) all our best stories. Adam and Jordan, like the Angel and Devil on either shoulder, that somehow manage to balance me out and keep me sane whilst letting out my inner weirdo. Skimming stones on Seil, going mad in Catty (#SpecialD4Lyf), and sparklers at Halloween - sure you're only the best (and my mammy loves you both, stop fighting). My soul sister, Nicole, every time we have a "quick" catch up I feel as though the weight of the world has been lifted from my shoulders. Santaniii, my agony aunt and booski, we WILL have a reunion soon. And that goes for you too Marjorie, Matt, and Selami, I miss you all so much and thank you for all your support.

Saving the most important for last, my family. My Nan, the most intelligent woman I know. She was always so proud that I never let anything get in the way of my studies. I wish nothing more than to have you here to celebrate this achievement. To my mam, who is there for me every single time I call (well, she'll call me back 'cos she didn't hear the phone ring even though it was right beside her). Every single day you're there listening to me shite on about science, bitch and whinge when it got hard, and cry when

I wanted to give up. I genuinely wouldn't have made it this far without you. My Dad, always there with solid advice and to tell me how I should do it (and he's never wrong, you know). You're my best friend, pops, and I always want to make you proud. My brother, Rich, who has always tried to help me through the stress of doing a PhD through the lens of the world class rugby player that he is. Now that I'm about to start a real job, it's my turn to bring us to the Caribbean. My sister, Jenny, there is no one in this world stronger than you and no one else I'd want (or need) in my corner. You're a terrifyingly amazing woman and I admire you so much. To Kaiden, Emmy, and Lainey, I've missed so many special occasions and key moments in your lives and I'm so sorry. I re-watch every video you send a thousand times, always laughing through the tears. And to the newest addition to the family, Ollie, arriving just in time to get a mention in these acknowledgements. Can't wait to meet you little us. Toby, Tiger, Bug, Lala, Muffin, Jack, Penny, Freddie, Red, Coby, Kuma, Tala, Captain, Poppy, Sal, Diego, Jasper, Bran, and Lily (Spud), the best little furballs, thanks for all the cuddles.

*“But in a way you can say that after leaving the sea, after all those millions of years of living inside of the sea, we took the ocean with us. When a woman makes a baby, she gives it water, inside her body, to grow in. That water inside her body is almost exactly the same as the water of the sea. It is salty, by just the same amount. She makes a little ocean, in her body. And not only this. Our blood and our sweating, they are both salty, almost exactly like the water from the sea is salty. We carry oceans inside of us, in our blood and our sweat. And we are crying the oceans, in our tears.”*

*- Gregory David Roberts, Shantaram*

*This thesis is dedicated to my Nan, Hannah Hughes, and my parents, Eileen and Oliver Hughes.*



## Contents

<b>Declaration</b> .....	<b>2</b>
<b>Publications</b> .....	<b>3</b>
<b>Acknowledgements</b> .....	<b>4</b>
<b>Contents</b> .....	<b>9</b>
<b>Abstract</b> .....	<b>12</b>
<b>1. Introduction</b> .....	<b>14</b>
1.1 Marine Natural Products .....	14
1.2 Microalgal Taxonomy and Classification .....	19
1.3 Culturing Microalgae .....	23
1.4 Applications of Microalgae and Their Natural Products .....	29
1.5 The Role of Stress in Stimulating Production of Natural Products .....	35
1.6 Elicitation of Metabolites from Microalgae Using Light.....	37
1.7 Metabolomics.....	44
1.8 Aims and Objectives .....	46
<b>2. Methods</b> .....	<b>48</b>
2.1 Materials.....	48
2.2 Strains.....	48
2.3 Media .....	52
2.4 Stock Cultures .....	54
2.5 Microscopy.....	54
2.6 Growth Calibration Curves .....	54
2.7 Growth Analysis .....	54
2.8 Phylogenetic Analysis.....	55
2.9 Culturing Under Experimental Conditions .....	57
2.10 Extraction of Metabolites.....	60
2.11 LC-MS and LC-MS/MS analysis.....	60
2.12 Molecular Networking .....	62
2.13 Bioactivity Screening .....	64
2.14 Fast Repetition Rate Fluorometry .....	66
<b>3. Strain Selection, Optimisation of Metabolite Extraction, and Exploring the Chemical Diversity of Eukaryotic Microalgae</b> .....	<b>67</b>
3.1.1 Introduction .....	67
3.1.2. Aims and Objectives .....	71

3.2 Results .....	72
3.2.1. Characterising Growth of Four Marine Microalgal Strains .....	72
3.2.2. Optimising Extraction Methods to Maximise Chemical Diversity .....	81
3.2.3. Exploring the Chemical Diversity of Eukaryotic Microalgae.....	91
3.3 Discussion .....	101
3.3.1. Growth of Four Marine Microalgal Strains .....	101
3.3.2. Optimising Extraction of Microalgal Metabolites .....	101
3.3.2. Unlocking the Chemical Potential of Microalgae .....	102
3.3.2. Diversity of Eukaryotic Microalgae.....	103
<b>4. Eliciting Specialised Metabolite Production by Marine Microalgae Using Abiotic Stress.....</b>	<b>105</b>
4.1.1 Introduction .....	105
4.1.2 Aims and Objectives .....	108
4.2 Results .....	109
4.2.1 The Effect of Abiotic Stress on the Growth of Three Marine Microalgal Strains.....	109
4.2.2 Overview of the Effect of Abiotic Stress on Metabolite Production .....	115
4.2.3 Salinity and NaCl Concentration .....	124
4.2.4 Nitrate Concentration .....	131
4.2.5 pH.....	136
4.3 Discussion .....	141
4.3.1 Evaluating Stress in Microalgae.....	141
4.3.2 Using Metabolomics Tools to Investigate Stress in Microalgae.....	142
<b>5. Investigating the Effect of 405 nm Light on Microalgal Growth and Metabolite Production .....</b>	<b>144</b>
5.1.1 Introduction .....	144
5.1.2 Aims and Objectives .....	148
5.2 Results .....	149
5.2.1 Effect of 405 nm on Growth and Photosynthetic Efficiency .....	149
5.2.2 Fractionation and Bioactivity Screening of Extracts .....	158
5.2.3 Chemical Analysis of Extracts from White and 405 nm LED Light .....	160
5.3 Discussion .....	168
5.3.1 Effect of 405 nm Illumination on Microalgal Growth.....	168
5.3.2 Antimicrobial Screening of Extracts and Fractions .....	169

<b>5.3.3 Effect of 405 nm Light on Metabolite Production</b> .....	170
<b>6. General Discussion and Future Work</b> .....	<b>172</b>
6.1 General Discussion.....	172
6.2 Future Work .....	175
6.3 Conclusion .....	176
<b>References</b> .....	<b>177</b>
<b>Appendices</b> .....	<b>200</b>
<b>8.1 Supplementary Information</b> .....	200
<b>8.1.1 Supplementary Tables</b> .....	200
<b>8.2.2 Supplementary Figures</b> .....	205

## Abstract

---

Microalgae form the base of the aquatic food chain and have important ecological functions, including nutrient cycling and carbon capturing. These microscopic eukaryotes are incredibly diverse, with an estimated 72,000 extant species. They have been investigated for their biotechnological potential in industries such as nutraceutical, cosmetic, and biofuel. Most research has focused on specific high-value metabolites such as astaxanthin or  $\beta$ -carotene for human health, or classes of natural products such as polyunsaturated fatty acids for biofuels. However, a systematic untargeted approach to exploring the chemical diversity of microalgal metabolites has yet to be performed. Unlocking this chemical potential could provide further applications and incentives to the microalgal biotechnology sector.

This thesis aims to fill this gap by exploring the chemical space of microalgae and the elicitation of further chemistry using abiotic stress. A comparative metabolomics study of 36 microalgal strains from both freshwater and marine environments showed that Haptophytes were a rich source of chemistry compared to the well-studied Chlorophytes. It also explored chemical diversity across strains of the same species, providing evidence that isolation environment rather than phylogenetic relationships could be used to group microalgae based on chemical profiles. To investigate the chemistry produced by three strains of marine microalgae, *Dunaliella primolecta*, *Nannochloropsis oculata*, and *Phaeodactylum tricornutum* were cultured under varying conditions of salinity, sodium chloride, nitrate, and pH and Global Natural Products Social (GNPS) molecular networking was used to gain insights into the effect of these stresses on metabolite production. A total of 2284 metabolites were detected across all strains and conditions, with 49% of those metabolites specific to cultures grown under stress conditions (i.e., not in the control). Salinity had the greatest effect with 22.8% of metabolites only produced under salinity stress. From comparison with over 33 libraries of mass spectral data, only five metabolites were identified, stressing the need for more open-access natural product -and specifically algal natural product - databases. Finally, we partnered with Xanthella Ltd., a marine biotechnology company in Scotland, to study the effect of 405 nm light on growth of four strains of

microalgae and the production of antimicrobial metabolites. This wavelength has been shown to reduce bacterial contamination in cultures but is an expensive regimen to apply at a large scale. The production of high-value metabolites under this light regimen could enable culturing under 405 nm illumination to be economically viable. Although no bioactivity was observed from extracts or fractions, molecular networking did show that 16-25% of metabolites were either exclusively produced under 405 nm illumination or absent from the white light control condition. This thesis offers a starting point for fundamental and comparative research into microalgal growth and metabolite production and their applications in human health.

## 1. Introduction

---

### 1.1 Marine Natural Products

Natural products, also known as secondary metabolites or specialised metabolites, are compounds produced by living organisms that are not required for the survival, growth, or reproduction of that organism. They are highly stereoselective and are believed to provide an evolutionary or adaptive advantage to the producer in their environment.<sup>1</sup> The study of natural products dates back approximately 5,000 years through the writings of ancient Egyptian, Greek and Chinese civilisations, amongst others. These civilisations believed that Gods and Demons were responsible for disease and looked to nature for gifts or cures for their ailments. The earliest surviving record of a natural products pharmacopeia, the Ebers Papyrus, was composed by the Egyptians in approximately 3,500 years ago and contains approximately 800 natural remedies and magical incantations.<sup>1</sup> The Charaka Samhita was written around 3,000 years ago and comprises over 300 plant-derived remedies used by the Indian Ayurveda (ancient medical system).<sup>2</sup> The Ancient Greeks also relied heavily on terrestrial plants as sources for cures, as is detailed in the Corpus Hippocraticum (2,400 years ago). This script contains 400 natural medicinal substances, including the use of *Atropa belladonna*, known commonly now as deadly nightshade, as an anaesthetic.<sup>3</sup> The philosophy of Traditional Chinese Medicine was believed to originate approximately 5000 years ago, however there are not many written sources to confirm this. The most primitive is the Wu Shi Er Bing Fang which lists over 200 natural substances and details 150 concoctions or combinatorial formulae for the treatment of ailments. The later published Shen Nong Ben Cao Jing (approximately 1,700 years ago), specified 252 plants and 67 animals that could be utilised for medicinal purposes.<sup>4</sup>

Many of the natural substances documented in these ancient texts formed the basis of modern medicine and have subsequently been proven to have therapeutic properties. The use of the willow tree (*Salix alba* L.) as a medicinal plant dates back to the Assyrians in 4000 B.C. who consumed an extract from the leaves in order to relieve pain and reduce fever.<sup>5</sup> This was an effective remedy and used throughout different civilizations in history. It was not until 1828 that the phenolic glycoside named salicin was extracted from *Salix alba* L. and purified by a German scientist, Johann Buchner.<sup>5</sup>

In the succeeding decade, improvements were made to the purification process and in 1838, the structure was solved.<sup>6</sup> In 1853, Charles von Gerhardt synthesised acetylsalicylic acid, or aspirin, from a salicin derivative. This example shows the history of natural products, from its use in ancient medicine to a drug that is still widely used today. Other such examples of this process that have stood the test of time are; the cardiac glycosides digoxin and digitoxin from the foxglove plant (*Digitalis purpurea*); paclitaxel, a potent chemotherapeutic originally isolated from the Pacific yew tree (*Taxus brevifolia*); and morphine, an opiate discovered from the milk of the poppy plant *Papaver somniferum*.<sup>7</sup> These drugs have all been sourced from terrestrial species and there are few reports of marine species being used for medicinal purposes during ancient times. One such example is that of *Chondrus crispus*, a red alga found on rocky shores along the Atlantic coast, which was used in the 19<sup>th</sup> century by boiling with milk and consuming the beverage to treat respiratory ailments. The alga, known commonly as Irish moss or carrageen, is still used today in gastronomy and nutraceuticals.<sup>8</sup>

Investigating marine environments began in earnest in the 20<sup>th</sup> Century, coinciding with the development of Self-Contained Underwater Breathing Apparatus (SCUBA). Since 1965, over 25,000 new metabolites isolated from marine organisms have been discovered from around the world, with approximately two-thirds exhibiting bioactivity.<sup>9</sup> In 1951, the bioactive nucleosides spongothymidine (**1**) and spongosine (**2**) were isolated from the Caribbean sponge *Cryptotethia crypta*<sup>10</sup> which led synthetic chemists to produce a library of ara-nucleosides and two such derivatives, cytarabine (**3**) and vidarabine (**4**) were approved for clinical use in the treatment of leukaemia and herpes simplex virus, respectively (**Figure 1.1**).<sup>11</sup> Ecteinascidin-743 (trabectedin), an anti-cancer metabolite extracted from the tunicate *Ecteinascidia turbinata*, only made it to the market after it was discovered that safracin B, a metabolite of *Pseudomonas fluorescens*, could be used as a precursor in the total synthesis.<sup>12</sup> The discovery of natural products from invertebrate microbiomes triggered a shift in marine natural products research in the early 2000s which continues today. Between 2017 and 2018, the number of new natural products isolated from marine bacterial, fungi, and cyanobacteria increased by 22%, 85%, and 61%, respectively.<sup>13</sup>

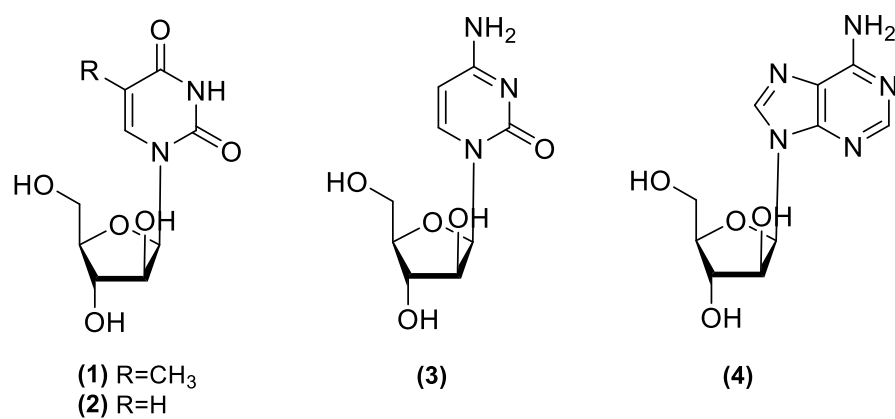


**Figure 1.1** Chemical structures of (1) spongothymidine<sup>10</sup>, (2) spongosine<sup>10</sup>, (3) cytarabine<sup>11</sup>, and (4) vidarabine<sup>11</sup>



Currently, eight marine drugs are available on the market for clinical use (**Figure 1..2**), five of which underwent structural modification during lead optimization.<sup>11</sup> Ziconotide, a synthetic derivative of a  $\omega$ -conotoxin isolated from *Conus magnus* is clinically approved to treat severe and chronic pain whilst Lovaza, a mixture of docosahexanoic and eicosapentanoic acids, is used to reduce triglyceride content in the blood. Four of the eight approved marine-derived drugs are used in the treatment of cancer including cytarabine and trabectedin. From 2012-2017, 262 marine compounds were involved in various stages of preclinical trials and there are currently thirteen marine natural products in clinical trials by the USA Food and Drug Administration (USFDA).<sup>4</sup> These include salinosporamide A<sup>14</sup> isolated from a marine bacterium, and the cryptophycins<sup>15</sup> and kahalalide F,<sup>16</sup> peptides from algae with anticancer activities.

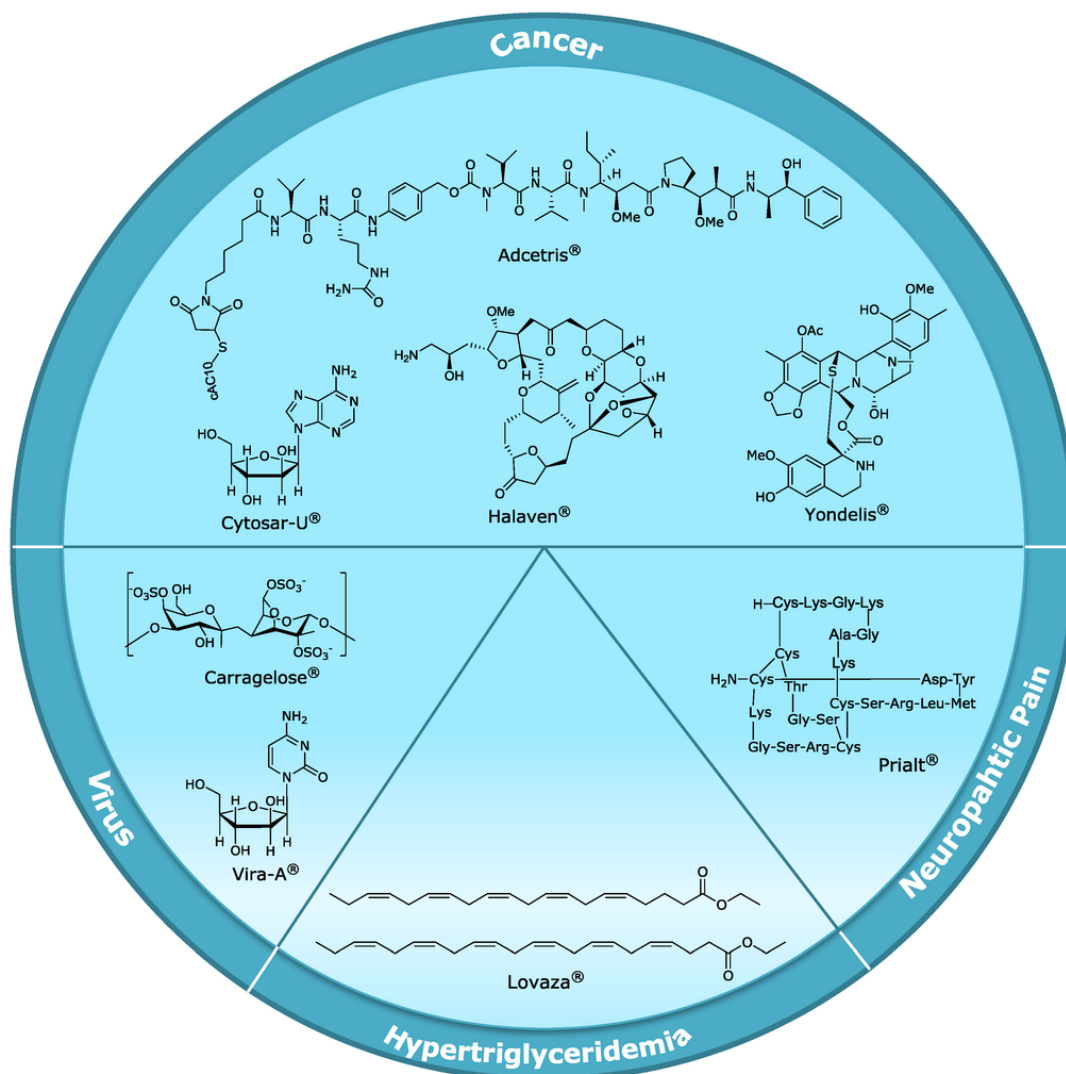


**Figure 1.2** Marine drugs approved for clinical use.<sup>11</sup> Adcetris (brentuximab vedotin), Cytosar-U (cytarabine), Halaven (eribulin mesylate), and Yondelis (trabectedin) are used to treat cancer; Carragelose and Vira-A (vidarabine) are used as antivirals; Lovaza (eicosapentanoic and docosahexanoic acid) is used to treat hyperglyceridemia; and Prialt (ziconotide) is used for severe and chronic pain.

## 1.2 Microalgal Taxonomy and Classification

Microalgae are microscopic eukaryotes which can be autotrophic, heterotrophic, or mixotrophic in nature.<sup>17</sup> Autotrophic microalgae require light, CO<sub>2</sub>, and basic inorganic nutrients to produce glucose via photosynthesis.<sup>18</sup> The origin of photosynthetic cyanobacteria (previously defined as “blue-green algae”) found in stromatolites and oncolites, has been dated to approximately 2.7 billion years ago. They are believed to be responsible for the oxygen-rich atmosphere we live in today.<sup>19</sup> Microalgae are incredibly diverse due to their evolutionary origins. Primary endosymbiotic events – the uptake of a chloroplast plastid from an unknown cyanobacterial source – led to the establishment of three clades of eukaryotic microalgae; Chlorophytes, Rhodophytes, and Glaucophytes.<sup>20</sup> Subsequent secondary (and in some cases tertiary) endosymbiotic events – the uptake of a plasmid from a Chlorophyte, Rhodophyte, or Glaucophyte – gave rise to further phylogenetic diversity, including the Heterokonts, which encompasses diatoms and Ochrophytes (**Figure 1.3**).<sup>21</sup> Their morphological diversity has led some taxonomists to declare that algae are in fact an artificial taxon. For example, Chlorarachniophytes are more closely related to Amoebae, as are Chlorophytes to higher plants, than they are to other algae.<sup>22</sup>

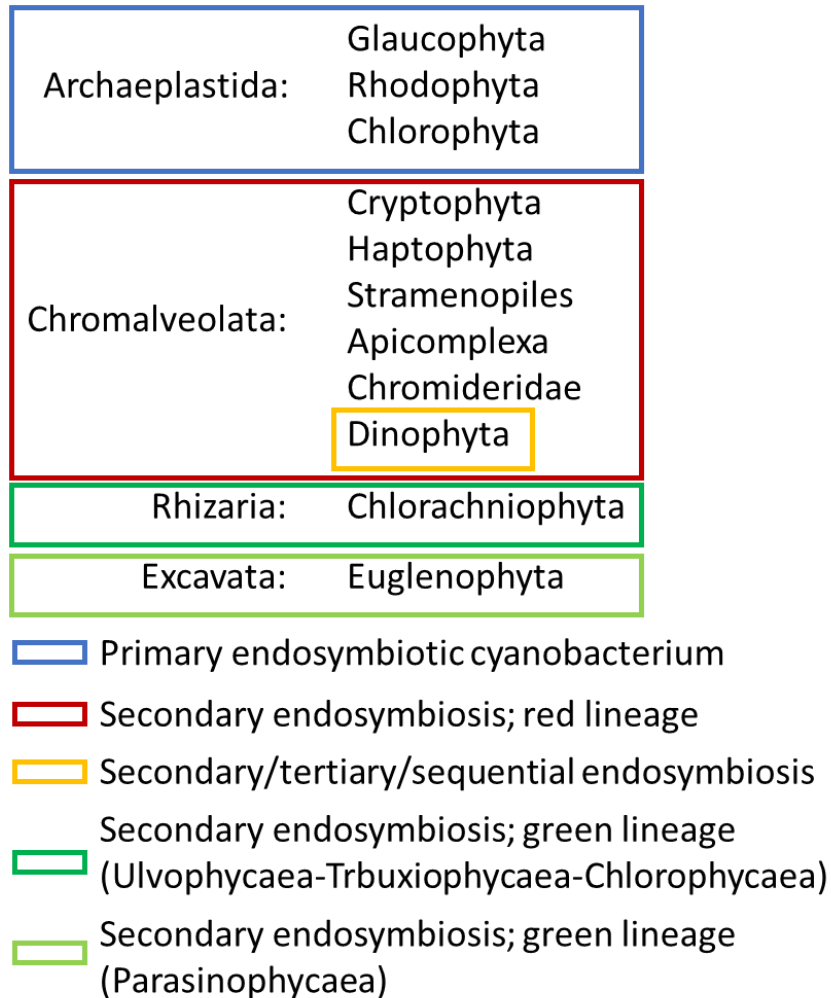


**Figure 1.3** Taxonomic classification of algal phyla based on plastid acquisition through endosymbiosis; primary endosymbiosis (blue), secondary endosymbiosis through red lineage (red), secondary/tertiary/sequential endosymbiosis (yellow), secondary endosymbiosis through green lineage leading to Ulvophyceae-Trebuxiophyceae-Chlorophyceae classes (green), secondary endosymbiosis through green lineage leading to Parasinophyceae class (light green). Adapted from Heimann *et al.*<sup>21</sup>

Despite the phylogenetic complexity of studying these organisms, five microalgal species (and the amoeba *Dictyostelium discoideum*) are defined as protist model organisms.<sup>23</sup> *Chlamydomonas reinhardtii* has been extensively used to study photosynthesis, flagellar motility, and cell-cell adhesion.<sup>24</sup> The whole genomes of the ciliate *Stentor coeruleus* and the diatom *Thalassiosira pseudonana* have been sequenced and act as models for single-cell regeneration, and silica biomineralization, respectively.<sup>25,26</sup> *Tetrahymena thermophila* is used as a model organism for gene expression as it exhibits nuclear dimorphism.<sup>27</sup> The ubiquitous phytoplankton, *Emiliana huxleyi* is used to study algal bloom phenomena.<sup>28</sup> As such, these polyphyletic and diverse organisms play important roles in fundamental research.

Microalgae are ubiquitous in nature and can be found in freshwater,<sup>29</sup> marine,<sup>30</sup> desert,<sup>31</sup> and rock habitats.<sup>32</sup> Isolates have been found in the extremely saline environments of the Great Salt Lake in the USA<sup>33</sup> and the Dead Sea in Israel,<sup>34</sup> and can survive at temperatures ranging from the Mediterranean Sea (>15 °C) to Antarctic snow (as low as -20 °C).<sup>35</sup> As they are photosynthetic, in aquatic environments, they are rarely found beyond the limits of the photic zone (200-300 m).<sup>18</sup> Chlorophytes are the most well-studied phylum with species found in both freshwater and marine habitats.<sup>18</sup> For example, members of the *Dunaliella* genus are almost exclusively found in marine and hyper-saline environments<sup>36</sup> whilst *Chlamydomonas* species are more commonly found in soil and freshwater habitats.<sup>29</sup> However, there are rare examples of microalgae found in unusual niches, such as the Atacama Desert, where a new subaerial species of *Dunaliella* was found growing on spiderwebs in caves.<sup>37</sup>

Michael D. Guiry, an accredited phycologist and taxonomist, considers algae to be “aquatic, oxygen-evolving photosynthetic autotrophs that are unicellular, colonial, or are constructed of filaments...” of which there are an estimated 72,000 species.<sup>38</sup> He is the founder of AlgaeBase<sup>39</sup>, a community curated database of algal taxonomy, nomenclature, and distribution which currently holds 163,046 entries (as of 31<sup>st</sup> August 2021).<sup>39</sup> Classifying microalgae based on traditional or Linnaean taxonomy is arduous as many species within a genus are morphologically diverse.<sup>40</sup> Microalgae comprise a variety of shapes and sizes, with some species using flagella for motility. They also differ in the composition of their outer cell walls. Diatoms produce a silicate frustule and coccolithophore cells are surrounded by intricate calcium carbonate

plates. This makes traditional taxonomic efforts of identifying and classifying microalgae difficult. However, cladistic approaches, such as phylogenetic studies, have also incurred challenges.<sup>41</sup> In bacteria, 16S rRNA gene sequences are used to study phylogenetic relationships between species. This gene is well conserved but with enough differences in variable regions (due to mutation) to allow genera and species to be distinguished.<sup>42</sup> No such gene marker exists for comparing microalgae, as they are polyphyletic in nature.<sup>43</sup> Guo *et al.*, compared potential ‘barcode’ genes for classifying diatoms by sequencing 18S rRNA, cytochrome c-oxidase subunit 1 (COI), carboxylase/oxygenase large subunit (*rbcL*), and the universal plastid amplicon (UPA) genes.<sup>44</sup> Base substitution saturation curves concluded that 18S rRNA and COI are too variable to be used in phylogenetic analysis, however UPA is too well conserved throughout this clade. They concluded that analysis using *rbcL* or the internal transcribed spacer-2 (ITS-2) region of the 18S rRNA gene alone could only be used to distinguish lower taxa, such as classes or families.<sup>44</sup> Other studies have shown that 18S small-subunit and 28S large-subunit rRNA genes can be used to classify diatoms into higher taxa levels (genera, species), however, universal primers are not readily available.<sup>45,46</sup>

The British island is surrounded by five distinct bodies of water – the Atlantic Ocean, North Sea, Celtic Sea, Irish Sea, and the English Channel. The North Atlantic Ocean has seen a massive shift in plankton populations and dynamics over the last 60 years (1958-2017). For example, dinoflagellate populations in the North Sea and Celtic Sea are decreasing which has been correlated with rising sea surface temperatures. Conversely, diatom populations have increased over the decades but do not show the same correlation to rising sea surface temperatures, suggesting that other factors – such as grazing pressure – may have an influence.<sup>47</sup> From 1992-2007, weekly water samples were collected from the Western English Channel and the phytoplankton community was characterised and monitored.<sup>48</sup> From this extensive study, 87% of the community was dominated by phyto-flagellate species with *Phaeocystis* spp. alone contributing an additional 4% of the community. Diatoms had an average abundance of 5% which increased in the summer due to *Pseudo-nitzschia* blooms whilst Coccolithophores and Dinoflagellate populations made up 2% and 3% of the community, respectively.<sup>48</sup> Studies like these are important for ecological and environmental understanding but

isolates of individual strains are required for fundamental and applied research. For this reason, the Culture Collection of Algae and Protozoa (CCAP) was established in 2004 at the Scottish Association for Marine Sciences.<sup>49</sup> This offered a repository of strains that could be purchased for academic and commercial research and has been invaluable in the development of the microalgal biotechnology industry in the UK. Companies such as Xanthella Ltd., MiAlgae, and Algenuity have used strains from this collection in the development of bioreactors, processes, and products using microalgae. However, there is still a gap in fundamental knowledge about the chemical potential of species already used in industrial practices. For this reason, four species of industrially relevant microalgae from British waters were chosen for untargeted metabolomics investigations. *Dunaliella primolecta* (Gross, 1936) is a Chlorophyte which contains chlorophyll *a* and *b*, and are the ancestors of land plants.<sup>22</sup> Although predominantly a freshwater phylum, the genus *Dunaliella* is most commonly found in marine environments.<sup>50</sup> They are biflagellate algae that lack a cell wall and can alter their pigment profile to change colour under certain environmental conditions. *Porphyridium cruentum* belongs to the Rhodophyte phylum that is defined by the presence of chlorophyll *a* and *c*, as well as phycobilins and phycobilisomes.<sup>51</sup> They are non-motile and often form aggregates or adhere to surfaces by producing exopolysaccharides.<sup>52</sup> *Nannochloropsis oculata* (Droop, 1953)<sup>53</sup> belongs to the Ochrophyta phylum which arose from the incorporation of a rhodophyte plastid into the genome. This genus is non-motile and only contains chlorophyll *a* but can build up high concentrations of other pigments required for photosynthesis. Finally, *Phaeodactylum tricornerutum* (De Martino and Ten-Hage 2003) belongs to the diatom clade which also evolved from a rhodophyte plasmid.<sup>54</sup> Diatoms are encapsulated by a hard frustule made of silica. *Phaeodactylum* is unusual in that it can exist in three different morphotypes; fusiform, oval, and triradiate and can survive without synthesising its silicified frustule.<sup>55</sup> The importance of these genera in the biotechnology industry will be discussed in **section 1.4**.

### **1.3 Culturing Microalgae**

In nature, microalgae co-exist with bacterial communities forming a symbiotic relationship that provides organic carbon for bacteria and remineralisation of nitrogen

and phosphorous for microalgae.<sup>56</sup> A survey of 326 algae showed that 52% of strains required bacterial symbionts to provide vitamin B<sub>12</sub> for growth.<sup>57</sup> However, even after supplementing culture media with vitamin B<sub>12</sub> and available nutrients, some microalgal cultures could not survive without their bacterial counterparts. This makes obtaining axenic cultures of microalgae difficult and time intensive, requiring techniques such as fluorescence-activated cell sorting (FACS), micropicking, or raman spectroscopy.<sup>58</sup> Advancements in microscopy and molecular tools has facilitated the establishment of international culture collections such as those at the Scottish Association for Marine Sciences, Marburg, and Göttingen university, each with over 1,500 strains. The availability of these axenic (or almost axenic) strains is therefore beneficial to the scientific community.

Once a suitable culture and medium has been obtained, there are several factors to consider when monitoring the growth of microalgal cultures. Microalgal growth can be monitored using cell counts, optical density, dry weight, and chlorophyll content.<sup>59</sup> The most accurate method is cell counting using a haemocytometer which is used to calculate the concentration of cells per volume of culture.<sup>59</sup> However, this method can only be used for single-celled microalgal species. For motile species, fixation of cells can be achieved using formaldehyde, propidium iodide, or Lugol's iodine.<sup>59</sup> To achieve >90% accuracy, it has been shown that at least 300 cells should be counted within each chamber.<sup>60</sup> This method can be time consuming due to the requirement for replicate measurements. For this reason, optical density has been shown to track relative densities of cultures using an absorbance at specific wavelengths between 600-750 nm.<sup>61</sup> Optical density is most commonly measured at 750 nm as pigments do not absorb in this region of the spectrum. Measuring chlorophyll *a* (680 nm) or *b* (650 nm) has also been used as a proxy for growth.<sup>61</sup> A linear relationship exists between absorbance and cell concentration and although this varies by species, it is simple to define through a calibration curve.<sup>60</sup> It should be noted that this method is not suitable for cultures that tend to clump.<sup>62</sup> Dry weight or ash-free dry weight measurements requires larger aliquots of sample to be removed and collected from liquid culture through filtration or centrifugation. Since marine species require salts in their medium, ash free dry weight is preferred as the salts are subtracted from the overall biomass after being ashed in a furnace.<sup>63</sup> According to Moheimani *et al.* ash free dry weight is



the most reliable method of biomass determination.<sup>60</sup> Flow cytometry is another method that is less commonly used to measure cell concentrations. Again, it is only suitable for single cells, however it is an automated and well established method that decreases the risk of gross error.<sup>64</sup> It also gives additional information such as fluorescence yields and fatty acid composition, which is particularly useful in biofuel research.<sup>65</sup>

Another important consideration in culturing microalgae is the scale and technology required to grow cultures efficiently. Large scale aquaculture of microalgae is desirable to produce sufficient biomass for nutraceuticals, feedstock, and biofuel industries.<sup>66</sup> This is achieved using open or closed systems, and natural or artificial light sources. Open systems, such as ponds and raceways (**Figure** ), leave cultures exposed to the outside environment which imposes a risk of contamination. Attempts to reduce environmental contamination involve growing cultures under extreme conditions. BASF is the world leader in the production of natural  $\beta$ -carotene from *Dunaliella salina*<sup>67</sup> and they have found that optimum  $\beta$ -carotene content is achieved in hypersaline (>27% W/V NaCl) and nitrogen-limiting conditions.<sup>68</sup> The cyanobacteria, *Arthrospira* spp. are commercially cultivated in a highly alkaline medium (up to 16 g/L sodium bicarbonate) for this same reason.<sup>69</sup> Open pond systems are much cheaper to run but cannot be finely tuned. Temperature fluctuates seasonally with the weather but also daily with diurnal rhythms and evaporation also affects culture volumes and may concentrate media components to an undesirable or toxic level during periods of intense sunlight.<sup>70</sup> Mixing of cultures is also very important to ensure cultures do not settle on the pond bottom and become hypoxic, and to facilitate consistent illumination of cells.<sup>71</sup>



**Figure 1.4** Production ponds in Hainan Province, China, containing *Arthrospira* (Spirulina) cultures.<sup>67</sup>

The need to control culturing conditions inspired the design of several types of closed systems, or photobioreactors, including vertical, horizontal tubular and flat panel (**Figure 1.5**), each with their advantages and drawbacks.<sup>71</sup> Mixing is also vitally important in closed systems to ensure consistent illumination of all cells, adequate gas exchange, and to prevent clumping or biofilm formation.<sup>70</sup> Mixing can be achieved by mechanical agitators or through sparging. Temperature and light parameters are usually maintained using a series of probes connected to a control module. Whilst the advantages of closed photobioreactors include no external contamination, finely controlled conditions, and batch-to-batch consistency;<sup>72</sup> open raceway ponds are by far the most common method of culturing microalgae on an industrial scale. It is actually more economically viable to grow microalgae in closed systems as they do not require as much land area but does require a large initial investment and technology to establish. In a financial assessment carried out by Richardson *et al.* in 2013, it was estimated that the total cost of crude bio-oil production was US\$109 per gallon in open raceway ponds and US\$77 per gallon in a photobioreactor.<sup>73</sup>

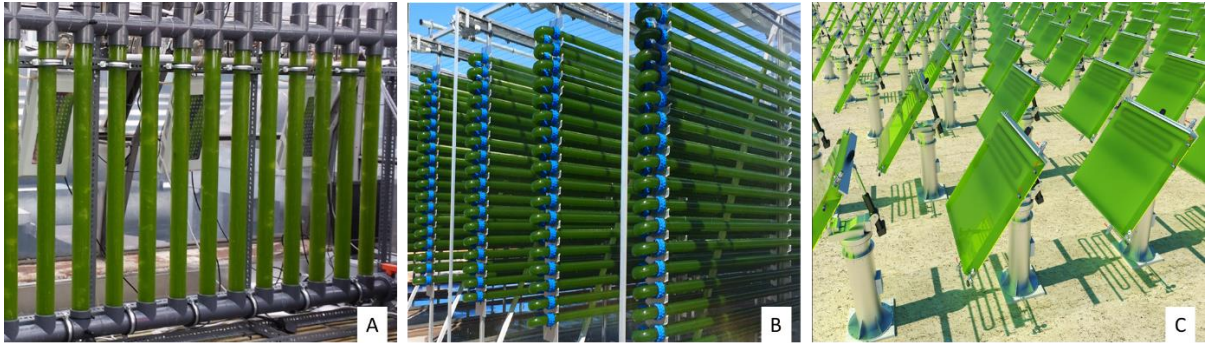


**Figure 1.5** Types of photobioreactors (A) vertical/column, (B) horizontal tubular, and (C) panel. Adapted from Murphy, *et al.* <sup>74</sup>

#### 1.4 Applications of Microalgae and Their Natural Products

Microalgal biomass and their extracted metabolites have a plethora of applications, including nutraceuticals,<sup>75</sup> biofuels,<sup>76</sup> and biomedicine.<sup>77</sup> Microalgal biomass is high in nutritional value and is commonly used in aquaculture, particularly for the farming of bivalve molluscs such as clams, oysters, and scallops, and is increasingly becoming known as a “super food” for human nutrition.<sup>78,79</sup> For example, the product Spirulina is made from two species of *Arthrospira*; *A. platensis*, and *A. maxima* which have a protein content as high as 60-70% whole cell dry weight.<sup>80</sup> Additionally, approximately 90% of its total fatty acid content is comprised of  $\gamma$ -linolenic, linoleic, and palmitic acid which have been reported to have prophylactic activity against diabetes, cardiovascular disease, and some cancers.<sup>81,80</sup> Dried *Chlorella* spp. biomass is also available as a health supplement as *Chlorella* spp. are rich in protein (53%) and carbohydrates (23%) and exhibit antimicrobial and antioxidative properties due to their high fatty acid and carotenoid concentrations.<sup>82</sup> A number of species are also used in aquaculture feeds. These include *Arthrospira* spp., *Chlorella* spp., *Tetraselmis* spp., and *Isochrysis galbana*. *Tetraselmis* spp. have a high arginine content whilst *Isochrysis galbana* offers a rich carbohydrate source.<sup>78</sup>

Another critical application of microalgal biomass and metabolites is in the production of biofuels. Fossil fuels are the leading contributor to greenhouse gases, with 288 megatonnes of CO<sub>2</sub> emitted in the UK in 2017.<sup>83</sup> In order to move away from the use of fossil fuels, research has focused on the production of biofuels – fuel derived from biomass. The first generation of biofuels utilised maize and sugarcane, however this move was met with controversy, as arable land was being utilised for bioethanol production rather than for food security.<sup>84</sup> Second generation biofuels intended to use non-food crops, whole plant matter, and forest harvesting residues, however the advancement of technology to allow commercial exploitation of these resources has been slow.<sup>85</sup> Third generation biofuels exclusively focuses on the extraction of algal biomass.<sup>86</sup> Transesterification of triacylglycerides to fatty acid methyl esters, followed by a cleavage step, produces biodiesel and glycerol.<sup>87</sup> Lipid content within microalgal cells depends on the species and culturing methods and ranges from 16-77% dry cell weight.<sup>88</sup> Since microalgae require minimal nutrient input, aquaculture farms can be built on non-arable land, reducing pressure on agriculture.<sup>70</sup> Large-scale production of

microalgae for biofuel is a great model for economic sustainability as waste water from distilleries and breweries can be used as a feedstock for the microalgae.<sup>66</sup> Additionally, 166 tonnes of CO<sub>2</sub> is fixed per 91 tonnes of biomass produced.<sup>88</sup> However, given the costs of developing microalgal biofuel plants, and the energy cost required to provide light and mixing to these plants, it is still not an economically viable route of producing biofuels. This is where biotechnology applications of microalgae could further benefit society as coupling the production of biodiesel to the extraction of high-value commercial products could significantly reduce the cost of biomass production.<sup>66</sup>

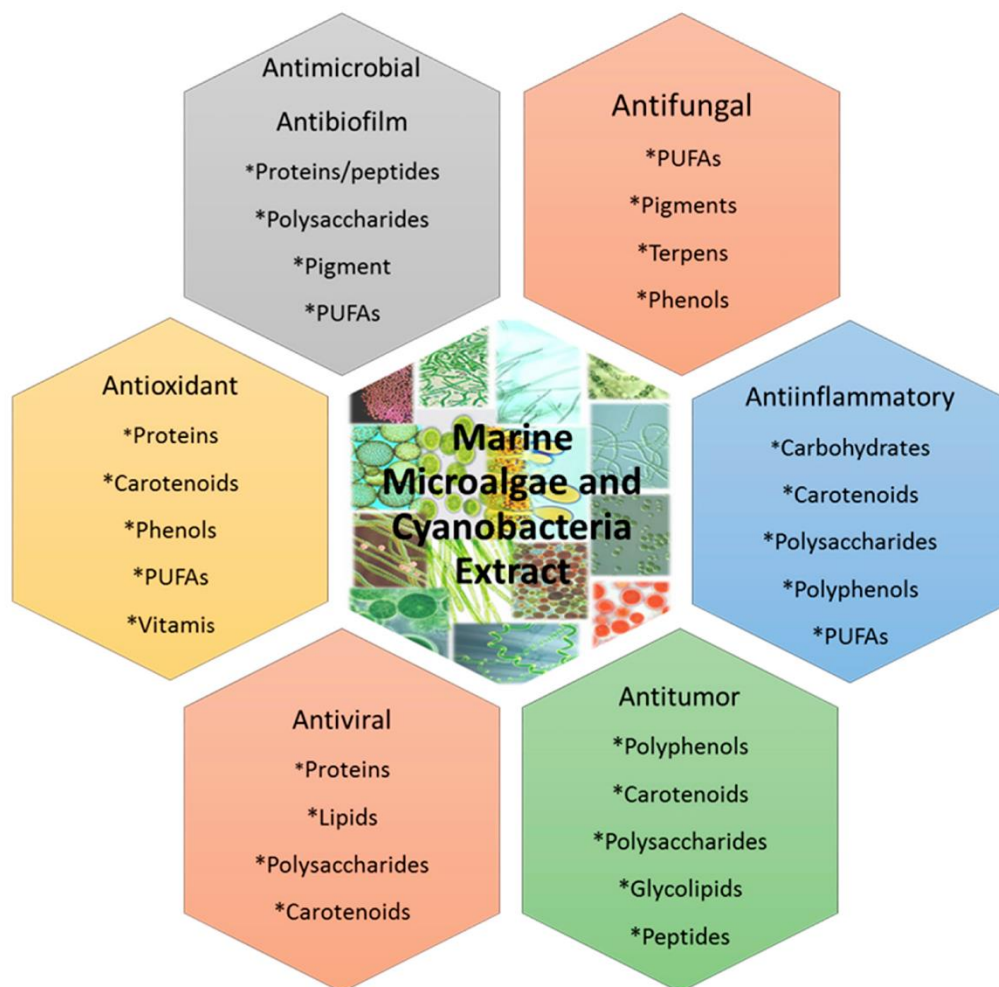


**Figure 1.6** Examples of bioactive microalgal metabolites and their bioactivities, including antioxidant, antitumour, and antimicrobial.<sup>89</sup>

Fortunately, bioactive metabolites are considered high-value products to the biotechnology industry and microalgae produce an abundance of metabolites with antitumour, antimicrobial, and immunomodulatory activities (**Figure 1.6**).<sup>77</sup>

### **Antimicrobial**

Antimicrobial activity is a blanket term used to describe inhibitory activity against any microorganisms, including bacteria, fungi, and viruses. Microalgal lipids not only have a role in biofuels, but also have interesting antimicrobial properties too. A study by McGee, *et al*, screened 80 microalgal extracts against *Escherichia coli*, *Pseudomonas aeruginosa*, *Bacillus subtilis*, *Enterococcus faecalis*, *Staphylococcus aureus*, and *Candida albicans*. They reported that 27% of extracts had activity against at least one pathogen and that lipophilic extracts showed the most activity (66%).<sup>90</sup> An additional study confirmed this by demonstrating that crude lipophilic extracts from *Dunaliella* spp. had moderate activity against clinically relevant strains of *Escherichia coli* and *Pseudomonas aeruginosa*, which they attributed to fatty acids such as eicosapentanoic acid (**8**) and palmitoleic acid (**9**).<sup>29</sup> Polysaccharides, in particular highly sulphated polysaccharides, have also been shown to have antimicrobial properties. Exopolysaccharides from *Porphyridium cruentum* have been reported to have antiviral activity against the Herpes Simplex virus,<sup>91</sup> Hepatitis B,<sup>92</sup> and Vesicular Stomatitis virus.<sup>93</sup>

### **Immunomodulatory**

Carotenoids, polyphenols, and polyunsaturated fatty acids produced by microalgae have great benefits to human health that include antioxidant, anti-inflammatory, and immunomodulatory activities.<sup>89</sup> *Dunaliella* spp. are prolific producers of  $\beta$ -carotene (**5**) (**Figure 1.7**), comprising up to 14% of dry weight.<sup>36</sup>  $\beta$ -carotene is a provitamin of vitamin A which plays an important role in strengthening the immune system and retaining good vision.<sup>94</sup> Other carotenoids such as astaxanthin (**6**) and zeaxanthin (**7**) act as powerful anti-oxidant and anti-inflammatory agents.<sup>82</sup> The protective properties of carotenoids, such as  $\beta$ -carotene and lutein, have been shown to prevent the onset of degenerative diseases like atherosclerosis, multiple sclerosis, and cognitive disability associated with Alzheimer's disease.<sup>34</sup> The marine derived drug Lovaza, which comprises eicosapentanoic and docosahexanoic acid (both found in high abundance in



microalgae), is used to protect against primary and secondary cardiovascular disease by reducing triglycerides and modulating cardiac ion channels.<sup>95</sup> A number of digalactosyldiacylglycerols and monogalactosyl analogues from *Nannochloropsis granulata* also exhibited strong immunomodulatory activity by inhibiting LPS-induced nitric oxide production in macrophage cells (RAW264.7).<sup>96</sup>

### **Anticancer**

Pigments from microalgae have also been shown to exhibit antitumour effects, alongside polysaccharides and peptides.<sup>89</sup> Fucoxanthin and lycopene extracted from *Chlorella ellipsoidea* and *C. vulgaris* inhibit growth of colon and prostate cancer, as well as stimulating apoptosis in other cancer cell lines.<sup>30,31</sup> Fucoxanthin is commonly found in macro- and micro-algae, with the diatom *Phaeodactylum tricornutum* reported to produce tenfold more fucoxanthin than macroalgae.<sup>97</sup> Another metabolite extracted from *P. tricornutum*, nonyl 8-acetoxy-6-methyloctanoate was also reported to have anticancer activity against human leukaemia (HL-60), lung carcinoma (A549), and mouse melanoma (B16F10) cell lines.<sup>98</sup> The depsipeptide dolastatin 10, produced by *Symploca* and *Lyngbya* species, made it to Phase II clinical trials as an anticancer agent in the 1990s. Unfortunately, dolastatin 10 treatment resulted in peripheral neuropathy in 40% of trial patients and it was discontinued.<sup>99</sup> However, a synthetic derivative of another depsipeptide, dolastatin 15, has successfully completed Phase I and Phase II clinical trials for the treatment of advanced stage metastatic melanoma.<sup>100</sup>



### 1.5 The Role of Stress in Stimulating Production of Natural Products

Investigation into microbial genomes often shows an inconsistency between the number of metabolites described by an organism and the number of biosynthetic gene clusters that encode the production of specialised metabolites.<sup>101</sup> It is widely believed that this is because most medically relevant metabolites are secondary metabolites and therefore only produced in response to biotic and abiotic pressures (i.e. they are not produced under standard laboratory culture conditions).<sup>102</sup> In bacteria, their chemical potential can be explored through genome mining using tools such as anti-SMASH (Antibiotics and Secondary Metabolites Analysis SHell),<sup>103</sup> and PRISM (PREdiction Informatics for Secondary Metabolites).<sup>104</sup> Unfortunately, due to the size and complexity of microalgal genomes, genome mining of microalgae is a difficult and arduous process (discussed in more detail in **chapter 4**).<sup>105</sup> As a result, unlocking the chemical potential of microalgae has largely been achieved through the elicitation of metabolites. The One Strain MAny Compound (OSMAC) approach<sup>102</sup> is one such method of chemical elicitation and it has been proven that small changes in growth conditions can lead to the production of specialised metabolites that would otherwise remain undiscovered.<sup>102</sup> For marine organisms, abiotic stresses such as nutrient levels, salinity, temperature, and pH have led to the discovery of new metabolites.<sup>101</sup>

The supply of nutrients and the stress caused by nutrient starvation can greatly affect the growth and metabolic capacity of microalgae.<sup>106,107</sup> In the most general of terms, microalgae require carbon, hydrogen, oxygen, nitrogen, and phosphorous. Diatoms also require silicon for their cell wall structure.<sup>18</sup> There are multiple studies showing the effect of nitrogen starvation, or use of alternative nitrogen sources, and their impact on metabolite production. For example, when *Parietochloris incisa* cultures were grown in nitrogen depleted BG-11 medium, arachidonic acid reached a level of 47% of total fatty acid content and this was extended to 60% when coupled with low light intensity (35  $\mu\text{mol}/\text{photons}/\text{m}^2/\text{s}$ ).<sup>108</sup> Converti *et al.*, also recorded a twofold and threefold increase in lipid content in *Nannochloropsis oculata* and *Chlorella vulgaris*, respectively, under nitrogen limiting (75% reduction) conditions.<sup>109</sup> Nitrogen starvation had a similar effect on carbohydrate production, with a fourfold increase recorded for *Tetraselmis subcordiformis*.<sup>110</sup> Phosphate, another important macronutrient for microalgal growth and development, has also been shown to

influence lipid composition. In a study by Khozin-Goldberg and Cohen, the total cellular lipid content increased in phosphate starved *Monodus subterraneus* cultures, however the target polyunsaturated fatty acid, eicosapentanoic acid, decreased by 13%.<sup>111</sup>

Trace nutrients, particularly metals, are important co-factors for photosynthesis as they facilitate efficient electron transport between metalloproteins.<sup>112</sup> The production of the commercially valuable carotenoid astaxanthin is increased (11-13 pg/cell) upon iron ( $\text{Fe}^{3+}$ ) starvation in *Haematococcus pluvialis* cultures,<sup>113</sup> whilst supplementation of media with  $1.2 \times 10^{-5}$  mol/L  $\text{FeCl}_3$  resulted in total lipid content increasing to 56.6% dry weight.<sup>114</sup> Introduction of copper or zinc increased the production of the neurotoxin domoic acid in *Pseudo-nitzschia australis*, whilst selenium and magnesium were attributed to a 58% rise in gymnodimine production in *Karenia selliformis* cultures.<sup>115</sup> The link between trace metal supplementation and the production of toxins by common bloom-forming microalgae may be important in predicting the onset of harmful algal blooms.<sup>116</sup> Vitamins are another important micronutrient for microalgae as they offer photoprotection and aid electron transport chains in the chloroplast.<sup>117</sup> Vitamins, or precursors thereof, are often supplied via symbiotic bacteria, however there are examples of microalgae synthesising some vitamins *de novo*.<sup>118</sup> Vitamin E ( $\alpha$ -tocopherol) is readily produced by the microalgae *Dunaliella tertiolecta* and *Tetraselmis suecica*.<sup>119</sup> Furthermore, production is increased up to  $2325.8 \pm 39$   $\mu\text{g/g}$  dry weight in *Nannochloropsis oculata* grown under nitrate limiting conditions.<sup>120</sup> Vitamin C (ascorbic acid) is also produced by a number of microalgae – including *Dunaliella tertiolecta* and *Nannochloropsis oculata* – in femtogram quantities.<sup>121</sup> Not only does photosynthesis require micronutrients such as metals and vitamins, it is also a temperature-dependent process in microalgae with optimum temperatures changing amongst freshwater and marine species. Sub-optimal temperature reduces RuBP carboxylase activity<sup>122</sup> but studies by Maxwell *et al.* demonstrated that *Chlorella vulgaris* adapted to being grown at 5 °C by lowering their chlorophyll content to offset the energy required.<sup>123</sup> Conversely, a 20% increase in the quantity of chloroplasts was observed for *Dunaliella salina* cultures that were chilled from 30 °C to 12 °C. This drop in temperature caused an increase in unsaturated fatty acids and digalactosyl diglycerides.<sup>124</sup> Converti *et al.* reported that lipid content of *Nannochloropsis oculata*

doubled to 14.9% when temperature was increased from 20 °C to 25 °C.<sup>109</sup> In that same study, the opposite effect was observed for *Chlorella sorokiniana*, with lipid content dropping from 14.7% to 5.9% when temperature was increased from 25 °C to 30 °C.<sup>109</sup>

Salinity levels can have a marked effect on carotenoid production of marine microalgae, but this varies remarkably amongst species. The accumulation of  $\beta$ -carotene in *Dunaliella salina* increases up to 10% dry weight under high saline conditions, and can tolerate up to 5.5 M salt concentration.<sup>50</sup> There is, however, an overall trend that halotolerant species can produce higher levels of carotenoids, namely  $\beta$ -carotene and astaxanthin, under high salinity levels as shown in *Nannochloropsis* sp. and *Tetraselmis* sp.<sup>125</sup> Gradual increase in the salinity of *Chaetoceros muelleri* saw the strain become halotolerant up to 45 ppt saline, coupled with increased production of fucoxanthin to 2.92 mg/g ash free dry weight.<sup>126</sup> A similar study using freshwater *Chlorella vulgaris* reported that lipid productivity of the strain doubled in saline conditions compared with freshwater conditions.<sup>127</sup> There are also a number of cases where salt stress is used to switch microalgal biosynthesis from starch to lipids. Kato *et al.* used heavy ion beam-coupled mutagenesis on *Chlamydomonas* sp. JSC4 cells to generate halotolerant mutants. Interestingly, they did not observe the shift in biosynthesis towards lipids as expected, suggesting that it is salt stress rather than simply the presence of salt which causes the change in biosynthesis.<sup>128</sup>

### **1.6 Elicitation of Metabolites from Microalgae Using Light**

As previously mentioned, the production and abundance of high-value metabolites from microalgae can be impacted by the conditions used for cultivation. Light and CO<sub>2</sub> are the most basic requirements for photosynthetic organisms. Whilst natural light is often used in open-pond systems (discussed in **section 1.3**), the fluctuation in intensity and photoperiod can greatly affect cell metabolism.<sup>70</sup> To achieve consistency, artificial light sources are often used, usually in the form of light emitting diodes (LED). It is important to supply energy in a form that is available to the algal cells and this depends on the ability of their accessory pigments to absorb light at different wavelengths (**Figure 1.8**).<sup>129</sup> This is known as Photosynthetically Active Radiation (PAR) and covers the range of 400-700 nm. Chlorophytes contain both chlorophyll *a* and *b*, as well as zeaxanthins, whereas Rhodophytes primarily absorb green and yellow light (500-650 nm) through phycocyanin and phycoerythrin.<sup>18</sup>



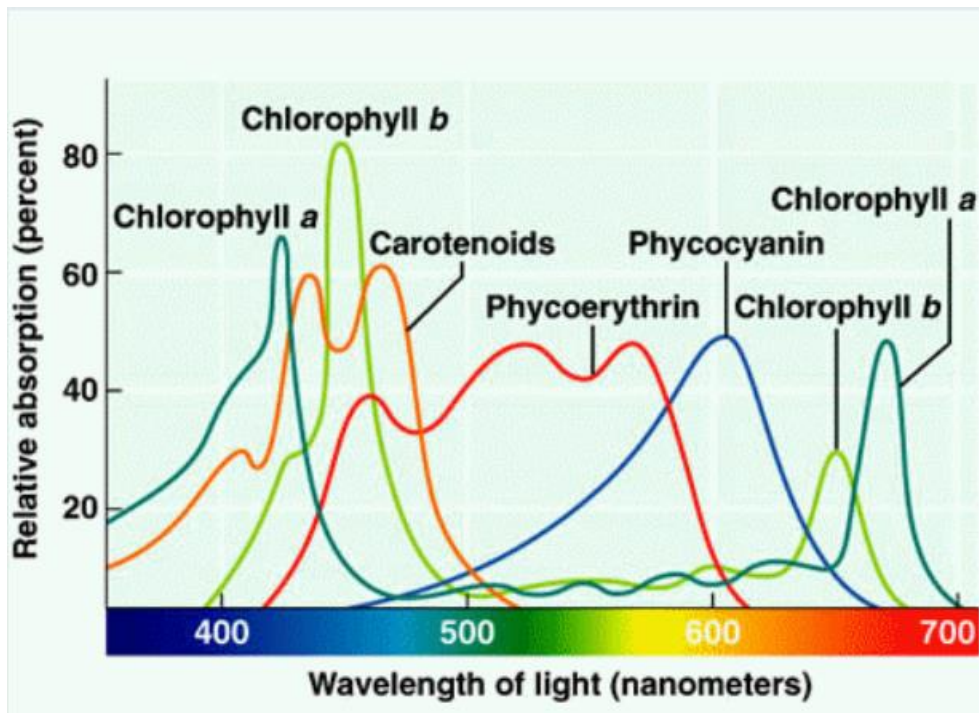


**Figure 1.8** Absorption spectra of algal accessory pigments across the visible light spectrum, illustrating the peak absorbance ranges for chlorophyll *a* (teal), chlorophyll *b* (green), carotenoids (orange), phycoerythrin (red), and phycocyanin (blue).<sup>129</sup>

The intensity and photoperiod of light has been shown to have considerable impact on growth and productivity of microalgae.<sup>17</sup> High light intensity or extended periods of illumination can cause photooxidative stress and damage the photosystems within chloroplasts.<sup>108</sup> Light intensity is directly proportional to the rate of photosynthesis, up to a saturation limit, as the supply of photons is responsible for ATP (adenosine triphosphate) and NADPH (reduced nicotinamide adenine dinucleotide phosphate) generation. Yeesang and Cheirslip studied the relationship between light intensity and nitrogen levels on *Botryococcus* strains. They found that maximum lipid content was achieved when strains were grown under a combination of high light intensity and nitrogen-deficient conditions.<sup>130</sup> In another case, high light intensity (400  $\mu\text{mol photons/m}^2/\text{s}$ ) alone was responsible for maximum total fatty acid content in cultures of *Parietochloris incisa*. However, when looking at the commercially valuable fatty acid, arachidonic acid, optimum production (60% total fatty acid content) occurred when *P. incisa* was grown under nitrogen-deficient conditions coupled with low light intensity (35  $\mu\text{mol photons/m}^2/\text{s}$ ).<sup>108</sup>

With advancements in LED technology and photobioreactor design, researchers have also been able to study the effect of wavelength ranges on growth and metabolite production, similar to studies on plants.<sup>131</sup> Xu and Harvey reported that although cell density remained the same when *Dunaliella salina* was grown under white, blue, red, or a mixture of red and blue; the total carotenoid and total chlorophyll content greatly differed. Chlorophyll content reached a maximum 5 pg/cell when illuminated with blue LED lights, however total carotenoid production increased from 30 to 40 pg/cell when grown under red illumination compared to white light.<sup>132</sup> Madhyastha *et al.* reported that cultivation of *Arthrospira* spp. under blue light increased the antioxidant activity of metabolite extracts.<sup>133</sup> Astaxanthin, the commercially important carotenoid produced by *Haematococcus pluvialis*, doubled in concentration when grown under blue light (450 nm) compared to red light (630 nm) reaching a maximum of 17 mg/L culture.<sup>134</sup> Although carotenoid production is greatly impacted by wavelength of light, this may be species or strain specific. McGee, *et al.*, reported a tenfold increase in zeaxanthin production by *Rhodella* sp. under high-intensity blue light, whilst medium-intensity blue and green light was required to elicit the same response from the Chlorophyte *Brachiomonas submarina*.<sup>135</sup>



Research into narrowband wavelengths led to the discovery that 405 nm light has bactericidal effects against a range of Gram-positive and Gram-negative bacteria.<sup>136</sup> This could be useful for microalgal culturing as bacterial communities often co-exist with microalgal cultures (as discussed in **section 1.2**), however they grow much faster and can out-compete the microalgal cultures for nutrients. It is hypothesised that cultivating microalgae under 405 nm illumination would keep bacterial cell counts at a minimum without affecting the growth of the eukaryotic microalgae. It has been shown that culturing *Nannochloropsis oculata* and *Tetraselmis chuii* under LEDs emitting 390-450 nm increased nutrient uptake and protein production compared to white light, and a combination of blue and red (630-690 nm) increased carbon fixation and carbohydrate production.<sup>137</sup> Therefore, narrowband 405 nm light could be beneficial in industry for improving microalgal growth whilst simultaneously reducing bacterial contaminants.

Although unrelated to the elicitation of metabolites, the naturally fluorescent properties of microalgae can be used to monitor their health and photosynthetic efficiency. This property can be used to measure the cell's response to stress. Auto-fluorescence is caused by the opening and closing of reaction centres in the photosystem, which is located in the chloroplast of the cell. There are two main stages to photosynthesis, the light phase and the dark phase which take place in photosystem II and photosystem I, respectively. The light phase reactions in photosystem II are first in the sequence and involves the absorption of a photon of light and the release of an electron into a redox cascade known as the z-scheme. This process is coupled with the conversion of water to molecular oxygen (**Figure 1.9**).<sup>138</sup> When the reaction centres of photosystem II are open, they can receive an electron which will then undergo charge separation to produce molecular oxygen. When the reaction centres are closed, electrons must dissipate their energy in a non-photosynthetic process, an example of which is fluorescence.<sup>139</sup> In fluorescence, the electron is given energy by an excitation wavelength ( $\lambda_A$ ) and elevated to an excited state. After a short time, that energy will be released as an emission wavelength ( $\lambda_B$ ) and heat to return the electron to the ground state. The emission wavelength can be measured using Fast Repetition Rate fluorometry and can give useful information about the physiological health and photosynthetic productivity of the organism.<sup>140</sup> This technique has primarily been used

to study environmental samples to determine the overall health of the populations,<sup>141</sup> study changes caused by climate change,<sup>142</sup> and monitoring of harmful blooms.<sup>143</sup> However, it can also be used to study laboratory cultures and has been shown to give insight into how various abiotic stresses affect the health and productivity of photosystem II. Yang *et al.* investigated the relationship between net photosynthetic rate and irradiance for three marine microalgal species: *Dunaliella salina*, *Isochrysis galbana*, and *Platymonas subcordiformis*. They observed that whilst net photosynthesis increased gradually with intensity for *I. galbana*, this relationship is steeply linear for both *D. salina* and *P. subcordiformis*.<sup>144</sup> This demonstrates that each species has a varying relationship between photosynthetic productivity and the intensity of light irradiance and may be important for understanding algal dynamics in the environment.

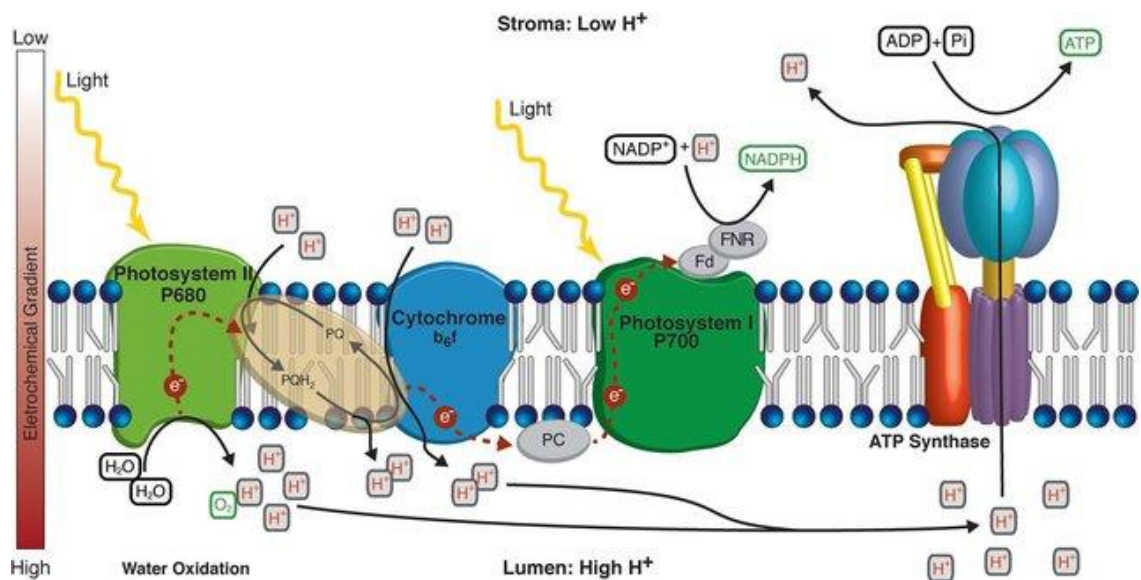


**Figure 1.9** Diagram of the light reactions in photosystem II.<sup>138</sup> Membrane-bound enzymes create a chemical gradient enabling the transport of protons (H<sup>+</sup>) from the stroma to the lumen. These protons are used by ATP synthase which drives the phosphorylation of adenosine diphosphate (ADP) to produce ATP.

## 1.7 Metabolomics

Traditionally, the discovery of new natural products was achieved through Nuclear Magnetic Resonance (NMR) spectroscopy- or bioassay-guided isolation before structure elucidation and identification of the metabolite could be confirmed.<sup>145</sup> This workflow required the use of expensive instrumentation (such as NMR and HPLC) and could often be a lengthy process as bioassays were performed by external collaborators. The advent of screening programmes such as the National Cancer Institute's 60 Human Tumour Cell Line Anticancer Screen (NCI60)<sup>146</sup> and Medicines for Malaria Venture (MMV)<sup>147</sup> in the 1980s and 1990s created streamlined bioassay screens to assist in the discovery of bioactive metabolites. The NCI60 screening programme led to the discovery of halichondrin B, a polyether macrolide isolated from the sponge *Halichondria okadai*.<sup>148</sup> This marine natural product was chemically modified to give the drug eribulin (marketed as Halaven) which is used to treat metastatic breast cancer.<sup>148</sup> These programmes greatly facilitated in the discovery of bioactive metabolites. Yet, as more natural products were being characterised, chemists were faced with the issue of rediscovery. The process from bioactive extract to a pure characterised metabolite is long and expensive, requiring multiple rounds of purification using HPLC and continued bioassay and NMR target confirmation.<sup>149</sup> The issue of rediscovery actually led to a large disinvestment in natural products research by pharmaceutical industries in the mid-1990s.<sup>145</sup> To address this bottleneck, dereplication strategies were employed which identified known metabolites from convoluted extracts or fractions.<sup>150</sup> This can be achieved using NMR and Liquid Chromatography Mass Spectrometry (LC-MS) tools and libraries and has rejuvenated the field of natural products drug discovery. For example, Shishido *et al.*, screened 62 extracts from 62 Brazilian cyanobacterial strains for the induction of apoptosis in acute myeloid leukaemia cells. Using molecular networking dereplication strategies, they identified nine known cyanotoxins as well as molecular family of five unknown chlorinated metabolites responsible for anticancer activity in some extracts.<sup>151</sup>

The natural products field continued to advance as metabolomics analysis became more commonplace. This included using LC-MS or tandem mass spectrometry (LC-MS/MS) and multivariate statistical analyses to compare crude metabolite extracts.<sup>150</sup> These methods enable dereplication and chemical prioritisation of parents ions of

interest (and thus metabolite extracts and fractions) which has further revolutionised the field of natural products.<sup>152</sup> Molecular networking, achieved through Global Natural Products Social (GNPS) ecosystem,<sup>153</sup> allows rapid, automated dereplication of tandem mass spectral data against a number of public and private libraries and produces a visual network of known/unknown fragments and their relatedness to each other.<sup>153</sup> Networks appear as clusters or molecular families of metabolites which are structurally similar based on their MS/MS fragmentation patterns, which act like a fingerprint of the molecule. Not only can previously isolated metabolites be identified through this platform, but analogues can be putatively identified within the molecular families. The potential for the discovery of novel metabolites can be achieved through chemical prioritisation of molecular families which are not linked to any known metabolites. Luzatto-Knaan *et al.* used molecular networking to investigate the chemical space of cyanobacterial and algal strains from over 300 field collections, which generated >15.6 million MS/MS spectra from 2600 extracted metabolite fractions. This analysis, which spanned 30 years' worth of fieldwork, could not be achieved manually, and was only made possible through the development of the GNPS platform. From this global analysis of marine cyanobacteria and microalgal fractions, only 13.7% of metabolites were identified as matches with the GNPS libraries.<sup>154</sup> This study illustrated that we have only captured “the tip of the iceberg” in terms of natural product discovery from cyanobacteria and microalgae. This molecular networking and dereplication approach has led to the discovery of several new metabolites from cyanobacteria, including yuvalamide A,<sup>154</sup> pagoamide A,<sup>155</sup> and palstimolide A which exhibited strong anti-parasitic activity (IC<sub>50</sub> of 223 nM against *Plasmodium falciparum* and 4.67 μM against *Leishmania donovani*).<sup>156</sup>

Unfortunately, the success of platforms such as GNPS relies on community sharing of data and public availability of natural product databases and libraries. There are a plethora of natural products databases such as MarinLit,<sup>157</sup> AntiBase,<sup>158</sup> and Dictionary of Natural Products.<sup>159</sup> However, these databases are hidden behind paywalls and dereplication must be done manually. There is no single platform that integrates all these libraries. In 2020, the GNPS libraries only contained approximately 2.5% of known natural products and this did not include any algal databases.<sup>160</sup> The Natural Products Atlas provides an open access repository of almost 25,000 natural

products isolated from microorganisms which has been integrated into the GNPS ecosystem and greatly improved the representation of natural products in the GNPS libraries.<sup>161</sup> Presently, it does not include natural products from eukaryotic microalgae and as such, discovery of new metabolites is still impeded by the lack of open access databases.

### **1.8 Aims and Objectives**

Research into the natural products of microalgae has primarily focused on lipids for biofuel production, carotenoids for cosmetics and nutraceuticals, and whole cell biomass for human health and aquaculture. However, there is a lack of understanding around the chemical space of microalgal metabolites and the role they play in their natural environment. Chemical space is a theoretical concept - based on physiochemical principles and constraints - of all possible molecular structures that could exist.<sup>162</sup> It has been evidenced in this chapter that microalgae produce a plethora of metabolites, covering several classes of natural products, but many studies have targeted specific metabolites or classes. Therefore, the true extent of their metabolite production remains unknown. This thesis aims to give insight into the chemical diversity of microalgae, and the impact of natural stress on the production of metabolites with specialised functions. It is hypothesised that culturing industrially relevant species under varying abiotic stress would elicit the production of previously undiscovered metabolites. These metabolites could uncover further applications of microalgae with more specialised activities which could benefit antimicrobial drug discovery efforts. This effect has been seen for other marine organisms such as bacteria and fungi, and biotechnological studies on microalgae has shown increased production of high-value metabolites when cultures were grown under varying conditions and provided rationale for this body of work.<sup>102, 101, 163</sup> This was achieved through the following objectives and aims:

#### **Objective 1: Chemical Characterisation of Microalgal Strains**

Chemical diversity of microalgal metabolites were explored through extraction optimisation and comparison of chemical profiles of microalgae from various phyla, species, and isolation environments.

Aim 1: To optimise the extraction of chemically diverse metabolites

Aim 2: To compare the metabolite profiles of 36 microalgal strains to understand species-specific and shared metabolites

**Objective 2: Quantify Growth and Metabolomic Profiles of Marine Microalgae Grown Under Abiotic Stress**

The strains *Dunaliella primolecta*, *Nannochloropsis oculata*, and *Phaeodactylum tricorutum* were cultured under high, low, and control concentrations of nitrate, salinity, NaCl, and pH.

Aim 1: To compare the growth characteristics of each strain in response to each stress.

Aim 2: To investigate the effect of abiotic stress conditions on the elicitation of metabolites.

**Objective 3: Investigate the Effect of 405 nm Light on Growth and Metabolite Production of Microalgal Strains.**

The strains *Dunaliella primolecta*, *Porphyridium cruentum*, *Nannochloropsis oculata*, and *Phaeodactylum tricorutum* were cultured under either white or 405 nm light only in 1 L MicroPharos™ photobioreactors.

Aim 1: To compare growth characteristics of cultures grown under either white or 405 nm light only.

Aim 2: To evaluate the antimicrobial activity of extracts and deconvoluted extract fractions resulting from growth under either white or 405 nm light only.

Aim 3: To investigate the effect of 405 nm light on the production of microalgal metabolites compared to a white light control.

## 2. Methods

---

### 2.1 Materials

The following common reagents were supplied from Fisher Scientific Ltd. or Sigma Aldrich; sodium chloride, sodium sulfate, potassium chloride, sodium hydrogen carbonate, potassium bromide, magnesium chloride hexahydrate, calcium chloride dihydrate, sodium nitrate, sodium dihydrogen phosphate monohydrate, sodium metasilicate nonahydrate, ferric chloride hexahydrate, disodium ethylenediaminetetraacetate dihydrate, manganese chloride tetrahydrate, zinc sulfate heptahydrate, cobalt chloride hexahydrate, copper sulfate pentahydrate, sodium molybdate dihydrate, thiamine hydrochloride, biotin, cyanocobalamin.

### 2.2 Strains

Strains used in this thesis are detailed in **Table 2. 1**. This includes strain identifications culturing medium, and collection site from which they were isolated.



**Table 2. 1** List of microalgal strains used including their strain identification and collection site.

<b>Species</b>	<b>Strain ID</b>	<b>Culture medium</b>	<b>Collection site</b>
<i>Dunaliella primolecta</i>	CCAP 11/34	<i>f</i> /2 (Guillard, 1975)	off Plymouth, Devon, England, UK
<i>Nannochloropsis oculata</i>	CCAP 849/1	<i>f</i> /2 (Guillard, 1975)	Skate Point, Isle of Cumbrae, Scotland, UK
<i>Phaeodactylum tricornutum</i>	CCAP 1055/15	<i>f</i> /2 (Guillard, 1975)	Blackpool, England, UK
<i>Porphyridium cruentum</i>	UTEX 161	<i>f</i> /2 (Guillard, 1975)	Basel, Switzerland
<i>Tetraselmis apiculata</i>	CCAP 66/15	<i>f</i> /2 (Guillard, 1975)	Brackish; salt marsh, Marine House, Lincolnshire, England, UK
<i>Tetraselmis suecica</i>	CCAP 66/22A	<i>f</i> /2 (Guillard, 1975)	Brackish; River Alde, Suffolk, England, UK
<i>Tetraselmis tetrathele</i>	CCAP 66/1A	<i>f</i> /2 (Guillard, 1975)	Brackish; salt marsh, Brancaster, Norfolk, England, UK
<i>Tetraselmis tetrathele</i>	CCAP 66/41	<i>f</i> /2 (Guillard, 1975)	Marine; Vancouver Island, British Columbia, Canada
<i>Chaetoceros calcitrans fo. pumilus</i>	CCAP 1010/11	<i>f</i> /2 (Guillard, 1975)	Marine; Urayasu, Chiba Prefecture, Japan
<i>Halamphora coffeaeformis</i>	CCAP 1001/2	<i>f</i> /2+Si (Guillard, 1975)	Brackish; tidal pool, La Jolla, California, USA
<i>Chlorocystis salina</i>	CCAP 233/1	<i>f</i> /2 (Guillard, 1975)	Marine; Ulva culture from Soulac, France
<i>Eustigmatos vischeri</i>	CCAP 860/7	3N-BBM+V (Aghajanian 1979)	Soil; Brixen, Austria
<i>Chlorella vulgaris</i>	CCAP 211/21A	<i>f</i> /2 (Guillard, 1975)	Brackish; River Crouch, Althorne, Essex, England, UK
<i>Pavlova gyrans</i>	CCAP 940/1C	<i>f</i> /2 (Guillard, 1975)	Marine; Cardigan Bay, Wales, UK
<i>Chrysothila carterae</i>	CCAP 944/6	<i>f</i> /2 (Guillard, 1975)	Marine; Station L2, English Channel
<i>Chrysothila carterae</i>	CCAP 961/5	<i>f</i> /2 (Guillard, 1975)	Marine; Port Erin, Isle of Man, British Isles

<i>Tisochrysis lutea</i>	CCAP 927/19	f/2 (Guillard, 1975)	Marine; Tahiti, Society Islands,
<i>Navicula sp.</i>	CCAP 1050/13	f/2+Si (Guillard, 1975)	Marine; Porcupine Abyssal Plain, North Atlantic
<i>Nannochloropsis oculata</i>	CCAP 849/1	f/2 (Guillard, 1975)	Marine; Skate Point, Isle of Cumbrae, Scotland, UK
<i>Cyclotella cryptica</i>	CCAP 1070/2	f/2+Si (Guillard, 1975)	Brackish; West Tisbury, Great Pond, Martha's Vineyard, Massachusetts, USA
<i>Tetraselmis chui</i>	CCAP 66/21A	f/2 (Guillard, 1975)	No record
<i>Diacronema lutheri</i>	CCAP 931/7	f/2 (Guillard, 1975)	Marine; pools, nr. pier, Millport, Isle of Cumbrae, Scotland, UK
<i>Isochrysis galbana</i>	CCAP 927/1	f/2 (Guillard, 1975)	Marine; fishpond, Port Erin Marine Station, Isle of Man, British Isles
<i>Rhodella violacea</i>	CCAP 1388/6	f/2 (Guillard, 1975)	Slightly brackish; öland Island, Baltic Sea, Sweden
<i>Diacronema lutheri</i>	CCAP 931/6	f/2 (Guillard, 1975)	Marine; pools, nr. pier, Millport, Isle of Cumbrae, Scotland, UK
<i>Diacronema vlkianum</i>	CCAP 914/1	f/2 (Guillard, 1975)	Marine; sea water, Ryde, Isle of Wight, England, UK
<i>Chrysotila carterae</i>	CCAP 961/1	f/2 (Guillard, 1975)	Marine; off Plymouth, Devon, England, UK
<i>Chrysotila carterae</i>	CCAP 961/8	f/2 (Guillard, 1975)	Brackish pool, Dunstaffnage Castle, Oban, UK
<i>Chrysotila carterae</i>	CCAP 961/2	f/2 (Guillard, 1975)	Marine; Station L2, English Channel
<i>Prymnesium parvum</i>	CCAP 941/1A	f/2 (Guillard, 1975)	Brackish; River Stour, Manningtree, Essex, England, UK
<i>Prymnesium parvum</i>	CCAP 946/6	f/2 (Guillard, 1975)	Marine; pool, nr. Pier, Millport, Isle of Cumbrae, Scotland, UK

<i>Prymnesium parvum</i>	CCAP 941/6	f/2 (Guillard, 1975)	Brackish; River Stour, Manningtree, Essex, England, UK
<i>Dunaliella tertiolecta</i>	CCAP 19/6B	f/2 (Guillard, 1975)	Brackish; Oslo Fjord, Norway
<i>Nannochloropsis oceanica</i>	CCAP 849/10	f/2 (Guillard, 1975)	Marine;
<i>Dunaliella tertiolecta</i>	CCAP 19/7C	f/2 (Guillard, 1975)	Brackish; River Crouch, Essex, England, UK
<i>Dunaliella tertiolecta</i>	CCAP 19/22	2ASW (Kester, 1967)	Marine
<i>Dunaliella tertiolecta</i>	CCAP 19/23	2ASW (Kester, 1967)	Marine
<i>Chlamydomonas reginae</i>	CCAP 11/78	f/2 (Guillard, 1975)	Marine; Per Haridy, Roscoff, France
<i>Chlamydomonas plethora</i>	CCAP 11/86B	Seawater Nutrient Agar (SNA)	Brackish; Butley River, Aldeburgh, Suffolk, England, UK
<i>Nannochloropsis oculata</i>	CCAP 849/7	SNA	Marine; Lake of Tunis, Tunisia

### 2.3 Media

For all in-house culturing, *f/2* (Guillard, 1975) in a modified version of Aquil synthetic seawater<sup>59</sup> was used (**Table 2. 2**)**Table 2. 2** List of reagents and final concentrations used to make *f/2* in Aquil medium.. NaNO<sub>3</sub> and NaH<sub>2</sub>PO<sub>4</sub>.H<sub>2</sub>O stocks were autoclaved at 121 °C for 15 mins. Trace metal and vitamin stock solutions were filter sterilised through 0.22 µm filter. The medium did not contain a buffer but pH was adjusted throughout experiments to maintain pH 7.6-7.8.

**Table 2. 2** List of reagents and final concentrations used to make f/2 in Aquil medium.

<b>Media component</b>	<b>Final concentration (M) in 1 L</b>
NaNO <sub>3</sub>	8.82x10 <sup>-4</sup>
NaH <sub>2</sub> PO <sub>4</sub> .H <sub>2</sub> O	3.62x10 <sup>-5</sup>
<b>Trace Metal Solution</b>	
FeCl <sub>3</sub> .6H <sub>2</sub> O	1.17x10 <sup>-5</sup>
Na <sub>2</sub> EDTA.2H <sub>2</sub> O	1.17x10 <sup>-5</sup>
MnCl <sub>2</sub> .4H <sub>2</sub> O	9.10x10 <sup>-7</sup>
ZnSO <sub>4</sub> .7H <sub>2</sub> O	7.62x10 <sup>-8</sup>
CoCl <sub>2</sub> .6H <sub>2</sub> O	4.20x10 <sup>-8</sup>
CuSO <sub>4</sub> .5H <sub>2</sub> O	3.93x10 <sup>-8</sup>
Na <sub>2</sub> MoO <sub>4</sub> .2H <sub>2</sub> O	2.60x10 <sup>-8</sup>
<b>Vitamin Solution</b>	
Thiamine HCl (vitamin B <sub>1</sub> )	2.96x10 <sup>-7</sup>
Biotin (vitamin H)	2.05x10 <sup>-9</sup>
Cyanocobalamin (vitamin B <sub>12</sub> )	3.69x10 <sup>-10</sup>
<b>Modified Aquil Synthetic Seawater</b>	
NaCl	4.20x10 <sup>-1</sup>
Na <sub>2</sub> SO <sub>4</sub>	2.88x10 <sup>-2</sup>
KCl	9.39x10 <sup>-3</sup>
NaHCO <sub>3</sub>	5.95x10 <sup>-3</sup>
KBr	8.40x10 <sup>-4</sup>
MgCl <sub>2</sub> .6H <sub>2</sub> O	5.46x10 <sup>-2</sup>
CaCl <sub>2</sub> .6H <sub>2</sub> O	6.38x10 <sup>-5</sup>

## 2.4 Stock Cultures

Strain stocks were maintained as 250 mL static cultures in f/2 enriched modified Aquil synthetic seawater with a 12-hour light, 12-hour dark cycle at  $75 \mu\text{mol}/\text{m}^2/\text{s}$  and  $20 \text{ }^\circ\text{C}$  in a Panasonic MIR-154-PE incubator. Media was replenished every month by removing 100 mL of culture and replacing with 100 mL fresh media. Cultures were manually agitated regularly to allow airflow and prevent biofilm formation.

## 2.5 Microscopy

Cells were suspended in 40% glycerol in modified Aquil synthetic seawater and a 10  $\mu\text{L}$  aliquot was placed onto a glass slide and a cover slip was placed on top. Cells were visualised using a TE2000-S inverted phase contrast microscope (Nikon) at x400 magnification. Images were acquired using a Hamamatsu C4742-95 camera at a 0.32  $\mu\text{m}/\text{pixel}$  scale and processed using the Image J.<sup>164</sup>

## 2.6 Growth Calibration Curves

The following 1 mL dilutions of stock cultures in distilled water were prepared in triplicate in Eppendorf tubes: 10:0, 9:1, 8:2, 7:2, 6:4, 5:5, 4:6, 3:7, 2:8, 1:9. The optical density at 600 nm (Eppendorf Biophotometer 6131) was recorded for each set of replicates. Cell concentration for each replicate was determined by adding a 10  $\mu\text{L}$  aliquot to a Marienfeld Neubauer improved bright light haemocytometer and visualising under Olympus CH20 light microscope at x40 magnification. The average cell concentration (cells/mL) for each triplicate was plotted against the average absorbance at 600 nm. The standard deviation between replicates of cell concentration (horizontal error bars) and optical density at 600 nm (vertical error bars) are represented on each graph.

## 2.7 Growth Analysis

Cultures of *Dunaliella primolecta* CCAP 11/34, *Nannochloropsis oculata* CCAP 849/1, *Phaeodactylum tricornutum* CCAP 1055/15, and *Porphyridium cruentum* UTEX 161 were prepared in triplicate and maintained under stock culture conditions (2.4 Stock Cultures). Growth was monitored by removing a 1 mL aliquot which was used to measure the optical density 600 nm and cell counts as above (2.6 Growth Calibration Curves).

Semi-log plots of raw growth data (cell counts or optical density at 600 nm) were used to determine start and end points for specific growth rate analysis. One-way ANOVA analysis was performed on specific growth rates using Origin 2021 software.

## **2.8 Phylogenetic Analysis**

18S rRNA gene sequences were retrieved from the European Nucleotide Archive (**Table 2. 3**) and aligned using Multiple Sequence Comparison by Log-Expectation (MUSCLE).<sup>165</sup> Alignments were filtered to remove gaps caused by partial sequence data. A nearest neighbour-joining phylogenetic tree was constructed using the Tamura-Nei method<sup>166</sup> (1000 bootstraps) in Mega 7 (v.7.0.26).<sup>167</sup>

**Table 2. 3** The strain codes, species names, and accession numbers of strains used in phylogenetic analysis.

<b>CCAP Code</b>	<b>Species</b>	<b>Accession Number</b>
66/15	<i>Tetraselmis apiculata</i>	KJ756817
66/22A	<i>Tetraselmis suecica</i>	FJ559377
66/1A	<i>Tetraselmis tetrathele</i>	MN720749
66/41	<i>Tetraselmis tetrathele</i>	MN721295
1010/11	<i>Chaetoceros calcitrans fo. pumilus</i>	EU240880
1001/2	<i>Halamphora coffeaeformis</i>	FR865481
233/1	<i>Chlorocystis salina</i>	FR865693
860/7	<i>Eustigmatos vischeri</i>	KJ713283
211/21A	<i>Chlorella vulgaris</i>	KJ756823
940/1C	<i>Pavlova gyrans</i>	FR865772
944/6	<i>Chrysotila carterae</i>	MN727054
961/5	<i>Chrysotila carterae</i>	MN727061
927/19	<i>Tisochrysis lutea</i>	MN723153
1050/13	<i>Navicula sp.</i>	MN722636
849/1	<i>Nannochloropsis oculata</i>	KJ756827
1070/2	<i>Cyclotella cryptica</i>	AY485499
66/21A	<i>Tetraselmis chui</i>	MN723167
931/7	<i>Diacronema lutheri</i>	MG022753
927/1	<i>Isochrysis galbana</i>	KC888106
931/6	<i>Diacronema lutheri</i>	MN723476
914/1	<i>Diacronema vlkianum</i>	FR865765
961/1	<i>Chrysotila carterae</i>	MG022757
961/8	<i>Chrysotila carterae</i>	HQ877918
961/2	<i>Chrysotila carterae</i>	MG022758
941/1A	<i>Prymnesium parvum</i>	MN723534
946/6	<i>Prymnesium parvum</i>	KJ756812
941/6	<i>Prymnesium parvum</i>	MN727031
19/6B	<i>Dunaliella tertiolecta</i>	KJ756820
849/10	<i>Nannochloropsis oceanica</i>	KJ756836
11/78	<i>Chlamydomonas reginae</i>	FR865614
11/86B	<i>Chlamydomonas plethora</i>	MN727030
849/7	<i>Nannochloropsis oculata</i>	KJ756833



## 2.9 Culturing Under Experimental Conditions

### *Abiotic stress*

Cultures of *Dunaliella primolecta* CCAP 11/34, *Nannochloropsis oculata* CCAP 849/1, and *Phaeodactylum tricornutum* CCAP 1055/15 were grown in triplicate in 250 mL Erlenmeyer flasks under the conditions above (**2.4 Stock Cultures**). All cultures were grown in f/2 enriched Aquil synthetic seawater with the following modifications: Sodium nitrate (NaNO<sub>3</sub>) concentration; 8.82x10<sup>3</sup> (high), 8.82x10<sup>4</sup> M (control) and 8.82x10<sup>5</sup> M (low).

Sodium chloride (NaCl) concentration: 0 g/L (deplete), 12 g/L (low), 24 g/L (control), 36 g/L (high).

Salinity (Aquil synthetic seawater concentration): 4.3 ppt (1/10 dilution, low), 43 ppt (control), 86 ppt (x2 concentrated, high).

pH: pH 4 buffered using 1 M (low), pH 7.6 not buffered (control), pH 10 using 1 M (high). pH was monitored throughout and adjusted using 1 M HCl or 1 M NaOH.

### *Photobioreactors*

Cultures of *Dunaliella primolecta* CCAP 11/34, *Nannochloropsis oculata* CCAP 849/1, *Phaeodactylum tricornutum* CCAP 1055/15, and *Porphyridium cruentum* UTEX 161 were grown in triplicate in 1 L MicroPharos™ (Xanthella Ltd., Oban, UK) at an average starting concentration of 4.5x10<sup>5</sup>, 1.9x10<sup>6</sup>, 3.8x10<sup>5</sup>, and 5.3x10<sup>4</sup> cells/mL, respectively. The MicroPharos™ photobioreactor included a temperature probe, air inlet, air outlet, and sampling port (**Figure 2 1**). Light intensity was maintained at 5 mA for *Porphyridium cruentum* and 10 mA for the *Nannochloropsis oculata*, *Dunaliella primolecta*, and *Phaeodactylum tricornutum*; **Figure 2.2** shows the linear relationship between current (mA) and light intensity (μmol). Temperature was maintained at 20±1 °C and mixing was achieved by bubbling air into the culture.

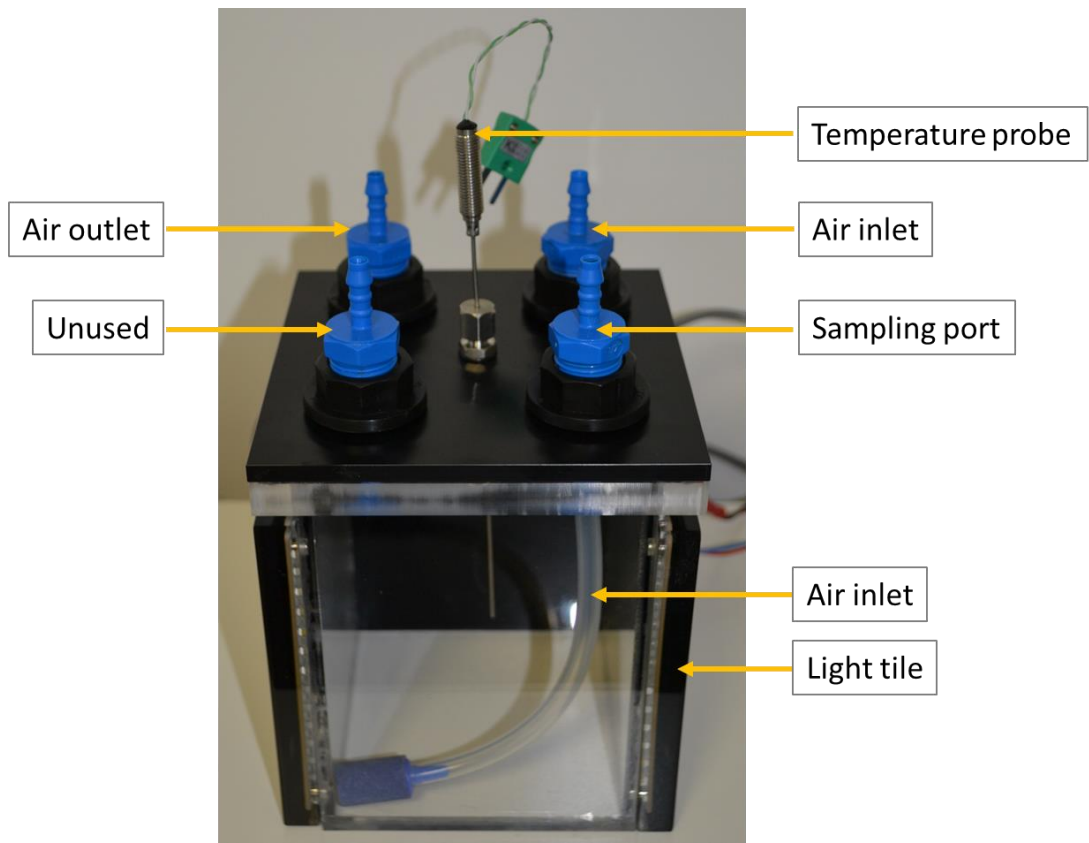


**Figure 2 1** Photo of the MicroPharos™ photobioreactor showing the temperature probe, air inlet and outlet ports, sampling port, and light tiles.

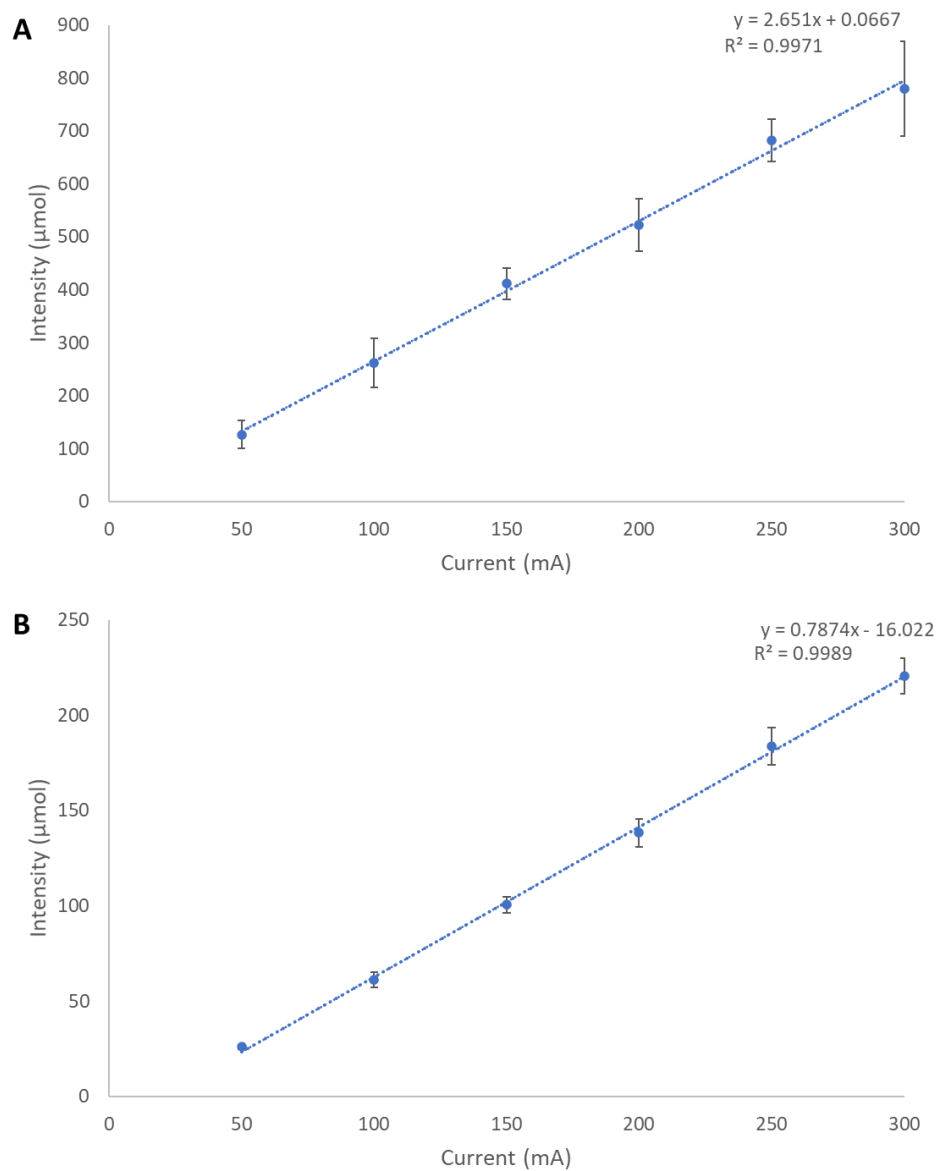


**Figure 2.2** Calibration curves showing the relationship between current (mA) and intensity ( $\mu\text{mol}$ ) for (A) white light tiles and (B) 405 nm light tiles. Error bars represent the standard deviation between four light tiles.

## **2.10 Extraction of Metabolites**

All extractions were performed on cultures once they had reached stationary phase (i.e., two consecutive readings were the same).

### *Extraction optimisation*

Liquid-liquid extractions: an equal volume (100 mL) of ethyl acetate was added to cultures and agitated overnight at 160 rpm (Stuart Orbital shaker SSL1). The organic layer was filtered through sterile cotton wool to remove cellular debris and dried under nitrogen.

HP-20 extractions: Diaionic HP-20 resin was activated by mixing in ethyl acetate for 10 min and vacuum filtered until dry. Dried resin was either used immediately or stored in ethyl acetate. Resin (5% w/v) was added to cultures and agitated overnight at 160 rpm. Cultures were centrifuged at 4200 rpm for 30 min (Thermo Scientific Heraeus Megafuge 40R) and the supernatant was removed. Frozen cell pellets with resin were lyophilised (Lab Conco Freezone 2.5) and extracted overnight with 50 mL of organic solvent (ethyl acetate, methanol, butanol, or 1:1 butanol:dichloromethane). Extracts were filtered through cotton wool and dried under nitrogen.

### *Extraction of small cultures (100 mL)*

HP-20 extractions were performed as above on all small cultures using 50 mL of ethyl acetate as the extraction solvent.

### *Extraction of large cultures (1 L)*

HP-20 extractions were performed as above with the following modifications: 3% w/v diaionic HP-20 was added to cultures and agitated overnight at 120 rpm and centrifuged at 9000 rpm for 30 min (Beckman Coulter Avanti JXN-26). Cell pellets were resuspended in a minimal volume of distilled water and centrifuged again at 4200 rpm for 30 min (Thermo Scientific Heraeus Megafuge 40R) and the supernatant was discarded. Freeze dried cell pellet and resin were extracted overnight in 200 mL of ethyl acetate and filtered through fluted filter before being dried under nitrogen.

## **2.11 LC-MS and LC-MS/MS analysis**

### *LC-MS analysis for extraction optimisation (Chapter 3.2.1)*

Crude metabolite extracts from liquid extraction were prepared at 1 mg/mL in acetonitrile and 10  $\mu$ L was injected onto an ACE C18 reversed-phase column (150 x 3.0 mm, 5  $\mu$ m; HiChrom, Reading, UK) connected to a Thermo UltiMate™ 3000 HPLC with a flow of 300  $\mu$ L/min. A binary gradient of solvent A (Millipore water with 0.1% formic acid) and solvent B (acetonitrile with 0.1% formic acid) was used, as follows: 5 min at 5% B, 20 min gradient from 5-100% B, 5 min at 100% B. Extracts were analysed using a Thermo Exactive mass spectrometer in positive mode electrospray ionisation (ESI), a mass range of 150/1500  $m/z$ , and a resolution of 30,000. Capillary temperature was maintained at 270 °C, ion spray voltage of 4.5 kV, and capillary voltage of 35V.

#### *LC-MS/MS analysis for exploring chemical diversity (Chapter 3.2.2)*

Metabolite extracts were prepared at 1 mg/mL in methanol and 10  $\mu$ L was injected onto an ACE C18 reversed-phase HPLC column (75 x 3.0 mm, 5  $\mu$ m; HiChrom, Reading UK) connected to an Accela HPLC (Thermo Scientific, Bremen, Germany). A binary gradient of solvent A (Millipore water with 0.1% formic acid) and solvent B (acetonitrile with 0.1% formic acid) was used: 30 min gradient from 10-100% B, 6 min at 100% B, 9 min gradient from 100-10%, with a flow rate of 300  $\mu$ L/min. Extracts were analysed using a Finnigan LTQ Orbitrap spectrometer using positive mode ESI, a mass range of 100-2000  $m/z$ , and a resolution of 30,000. Samples were analysed using a Finnigan LTQ Orbitrap spectrometer (Thermo Fisher, Bremen, Germany) and data dependent MS<sup>2</sup> experiments were performed on the 1<sup>st</sup>, 2<sup>nd</sup>, and 3<sup>rd</sup> most intense peaks using collision-induced dissociation (CID) with a resolution of 15,000 and minimum ion signal threshold of 500. The capillary voltage was set at 35 V, capillary temperature was 270 °C, ion spray voltage was 4.5 kV, and tube lens voltage was 110 V. MS<sup>2</sup> signals were not sufficiently amplified for informative analysis and so MS<sup>1</sup> data was extracted using the Proteowizard MSConvert tool.<sup>168</sup>

#### *LC-MS/MS analysis for abiotic stress and light extracts (Chapter 4.2 and 5.2.3)*

Extracts were prepared at 1 mg/mL in 2:2:1 acetonitrile:methanol:water and 10  $\mu$ L was injected onto a Kinetex C18 reversed-phase column (100 x 2.1 mm, 1.7  $\mu$ m; Phenomenex, Cheshire, UK) connected to a Thermo UltiMate™ 3000 UPLC with a flow of 300  $\mu$ L/min. A binary gradient of solvent A (Millipore water with 0.1% formic acid)

acid) and solvent B (acetonitrile with 0.1% formic acid) was used, as follows: 0.5 min at 5% B, 8 min gradient from 5-50%, 2 min gradient from 50-99% B, 2 min at 99% B, 1 min gradient from 99-5% B, 2 min at 5% B. Extracts were analysed using a Thermo Scientific Q-Exactive in positive mode ESI, a mass range of 150-1500  $m/z$ , and a resolution of 35,000. Data dependent MS<sup>2</sup> scans were performed on the 1<sup>st</sup>, 2<sup>nd</sup>, and 3<sup>rd</sup> most intense peaks using CID with a resolution of 17,500. The ion spray voltage was set to 4.2 kV, the capillary temperature was 310 °C.

#### *Data filtering using MZmine*

All data was converted to centroid .mzML files using the ProteoWizard MSConvert tool<sup>168</sup> and processed using MZmine v2.53.<sup>169</sup> Mass detection was performed using a minimum intensity value of  $1 \times 10^5$ . The Automated Data Analysis Pipeline (ADAP)<sup>170</sup> was used to build chromatograms using a minimum group size of 5 scans, group intensity threshold of 500, and an  $m/z$  tolerance of 0.01. Chromatograms were deconvoluted using the local minimum search algorithm with a 90% chromatographic threshold, 0.4 min minimum retention time range, minimum relative height of 5%, minimum ratio of peak top/edge of 2, and a peak duration of 0.2-5 min. The MS2 scan pairing range was 0.025 Da and retention time range of 0.3 min. Grouping of isotope peaks was then performed, and data was aligned using a 5% retention time tolerance, and 20 as the weight for both  $m/z$  and retention time. Finally, gap filling was achieved using the peak finder tool with a 25% intensity tolerance and 0.5 min retention time tolerance. Mass spectral values that were detected in solvent blanks were removed and peaklists were exported.

#### *Multivariate statistical analysis using MetaboAnalyst*

Peaklists generated using MZmine v2.53 were uploaded to MetaboAnalyst<sup>171</sup> where log transformation and auto or pareto scaling was used to normalise data. Principal Component Analysis (PCA) and/or Partial Least Squares – Discriminant Analysis (PLS-DA) was performed. Hierarchical clustering produced heatmaps of chemical profiles.

## **2.12 Molecular Networking**

### *Classical Molecular Networking*

Converted .mzML spectral files were uploaded to the GNPS<sup>153</sup> platform and the medium data preset was selected. The precursor ion mass tolerance was set at 2 Da and the fragment ion tolerance was 0.5 Da. The minimum pairs cosine value was 0.7, network topK was 10, maximum connected component size of 100, minimum matched fragment ions was set to 3, minimum cluster size of 2, and minimum peak intensity was  $1 \times 10^4$ . The same parameters were used for the library search and solvent blanks were filtered from the data before networking. The resultant GraphML file and cluster table were imported to Cytoscape v3.8.2 for annotation.<sup>172</sup>

#### *Feature Based Molecular Networking (FBMN)*

Peaklists and quantification tables were generated using MZmine 2.53 and these tables, as well as converted .mzML files, were uploaded to the FBMN<sup>173</sup> workflow on GNPS. The precursor fragment ion mass tolerance was 0.02, minimum pairs cosine was 0.6, network topK was 10, minimum matched fragment ions was set to 6, maximum connected component size was 100, maximum shift between precursors was 500 Da, and run dereplicator was selected.

#### *MS<sup>2</sup> Latent Dirichlet Allocation (MS2LDA) analysis*

The spectral data (MGF) and networkedges\_selfloop files from the FBMN were uploaded to the MS2LDA<sup>174</sup> and MotifDB substructure workflow on GNPS, along with the quantification table from MZmine 2.53. The bin width was set at 0.1, number of LDA iterations was 1000, minimum MS<sup>2</sup> intensity was 1000, and LDA free motifs was 300. All MotifDB databases were selected except Urine Motif and *Streptomyces* and *Salinisporus* Motif.

#### *Molecular Network Enhancer (MolNetEnhancer) analysis*

The task ID for the FBMN and MS2LDA analyses were copied into the MolNetEnhancer<sup>175</sup> workflow on GNPS.

#### *Data Repository*

Data for Chapter 3.2.2 can be found at:

<https://massive.ucsd.edu/ProteoSAFe/dataset.jsp?task=67a921a87cce46be896d698c9ec40526>

Data for Chapter 3.2.3 can be found at:

<https://massive.ucsd.edu/ProteoSAFe/dataset.jsp?task=ee87edeec73f43d18e1596f35c055eb4>

Data for Chapter 4.2 can be found at:

<https://massive.ucsd.edu/ProteoSAFe/dataset.jsp?task=862a5b30ee0c45c8bc54c2760cea33ec>

Data for Chapter 5.2.3 can be found at:

<https://massive.ucsd.edu/ProteoSAFe/dataset.jsp?task=236d3090b23648ab951b40f9213f74e6>

## 2.13 Bioactivity Screening

### *Disk diffusion assays*

Disk diffusion assays against the pathogens *Escherichia coli* ATCC 25922, *Staphylococcus aureus* ATCC 43300, *Klebsiella pneumoniae* ATCC 700603, *Acinetobacter baumannii* ATCC 19606, *Pseudomonas aeruginosa* CIP A14, *Enterococcus faecalis* ATCC 51299, *Bacillus subtilis* ATCC 23857, *Candida albicans* DSM 1386, and *Rhizopus oryzae* were performed. For the bacteria and *C. albicans*, a single colony was inoculated into 5 mL of media (**Table 2. 4**) and incubated overnight. 5 mL of sterile water was added to an agar plate with *R. oryzae* and the mycelium and water were transferred to a universal tube. The cultures were diluted to an optical density of 0.01 (0.1 for *E. faecalis*) into molten soft nutrient agar (50 °C) and poured over agar plates (**Table 2. 4**). Crude metabolite extracts were dissolved in ethyl acetate and transferred to sterile filter disks at a final concentration of 100 µg/disk. Negative controls included ethyl acetate disks and extracted f/2 with Aquil medium. Positive controls are listed in **Table 2. 4**. Extracts were considered active if a zone of inhibition was observed after 24 hours incubation and the diameter of the zone was measured (mm).



**Table 2. 4** List of pathogens, the medium they were cultured in, incubation temperature, and the reagent used as a positive control in bioassays.

Pathogen	Medium	Temperature (°C)	Positive Control
<i>E. coli</i>	LB (peptone 10 g/L, yeast extract 5g/L, sodium chloride 5 g/L)	37	Chloramphenicol 25 µg/mL
<i>S. aureus</i>	LB	37	Chloramphenicol 25 µg/mL
<i>K. pneumoniae</i>	LB	37	Imipenem 50 µg/mL
<i>A. baumannii</i>	LB	37	Imipenem 50 µg/mL
<i>P. aeruginosa</i>	NA (ThermoFisher Scientific)	37	Imipenem 50 µg/mL
<i>E. faecalis</i>	LB	37	Imipenem 50 µg/mL
<i>B. subtilis</i>	NA	30	Chloramphenicol 25 µg/mL
<i>R. oryzae</i>	MS (mannitol 20 g/L, soya flour 20 g/L)	30	Nystatin 25 µg/mL
<i>C. albicans</i>	NA	30	Amphotericin B 0.25 µg/mL

### *Liquid bioassays*

Pathogen cultures were prepared as above and diluted to an optical density of 0.2 (0.02 for *E. faecalis*) in liquid media and 100  $\mu\text{L}$  aliquots were added to 96-well plates. An additional 98  $\mu\text{L}$  of media were also added to each well. Crude metabolite extracts were prepared at 5 mg/mL in dimethyl sulfoxide and 2  $\mu\text{L}$  aliquots were added to give a final concentration of 0.05  $\mu\text{g}/\text{mL}$ . The optical density at 600 nm was recorded before plates were incubated overnight in a shaking incubator (Infors HT Multitron Standard) and the optical density was measured again after incubation. The change in absorbance measurements was compared to the positive controls.

#### **2.14 Fast Repetition Rate Fluorometry**

Single turnover measurements were carried out using a fast repetition rate fluorometer (fRRF, Chelsea Technologies Ltd., Surrey, UK). The single turnover protocol consisted of 100 flashlets on a 2  $\mu\text{s}$  pitch followed by a relaxation period of 40 flashlets on a 50  $\mu\text{s}$  pitch. Stock cultures of each strain were used to optimise the excitation of 450, 530, and 624 nm LEDs and the voltage of the photon multiplier tube (PMT) to achieve a  $R\sigma_{\text{PSII}}$  between 0.04-0.05 and 20-70% ADC. Once optimised, 1 mL samples were quickly transferred to the fluorometer for measurement (i.e., dark adaptation was not completed).  $F/2$  in Aquil medium was used as a control and subtracted from  $F_v/F_m$  values.

### 3. Strain Selection, Optimisation of Metabolite Extraction, and Exploring the Chemical Diversity of Eukaryotic Microalgae

---

#### 3.1.1 Introduction

This chapter focuses on characterising the growth of four marine microalgal strains *Nannochloropsis oculata* CCAP 849/1, *Dunaliella primolecta* CCAP 11/34, *Phaeodactylum tricornutum* CCAP 1055/15, and *Porphyridium cruentum* UTEX 161. These strains were selected due to their biotechnological potential, which is discussed in **Chapter 1**. Cell counting, which in this case was done manually using a haemocytometer, is considered the most accurate method for measuring growth.<sup>60</sup> However, it is time consuming and susceptible to human error. For this reason, absorbance is often used as a quick and easy replacement. Due to the absorption wavelengths of carotenoids, microalgal density is typically measured at 750 nm but there is also a minimum absorption at 600 nm.<sup>176</sup> Meanwhile, specific growth rates ( $\mu$ ) offer a snapshot of the information obtained from the growth curves as well as allowing statistical analysis of growth to be performed.

To assist in characterising the growth of these species, basic physiological traits of these strains are important to note. *Phaeodactylum tricornutum* CCAP 1055/15 (**Figure 3.1 (A)**) is a pennate diatom isolated from Blackpool, England, UK. Although it has silicified frustules, it does not require silicon for growth and this strain has been grown in Guillard's f/2 medium<sup>177</sup> without sodium silicate supplementation. *P. tricornutum* is the only species in this genus that has been discovered and is described as polymorphic, with three main morphologies: fusiform, triradiate, and oval.<sup>55</sup> *Nannochloropsis oculata* CCAP 849/1 is an Ochrophyte and the holotype of the genus which comprises six strains.<sup>178</sup> It was isolated at Skate Point, Isle of Cumbrae, Scotland and is described as a unicellular small green alga with a spherical shape (**Figure 3.1 (B)**). *Dunaliella primolecta* CCAP 11/34 is unicellular biflagellate Chlorophyte (7-12  $\mu\text{m}$  in length) isolated off the coast of Plymouth, England, UK (**Figure 3.1 (C)**).<sup>179</sup> They are exceptionally halotolerant and lack rigidity in their cell wall.<sup>180</sup> *Porphyridium cruentum* UTEX 161 is a spherical Rhodophyte (5-8  $\mu\text{m}$  long) isolated from Basel,

Switzerland (**Figure 3.1 (D)**) that lacks a true cell wall but is surrounded by a mucosal layer which can cause cell aggregation and biofilm formation.<sup>181</sup>

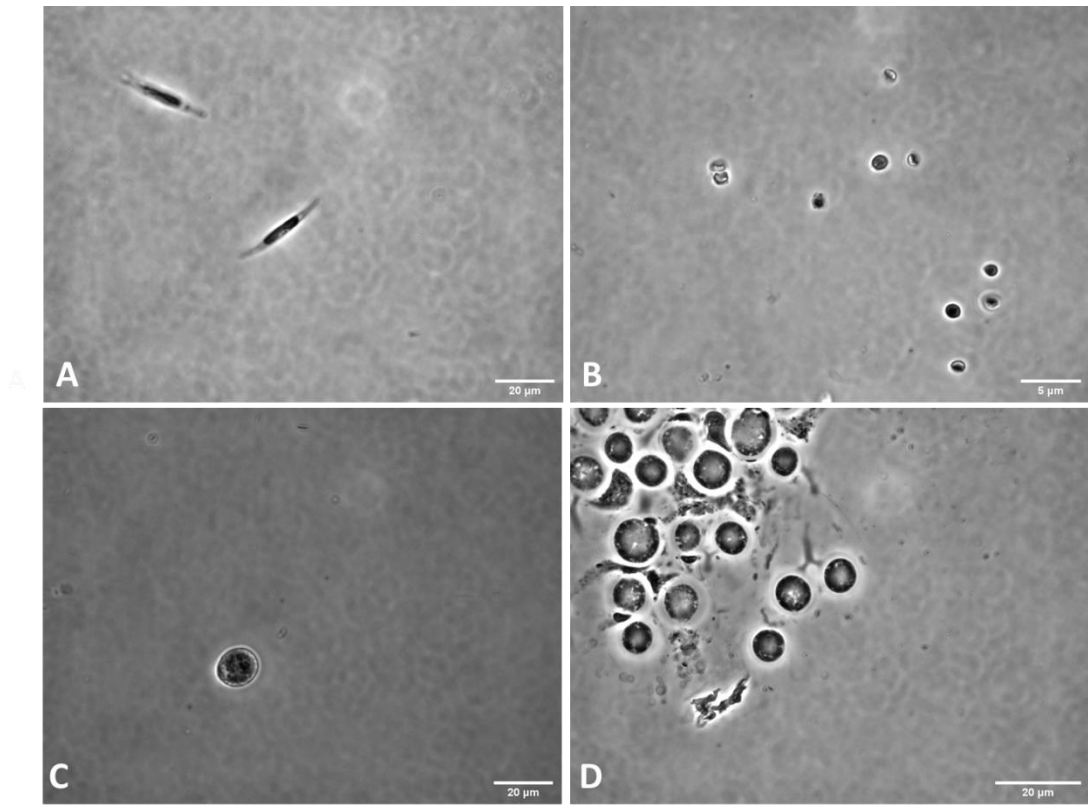


**Figure 3.1** Phase-contrast microscopy images of (A) *Phaeodactylum tricornutum*, (B) *Nannochloropsis oculata*, (C) *Dunaliella primolecta*, and (D) *Porphyridium cruentum* taken on a Nikon Eclipse TE2000-S inverted microscope.

A number of microalgal strains (including *N. oculata*) have been shown to be a promising source of biofuels capable of producing up to 58,700 L/hac oil which can be converted into 121,104 L/hac biodiesel.<sup>182</sup> Unfortunately, there is a high production cost associated with microalgal biofuels which is currently not able to compete economically with fossil fuels or first-generation biofuels that use food crops. The extraction of microalgal lipids, and also carotenoids, requires the use of polar solvents such as acetone, methanol, and water, or chlorinated and/or ethereal solvents which can be toxic.<sup>183, 184</sup> Although these metabolites have exceptional biotechnological potential, they are often not considered as promising drug leads as they do not abide by Lipinski's Rule of 5 for orally active drugs.<sup>185</sup> Lipinski's rules are chemical properties of a drug that make them more likely to be orally active. Essentially this means that whilst these metabolites are used with great benefit in the nutraceutical and food industries as supplements and food additives, they are of little interest to the pharmaceutical industry due to their poor physiochemical properties.<sup>186</sup> In order to uncover the potential of microalgal metabolites as pharmaceuticals, an untargeted approach to investigating the chemistry they produce must be undertaken.

Multivariate statistical tools, such as MetaboAnalyst<sup>187</sup>, uses either MS1 or MS2 data to compare repeatability between replicates and evaluate the differences in chemical profiles from a range of sample "groups" which can be predefined (supervised) or algorithmically generated (unsupervised). Both Principal Component Analysis (PCA, unsupervised) and Partial Least Squares – Discriminant Analysis (PLS-DA, supervised) are regression models that predict the variability of Y values (metabolites) based on known information of the X variables (samples). As PLS-DA is a supervised method, it requires binning samples into groups (e.g., taxa, condition) and thus acts as a classification tool as well as a regression model. Paliwal *et al.*, used PCA and hierarchical clustering to distinguish Chlorophytes from Cyanophytes based on their carotenoid profiles. Based on this analysis, they concluded that lutein and violaxanthin could be used as biomarkers to distinguish Chlorophytes from their cyanobacterial counterparts.<sup>188</sup> Additional tools, such as those hosted on the Global Natural Products Social (GNPS)<sup>153</sup> molecular networking platform, can be used to gain insights into the structural relationships and putative identification of metabolites through dereplication. Although GNPS houses 33 libraries of characterised metabolites, drugs,

and synthetic compounds, very few small molecules from eukaryotic microalgae have been isolated and characterised and so dereplication (identifying known metabolites) attempts are often fruitless. This is where advanced tools such as Feature Based Molecular Networking (FBMN)<sup>173</sup> and MolNetEnhancer<sup>175</sup> are particularly useful. FBMN offers improved annotation (compared to the classical molecular networking approach) whilst MolNetEnhancer uses outputs from MS2LDA<sup>174</sup> to “enhance” the FBMN by providing substructural and metabolite class information. This is achieved by matching patterns from mass fragments and neutral losses commonly observed in the spectra of metabolites belonging to the same class of natural products. This information is incorporated into the FBMN to putatively classify metabolites in molecular families when dereplication/annotation attempts have been unsuccessful. For example, Remy *et al.*, screened 594 plant extracts for activity against Chikungya virus replication and used FBMN to dereplicate samples with known bioactive metabolites. They also identify a molecular family of phorbol esters that could be responsible for the antiviral activity observed.<sup>189</sup> These tools have revolutionised the metabolomics and natural product discovery fields and have numerous applications, some of which will be explored in this chapter.

### 3.1.2. Aims and Objectives

There are few studies of untargeted metabolomics studies carried out on eukaryotic microalgae, therefore an optimised extraction protocol was required to capture the diversity of metabolites produced by microalgae. This protocol was then used to gain insights into the chemical space occupied by microalgal metabolites across taxonomic boundaries with the hypothesis that their biological diversity would translate into chemical diversity. Finally, the influence of the isolation environment (freshwater/brackish and marine) was investigated.

Objective 1: To characterise physiology and growth of four microalgal strains *Dunaliella primolecta* CCAP 11/34, *Nannochloropsis oculata* CCAP 849/1, *Phaeodactylum tricornutum* CCAP 1055/15, and *Porphyridium cruentum* UTEX 161.

- Compare growth curves generated using cell counts and absorbance methods.
- Determine the relationship between the two methods.
- Evaluate specific growth rates for both methods.

Objective 2: To determine the most efficient extraction process in terms of extract mass, repeatability, and diversity of metabolites.

- Examine repeatability amongst replicates using the multivariate statistical tool MetaboAnalyst for different extraction solvent systems.
- Evaluate chemical diversity of metabolites extracted using GNPS advanced tools FBMN and MolNetEnhancer.

Objective 3: To explore the chemical diversity of microalgae across taxonomic boundaries and environments.

- Investigate presence of a shared metabolome across various phyla.
- Gain insight into the diversity of metabolites produced by different taxa.
- Examine whether there is a connection between isolation habitat and number of metabolites produced.

## 3.2 Results

### 3.2.1. Characterising Growth of Four Marine Microalgal Strains

Four strains were grown in triplicate in f/2 medium as static cultures and their growth was evaluated using optical density at 600 nm and manual cell counting. Calibration curves were produced based on dilutions of stock cultures (culture: medium: 10:0, 9:1, 8:2, etc.) to determine the relationship between absorbance and cell concentration.

The growth curves for all four strains followed a sigmoidal trend with a lag phase lasting 1-8 days and a phase of linear growth lasting 14-20 days. *Porphyridium cruentum* had the longest lag phase, with increased growth observed after 11 days of culturing. Although the growth curves had a similar shape and progression for both cell counts and optical density, the standard deviation (represented as error bars in **Figure 3.2-3.5**) amongst replicates was more consistent for optical density measurements and therefore offered a more precise method for measuring growth. Large standard deviation amongst replicates at higher densities was evident for all strains for the cell count method but not for the optical density method. Large standard deviations can be seen for *Phaeodactylum tricornutum* ( $1.37 \times 10^5$  for day 18 and  $1.75 \times 10^5$  for day 22, **Figure 3.4, Appendix Table A1**). This is due to the sexual reproduction of *P. tricornutum* through conjugation which requires cells to align



lengthwise making them difficult to distinguish under the microscope. Large standard deviations were also noticed for *Porphyridium cruentum* ( $3.46 \times 10^5$  cells/mL on day 22, **Figure 3.5, Appendix Table A1**), especially as the culture became denser and this is likely due to the accumulation of exopolysaccharides in the medium which causes aggregation of cells and biofilm formation on the surface of flasks. From day 15 onwards, there were consistently two measurements that agreed well with one another and a third that was notably different. However, this was spread across all three replicates (i.e., the sample giving the outlying value did not always come from the same flask). Resampling was performed on the outlying culture, but this did not result in measurements that agreed with the others from that same day. Since aggregates of cells were visible in the sample aliquots, this also caused higher standard deviations in optical density values. It should also be noted that the lower limit for achieving accurate cell counts with a haemocytometer is approximately  $2.5 \times 10^5$  cells/mL (Bio-Rad specifications sheet) and these cultures had a maximum cell concentration of  $5.97 \times 10^5$  cells/mL.

As mentioned, a single aliquot was used for both cell counts and optical density readings which accounts for some other deviations in the growth curves. This is particularly notable in the growth curves of *Dunaliella primolecta* on day 18 where both cell counts and optical density values were lower than expected (**Figure 3.2**). Similarly, a “dip” in the growth of *Nannochloropsis oculata* was observed on Day 15. However, this was only noticeable for the cell counts method and not the optical density (**Figure 3.3**). Due to the small size of *N. oculata* cells (2-5  $\mu\text{m}$ ), this discrepancy may be due to human error in either diluting the sample or counting the cells under the microscope.

The calibration curves for each strain showed a strong linear relationship between cell counts and optical density values. The co-efficient of determination ( $R^2$ ) which measures how well the linear regression fits the data was 0.8817 for *D. primolecta*, 0.969 for *N. oculata*, 0.975 for *P. tricornutum*, and 0.946 for *P. cruentum* (**Figure 3.2-3.5 (C)**). These calibration curves were produced using stock cultures rather than the cultures used for producing growth curves, but the data was well corroborated between the two. The standard deviations for *P. cruentum* are much smaller than for the growth curve measurements (**Figure 3.5**). The stock culture, from which the growth curve

cultures were inoculated, did not form a biofilm at the bottom of the flask whilst the growth curve cultures did form biofilms and observably larger aggregations of cells. The reason for this is unknown as all cultures were maintained under the same conditions. One possibility is that the stock culture was generated at an earlier date (i.e., “older”) and therefore biofilms may have broken down over time which allowed cells to resuspend in the medium and continue to proliferate to a higher density. This is supported by the fact that the cultures used for measuring growth reached a maximum density of  $5.97 \times 10^5$  cells/mL whilst the stock cultures had a maximum density of  $1.52 \times 10^6$  cells/mL.

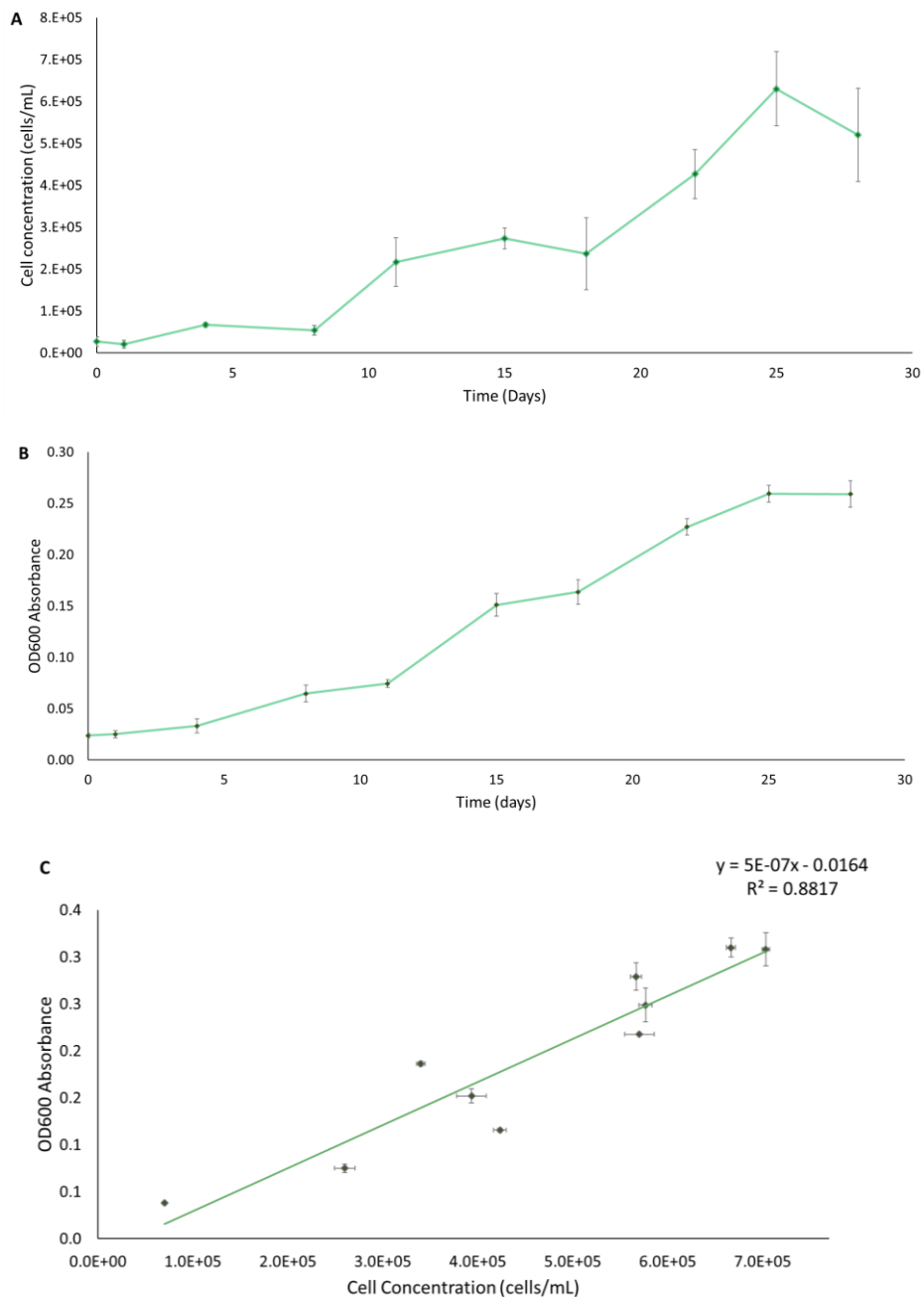


**Figure 3.2** Growth curve of *Dunaliella primolecta* CCAP 11/34 with time (days) on the x-axis and (A) cell concentration (cells/mL), (B) optical density at 600 nm on the y-axis, and (C) calibration curve of cell concentration (x-axis) and optical density at 600 nm (y-axis). Data points represent the average value of three replicates. Error bars represent the standard deviation of (A) cell concentration (cells/mL), (B) optical density at 600 nm, and (C) optical density at 600 nm (vertical) and cell concentration (horizontal) between replicates.

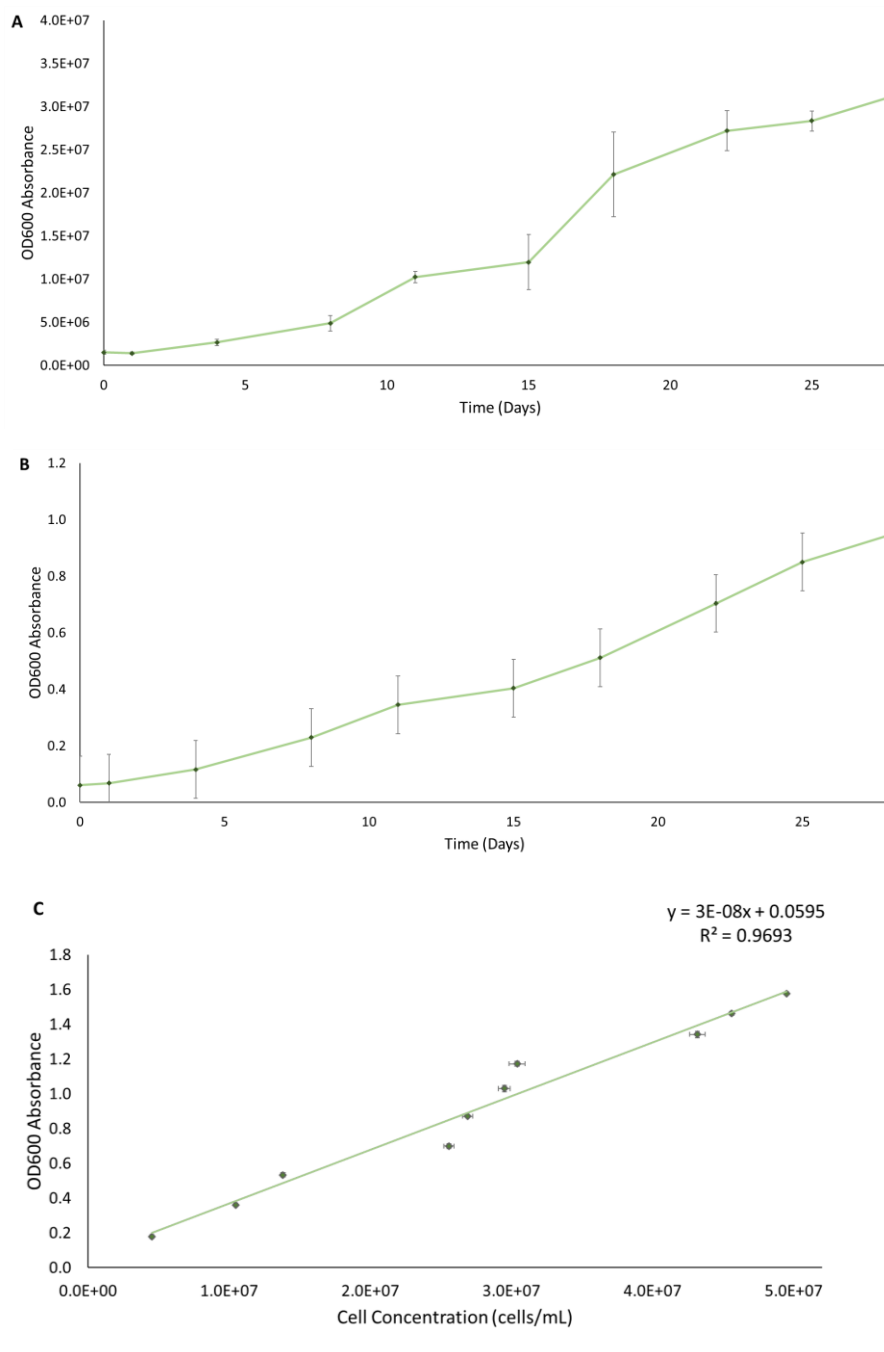


**Figure 3.3** Growth curve of *Nannochloropsis oculata* CCAP 849/1 with time (days) on the x-axis and (A) cell concentration (cells/mL), (B) optical density at 600 nm on the y-axis, and (C) calibration curve of cell concentration (x-axis) and optical density at 600 nm (y-axis). Data points represent the average value of three replicates. Error bars represent the standard deviation of (A) cell concentration (cells/mL), (B) optical density at 600 nm, and (C) optical density at 600 nm (vertical) and cell concentration (horizontal) between replicates.

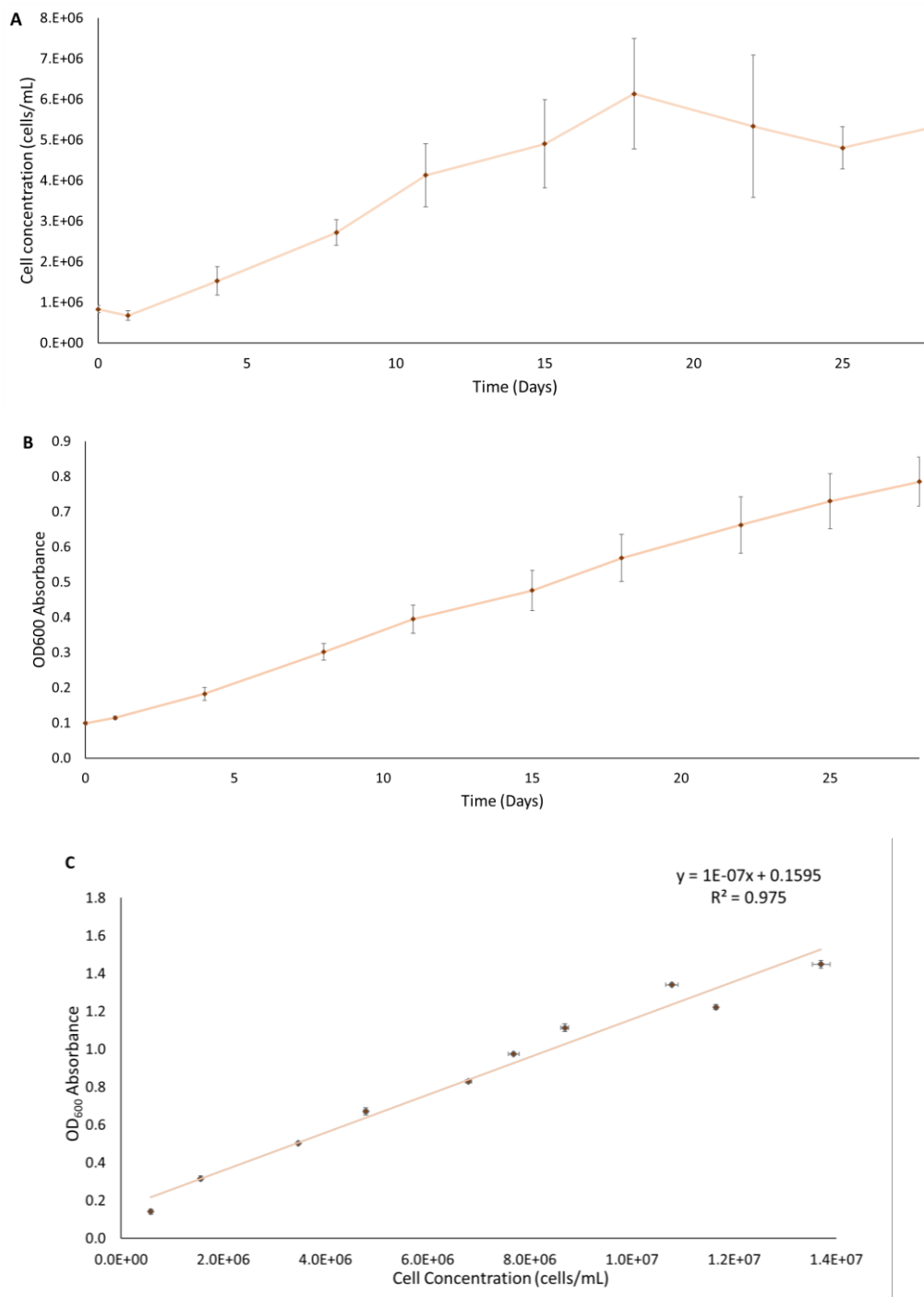


**Figure 3.4** Growth curve of *Phaeodactylum tricornutum* CCAP 1055/15 with time (days) on the x-axis and (A) cell concentration (cells/mL), (B) optical density at 600 nm on the y-axis, and (C) calibration curve of cell concentration (x-axis) and optical density at 600 nm (y-axis). Data points represent the average value of three replicates. Error bars represent the standard deviation of (A) cell concentration

(cells/mL), (B) optical density at 600 nm, and (C) absorbance at 600 nm (vertical) and cell concentration (horizontal) between replicates.

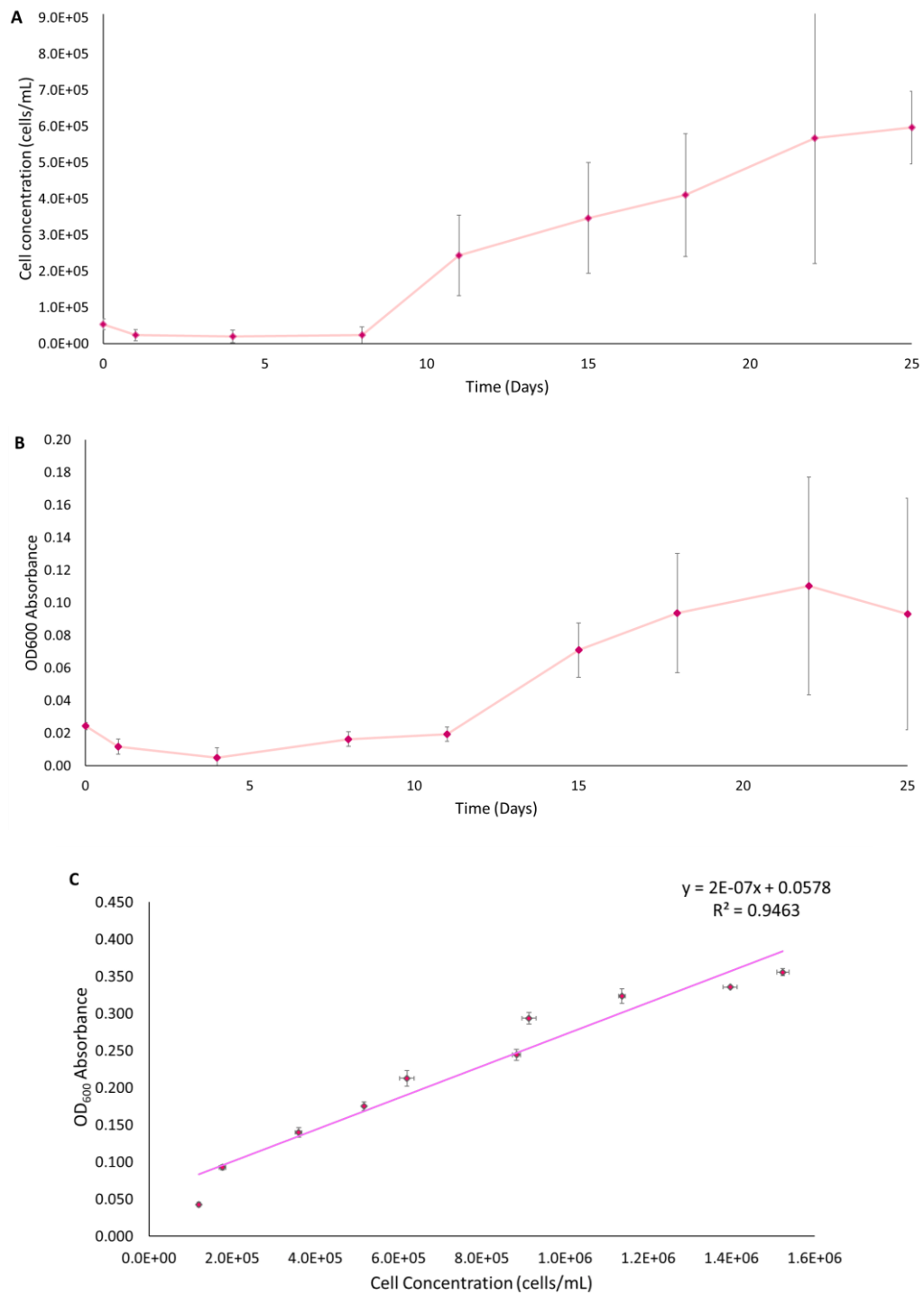


**Figure 3.5** Growth curve of *Porphyridium cruentum* UTEX 161 with time (days) on the x-axis and (A) cell concentration (cells/mL), (B) optical density at 600 nm on the y-axis, and (C) calibration curve of cell concentration (x-axis) and optical density at

600 nm (y-axis). Data points represent the average value of three replicates. Error bars represent the standard deviation of (A) cell concentration (cells/mL), (B) optical density at 600 nm, and (C) optical density at 600 nm (vertical) and cell concentration (horizontal) between replicates.

The specific growth rate ( $\mu$ , day<sup>-1</sup>) was calculated for each strain based on the natural log (ln) of the linear portion of the growth curves (**Figure 3.6**). This analysis was included as it gives a snapshot of the growth curves and is a more easily digestible way to compare the growth of different species or conditions which will be seen in **chapter 4** and **5**. It also allows the growth of cultures to be compared statistically using a t-test. All four strains have a similar mean value (0.066-0.118 for cell concentration and 0.074-0.089 for optical density), (**Figure 3.6, Appendix Table A2**). In all cases except *P. cruentum*, the specific growth rate was significantly greater for cell concentration than optical density at 600 nm. The *p*-value for each were *D. primolecta* 0.01, *N. oculata* 0.01, and *P. tricornutum* 0.005. The data points for *P. cruentum* are skewed due to the triplicate specific growth rate values of 0.130, 0.125, and 0.014 for optical density at 600 nm (**Appendix Table A2**). This is evident in the spread of the data as the optical density median is 0.125 but the mean is 0.09. For all other strains, the mean and median were quite similar, and the range of values was smaller for optical density compared to cell concentration.

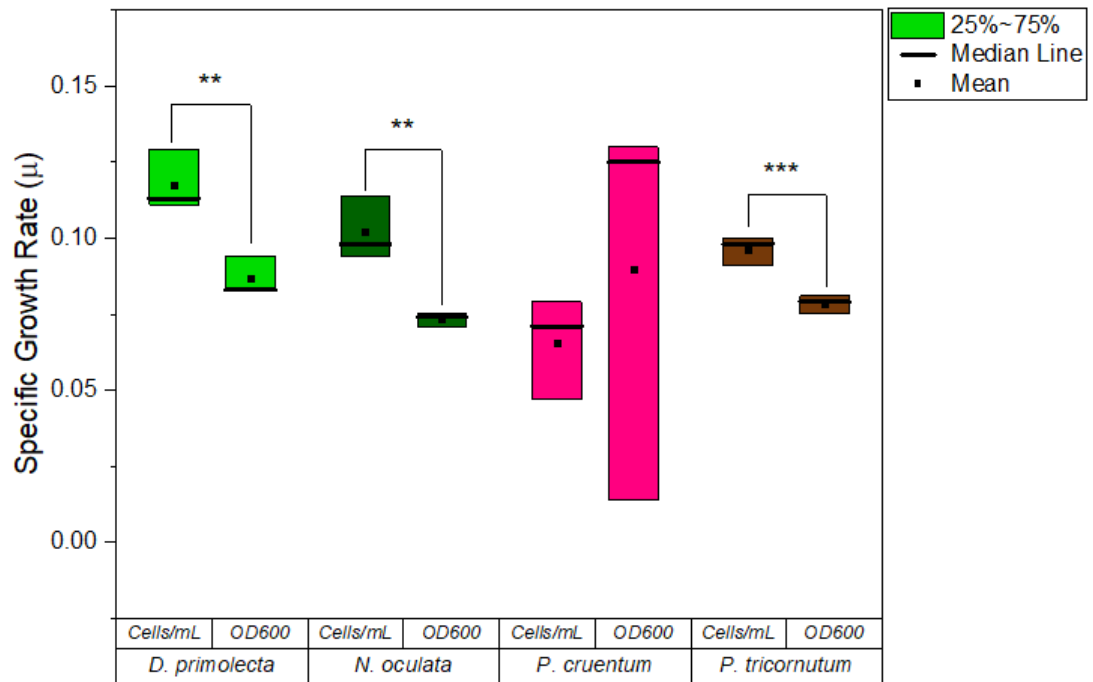


**Figure 3.6** Boxplots showing the specific growth rates of triplicate cultures of *Dunaliella primolecta* (light green), *Nannochloropsis oculata* (dark green), *Phaeodactylum tricorutum* (brown) and *Porphyridium cruentum* (pink). Coloured box shows 25-75 percentile, the black line represents the median value, and the black square represents the mean. *P*-values are represented as \* ( $\leq 0.05$ ), \*\* ( $\leq 0.01$ ), or \*\*\* ( $\leq 0.001$ ).



### 3.2.2. Optimising Extraction Methods to Maximise Chemical Diversity

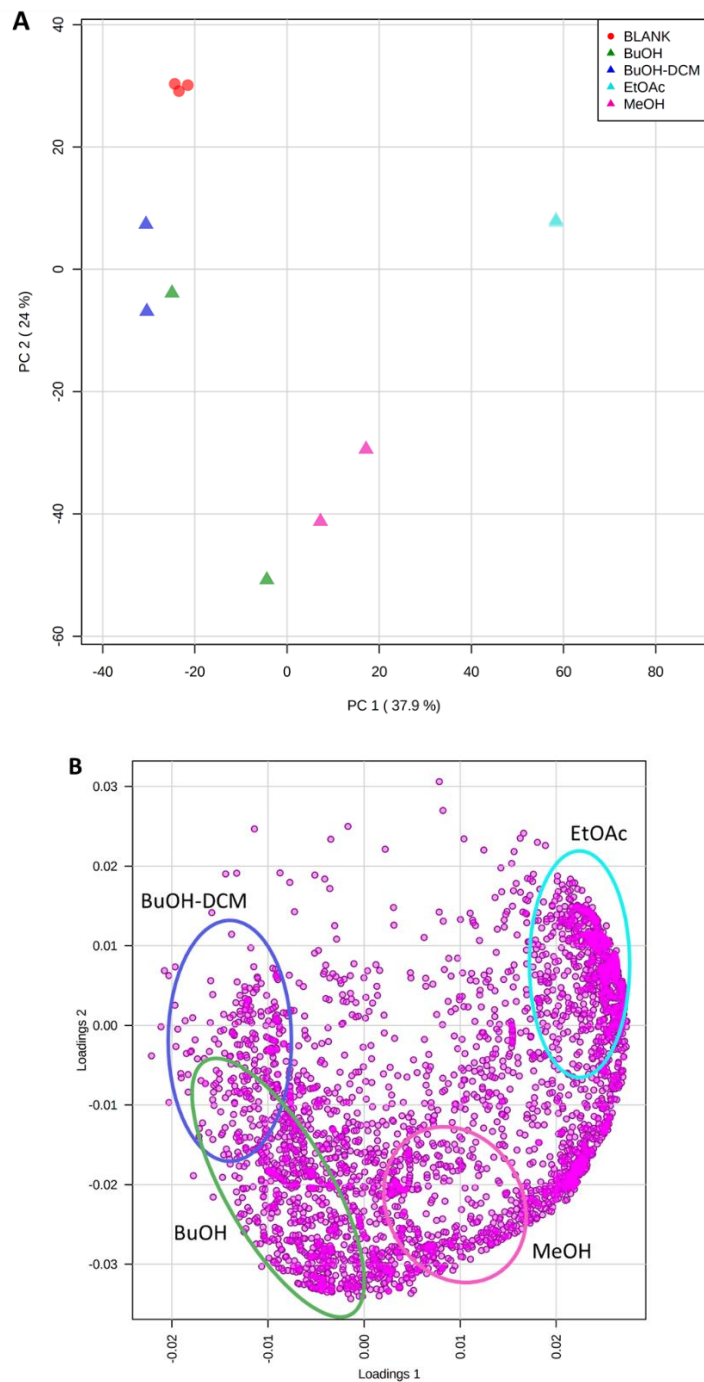
The key factors considered in optimising extraction methods for this thesis were extract mass, repeatability, and diversity of metabolites. Initially, liquid cultures were extracted by adding organic solvent and shaking overnight. However, the extract mass from a 100 mL static culture was <2 mg which was not sufficient for performing LC-MS analysis and bioactivity screening of extracts. The small extract mass was likely a result of not breaking cells before extraction and the immiscibility of the culture and solvent layer, leading to inefficient extraction. For this reason, HP-20 diaionic resin was added to cultures once they reached stationary phase to attract small organic molecules that had been excreted into the culture medium. Resin and cell pellets were then freeze dried to break cell walls and release intracellular metabolites before being extracted overnight with organic solvents. This extraction method led to extracts with masses ranging from 10-100 mg (depending on the solvent) which was sufficient for analysis.

Small organic metabolites were targeted by testing four solvents of medium polarity: ethyl acetate, 1:1 butanol:dichloromethane, butanol, and methanol. Dielectric constants (also known as relative permeability) are a relative measure of chemical polarity with ethyl acetate having the lowest value 8.7 and methanol with the highest 32.6 (**Table 3. 1**). A synthetic seawater was used to culture the microalgal strains and it was important to use solvents that would not readily dissolve these salts as it would then require partitioning of a small extract to remove the salts which otherwise could damage LC-MS columns or influence bioassay results since many of the pathogens used were not halotolerant.

**Table 3. 1** The names, abbreviations, and dielectric constants of solvents used to optimise extraction of microalgal metabolites. \*Dielectric constants measured at 20 °C unless otherwise stated. Calc = average of dielectric constants of both solvents.

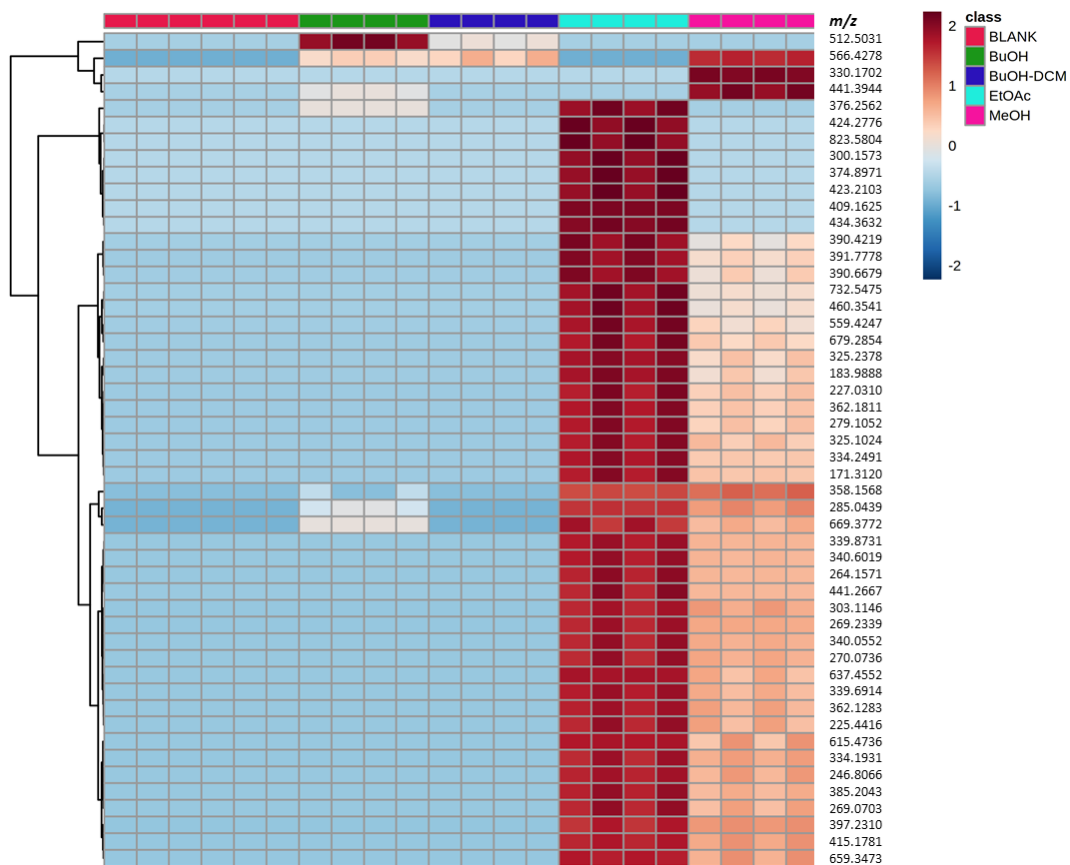
Name	Abbreviation	Dielectric constant*, $\kappa$
Ethyl acetate	EtOAc	8.7
1:1 2-butanol:dichloromethane	BuOH:DCM	13.1 (calc)
2-butanol	BuOH	17.26
Methanol	MeOH	32.6 (25 °C)

To evaluate the repeatability amongst replicates, the extracts generated from the four solvents were compared using Principal Component Analysis (PCA). This is an unsupervised analysis where the algorithm determines the groupings and so will show how the samples cluster solely based on Y variables (metabolites). The PCA scores plot (**Figure 3.7**) shows that all four solvents generated metabolite profiles distinct from that of the media controls. Only the two ethyl acetate replicates showed repeatability as the nodes representing these samples overlapped when viewing the variation according to principal components 1 (PC1, 37.9%) and 2 (PC2, 24%) which accounted for the greatest variance across all samples. Butanol:dichloromethane and methanol also showed good repeatability, however the replicates from butanol showed a large variation along PC2. Whilst the score plot gives an overall score of each sample (extract), the loadings plot shows each variable (metabolite). It typically ranges from -1 to 1, with variables at the outer edges driving variation along that component or axis. Those clustered around the centre point have either a weak influence or no influence at all on the variation between samples. Each variable from the loadings and each sample from the score plot comprises a vector and so the position of these data points correlate to one another (i.e., the position of variables on the loadings plot correspond to the position of samples in the scores plot). In this case, the loadings plot (**Figure 3.7 (B)**) shows that there is not much variation between the different extraction solvents as the scale only ranges from -0.02 to 0.02. There is a density of metabolites along the 0.02 x-axis range which indicates the metabolites driving the differences are between ethyl acetate, the least polar solvent, and the other solvents. Similarly, the density of metabolites on the -0.02 x-axis range shows the variation is driven by metabolites from butanol and butanol:dichloromethane.



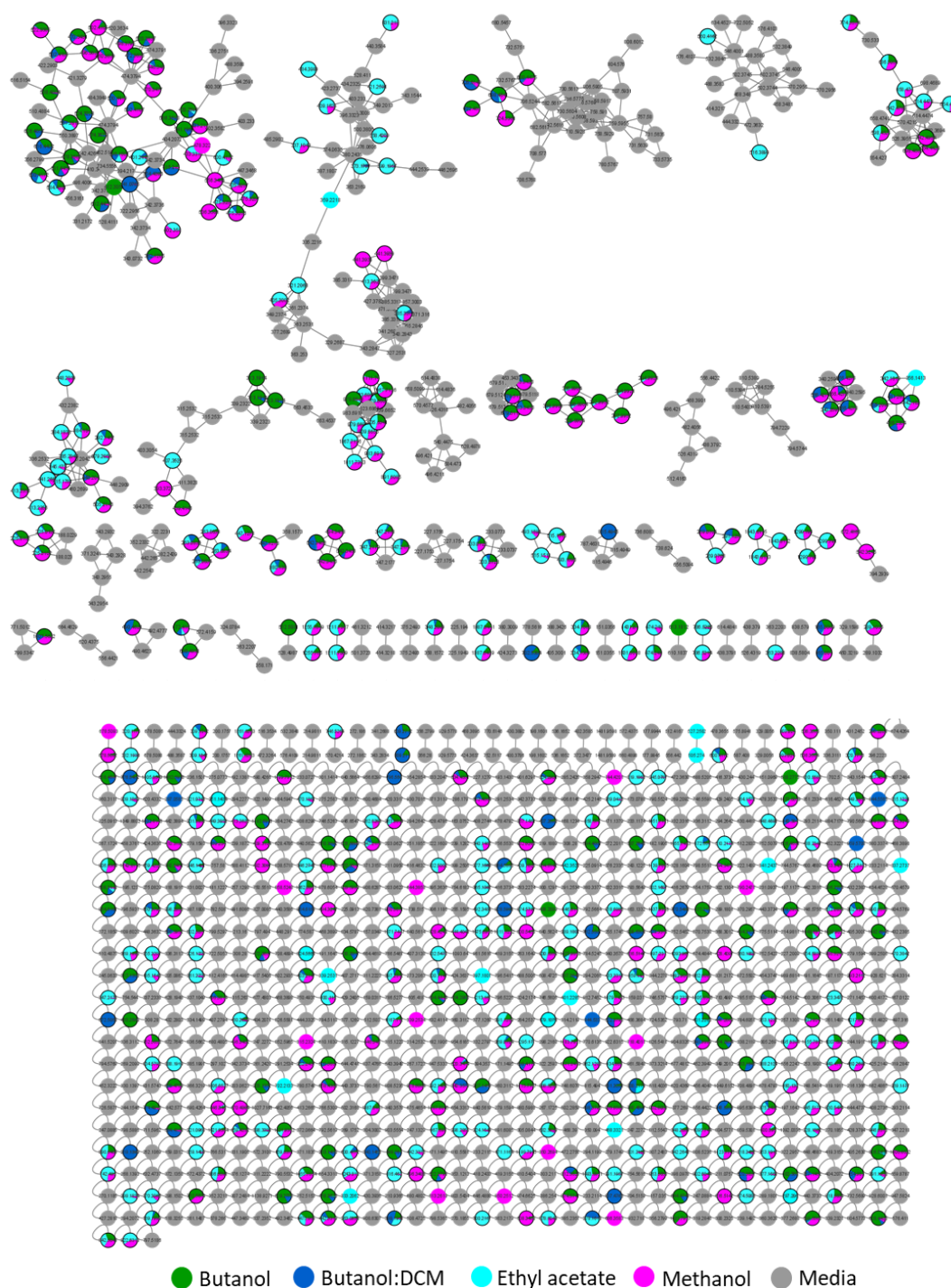
**Figure 3.7** Principal component analysis of *Chlorella sorokiniana* cultures extracted with butanol (BuOH, green), 1:1 butanol: dichloromethane (BuOH-DCM, dark blue), ethyl acetate (EtOAc, light blue), and methanol (MeOH, pink). **(A)** Scores plot with PC1 (37.9%) on the x-axis and PC2 (24%) on the y-axis. Solvent and f/2 media controls represented by red circles. **(B)** Loadings plot showing the distribution of metabolites across samples.

A closer look at the distribution of metabolites across all four solvent conditions can be seen in the heatmap of top 50 features driving the differences between samples. Heatmaps look at each variable (metabolite) and shows the relative intensity of that metabolite across each sample. Red indicates higher intensity whilst blue represents lower intensity. In qualitative LC-MS, intensity is related to the abundance of the metabolite but without the use of standards, this is a measure of relative intensity or abundance and is not quantitative. The dendrogram illustrates the output of hierarchical clustering with similarities or groupings being determined by Euclidean distances. Except for the features 512.5031 *m/z*, 566.4278 *m/z*, 330.1702 *m/z*, 441.3944 *m/z* which forms a cluster in the dendrogram, all features in the top 50 were detected at a high relative intensity in the ethyl acetate extracts. Methanol was also efficient at extracting these metabolites but at much lower relative intensities and did not extract any metabolites belonging to the second cluster on the dendrogram, which had a mass range of 300.1573-823.5804 *m/z*. The extended heatmap of all features detected (**Appendix Fig A1**) shows that extracts from methanol, ethyl acetate, and butanol solvent systems have distinct chemical profiles. It also illustrates the variability amongst replicates for the butanol and butanol:dichloromethane as seen in the PCA scores plot (**Figure 3.7**).



**Figure 3.8** Heatmap illustrating the top 50 features driving differences between the extracts produced using different solvent; butanol (BuOH, green), 1:1 butanol: dichloromethane (BuOH-DCM, dark blue), ethyl acetate (EtOAc, light blue), and methanol (MeOH, pink). The dendrogram shows the output of hierarchical clustering based on Euclidean distances. Relative intensity is represented by red (high) and blue (low) colouring across a scale ranging from -2 to 2.

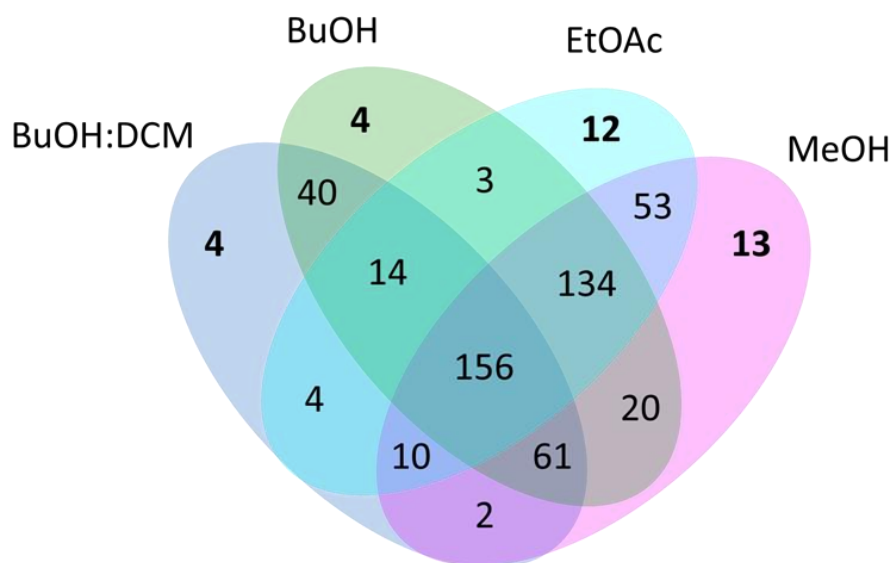
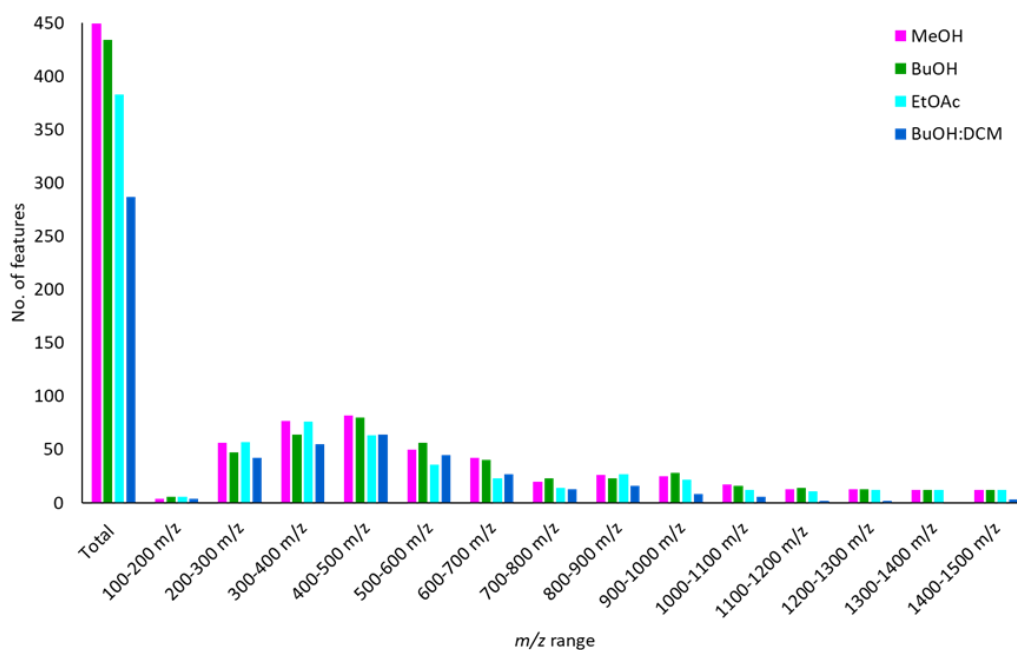
Finally, to understand the chemical diversity of metabolites being extracted according to structure and class of natural products, FBMN and MolNetEnhancer, both in the GNPS ecosystem, were used. Whilst multivariate statistical analysis uses MS1 data to illustrate the variation between samples, molecular networking uses MS2 data which gives more structural information on the metabolites being extracted and the relationship between these metabolites by clustering them into molecular families. MS2 data essentially acts like a fingerprint for a metabolite which holds structural information based on the pattern of fragmentation created when the metabolite is ionised. Metabolites with similar fragmentation patterns means they have similar structural characteristics and therefore will be clustered together into molecular families.<sup>153</sup> A total of 1290 features were detected in this network, with 760 of those present in media controls (grey nodes) and 530 (41%) resulting from the extraction of metabolites from *Chlorella sorokiniana* cultures (**Figure 3.9**). *F/2* is a minimal medium, however a high percentage of features were found in the media controls. From the 530 features detected from *C. sorokiniana*, 156 (29%) were found in all four solvent conditions which is interesting considering the polarity (dielectric constants) of these solvents ranged from 8.7-32.6. Each pie chart within the molecular network (**Figure 3.9**) illustrates the relative intensity of that specific metabolite extracted using each of the solvents. From the MolNetEnhancer natural product class analysis, only one molecular family that comprised 54 nodes were annotated as fatty acid esters (**Appendix Fig A2**).



**Figure 3.9** Feature Based Molecular Network of a *Chlorella sorokiniana* culture extracted using butanol (green), 1:1 butanol:dichloromethane (dark blue), ethyl acetate (light blue), and methanol (pink). Features from f/2 medium and solvent blanks are depicted in grey. Solid colour represents that the feature was only detected in that condition, pie charts represent the relative intensity of that feature in all conditions that it was present.



Taking a closer look at the distribution of features amongst samples revealed that methanol extracted the highest number of metabolites overall (449, 84.7%), followed by butanol (432, 81.5%), ethyl acetate (386, 72.8%), and 1:1 butanol:dichloromethane (291, 54.9%) (**Figure 3.10 (A)**). Butanol:dichloromethane was eliminated as a potential solvent of choice due to the small number of metabolites it extracted and the fact that 98.6% of those metabolites were also extracted using one of the other solvents. Although butanol samples contained the second highest number of metabolites, these mostly overlapped with those extracted using methanol (371, 86%). Considering the relative cost of these two solvents, and that methanol extracted more distinct metabolites (i.e., metabolites not extracted by other solvents), butanol was also eliminated as the solvent of choice. Ethyl acetate was just as efficient at extracting polar metabolites as the alcohol-containing solvent systems with 374/386 (96.9%) of metabolites extracted by ethyl acetate and one of the other solvents. This is a testament to ethyl acetate as an extraction solvent as although it is efficient at extracting small organic metabolites, the polar acetate head group also allows extraction of more polar metabolites. This is also evident in the rank abundance curves (**Figure 3.10 (B)**) which shows the distribution of metabolites extracted from each solvent according to their  $m/z$  values. Over 50 features were detected in the 200-300, 300-400, 400-500, and 500-600  $m/z$  bins which represented the highest density of metabolites extracted. There is an even trend across each bin up until 900  $m/z$  when the number of metabolites extracted using butanol:dichloromethane began to taper off, which correlates with the low overall number of metabolites extracted using this solvent. Ethyl acetate and methanol (the two remaining “horses in the race”) had a similar trend across the rank abundance curves, a similar number of distinct metabolites (12 and 13, respectively), and both solvents extracted 66.6% (353/530) of metabolites detected. However, when considering other factors such as cost, vapour pressure (how easy to evaporate), and toxicity, it was decided that ethyl acetate would be chosen as the solvent of choice. It has a high vapour pressure of 70 mmHg at 20 °C (compared to 13.02 mmHg for methanol) which means it can be easily evaporated using nitrogen or through rotary evaporation.

**A****B**

**Figure 3.10** (A) Venn diagram illustrating the overlap of features detected from each solvent extraction condition and (B) rank abundance curves illustrating the distribution of features according to their  $m/z$  values. Butanol (BuOH, green), 1:1 butanol:dichloromethane (BuOH:DCM, dark blue), ethyl acetate (EtOAc, light blue), methanol (MeOH, pink).

### 3.2.3. Exploring the Chemical Diversity of Eukaryotic Microalgae

There are few studies of untargeted metabolomics analysis of eukaryotic microalgae and these investigations are critical for understanding the potential of these organisms in the nutraceutical, pharmaceutical, and cosmetics industries. To gain an understanding into the chemical diversity produced by these prolific organisms, 36 strains of microalgae were analysed based on their phylogeny and chemical profiles. Crude metabolite extracts from all 36 strains, and their 18S rRNA gene sequences were provided by the Scottish Association for Marine Science (Dunstaffnage, Oban, UK) as part of the SeaBiotech EU-FP7 project. Only partial gene sequences were obtained for *Dunaliella tertiolecta* strains CCAP 19/7C, CCAP 19/22, and CCAP 19/23, and so they were excluded from the phylogenetic analysis. A nearest-neighbour joining phylogenetic tree was produced, using MEGA 7 software, showing distinct clustering for Chlorophytes, Rhodophytes, and Haptophytes, whilst the Heterokonta (diatoms) and Ochrophyta had a distant ancestor in common (**Figure 3.11**).

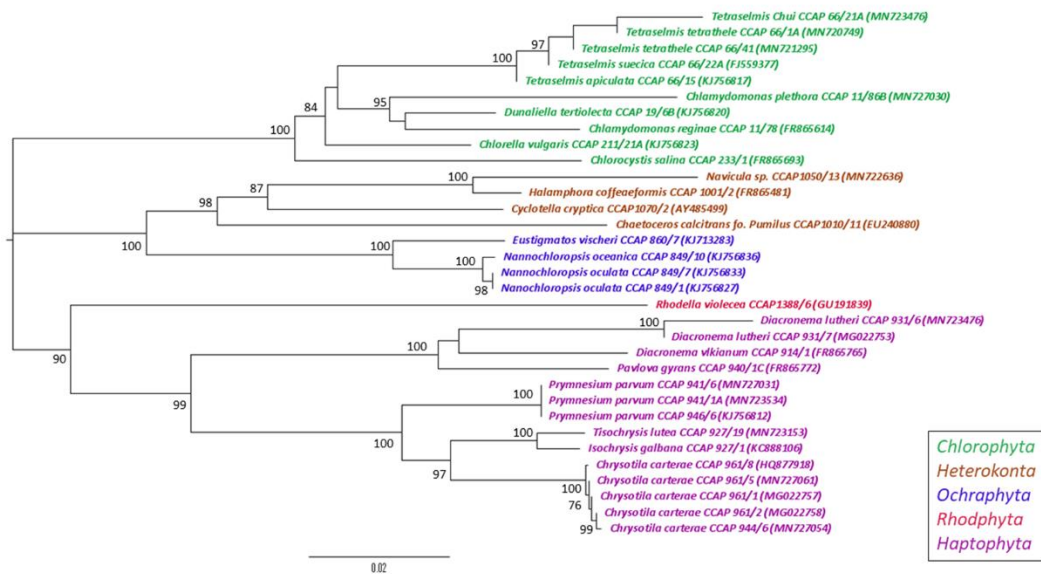


**Figure 3.11** Nearest Neighbour-Joining phylogenetic tree of 18S rRNA gene sequences. Taxa colouring represents the phyla; green, Chlorophyta; brown, Heterokonta; blue, Ochrophyta; red, Rhodophyta; purple, Haptophyta. Bootstrap values above 70% are indicated on the branches.

After establishing a phylogenetic relationship between the microalgal strains based on 18S rRNA gene sequences, 20 of these strains (seven Chlorophytes, six Haptophytes, four diatoms, two Ochrophytes, and one Rhodophyte) were chosen for metabolomic comparison. Peaklists generated from filtered positive mode mass spectral data were analysed using MetaboAnalyst after ions present in solvent and media blanks were removed from the analysis to prevent uninformative skewing of the results. A total of 879 features were detected, with each feature representing a unique combination of the  $m/z$  value and chromatogram peak characteristics (**Figure 3.12**).

Haptophytes showed the greatest variability in their chemical profiles. *Tisochrysis lutea* (CCAP 927/19, marine, Tahiti), *Isochrysis galbana* (CCAP 927/1, marine, UK), and *Pavlova gyrans* (CCAP 940/1C, marine, UK) clustered together, whilst *Diacronema lutheri* (CCAP 931/7, marine, UK) and the two *Chrysotila carterae* strains (CCAP 944/6, marine, UK; CCAP 961/5, marine, UK) had very disparate chemical profiles. Haptophytes also represented the phylum with the greatest number of metabolites, with an average of 370 features detected per strain (**Figure 3.12, Appendix Fig A3**). Conversely, Rhodophytes, represented by a single strain – *Rhodella violacea* CCAP 1388/6 – had the lowest number of detected features at 123. Strains from the diatom phylum cluster closely together and show some overlap in chemical features with the Ochrophyte *Eustigmatos vischeri* CCAP 860/7, their closest neighbour from the phylogenetic analysis. All seven strains belonging to the Chlorophyte phylum clustered closely together and shared many features in their chemical profiles. However, it must be noted that five of the seven strains included belong to the genus *Tetraselmis*. Despite Chlorophytes being well-studied for the natural products they produce, this phylum had an average of 200 detected features per strain, which was comparatively low.

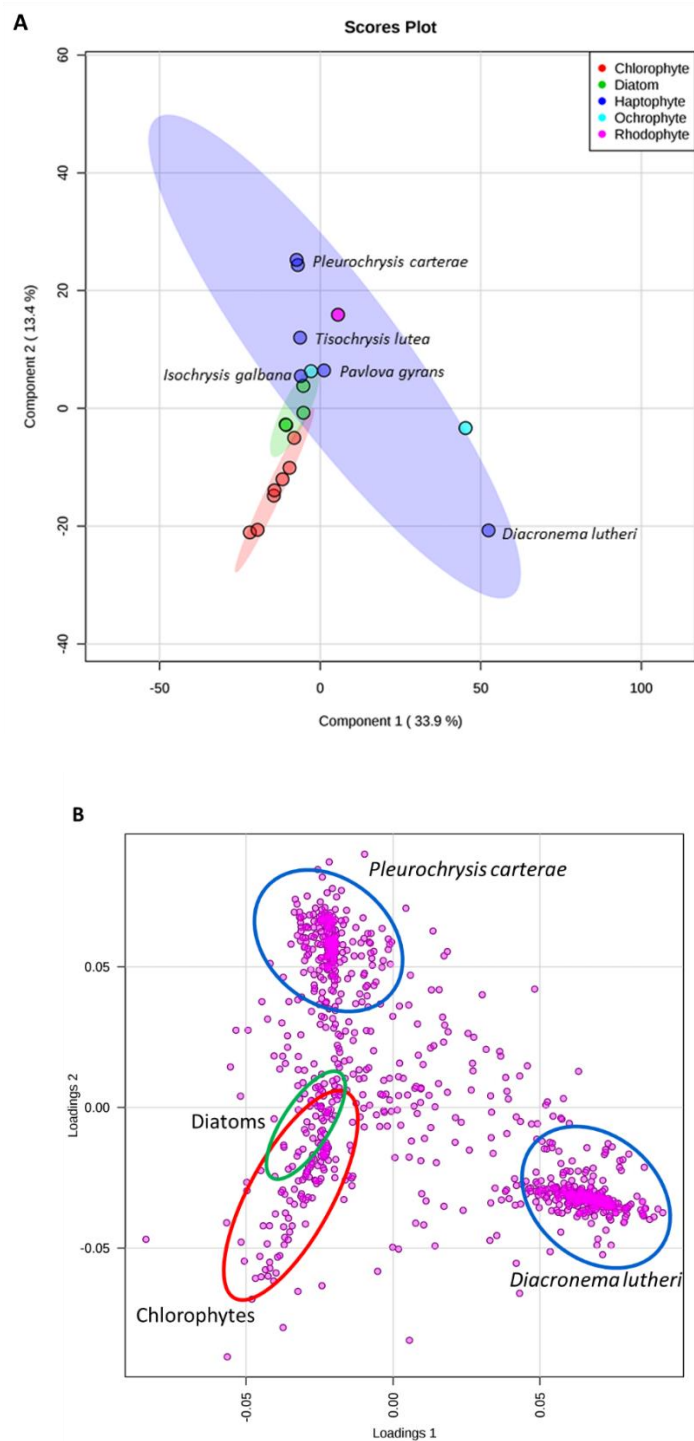


**Figure 3.12** Partial Least Squares-Discriminant Analysis (PLS-DA) scores plot for Chlorophytes (red), diatoms (green), Haptophytes (dark blue), Ochrophytes (light blue), and Rhodophytes (pink). **(A)** Scores plot with PC1 (33.9%) on the x-axis and PC2 (13.4%) on the y-axis. **(B)** Loadings plot showing the distribution of metabolites across samples.

It was observed that the chemical diversity expanded beyond taxonomic boundaries. Indeed, Haptophyte, Ochrophyte, and diatom samples did not cluster solely according to their phyla. However, the lower number of samples within the Ochrophyte (2 strains) and Rhodophyte (1 strain) clades meant that this pattern could not be confirmed. The Haptophyte clade produced the most diverse metabolites, with *Chrysothila carterae* producing a greater abundance of low molecular weight metabolites ranging from 219-678  $m/z$  compared to the other Haptophyte strains screened (**Figure 3.13**). Although they clustered together in the PCA analysis, there were no notable patterns in the hierarchical clustering (heatmap) that either grouped the five *Tetraselmis* species together, or differentiated them from the two other Chlorophyte strains, *Chlorocystis salina* CCAP 233/1 and *Chlorella vulgaris* CCAP 211/21A.

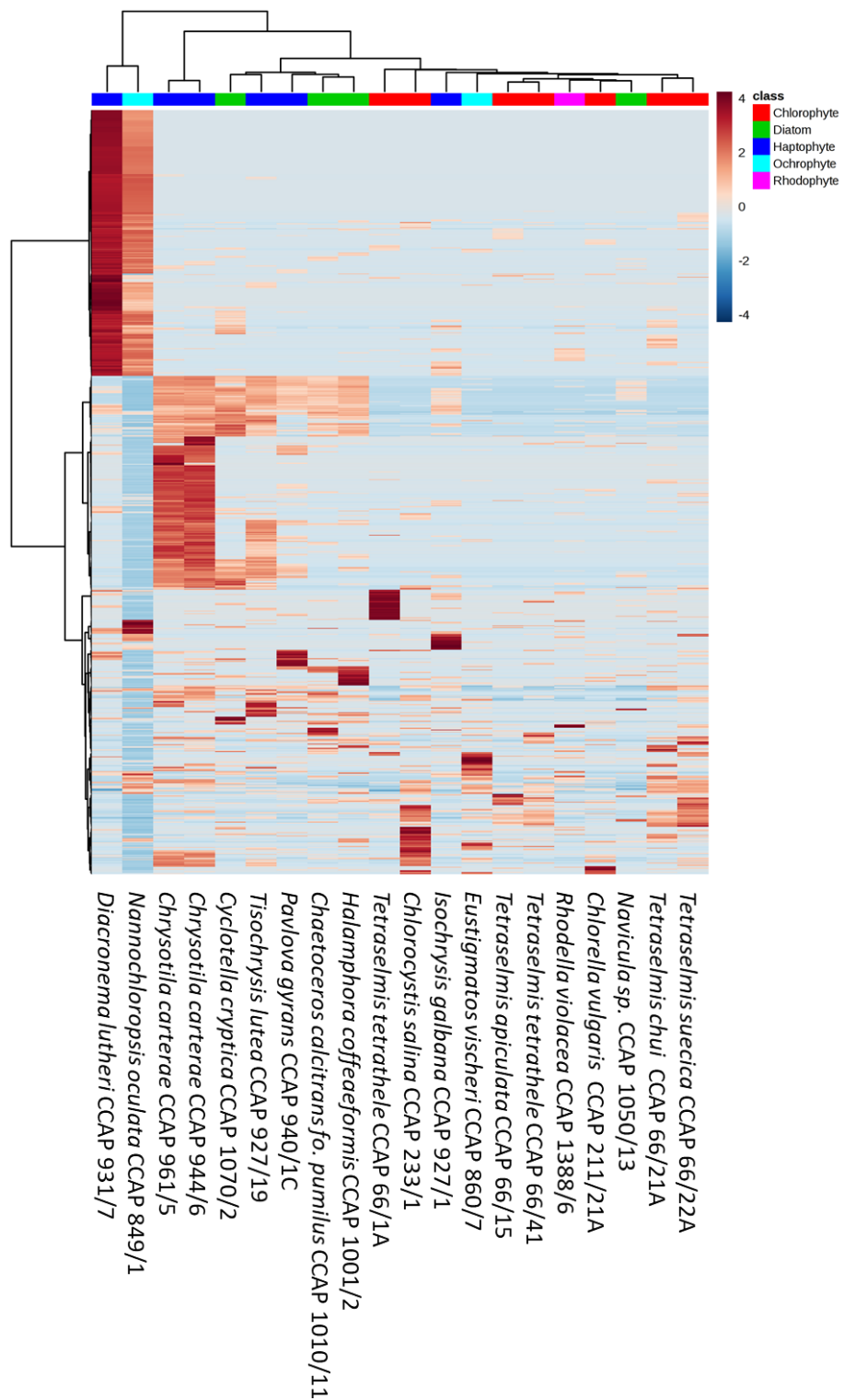


**Figure 3.13** Hierarchical clustering of all detected ions across Chlorophytes (red), diatoms (green), Haptophytes (dark blue), Ochrophytes (light blue), and Rhodophytes (pink). Heatmap shows relative abundance (low; blue, high; red) of respective features.



A second comparative metabolomics experiment was designed to understand the diversity of microalgal chemical profiles on a species/strain level, often referred to as chemotypes. A total of 16 strains belonging to the genera *Dunaliella* (4), *Chrysotila* (3), *Chlamydomonas* (2), *Diacronema* (2), *Nannochloropsis* (2), and *Prymnesium* (3) were selected as Chlorophytes are a well-studied phylum and Haptophytes represented the greatest chemical diversity in the above analysis. Interestingly, the number of features detected in each of the samples varied considerably within species. The greatest variation was seen between the three *Chrysotila carterae* strains. CCAP 961/1 and CCAP 961/2 were both isolated from the English Channel and share similar chemical profiles (**Figure 3.14**) and had a similar number of features (90 and 83, respectively, **Figure 3.15**). However, CCAP 961/8 is distinctly different along the Component 2 axis and had almost half (46) of the features detected in the other two strains. CCAP 961/8 was isolated from a brackish environment in Oban, Scotland, UK which suggests it may be a different chemotype to the other two strains, based on the environment from which they were isolated. This can also be observed for the four strains of *Dunaliella tertiolecta* analysed. CCAP 19/6B originated from an Oslofjord in Norway, CCAP 19/7C came from the river Crouch in Essex, England, and the other two strains, CCAP 19/22 and CCAP 19/23, are from unknown marine locations. The Oslofjord in particular has a comparatively thin layer of brackish water underneath which is seawater with a salinity of 32-34.<sup>190</sup> Taking this into consideration, it could be postulated that CCAP 19/6B, CCAP 19/22, and CCAP 19/23 have a similar abundance (164, 151, and 154, respectively, **Figure 3.15**) and distribution (**Figure 3.16**) of metabolites compared to the brackish strain 19/7B (129). A similar trend can be seen for the strains belonging to the *Diacronema*, *Nannochloropsis*, and *Chlamydomonas* (**Figure 3.15**). In each case, strains belonging to the same species/genus will differ in number and distribution of metabolites if they were isolated from different environments (e.g., marine, brackish). However, for *Nannochloropsis*, *Chlamydomonas*, and *Prymnesium*, the brackish strains had a higher number of metabolites compared to the marine strains. In fact, the three *Prymnesium* strains are the only ones that cluster together in the hierarchical analysis of metabolites detected from each culture (**Figure 3.16**). This data supports the argument for chemotypes based on populations of microalgae rather than phylogenetic relationships.

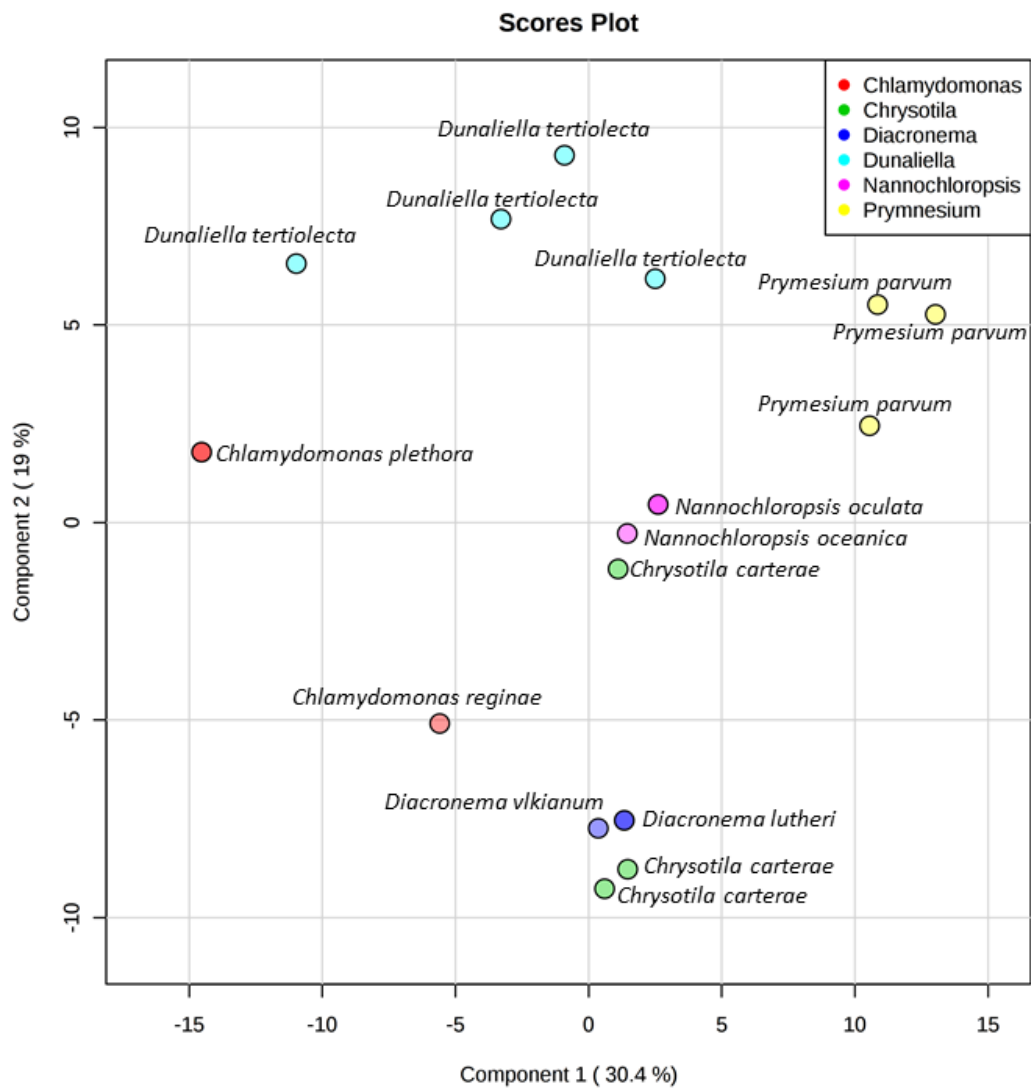


**Figure 3.14** PLS-DA scores plot for *Chlamydomonas* (red), *Chrysotila* (green), *Diacronema* (dark blue), *Dunaliella* (light blue), and *Nannochloropsis* (pink), and *Prymesium* (yellow) using component 1 (33.9%) and component 2 (13.4%) as axes.

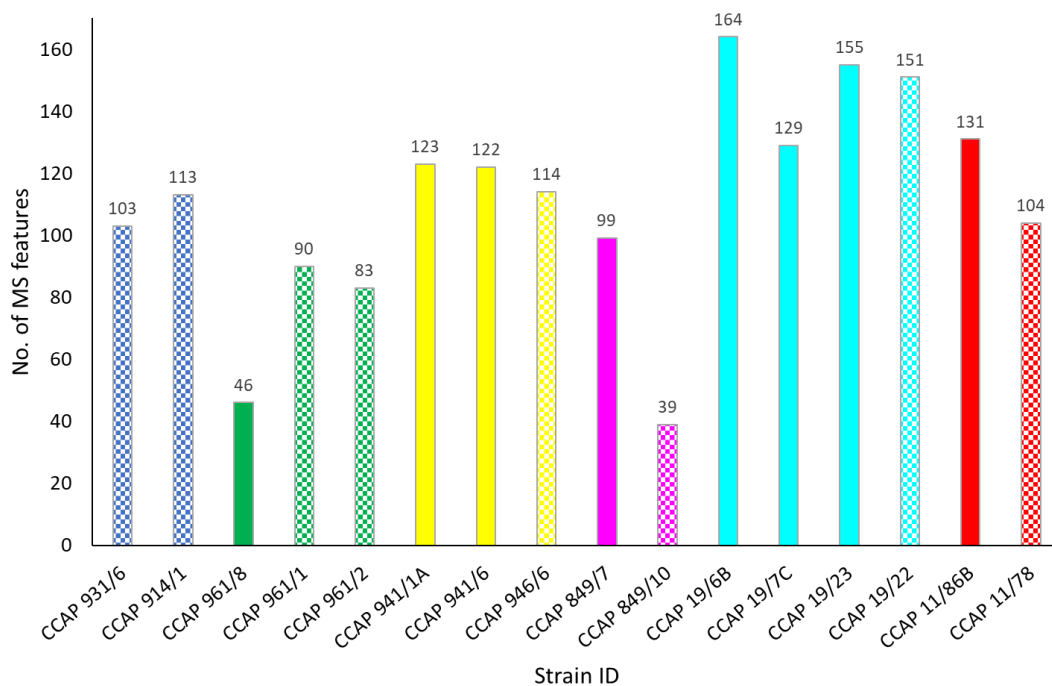


**Figure 3.15** Bar chart showing the number of mass spectral features detected for each strain (*Diacronema*, blue; *Chrysotila*, green; *Prymnesium*, yellow; *Nannochloropsis*, pink; *Dunaliella*, cyan; *Chlamydomonas*, red). Bars with checkerboard filling were isolated from marine environments and those with solid fill were isolated from brackish environments.

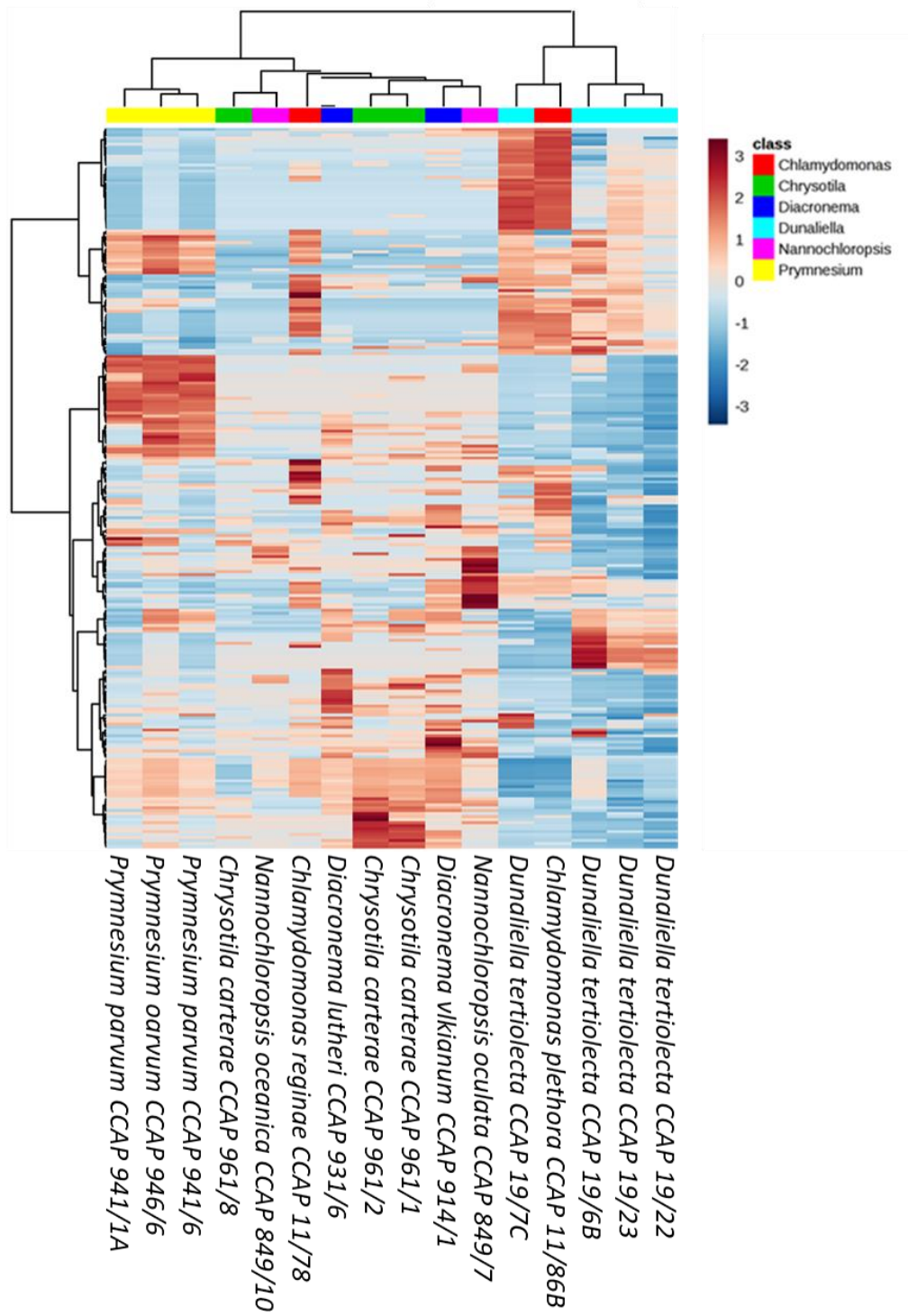


**Figure 3.16** Hierarchical clustering of all detected ions across *Prymnesium* (yellow), *Chlamydomonas* (red), *Chrysotila* (green), *Diacronema* (dark blue), *Dunaliella* (light blue), and *Nannochloropsis* (pink). Heatmap shows relative abundance (low; blue, high; red) of respective features.

### 3.3 Discussion

#### 3.3.1. Growth of Four Marine Microalgal Strains

Four strains of marine microalgae *Nannochloropsis oculata* CCAP 849/1, *Dunaliella primolecta* CCAP 11/34, *Phaeodactylum tricornutum* CCAP 1055/15, and *Porphyridium cruentum* UTEX 161 were selected for their biotechnological potential and will be the strains of focus for the remainder of this thesis. Their growth was characterised by plotting growth curves based on manual cell counting, optical density at 600 nm, and specific growth rates. All four growth curves were sigmoidal in shape as expected and consisted of a lag phase lasting 1-8 days followed by a period of linear growth lasting 15-21 days. Interestingly, You and Barnett also observed a longer lag phase of 6 days when culturing the same strain of *P. cruentum* (UTEX 161).<sup>191</sup> Using a photobioreactor, they were able to achieve a higher cell concentration of  $4 \times 10^9$  cells/mL and a growth rate of 0.32 (compared to 0.09 from our study). Manual cell counting does offer the advantage of being able to inspect cell health and contamination of cultures, however it is a time-consuming task. It also has quite a high threshold for obtaining accurate results with the lower limit for achieving accurate cell counts with a haemocytometer being  $2.5 \times 10^5$  cells/mL (Bio-Rad specifications sheet). *D. primolecta* and *P. cruentum* reached maximum cell densities of  $5.2 \times 10^5$  and  $5.97 \times 10^5$  cells/mL, respectively. Working close to and below the lower limit of accuracy created issues amongst replicates with high standard deviations being recorded. Based on time and inaccuracy, it was decided that optical density at 600 nm would be used as a proxy for growth for higher throughput experiments and that cell counts would be used for the larger photobioreactor cultures (**Chapter 5**) that were expected to reach much higher densities than the small-scale static cultures. Whilst using optical density at 600 nm may mean that cultures will appear to reach stationary phase later than using cell counts, this will be consistent across all replicates and therefore should not interfere with the resultant extracts.

#### 3.3.2. Optimising Extraction of Microalgal Metabolites

The original bottleneck in this work was the insufficient extract masses obtained which was rectified by using HP-20 diaionic resin and physically disrupting cells through lyophilisation. Each 100 mL culture of *Chlorella sorokiniana* was split in two to give two technical replicates for each solvent. Although it would have been desirable to

have more replicates for statistical testing, the biomass and subsequent extract mass was too small to allow this. Repeatability amongst the technical replicates was poor for butanol, butanol:dichloromethane, and methanol. It is unclear why the butanol extracts were so disparate, however the bottle used (Sigma Aldrich, 71-36-3, 99.5% purity) had been opened and in storage for some time before use and may have contained impurities such as butyl ether. Whilst HPLC-grade methanol (Fisher, 67-56-1, 99.8% purity) was used, it is a hygroscopic solvent which may account for the small variation seen between replicates as extractions were not performed under anhydrous conditions. From the 530 metabolites extracted from the *Chlorella sorokiniana*, 29% were extracted in some quantity by all four solvents. Although methanol extracted the highest number of metabolites overall, and the highest number of metabolites that were not extracted by any other solvent, many of these metabolites were structurally related and thus clustered together in the molecular networks. Ethyl acetate extracted 386 (73%) of the metabolites detected from extracts and their diversity was represented across 18 of the 27 molecular families, often in high relative intensity. Wu *et al.*, also used MetaboAnalyst to look at the differences in chemical profiles between a wild-type and starch mutant strain of *Chlorella sorokiniana*. They extracted cultures after six days using a combination of acetonitrile and water and extracted a total of 316 metabolites.<sup>192</sup> This example illustrates that the growth stage of the culture (e.g., after six days compared to stationary phase) may also influence the abundance - and potentially diversity - of metabolites extracted. The diversity of the metabolites extracted by ethyl acetate, the similarity between both replicates, and the fact that it is an inexpensive and green solvent produced by processing corn, led to ethyl acetate being selected as the solvent of choice for the work depicted in this thesis.

### **3.3.2. Unlocking the Chemical Potential of Microalgae**

Based on the comparative metabolomics results, microalgae are a rich source of metabolites, many of which remain uncharacterised. By using an untargeted metabolomics approach, we were able to illustrate that microalgae produce diverse suites of metabolites and that there is little evidence that a core metabolome exists that is shared across taxonomic boundaries as there is no region in the scores plot (**Figure 3.12**) that shows an overlap with all phyla. This is surprising as various classes of microalgae are distinguished by their carotenoid profiles, as well as morphology and

genetic phylogeny.<sup>193</sup> However, since ethyl acetate was the solvent of choice for this analysis, many carotenoids were not efficiently extracted due to their high polarity.<sup>194</sup> A total of 530 metabolomic features were detected for a *Chlorella sorokiniana* culture, simply by using solvents of different polarity when extracting. For chemically rich strains such as *Chrysothila carterae* CCAP 944/6, 573 metabolomic features were detected using only one solvent (ethyl acetate) for extraction. What is even more exciting (and challenging) is that the vast majority of these metabolites have yet to be characterised. From the 530 features detected from *Chlorella sorokiniana*, a well-studied genus of Chlorophytes, none of the features matched with spectra from the GNPS libraries. A study by Luzzatto-Knaan *et al.* obtained over 15 million ultra-high performance liquid chromatography–tandem mass spectrometry (UPLC-MS/MS) spectra from 2600 fractions belonging to cyanobacteria and algae and compared these to Actinobacteria (marine and terrestrial) and lichens, reporting that 86.3% of chemical features were unique to cyanobacteria and algae., and from this only 0.04% of those metabolites could be identified through the GNPS libraries which hold mass spectral data on more than 18,000 compounds.<sup>154</sup> Untargeted metabolomics and comparative techniques are powerful tools in gaining insights into the potential chemical space and biotechnological applications of these organisms. However, without characterising these metabolites and creating databases to assist dereplication and prioritisation of metabolites of interest, understanding the chemical space and role of specialised metabolites remains challenging.

### **3.3.2. Diversity of Eukaryotic Microalgae**

With almost 160,000 described species of algae, it is expected that their vast biological diversity will translate into chemical diversity.<sup>39</sup> Haptophytes, in particular, were rich in chemistry with over 300 features detected from each strain and represent an understudied phylum in terms of biotechnological potential. The majority of species described within the phylum are coccolithophores, which are abundant in the marine environment as they form chalk deposits ([www.algaebase.org/haptophytes](http://www.algaebase.org/haptophytes)).<sup>39</sup> Other species belonging to this phylum that are commonly studied are *Prymnesium* and *Phaocystis*, which form toxic algal blooms and use allelopathic strategies to achieve this.<sup>195</sup> Metabolomics approaches to investigating their chemical profiles could also be used to predict favourable conditions for algal bloom formations or aid in the

identification of stresses that trigger the production of algal toxins.<sup>196</sup> Due to Haptophytes' involvement in chemical warfare, it is not surprising that they produce a plethora of metabolites with specialised functions that could be utilised in biotechnology and pharmaceutical sectors. This study also highlighted the disparity in chemical profiles between strains isolated from different environments. In each of the examples in **Figure 3.14**, strains isolated from similar environments (e.g., marine, brackish) had a similar number of features detected from their extracts and their chemical profiles occupied similar areas of chemical space, despite being categorised according to their species/genus in the PLS-DA. At a minimum, this highlights the importance of using strain identifications (i.e., CCAP code) when reporting genomic and metabolomic observations. Despite being a very small study that was not intended on investigating the existence of chemotypes, the observations do support this argument.

This study suggested that environment may have a large influence on metabolite production. Despite strains belonging to the same species or genus, and despite having a strong phylogenetic relationship (based on 18S rRNA gene sequences only), they can produce distinct chemical profiles. Further evidence through addition of more strains and more replicates would be required to strengthen this argument. It was also demonstrated that using a single culture condition or using a single extraction solvent merely gives a snapshot of the metabolome of these ubiquitous organisms. The remainder of this thesis will focus on four strains of microalgae (*Dunaliella primolecta* CCAP 11/34, *Nannochloropsis oculata* CCAP 849/1, *Phaeodactylum tricornutum* CCAP 1055/15, and *Porphyridium cruentum* UTEX 161) that have promising biotechnological potential, and how we can unlock that potential through the One Strain Many Compounds (OSMAC) approach<sup>101</sup> using abiotic and light stress to induce the production of specialised metabolites.



## 4. Eliciting Specialised Metabolite Production by Marine Microalgae Using Abiotic Stress

---

### 4.1.1 Introduction

Microalgae produce a variety of metabolites, many with specialised functions that can be utilised for biofuels, textiles, cosmetics, and nutraceuticals, some of which are detailed in **Chapter 1**. The most common classes of natural products found in microalgae are isoprenoids and polyunsaturated fatty acids.<sup>197</sup> Isoprenoids, which include the light-harvesting carotenoids, sterols, and phytohormones, are produced from a C5 precursor using either the mevalonate or methylerythol phosphate (MEP) pathway. Interestingly, there is no evidence that Chlorophytes have a mevalonate pathway from mining of available genomes.<sup>198</sup> In fact, it has been shown that they do not possess homologues of plant terpene synthases, meaning that the molecular details of isoprenoid synthesis in microalgae remains unknown.<sup>199</sup> Polyunsaturated fatty acids (PUFAs) include omega-3 and omega-6 fatty acids that mostly exist in the *cis* conformation. Whilst microalgae and plants share many PUFAs, there are some, such as the neuroprotectant docasahexanoic acid, that are found in algae but not terrestrial plants.<sup>197</sup> Highly oxygenated fatty acids, known as oxylipins, are also commonly found in diatoms with about 30% of marine diatoms capable of producing oxylipin metabolites.<sup>200</sup> Some species of microalgae produce toxins belonging to the polyketide or alkaloid natural product classes.<sup>197</sup> Examples of these include the brevetoxins and spirolides from the dinoflagellates *Karenia brevis* and *Alexandrium ostenfeldii*, respectively.<sup>201, 202</sup>

Whilst microalgae, like many other organisms, have the machinery to produce a plethora of diverse metabolites, they cannot always be detected from laboratory cultures of these organisms. According to evidence from genome mining, even the well-investigated *Streptomyces* genus encode the production of metabolites that are yet to be discovered.<sup>203</sup> Various strategies have been used to unlock the chemical potential of microorganisms, including genome mining, genetic engineering, and synthetic biology. Genome mining of 13 Subsection V cyanobacteria revealed that up to 3.5% of their genomes are dedicated to secondary metabolite biosynthesis and a

total of 103 orphan Non-Ribosomal Polyketide Synthase/Polyketide Synthase/Hybrid (NRPS/PKS/Hybrid) gene clusters were discovered which encode for unknown metabolites.<sup>204</sup> The existence of biosynthetic gene clusters – groups of genes that encode a particular product – is common in bacteria and filamentous fungi, however there are few examples of this in eukaryotic microalgae.<sup>205</sup> In 2018, the biosynthetic gene cluster that encodes domoic acid was discovered and the biosynthesis of the neurotoxin through a four gene (8 kb) cascade was uncovered.<sup>206</sup> This provided evidence of biosynthetic gene clusters in microalgae, although it is still believed that this is an exception rather than a rule.<sup>205</sup> Even when putative gene clusters are identified, it can be difficult to stimulate the production of the metabolite they encode due to the size and complexity of the microalgal genome. For example, the dinoflagellate *Karenia brevis* has a genome size of approximately  $10^{11}$  base pairs – 30 times the size of the human genome – and contains at least 12,000 unique genes.<sup>207</sup> However, advancements in sequencing and molecular toolkits have been made in recent years including the use of Clustered Regularly Interspaced Short Palindromic Repeats/CRISPR-Associated Protein 9 (CRISPR/Cas9) systems to edit genes in *P. tricornutum*,<sup>208</sup> genetic engineering of *Nannochloropsis oceanica* for increased polyunsaturated fatty acid production,<sup>209</sup> and the addition of introns into *Chlamydomonas* genes to improve transgene expression.<sup>210</sup> Although this is an exciting time of advancement in molecular techniques for microalgae, progress is slow and incredibly expensive.<sup>211</sup> Simpler, yet untargeted, approaches to unlocking the chemical potential of microalgae is still commonly achieved through the elicitation of metabolites by manipulating culture conditions.

One such way of driving the production of diverse metabolites is the One Strain MAny Compounds (OSMAC) approach,<sup>102</sup> which has proven that small changes in growth conditions can lead to the production of specialised metabolites that would otherwise remain undiscovered when grown in standard laboratory conditions. This approach also has ecological relevance as some metabolites will be triggered in response to specific stress. When the Chlorophyte *Dunaliella salina* was subjected to salt stress (up to 5 M), the level of reactive oxygen species such as hydrogen peroxide increases.<sup>212</sup> To counteract this, the alga produced the powerful antioxidant  $\beta$ -carotene in large quantities (up to 10% dry weight).<sup>132</sup> This natural response by *D. salina* has

been exploited by the biotechnology industry to produce natural  $\beta$ -carotene which has a global market worth US\$155 million (2015).<sup>213</sup> Salt stress not only affects carotenoid production but also glycerol metabolism through the activity of glycerol-3-phosphate dehydrogenase isozymes.<sup>214</sup> Salt concentration is a common stress used for marine microorganisms as they have metabolic mechanisms in place for osmoregulation in response to fluctuating salinity encountered in their native environment. Salinity in the oceans varies from 30 ppt in the Arctic Ocean to 37 ppt in the North Atlantic Ocean,<sup>215, 216</sup> and these values shift according to climate, season, and vicinity to fresh water sources such as rivers and glaciers. Therefore, marine organisms must be able to adapt to the osmotic pressure created by shifting salinities, as well as the change in mineral and nutrient concentrations of the seawater. This mineral composition is important for marine organisms and often, in laboratory settings, sodium chloride is used as a proxy for seawater despite the fact that seawater comprises at least 41 elements in different charged ion and salt complexes.<sup>217</sup> Due to the complexity of natural seawater, synthetic seawaters such as Instant Ocean<sup>®</sup> and Aquil synthetic seawater<sup>218</sup> can also be used. Seawater also contains dissolved nutrients which are required for all organisms in the ocean to survive. Phytoplankton require a specific ratio, known as the Redfield ratio, of 106:16:1 carbon, nitrogen, and phosphorous, respectively.<sup>219</sup> Varying nitrogen sources including ammonium ( $\text{NH}_4^+$ ), nitrate ( $\text{NO}_3^-$ ), nitrite ( $\text{NO}_2^-$ ), and urea ( $\text{NH}_4\text{N}_2\text{O}$ ) have been studied for their bioavailability and both nitrogen source and nitrogen concentrations have been used in the OSMAC approach to elicit production of specific metabolites.<sup>220,221</sup> One promising example of this is in the search for sustainable biofuel sources. *Nannochloropsis* spp. have been shown to accumulate up to 60% lipid content in response to nitrogen starvation and up to 50% fatty acid accumulation under nitrogen and phosphorous starvation.<sup>28</sup> Not only is this an important discovery in our search for sustainable biofuels that do not interfere with food security, but it has wider ecological importance as our lakes and oceans undergo eutrophication from fertilizer runoff, sewage disposal, and climate change.<sup>222</sup> Eutrophication leads to the explosion of harmful algal blooms in both freshwater and marine habitats leading to hypoxic conditions and poisoning of animals through the production of harmful algal toxins.<sup>223</sup> Coinciding with eutrophication of waters is the acidification of the oceans which also leads to harmful algal blooms, often referred to

as red tides.<sup>224</sup> The reduction in the pH of oceans has been shown to reduce the buffering capacity of the ocean such as increasing carbonate mineral dissolution and hydrogen sulfide oxidation.<sup>225</sup> It has also been reported that certain microalgal toxins (known as M-toxins) that cause paralytic shellfish poisoning are actually more stable and less likely to degrade under lower pH values which could result in harmful algal blooms having a longer lasting impact as a result of ocean acidification.<sup>226</sup> On the other hand, the effect of low pH has also been used to increase the production of beneficial microalgal metabolites in controlled settings. Culturing *Haematococcus pluvialis* at pH 4 not only significantly reduces the fungal contaminant *Paraphysoderma sedebokerensis* but the combination of acidic pH and nitrogen deficiency led to a 141-fold increase in astaxanthin production.<sup>227</sup> After studying the ecological and biotechnological potential of abiotic stress on microalgae, salinity (both sodium chloride and Aquil synthetic seawater concentrations), nitrate concentration, and pH were chosen for further investigation.

In order to systematically evaluate the effect of individual abiotic stresses on marine microalgae, three strains (*Nannochloropsis oculata* CCAP 849/1, *Dunaliella primolecta* CCAP 11/34, and *Phaeodactylum tricornutum* CCAP 1055/15) were grown under varying concentrations of sodium chloride (deplete 0 g/L, low 12 g/L, control 24 g/L, and high 36 g/L), Aquil synthetic seawater (low 4.3 ppt, control 43 ppt, and high 86 ppt), and sodium nitrate (low  $8.82 \times 10^{-5}$  M, control  $8.82 \times 10^{-4}$  M, and high  $8.82 \times 10^{-3}$  M), and varying pH (low pH 4, control pH 7.6, and high pH 10). Comparative metabolomics was then used to compare the effects across strains and conditions.

#### **4.1.2 Aims and Objectives**

Whilst the effect of abiotic stresses on the production of specific metabolites (or classes of metabolites) has been well studied, a systematic and untargeted approach to evaluating the effect of abiotic stress on marine microalgal strains has not been done before. Microalgae produce a number of metabolites to maintain homeostasis throughout different life stages. It is hypothesised that microalgae will respond to the stress conditions used in this chapter through the expression of otherwise latent

metabolites. The extent to which each individual stress effects metabolite production, and general trends across strains of different phyla remains unknown.

Objective 1: Quantify growth of marine microalgal strains cultured under various abiotic stress

- Evaluate growth of cultures under varying NaCl, salinity, nitrate, and pH conditions using optical density measurements at 600 nm.
- Compare specific growth rates of cultures grown under each condition to control cultures.

Objective 2: Investigate the influence of abiotic stress on metabolite production in marine microalgal strains

- Examine trends in the response of each strain to varying conditions.
- Explore the effect of each stress (NaCl, salinity, nitrate, and pH) on the chemical profiles of each strain (i.e., an untargeted analysis approach).

## 4.2 Results

### 4.2.1 The Effect of Abiotic Stress on the Growth of Three Marine Microalgal Strains

Three strains of marine microalgae, *Nannochloropsis oculata*, *Dunaliella primolecta*, and *Phaeodactylum tricornutum*, were cultured under varying concentrations of nitrate, sodium chloride (NaCl), Aquil synthetic seawater (salinity), and pH.

#### *Nannochloropsis oculata*

The growth of *N. oculata* was significantly affected by changes in nitrate, NaCl, and salinity, however changes in pH had little impact on growth (**Figure 4.1**). The specific growth rate was reduced for both low ( $8.82 \times 10^{-5}$  M) and high ( $8.82 \times 10^{-3}$  M) nitrate which may indicate that the 10-fold increase in nitrate concentration may have pushed the equilibrium to a point that was no longer productive for the strain. For both NaCl and salinity concentrations, *N. oculata* growth decreased under low and deplete conditions, but increased under the high conditions of 36 g/L NaCl and 86 ppt Aquil synthetic seawater. As this strain was isolated from the Firth of Clyde (off the coast of Isle of Cumbrae, UK), this is a surprising result as there is an influx of freshwater in

this area from the River Clyde. Altering NaCl and salinity had significant changes in the specific growth rates with average values of 14.75 day<sup>-1</sup> and 10.56 day<sup>-1</sup> for controls (24 g/L NaCl and 8.82x10<sup>-4</sup> M salinity), 10.78 day<sup>-1</sup> and 8.12 day<sup>-1</sup> for low (12 g/L NaCl, 8.82x10<sup>-5</sup> M salinity), and 26.16 day<sup>-1</sup> and 12.57 day<sup>-1</sup> for high (36 g/L NaCl and 8.82x10<sup>-3</sup> M salinity) (**Appendix Table A3**). This suggests that other elements, not just NaCl, plays a role in salinity stress.

### ***Dunaliella primolecta***

The growth of *D. primolecta* was reduced under low nitrate conditions although the full extent of this reduction is difficult to conclude as specific growth rate values differed between replicates (replicate 1 2.76 day<sup>-1</sup>, replicate 2 11.83 day<sup>-1</sup>, replicate 3 -6.74 day<sup>-1</sup>) (**Figure 4.2, Appendix Table A3**). This marine strain grew poorly under deplete (0 g/L) NaCl but had a similar specific growth rate to the control for the low NaCl condition (4.23 day<sup>-1</sup> and 4.34 day<sup>-1</sup>, respectively). Growth was significantly reduced ( $p = 2.5 \times 10^{-5}$ ) under low salinity conditions but this would equate to 2.4 g/L NaCl and therefore would be closer to deplete NaCl conditions than low NaCl conditions in this study. *Dunaliella* spp. are known to be particularly halotolerant and therefore it is surprising that growth was also reduced under high salinity conditions. The high salinity condition equates to 48 g/L NaCl which may be why a similar reduction in growth was not observed when the strain was grown at 36 g/L NaCl (high NaCl condition). Another unexpected result was the increased growth of *D. primolecta* under acidic conditions (pH 4) which saw an increase in specific growth rate from 4.74 day<sup>-1</sup> to 6.17 day<sup>-1</sup> (**Appendix Table A3**).

### ***Phaeodactylum tricornutum***

The growth of the diatom *P. tricornutum* was unaffected by high nitrate conditions but was significantly reduced under low nitrate conditions ( $p = 0.003$ ) (**Figure 4. 3, Appendix Table A3**). Most interestingly, the specific growth rate decreased under high NaCl (36 g/L) but not under high salinity (86 ppt) which contained 48 g/L NaCl. It is unknown what might have caused this effect but does demonstrate that NaCl is not always the best proxy for seawater salinity. *P. tricornutum* was the only strain in which growth was decreased under both acidic and basic (pH 10 conditions) with average specific growth rates of 13.38 day<sup>-1</sup> for the control, 11.26 day<sup>-1</sup> for low, and

7.94 day<sup>-1</sup> for high (**Appendix Table A3**). This is likely due to the formation of silicified frustules around the cell wall being disturbed by the changes in pH.

### Trends between strains

As expected, lowering the concentration of nitrate tenfold to 8.82x10<sup>-5</sup> M decreased the growth of all three strains (**Figure 4.1, 4.2, and 4.3**). This decrease was significant for *N. oculata* ( $p = 0.006$ ) and *P. tricornutum* ( $p = 0.003$ ) (**Appendix Table A3**) but due to the spread of measurements for the *D. primolecta* replicates, it is unclear just how much of an impact low nitrate concentration had on this strain. We expected to see a similar trend for both the NaCl concentration and varying salinity concentrations as NaCl is the main component of Aquil synthetic seawater at 24 g/L. However, Aquil synthetic seawater is a mixture of seven salts affecting the salinity, buffering potential, and minerality of the medium. For each strain, 0 g/L NaCl resulted in a significant decrease in growth which is expected as they had been isolated from a marine environment and maintained in saline conditions. The specific growth rates of *D. salina* remained unaffected under growth at 12 g/L, 24 g/L, and 36 g/L NaCl (average  $\mu = 4.34, 5.05, \text{ and } 4.27 \text{ day}^{-1}$ , respectively) (**Appendix Table A3**). In comparison, growth under varying salinity which was significantly reduced for both low (4.3 ppt) and high (86 ppt) conditions. *Dunaliella* spp., are suspected to be obligate marine microalgae as there have been no freshwater species described so far. Furthermore, *D. salina* is used as a model organism for studying halotolerance and osmotic stress.<sup>228</sup> It was therefore expected that the growth *D. salina* would be unaffected by increases in NaCl and salinity, however growth was reduced under high salinity. The specific growth rate of *N. oculata* almost doubled when grown in 36 g/L NaCl from 14.75 day<sup>-1</sup> to 26.26 day<sup>-1</sup>. This increase was not as large as when *N. oculata* was grown under high salinity. Conversely, growth of the diatom *P. tricornutum* decreased by 71% when grown under high NaCl but growth only decreased by 13% when grown under high salinity. Finally, *P. tricornutum* was the only strain to be significantly affected by pH stress with average specific growth rates of 11.26, 13.38, and 7.94 day<sup>-1</sup> for pH 4, 7.6, and 10, respectively. In contrast, growth of *N. oculata* and *D. primolecta* remained unaffected by acidic or basic pH conditions, whilst growth of *P. tricornutum* was significantly reduced under acidic and basic conditions ( $p = 0.02$  and  $1.18 \times 10^{-5}$ , respectively)

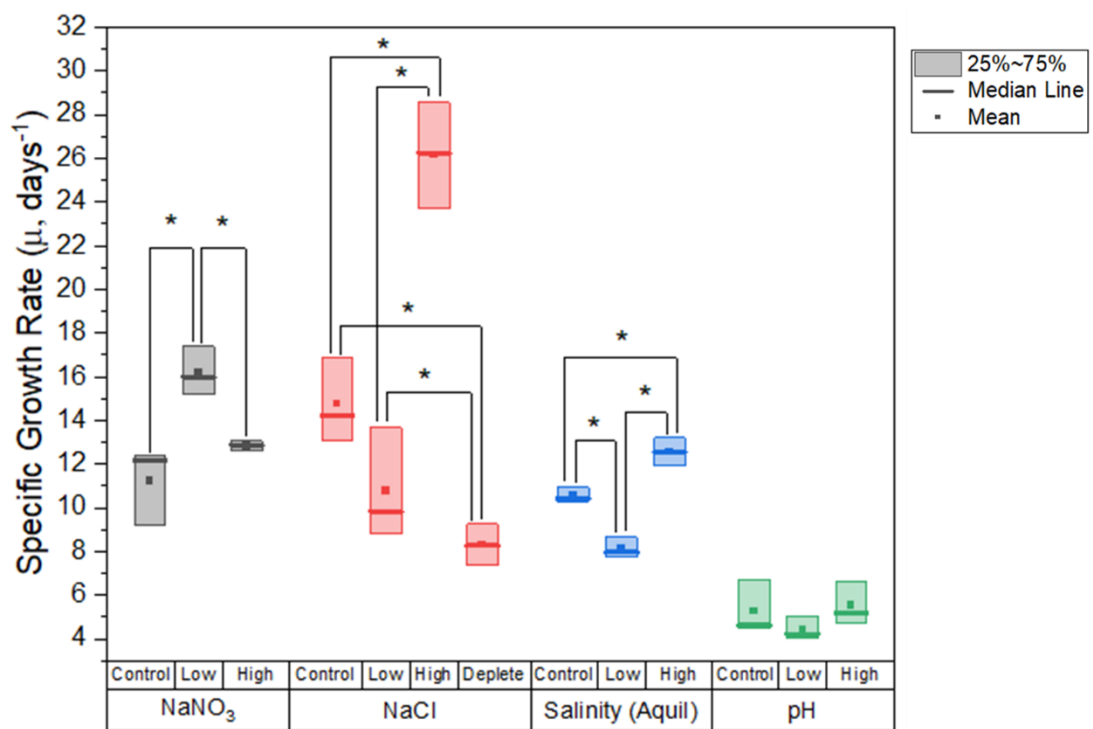


**Figure 4.1** Box plots summarising growth rates of *Nannochloropsis oculata* grown under varying conditions with box plots showing the 25-75% range, median values as thick lines and mean values as solid squares. Conditions are as follows: NaNO<sub>3</sub> (grey); control ( $8.82 \times 10^{-4}$  M), low ( $8.82 \times 10^{-5}$  M), high ( $8.82 \times 10^{-3}$  M); NaCl (red); control (24 g/L), low (12 g/L), high (36 g/L), deplete (0 g/L); salinity (blue); control (43 ppt), low (4.3 ppt), high (86 ppt); and pH (green); control (7.6), low (4), high (10). P-values are based on a t-test between condition and control for each stress.



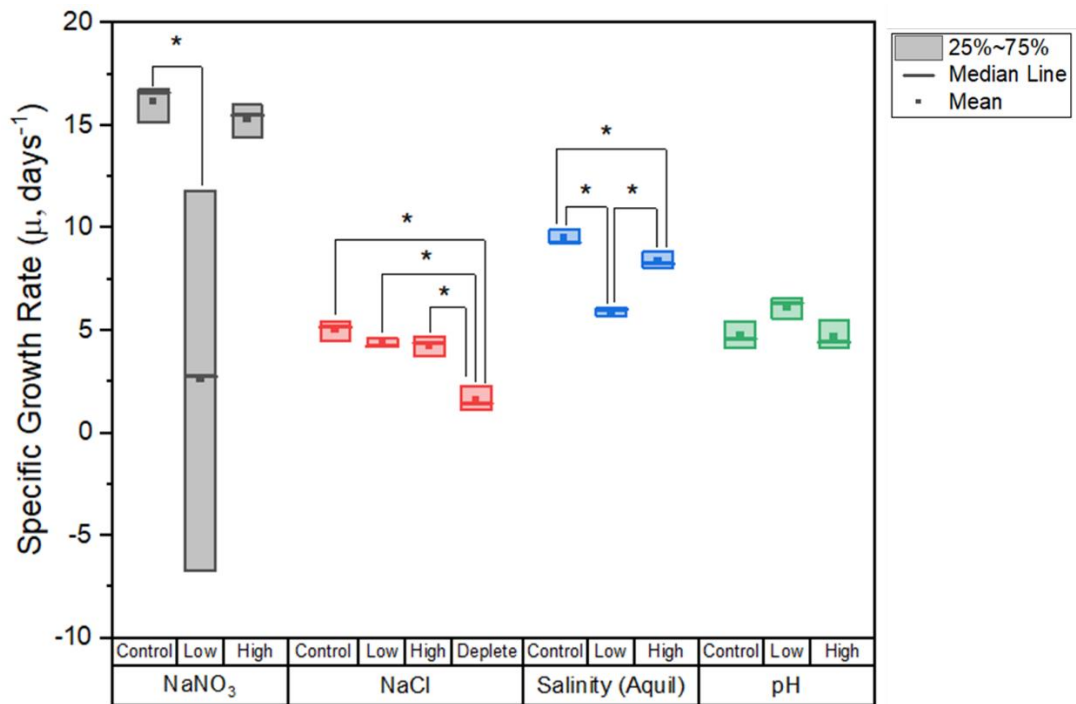


**Figure 4.2** Box plots summarising growth rates of *Dunaliella primolecta* grown under varying conditions with box plots showing the 25-75% range, median values as thick lines and mean values as solid squares. Conditions are as follows: NaNO<sub>3</sub> (grey); control ( $8.82 \times 10^{-4}$  M), low ( $8.82 \times 10^{-5}$  M), high ( $8.82 \times 10^{-3}$  M); NaCl (red); control (24 g/L), low (12 g/L), high (36 g/L), deplete (0 g/L); salinity (blue); control (43 ppt), low (4.3 ppt), high (86 ppt); and pH (green); control (7.6), low (4), high (10). P-values are based on a t-test between condition and control for each stress.

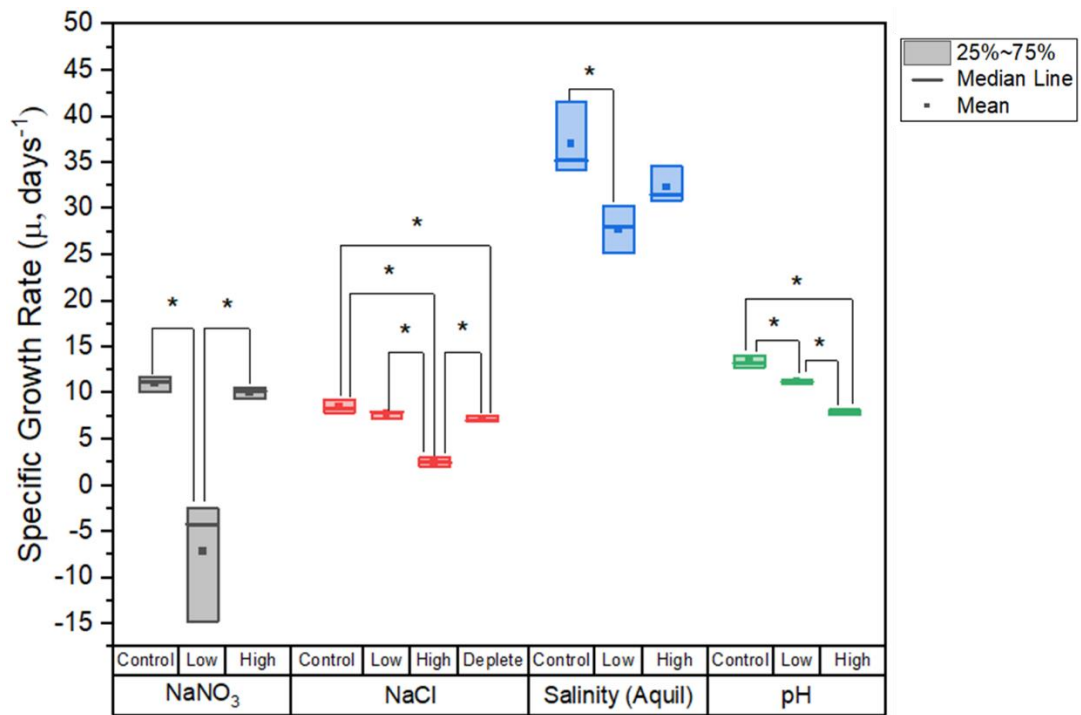
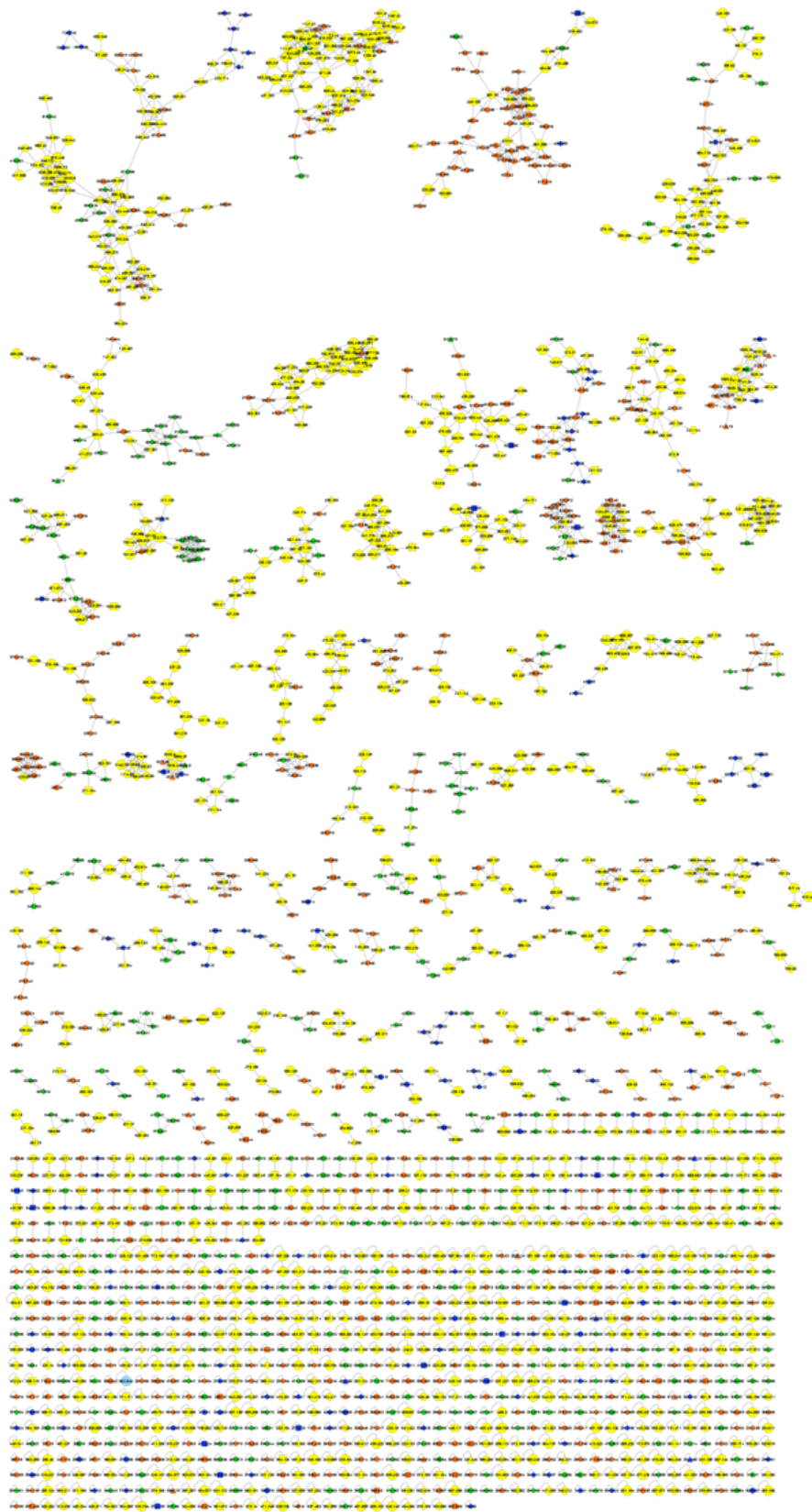


**Figure 4. 3** Box plots summarising growth rates of *Phaeodactylum tricornerutum* grown under varying conditions with box plots showing the 25-75% range, median values as thick lines and mean values as solid squares. Conditions are as follows: NaNO<sub>3</sub> (grey); control ( $8.82 \times 10^{-4}$  M), low ( $8.82 \times 10^{-5}$  M), high ( $8.82 \times 10^{-3}$  M); NaCl (red); control (24 g/L), low (12 g/L), high (36 g/L), deplete (0 g/L); salinity (blue); control (43 ppt), low (4.3 ppt), high (86 ppt); and pH (green); control (7.6), low (4), high (10). P-values are based on a t-test between condition and control for each stress.

#### 4.2.2 Overview of the Effect of Abiotic Stress on Metabolite Production

A molecular network of extracts from the three strains grown under each abiotic condition in triplicate comprised 2284 nodes, of which 51.2% were shared between at least two of the three strains (**Figure 4.4, Figure 4.5**). In **chapter 3**, we saw that when grown under standard laboratory conditions, the chemical profiles of particular clades and strains were distinct from one another. After taking a more in depth look in this chapter at their chemical profiles (through LC-MS/MS and molecular networking analysis), it can be seen that there is a shared chemical space between different phyla of microalgae, particularly when some of their chemical potential is unlocked using the OSMAC approach. However, there are still distinct differences in the chemical profiles at the genus level for these strains, with 24.1% (550) of features only found in *P. tricornutum* extracts, 17.3% (391) of features are unique to *D. primolecta*, and 7.4% (169) of features are distinct to *N. oculata* extracts (**Figure 4.5**). These distinct features for each strain tend to cluster within specific molecular families of metabolites with related structural moieties. Not only does each strain have a set of distinct features, but so does each stress. Focusing on features that were only produced in response to stress (i.e., NaCl, salinity, nitrate, or pH) revealed that 49% of features were only produced by strains grown under a particular stress: 22.8% of features were only produced in response to salinity stress, 17.1% in response to nitrate stress, 7.7% in response to NaCl stress, and 1.4% in response to pH stress (**Figure 4.6**). This aligns with the effect seen on the growth of these organisms with salinity having the greatest effect on the growth of all three strains, followed by nitrate, NaCl, and finally pH which only had a significant effect on the growth of *P. tricornutum*.



● *Dunaliella primolecta*   
 ● *Nannochloropsis oculata*   
 ● *Phaeodactylum tricorutum*   
 ● Shared between strains  
 ▲ pH    ◆ Salinity    ■ NaCl conc.    ⬡ NaNO<sub>3</sub> conc.    ● Shared between conditions

**Figure 4.4** GNPS classical molecular network of MS/MS features detected from extracts of *Nannochloropsis oculata* (blue), *Dunaliella primolecta* (green), and *Phaeodactylum tricornutum* (orange) grown under varying pH (triangles), salinity (diamonds), NaCl concentrations (squares), and nitrate concentrations (hexagons). Features shared between strains are in yellow while features shared across conditions are presented as circles.

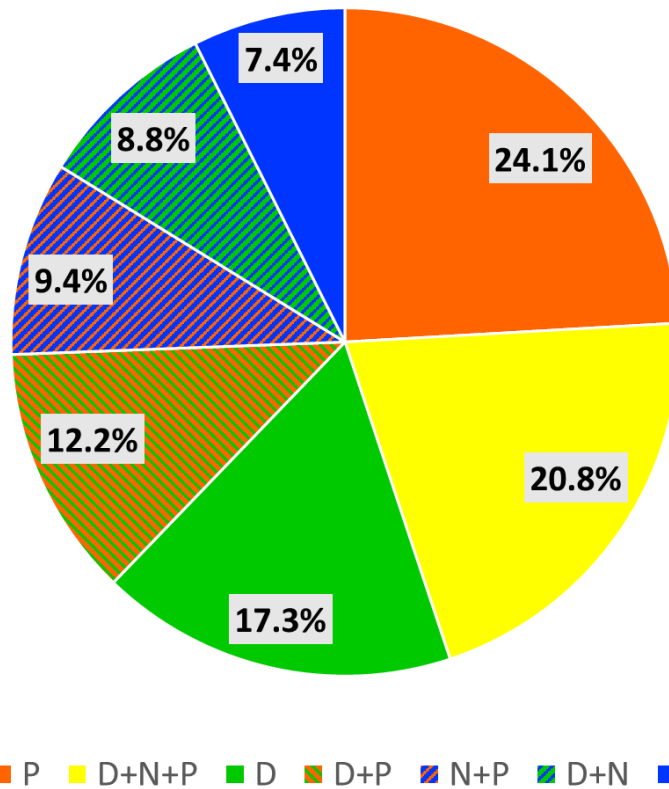


**Figure 4.5** Pie chart showing the distribution of MS/MS features across strains: P = *Phaeodactylum tricornutum*, orange; D = *Dunaliella primolecta*, green; N = *Nannochloropsis oculata*, blue; D+P = features shared between *D. primolecta* and *P. tricornutum*, green and orange stripes, D+N = features shared between *D. primolecta* and *N. oculata*, green and blue stripes, N+P = features shared between *N. oculata* and *P. tricornutum*, blue and orange stripes, D+N+P = features shared between all three strains, yellow.

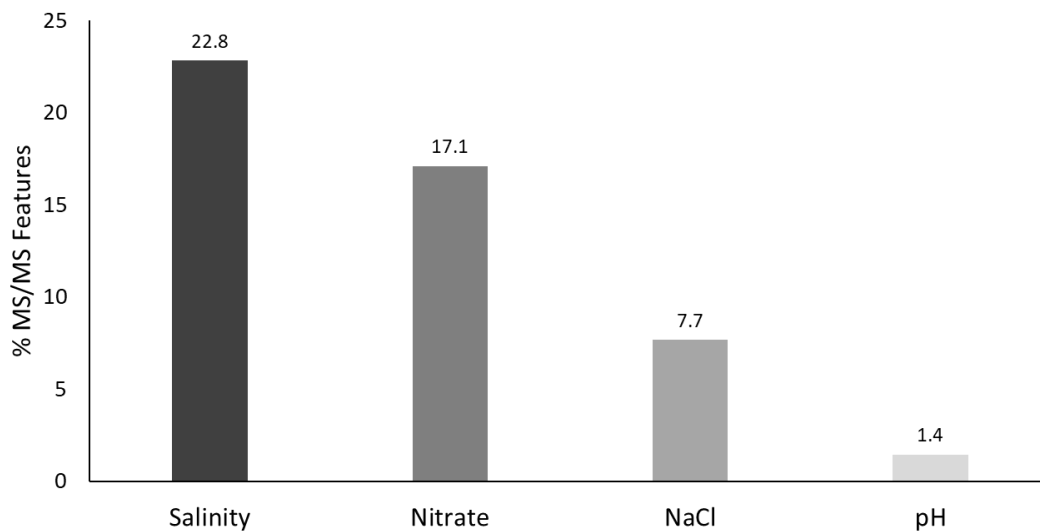


**Figure 4.6** Bar chart of the percentage of total MS/MS features only detected in response to specific stresses; varying salinity (Aquil synthetic seawater), nitrate concentrations, NaCl concentrations, and pH. The percentages are listed above each bar.

From the overview molecular network (**Figure 4.4**), salinity had the greatest effect on metabolite production with 22.8% of features detected from microalgal extracts from salinity stress. It also had the greatest effect on growth with specific growth rates being significantly reduced under low salinity (4.3 ppt) for all three strains. These changes in growth were coupled with large changes in metabolite production with 17.9-23.6% of metabolites only produced under low salinity (

**Figure 4.7**). This effect can also be seen in deplete and low NaCl conditions with 6.6-17.1% and 4.4-10.8% of metabolites only produced under these conditions. In fact, the spread of metabolites across each condition was similar for each strain, suggesting that these marine strains may have common strategies for responding to salt stress. Interestingly, high salinity and NaCl concentration had a much smaller effect (3.6-5.4% for salinity and 2.9-6.3% for NaCl) which shows that hypoosmotic stress has a greater influence on metabolite production than hyperosmotic stress (

**Figure 4.7**). This also agrees well with the growth data, as high salinity and NaCl did not impact growth in the same way that low conditions did. One notable difference across strains is that of *D. primolecta* grown under deplete NaCl which stimulated the production of 191 (17.1%) metabolites that are not found in the other conditions. The poor growth and large change in metabolism gives further support that *Dunaliella* spp. are obligate marine microalgae.

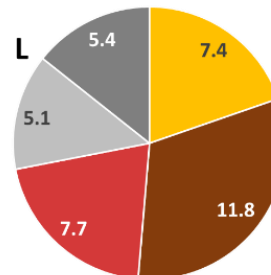
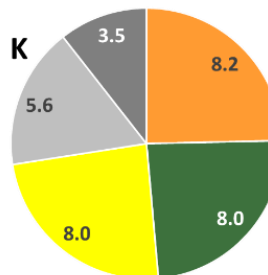
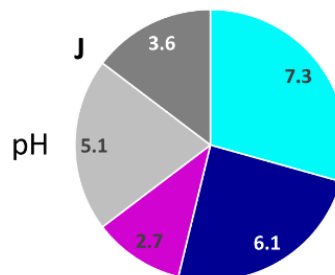
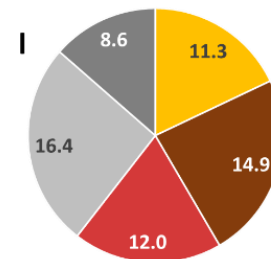
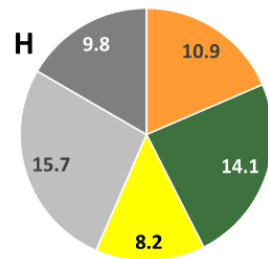
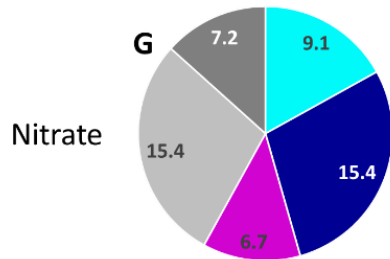
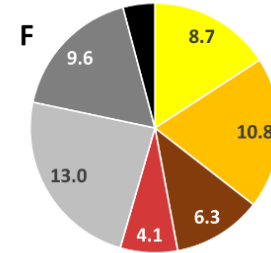
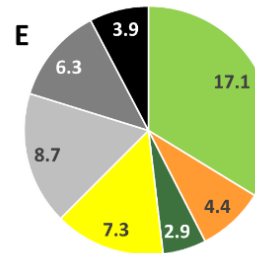
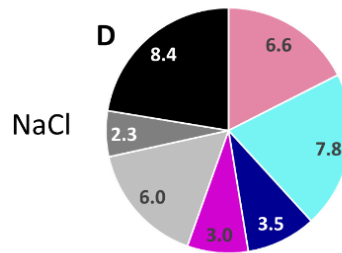
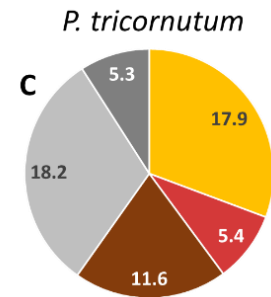
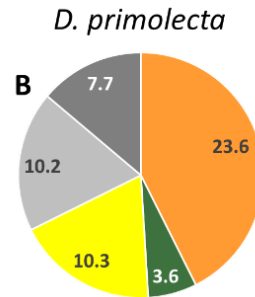
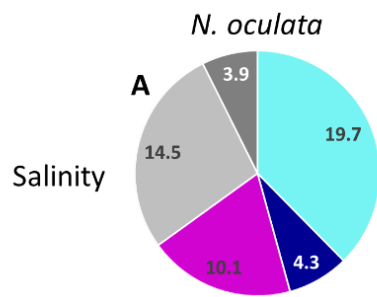
After salinity, varying nitrate concentrations had the second largest impact on the metabolite profiles with 17.1% of metabolites only detected when strains were grown under nitrate stress. Although low nitrate ( $8.82 \times 10^{-5}$  M) had the greatest effect of the specific growth rates of all strains, it had less of an influence on metabolite production with 9.1-11.3% of metabolites only produced under low nitrate conditions compared with 14.1-15.4% of metabolites detected in extracts from high nitrate ( $8.82 \times 10^{-3}$  M) cultures. This is interesting from an ecological point of view, as eutrophication has caused an increase of nitrate in the oceans causing increased growth of microalgae (algal blooms). However, the effect of these increased nitrate levels on the metabolism of these organisms and how this may impact the food chain remains underexplored. As with salinity, the distribution of metabolites across control, low, and high conditions is similar for all three strains (



**Figure 4.7**), again demonstrating that there could be common response mechanisms to nitrate stress.

Finally, pH stress had the lowest impact on growth with only the specific growth rate of *P. tricornutum* decreasing significantly under low (pH 4) and high (pH 10) conditions, and *D. primolecta* seeing an increase in growth under pH 4. As seen with the other stresses, the impact on growth correlates well with the impact on metabolite production with only 1.4% of metabolites produced specifically under pH stress. Once again, the distribution of metabolites according to each condition was very similar for all strains with 6.1-11.8% only detected under high pH conditions, 6.1-8.0% only detected in control samples, and 7.3-8.2% of features only detected under low pH conditions. *D. primolecta* had a higher specific growth rate under acidic (low pH) conditions and this did correlate with a slightly higher (8.2% compared to 7.3% and 7.4%) number of metabolites detected for *D. primolecta* compared to the other two strains.

The sheer amount of data presented in **Figure 4.4** makes it difficult to understand the influence of varying levels of each stress and therefore only provides a global overview on which types of stress are having the greatest overall effect. To gain greater insights into the influence of each stress, and the varying levels of those stresses, classical molecular networks were produced for each stress and for each strain grown under each stress. Below offers some of the insights from this in-depth analysis. There is still much more to be explored in terms of metabolite discovery and piecing together the influence of particular stresses on metabolic and biosynthetic pathways.



*N. oculata* (A, D, G, J)    Low    Control    High    Deplete

*D. primolecta* (B, E, H, K)    Low    Control    High    Deplete

*P. tricorutum* (C, F, I, L)    Low    Control    High    Deplete

Two conditions    Three conditions    All conditions

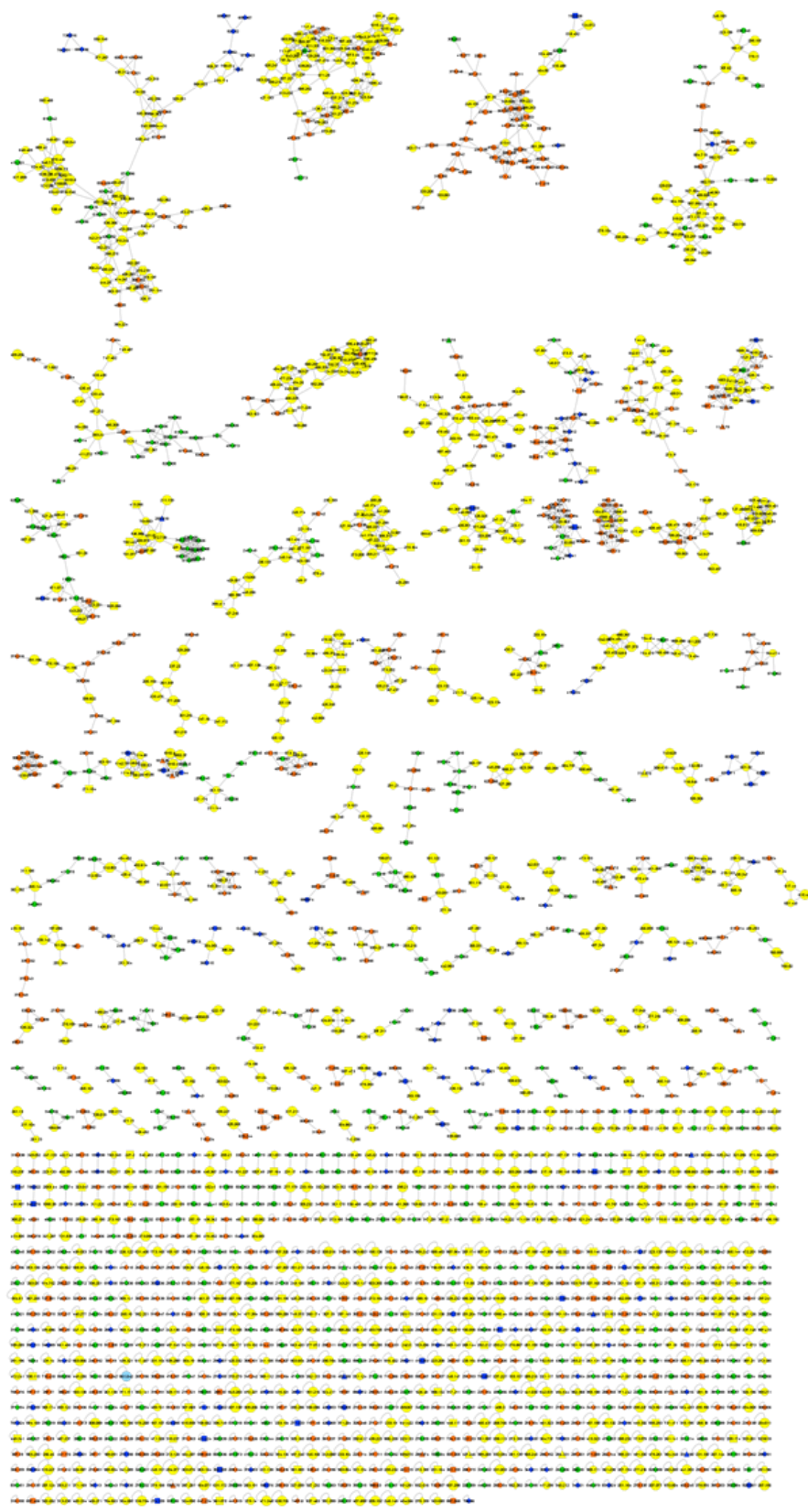
**Figure 4.7** Pie charts illustrating the distribution of MS/MS features as percentages (given in figure) for all three strains under all four stresses: **(A)** *N. oculata* grown under varying salinity, **(B)** *D. primolecta* grown under varying salinity, **(C)** *P. tricornutum* grown under varying salinity, **(D)** *N. oculata* grown under varying NaCl concentrations, **(E)** *D. primolecta* grown under varying NaCl concentrations, **(F)** *P. tricornutum* grown under varying NaCl concentrations, **(G)** *N. oculata* grown under varying nitrate concentrations, **(H)** *D. primolecta* grown under varying nitrate concentrations, **(I)** *P. tricornutum* grown under varying nitrate concentrations, **(J)** *N. oculata* grown under varying pH, **(K)** *D. primolecta* grown under varying pH, and **(L)** *P. tricornutum* grown under varying pH.

### 4.2.3 Salinity and NaCl Concentration

From the salinity molecular network (**Figure 4.8**), 2749 features were detected, 28% of those coming from the media and solvent controls. Individual networks were created for each strain with the highest number of features detected for *P. tricornutum* at 701, followed by *D. primolecta* with 584 features, and *N. oculata* with 348 (**Appendix Fig A4, A8, A12**). As mentioned above, all three strains have a similar distribution of MS/MS features across the three conditions of low salinity (4.3 ppt), control (43 ppt), and high salinity (86 ppt). Following a similar trend to growth, low salinity had the greatest effect on metabolite production with 17.9-23.6% of metabolites only produced when strains were grown under low salinity. This is five times the number of metabolites detected when strains are grown in high salinity (3.6-5.4%) with the remaining metabolites being distributed across control samples (10.1-11.6%) or shared between two or three conditions. A similar trend can be observed from the NaCl molecular network, however with far fewer overall features at 1882, 32% of which are from media and control blanks (**Figure 4.9**). Deplete (0 g/L NaCl) and low (12 g/L NaCl) conditions again had the greatest impact on metabolite production with 6.6-17.1% and 4.4-10.8%, respectively. *D. primolecta*, in particular, saw the greatest change in its metabolite profile in response to low salinity/NaCl concentration with 23.6% of metabolites only produced under low salinity and 20% of metabolites only produced when cultures were grown in medium deplete of NaCl or under low NaCl conditions (**Figure 4.5**). The only metabolites identified through comparison with the GNPS libraries were monopalmitolein and 1-octadecanamide (stearamide) which were found in all strains grown under all salinity and NaCl conditions. The lack of matches to previously discovered metabolites makes dereplication and putative identification of derivatives an incredibly difficult task.

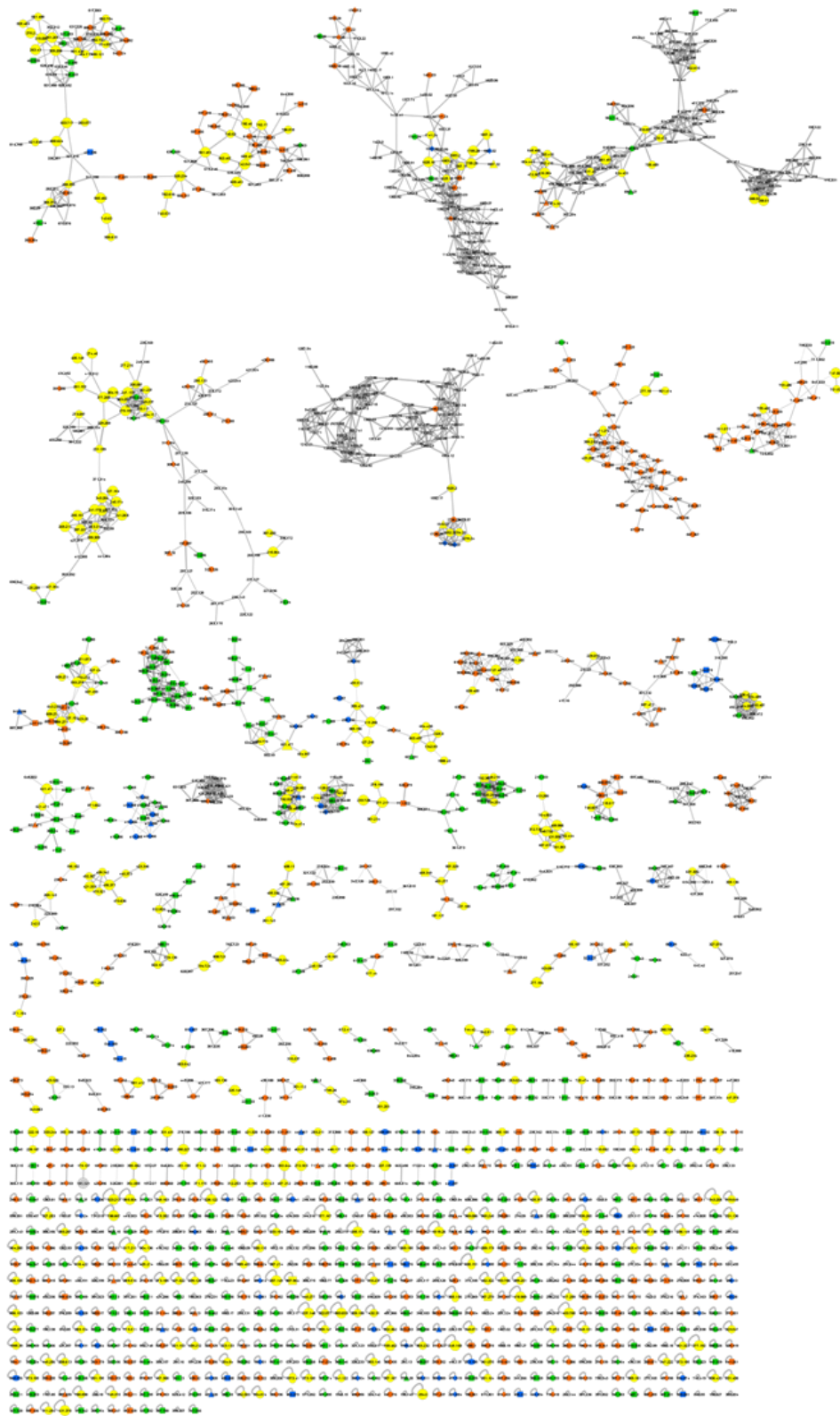
Metabolites that are only detected from a specific strain tend to cluster together into molecular families and this can be seen in the salinity and NaCl molecular networks. For example, **Figure 4.10 A** shows that 24 of the 35 metabolites in this molecular family were only detected in samples from *P. tricornutum*. More interestingly, 25 of these metabolites are only found under low salinity conditions, with the majority of these being medium-high molecular weight (721.382-1177.67 *m/z*) metabolites coming from *P. tricornutum*. Another molecular family (**Figure 4.10 B**) of structurally

similar (cosine score >0.7) medium-high molecular weight metabolites (672.406-1233.76  $m/z$ ) were only produced by *P. tricornutum* under low salinity, and another molecular family of seven low molecular weight metabolites (372.738-781.545  $m/z$ ) were only produced under high salinity. This can also be observed for *N. oculata* (**Figure 4.10 C**) with a molecular family of high molecular weight metabolites (833.472-2284.49  $m/z$ ) only being detected for *N. oculata* grown under low salinity conditions. This trend is not as clear for *D. primolecta*, however there are some small molecular families with 3-4 members that again are only produced under low salinity conditions (**Figure 4.10 D**). From the molecular networks it can be seen that there were at least four molecular families of metabolites that were solely detected in that strain for salinity (four by *N. oculata*, five by *D. primolecta*, and seven by *P. tricornutum*) and at least two molecular families solely detected for that strain under NaCl (two for *N. oculata*, five for *D. primolecta*, and 13 for *P. tricornutum*). Not only does this support conclusions from **chapter 3** that diatoms are a rich source of novel chemistry, but it could also allow for MS/MS “fingerprinting” of environmental cultures to rapidly identify populations to genus or species level.



● *Dunaliella primolecta*   
 ● *Nannochloropsis oculata*   
 ● *Phaeodactylum tricornerum*   
 ● Shared between strains  
◆ Low, 4.3 ppt   
 ● Control, 43 ppt   
 ▲ High, 86 ppt

**Figure 4.8** GNPS classical molecular network of MS/MS features detected from extracts of *Nannochloropsis oculata* (blue), *Dunaliella primolecta* (green), and *Phaeodactylum tricornutum* (orange) grown under varying salinity: low = 4.3 ppt Aquil, diamond; control = 43 ppt Aquil, circle; high = 86 ppt Aquil, triangle). Features shared between conditions are presented as yellow circles.



● *Dunaliella primolecta*  
 ● *Nannochloropsis oculata*  
 ● *Phaeodactylum tricorutum*  
 ● Shared between strains  
 Deplete, 0 g/L  
 ◆ Low, 12 g/L  
 ● Control, 24 g/L  
 ▲ High, 36 g/L



**Figure 4.9** GNPS classical molecular network of MS/MS features detected from extracts of *Nannochloropsis oculata* (blue), *Dunaliella primolecta* (green), and *Phaeodactylum tricornutum* (orange) grown under varying NaCl concentrations: deplete = 0 g/L NaCl, square; low = 12 g/L NaCl, diamond; control = 24 g/L NaCl, circle; high = 36 g/L NaCl, triangle). Features shared between conditions are presented as yellow circles.

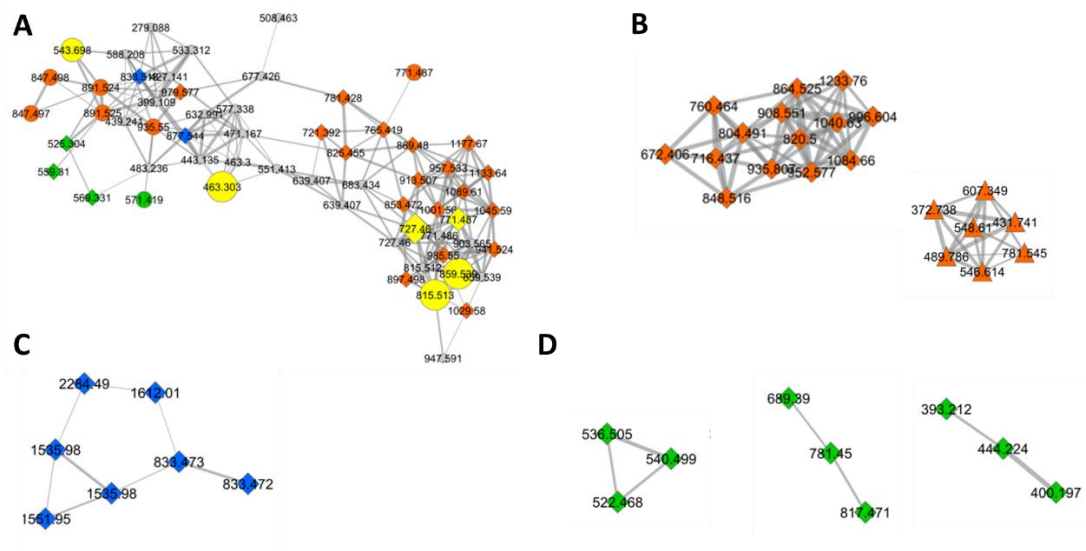


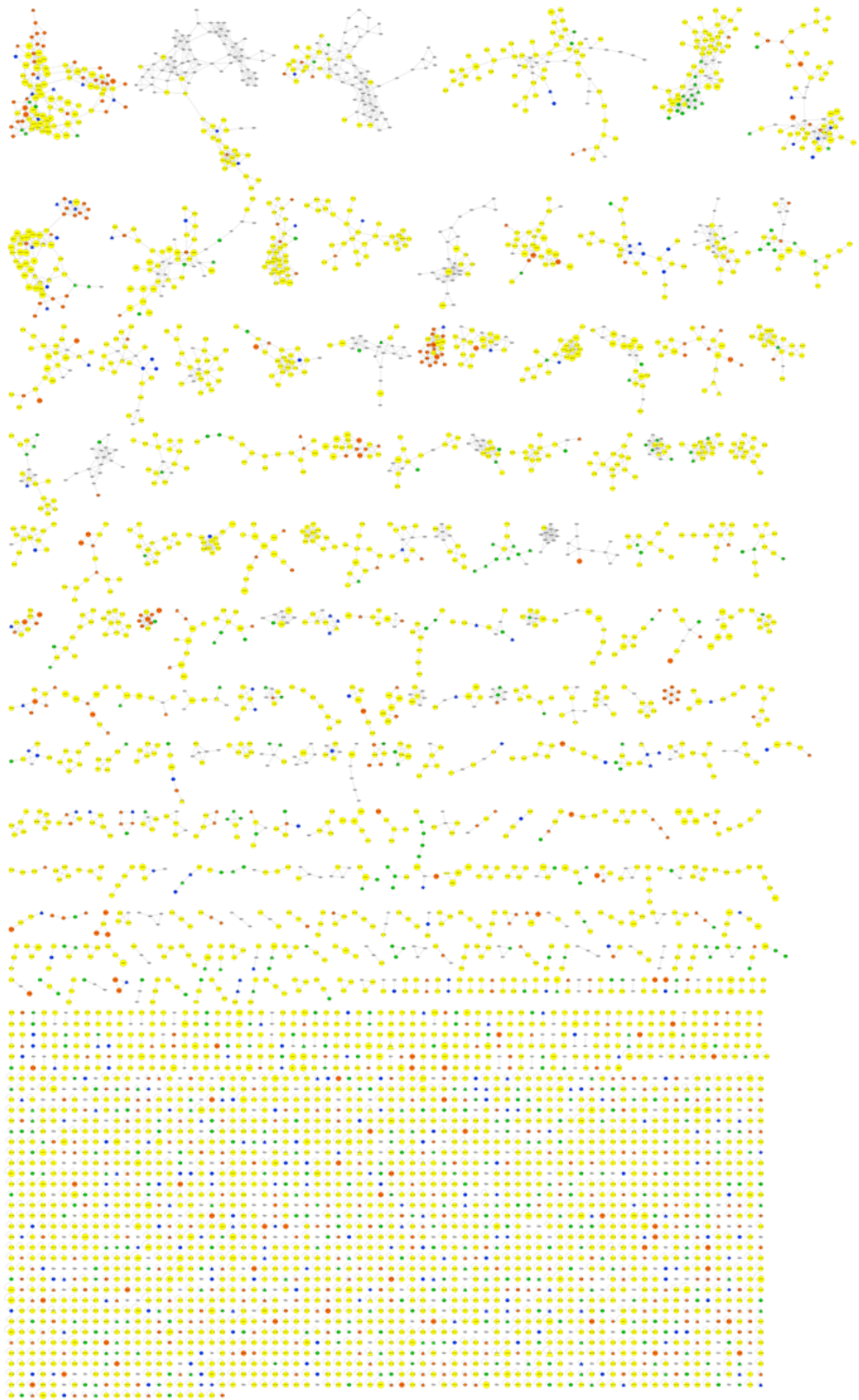
**Figure 4.10** Examples of molecular families detected under specific conditions: **(A)** metabolites in orange are only produced by *P. tricornutum* with diamonds representing metabolites only produced under low salinity, **(B)** metabolites only produced by *P. tricornutum* (orange) under low salinity (diamonds) or high salinity (triangles), **(C)** molecular family produced in response to low salinity by *N. oculata*, **(D)** molecular families produced in response to low salinity by *D. primolecta*.

#### 4.2.4 Nitrate Concentration

The nitrate molecular network (**Figure 4.11**) had the highest overall number of 4982 features detected with 12.6% from media and solvent controls. Individual networks were created for each strain with 1003 features detected for *P. tricornutum*, 843 for *D. primolecta*, and 667 for *N. oculata* (**Appendix Fig A6, A10, A14**). Whilst low nitrate had the greatest impact on the growth of each strain, in the chemical analysis it was the high nitrate concentration that had the greatest impact. For high nitrate, 14.1-15.4% of metabolites were only produced under this condition compared to 9.1-11.3% for low nitrate. This somewhat contradicts the trend seen with salinity and NaCl where reduced growth correlated with increased metabolite production. As well as 1-octadecanamine, three other metabolites were identified in all strains across all conditions – hexanedioic acid, 13-keto-9Z,11E-octadecadienoic acid, and 9,12-octadecadien-1-ol. These were all matches to the MassBank<sup>229</sup> library which is an open access repository of small molecules (<3000 Da) of compounds (natural and synthetic) relevant to life sciences.

Comparing the nitrate molecular network to those of salinity and NaCl, there are far more molecular families with smaller numbers of metabolites in each in the nitrate network. The reason for this is unclear as the same parameters were used to construct all networks so they could be easily compared to one another. There is also much more shared chemistry across the strains with 886 (20.3%) of metabolites shared between at least two strains. In terms of strain specific molecular families, there was only one detected for *P. tricornutum* and *D. primolecta*. The effect of varying nitrate conditions affected the production of metabolites belonging to most molecular families rather than specific molecular families as seen with salinity and NaCl. After light and inorganic carbon, nitrogen is the most prominent nutrient required for the growth and survival of microalgae so it not surprising that all aspects of metabolism are affected by a 10-fold increase or decrease in nitrate concentration. Only one molecular family predominantly comprised of metabolites (913.507-1221.68  $m/z$ ) solely detected when *D. primolecta* was cultured under high nitrate (**Figure 4.12 A**). A number of other molecular families showed examples of metabolites that were only produced in response to high or low nitrate in all three strains. For example, **Figure 4.12 B** shows three metabolites with parent masses 635.385, 679.277, and 784.491  $m/z$  which are

detected in samples from all three strains under low nitrate conditions. Similarly, **Figure 4.12 C** shows a molecular family with four metabolites (477.234, 563.27, 649.308, and 838.408  $m/z$ ) which were produced by all three strains under high nitrate. It is remarkable that the high nitrate concentration had such an impact on metabolite production in these strains and this result could be important for understanding how the eutrophication of our waters affect the aquatic food chain. It has been shown that high nitrogen and phosphorous levels lead to more blooms of toxic microalgae and cyanobacteria, but the effect it has on non-toxic or non-bloom forming microalgae requires further investigation.



● *Dunaliella primolecta*   ● *Nannochloropsis oculata*   ● *Phaeodactylum tricornutum*   ● Shared between strains  
 ◆ Low,  $8.2 \times 10^{-5}$  M   ● Control,  $8.2 \times 10^{-4}$  M   ▲ High,  $8.2 \times 10^{-3}$  M

**Figure 4.11** GNPS classical molecular network of MS/MS features detected from extracts of *Nannochloropsis oculata* (blue), *Dunaliella primolecta* (green), and *Phaeodactylum tricornutum* (orange) grown under varying nitrate concentrations: low =  $8.82 \times 10^{-5}$  M NaNO<sub>3</sub>, diamond; control =  $8.82 \times 10^{-4}$  M NaNO<sub>3</sub>, circle; high =  $8.82 \times 10^{-3}$  M NaNO<sub>3</sub>, triangle). Features shared between conditions are presented as yellow circles.

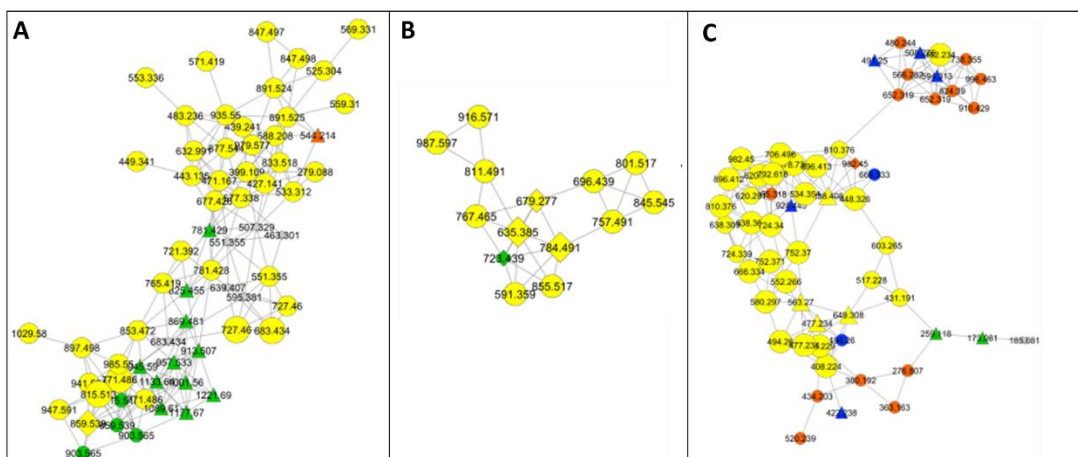


**Figure 4.12** Examples of molecular families detected under specific conditions: **(A)** metabolites in green are only produced by *D. primolecta* with triangles representing metabolites only produced under high nitrate, **(B)** molecular family produced in response to low nitrate (diamonds) by all strains (yellow) and *D. primolecta* (green), and **(C)** metabolites only produced under high nitrate (triangles) by all three strains (yellow).

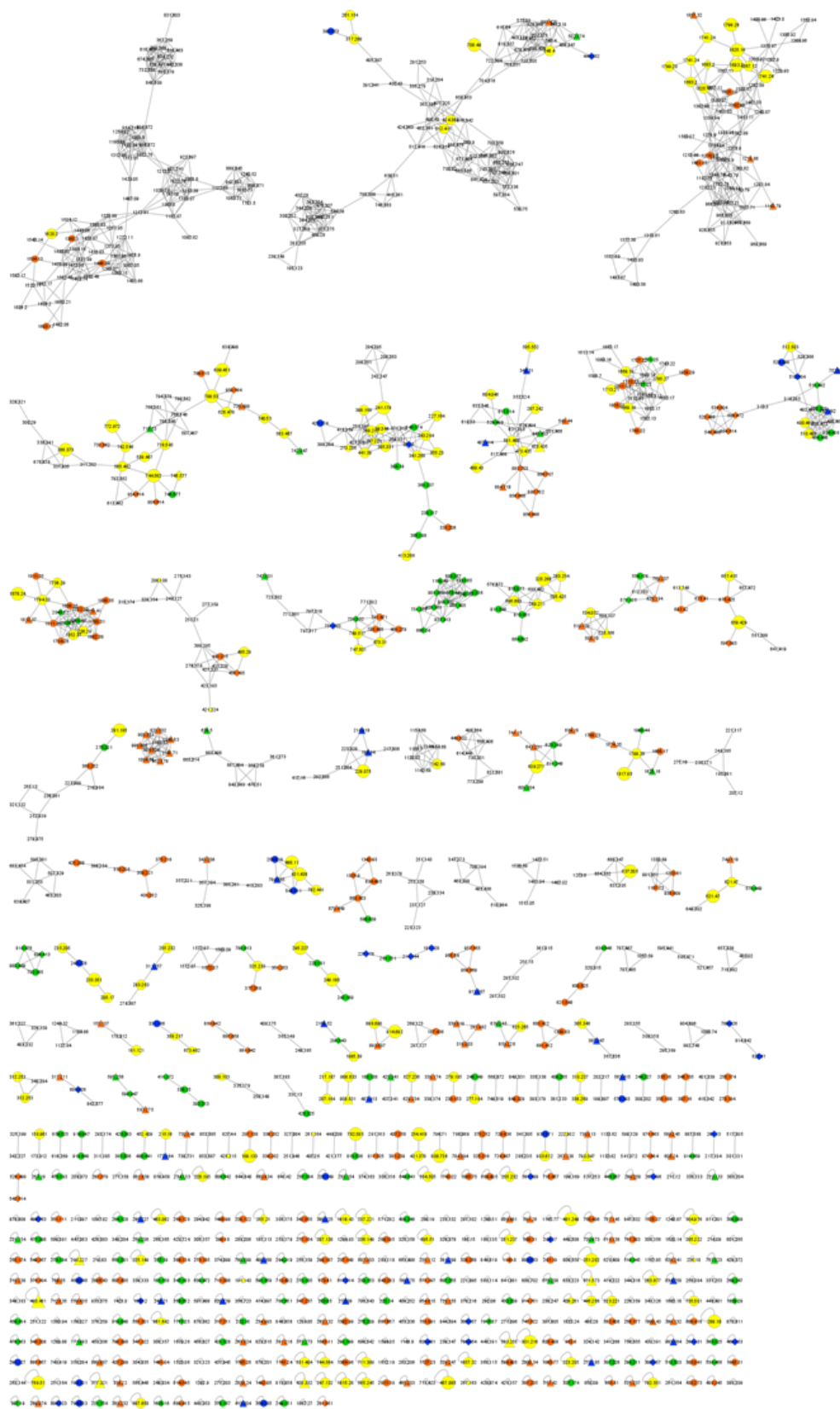
#### 4.2.5 pH

The pH network shows a total of 1197 features detected, with 48% coming from the media and solvent controls (**Figure 4.13**). This is much higher than for the salinity (28%), NaCl (32%), and nitrate (12.6%) networks and this may be due to degradation of extracts over time as these experiments were performed at a much earlier stage in the project. However, extracts were analysed together so comparisons across all strains and conditions could be made. With that being noted, from the networks of each individual strain, *P. tricornutum* still had the highest number of features detected with 335, followed by *D. primolecta* with 284, and *N. oculata* with 184 (**Appendix Fig A7, A11, A15**). As with salinity and NaCl concentrations, conditions that had the greatest impact on growth also had the greatest impact on metabolite production. For *D. primolecta* growth was increased under acidic conditions which resulted in 8.2% (23) of metabolites only being detected under this condition. However, this is negligible as 8% (22) metabolites were only produced under both control and basic pH conditions. Monopalmitolein and 9,12-octadecadien-1-ol were again the only metabolites identified through matching with the GNPS spectral libraries and was detected in all strains grown under all conditions. The effect is more pronounced in *P. tricornutum* as the 41% reduction of growth (**Figure 4. 3**) under basic conditions resulted in 11.8% (40) of metabolites only being detected in samples from this condition (**Figure 4.5**). Growth was also reduced under acidic pH but only by 14% which was coupled with 7.4% (25) of metabolites specifically detected under this condition.

As seen in the nitrate network, 25.7% of chemistry is shared between two or more of the strains. Although changes in nitrate concentration affected metabolites shared by all three strains, changes in pH affected metabolites that were strain specific. In fact, only one metabolite with a parent mass of 764.577  $m/z$  was detected in samples from all three strains in response to acidic conditions (**Figure 4.14 A**). Molecular families included metabolites that were strain-specific but only detected under a particular condition. For example, **Figure 4.14 B** shows a molecular family of 19 metabolites, six of which are present in control samples from all strains, one (473.435  $m/z$ ) which is only found in samples from all strains grown in basic conditions, and five metabolites that are strain-specific under basic conditions. Two of those metabolites were specific to *N. oculata* (487.414 and 349.31), another two were specific to *P.*



*tricornutum* (543.44, 884.712  $m/z$ ) and one for *D. primolecta* (445.403  $m/z$ ). Interestingly, this molecular family also contained a sub-cluster of five metabolites detected from *P. tricornutum* acidic samples and had higher molecular weights than the rest of the molecular family with a range 856.686-886.707  $m/z$ . There is the possibility that some of the features detected in these networks are actually degradation products due to the age of the extracts when analysis was performed. From the analysis provided here, pH stress results in minimal changes to metabolite production and these changes appear to be strain specific rather than shared mechanisms of adapting to pH stress.



● *Dunalialla primolecta*   
 ● *Nannochloropsis oculata*   
 ● *Phaeodactylum tricornutum*   
 ● Shared between strains  
 ◆ Low, pH 4    ● Control, pH 7.6    ▲ High, pH 10

**Figure 4.13** GNPS classical molecular network of MS/MS features detected from extracts of *Nannochloropsis oculata* (blue), *Dunaliella primolecta* (green), and *Phaeodactylum tricornutum* (orange) grown under varying pH: low = pH 4, diamond; control = pH 7.6, circle; high = pH 10, triangle). Features shared between conditions are presented as yellow circles.

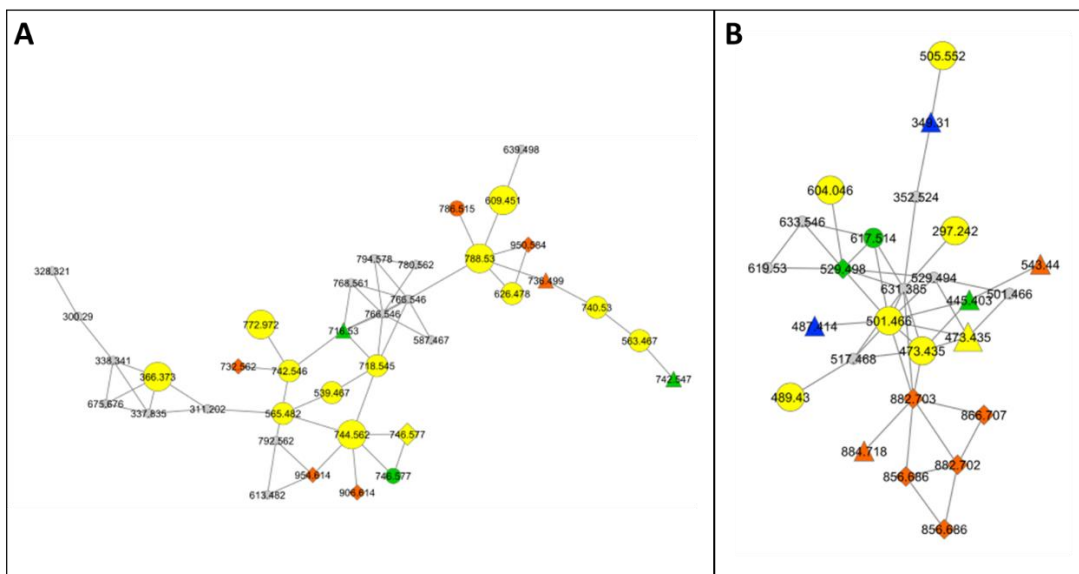


**Figure 4.14** Examples of molecular families detected under specific conditions (**A**) metabolites produced by all strains (yellow) under low pH (diamonds), (**B**) metabolites produced by all strains (yellow), *D. primolecta* (green), *N. oculata* (blue), or *P. tricornutum* (orange) under control (circles), low pH (diamonds), or high pH (triangles).

## 4.3 Discussion

### 4.3.1 Evaluating Stress in Microalgae

From this analysis, there was a general trend that a decrease in growth resulted in an increase in metabolite production. A study by Renaud and Parry observed that total lipid content increased with salinity (from 10-35 ppt) for *Nannochloropsis oculata*, with *cis*-9-hexadecanoic acid [16:1 (n-7)] increasing up to 24.1% of total fatty acids when grown under 35 ppt salinity. However, this was coupled with a significant reduction in the specific growth rate of *N. oculata* at 35 ppt.<sup>230</sup> Another study which used homology-based proteomics observed that under hypersaline (3 M NaCl) conditions, *Dunaliella primolecta* increases production of enzymes key to the Calvin cycle and regulating protein biosynthesis.<sup>231</sup> This is believed to contribute to the organism's tolerance of hypersaline environments. As such, this could explain the variation in metabolite profile under low or deplete NaCl conditions when these metabolic pathways may be suppressed in favour of other pathways that protect the cell from hyposaline conditions. In both of the above studies, hypersaline or high salinity were defined differently. In Renaud and Parry's study, 35 ppt is equivalent to 0.6 M NaCl whilst the proteomics study defined 3 M NaCl as hypersaline. This makes comparison of results across studies very difficult. It also brings into question whether "high" and "low" conditions could be strain specific. *Dunaliella* spp. are known to be halotolerant and *D. salina* is grown commercially in media with up to 5 M NaCl in order to maximise  $\beta$ -carotene production. On the other hand, 0.6 M NaCl was sufficient to cause stress to *N. oculata* resulting in reduced growth and increased total fatty acid content. To conflict with this result, the specific growth rate of our *N. oculata* CCAP 849/1 strain almost doubled when grown under 0.62 M NaCl. This variation in defining high versus low conditions, and the response to individual strains to these conditions makes systematic investigations difficult to achieve and comparison to literature almost impossible. Perhaps wider transcriptomic analyses could provide a solution to this problem and using microarrays would allow this to be done in a systematic and high-throughput way. Nagappan, *et al.*, published a thorough review on the physiological changes in microalgae in response to nitrogen starvation which included metabolomic, transcriptomic, proteomic, and biochemical analyses from across the literature. This review illustrated the complexity of this area of research as

nitrogen deprivation affected the production of chlorophyll, carbohydrates, carotenoids, lipids, and biomass, as well as altering the regulation of the Calvin cycle, glycolysis, the pentose phosphate pathway, and photosynthesis.<sup>232</sup> It is undeniable that the OSMAC approach is useful as it has led to the commercialisation of high-value products from microalgae, such as  $\beta$ -carotene and astaxanthin, which globally are worth US\$155 million (2015) and US\$770 (expected by 2024).<sup>213</sup> It is still unknown how these stressful culturing conditions stimulate the production of these specialised metabolites. There is also huge relevance to linking these findings to phenomena in their natural ecosystem, particularly since anthropogenic climate change continues to cause extreme weather events, eutrophication, ocean acidification, and global warming.<sup>233</sup>

#### **4.3.2 Using Metabolomics Tools to Investigate Stress in Microalgae**

The GNPS ecosystem allows networks of structurally similar metabolites to be created and screened against 33 libraries of compounds. One downfall of this screening is that GNPS contains libraries such as MassBank<sup>229</sup> and the National Institute of Standards and Technology (NIST) databases which also contain synthetic molecules not found in nature. Due to the paywall behind natural product libraries such as MarinLit,<sup>157</sup> AntiBase<sup>158</sup>, and Dictionary of Natural Products,<sup>159</sup> they are not included in the GNPS libraries. This lack of available natural product - and specifically algal natural products - libraries makes annotation and dereplication a frustrating and unfruitful endeavour. From the analysis above of 2284 metabolites only five metabolites were identified: monopalmitolein, 1-octadecanamine, hexanedioic acid, 13-keto-9Z,11E-octadecadienoic acid, and 9,12-octadecadien-1-ol. Gaining meaningful information from large MS2 datasets without the aid of dereplication requires the use of expensive instrumentation such as NMR and HPLC which give more detailed structural information and aid in isolation of metabolites, respectively. Even using NMR to guide the isolation of metabolites through HPLC can result in the isolation of known metabolites which is a huge loss of money and time when researchers are working within strict grant budgets and timeframes. One method to aid in the prioritisation of metabolites from molecular networking is coupling this mass spectral data with bioactivity data. The bioactivity-based molecular networking platform was developed in 2018 and led to the discovery of new antiviral metabolites from the well-studied

plant *Euphorbia dendroides*.<sup>234</sup> Since then, a database of *Euphorbia* metabolites was created and implemented into the MolNetEnhancer framework<sup>175</sup> through Mass2Motifs.<sup>174</sup> Another development from the GNPS ecosystem was the Mass Spectrometry Interactive Virtual Environment (MassIVE) data repository, an open-access platform for researchers to search other publicly available datasets, integrate annotations from these datasets, or conduct comparative analysis with their own datasets. Unfortunately, when searching this repository for microalgae, only one dataset can be found which belongs to our published work from **Chapter 3**. Searching for algae returns 27 datasets and there are 51 datasets on cyanobacteria. In comparison, there are 121 datasets on the genus *Streptomyces* ([www.massive.ucsd.edu](http://www.massive.ucsd.edu), accessed 09/09/2021).

## 5. Investigating the Effect of 405 nm Light on Microalgal Growth and Metabolite Production

---

### 5.1.1 Introduction

Photosynthesis is the process of utilising light, carbon dioxide, and water to produce oxygen and sugar that fuels the cell. It is a complex process that occurs in the thylakoid region of the chloroplasts where light is harvested by pigments and converted into chemical energy, namely the molecules ATP and NADPH. These molecules then enter the stroma and drive the reactions of the Calvin cycle where carbon dioxide binds to RuBisCo (Ribulose-1,5-bisphosphate carboxylase-oxygenase) and undergoes chemical transformation into sugars.<sup>235</sup> This entire process is made possible by the energy supplied through light, specifically light in photosynthetic active radiation (PAR) range of 400-700 nm.<sup>236</sup> Light of varying wavelengths are captured by pigments in the thylakoids and some common pigments and the wavelengths of light they absorb are given in **Table 5. 1**. Chlorophyll *a* is found in all photosynthetic organisms and has peak absorption at 663 nm which is higher than both chlorophyll *b* (648 nm), and chlorophyll *c* (588 nm).<sup>237, 238</sup> Most carotenoids have an absorption peak between 400 and 500 nm.<sup>237</sup> Pigments are selective in the range of light they can harvest as each wavelength has a frequency and energy associated with it. These parameters are inversely proportional to one another e.g., violet light with a wavelength of 400 nm has a frequency of  $7.50 \times 10^{14}$  Hz and 3.10 eV of energy compared to red light with a longer wavelength of 700 nm but a lower frequency ( $4.29 \times 10^{14}$  Hz) and energy (1.77 eV) value.



**Table 5. 1** List of pigments commonly found in microalgae and the wavelengths at which their absorption peaks.

<b>Pigment</b>	<b>Lambda Max (nm)</b>
Chlorophyll a <sup>237</sup>	430, 663
Chlorophyll b <sup>237</sup>	463, 648
Chlorophyll c <sup>238</sup>	419, 568, 588
$\beta$ -carotene <sup>237</sup>	449, 473
Violaxanthin <sup>237</sup>	417, 440, 469
Fucoxanthin <sup>239</sup>	445, 663, 750
Lutein <sup>237</sup>	423, 445, 474
Zeaxanthin <sup>237</sup>	452, 478
Phycoerythrin <sup>240</sup>	498, 539, 565
Diadinoxanthin <sup>241</sup>	440, 462, 490
Diatoxanthin <sup>241</sup>	453, 483
Cryptoxanthin <sup>242</sup>	448

Photosynthesis is the basis of primary metabolism in plants and algae. Therefore, light of varying intensity, wavelength, and photoperiod greatly influences the growth and metabolism of photosynthetic organisms. For example, Xu and Harvey cultured several subspecies of *D. salina* under high light intensity (1000  $\mu\text{mol photons/m}^2/\text{s}$ ) blue and white LED and reported that whilst growth was unaffected, chlorophyll content was higher under blue light but in all strains, except one, carotenoid production was significantly lower.<sup>132</sup> For *Nannochloropsis* sp. although growth (specific growth rate,  $\mu$ ) was lower under blue light (400-525 nm), the biomass productivity per number of photons supplied was 32% higher compared to white light and lipid content increased from 50% to 60% of organic weight. It was suspected this was due to the enhanced activity of enzymes such as RuBisCo.<sup>243</sup> On the other hand, blue light irradiance caused the specific growth rate of the Rhodophyte *Porphyridium cruentum* to double to 0.44 and this was coupled with increased polysaccharide production at the same maximum cell density of  $4 \times 10^9$  cells/L.<sup>191</sup>

As well as blue light having promising effects on growth and metabolite production on microalgae, research into narrowband wavelengths has led to the discovery that 405 nm light has bactericidal effects against a range of Gram-positive and Gram-negative bacteria.<sup>136</sup> This is useful for industrial microalgal culturing as bacterial communities often co-exist with microalgal cultures and grow at much faster rates which can out-compete the microalgal cultures for nutrients. Preliminary tests by Xanthella Ltd. (Oban, Scotland, UK) demonstrated that cultivating microalgae under 405 nm illumination keeps bacterial cell counts at a minimum without affecting the growth of the eukaryotic microalga *Chlorella sorokiniana* (not published). It has also been shown that culturing *Nannochloropsis oculata* and *Tetraselmis chuii* under LEDs emitting 390-450 nm wavelengths increased nutrient uptake and protein production compared to white light. Therefore, growing microalgae under 405 nm light at an industrial scale may be advantageous.<sup>137</sup>

To evaluate the effect of narrowband 405 nm light, one litre MicroPharos™ photobioreactors designed and built by Xanthella Ltd. (Oban, Scotland, UK) were used. Algae are often grown in bags, flasks, or carboys for research purposes and whilst these are efficient methods, they lack the same control that a bioreactor allows. For example, bags, flasks, and carboys are often kept in temperature-controlled rooms

where temperature and light may be interrupted by opening and closing of the door. With photobioreactors, the culture is closed off from the outside environment with probes monitoring the temperature of the culture (rather than the room the culture is in) and illumination only coming from the light tiles attached to the photobioreactor.<sup>244, 245, 246</sup> It is important to note that the frequency and energy output from broad spectrum white light and narrowband 405nm light differs considerably and therefore an equal current of light was provided for cultures grown under both light conditions.

Along with assessing growth of cultures under white and 405 nm LED illumination, we also measured the quantum efficiency of Photosystem II. This is achieved through calculating  $F_v/F_m$ , where  $F_v$  is the variable fluorescence (maximum fluorescence minus minimum fluorescence) and  $F_m$  is the maximum fluorescence. This ratio is a good indication of stress to the photosynthetic machinery as when the chloroplast experiences light stress, it closes more reaction centres and light energy must be dissipated in a non-photosynthetic process, such as fluorescence or heat.<sup>247</sup> Therefore, stress lowers the  $F_v/F_m$  value which means the quantum efficiency of Photosystem II is reduced. For example, iron supplementation in parts of the Southern Ocean that were depleted in iron led to increased  $F_v/F_m$  values of the phytoplankton community from 0.23 to 0.39 in 5 days.<sup>248</sup> For these experiments, cultures did not undergo dark adaptation before measurements were taken as reaction centres can open rapidly when light stress is removed and therefore  $F_v'/F_m'$  was measured.

In order to assess the impact of light on metabolite production, cultures from both conditions (either 405 nm or white light only) were extracted and subjected to LC-MS/MS analysis. Crude extracts contain a complex mixture of metabolites and therefore bioactive metabolites may exist in such a low relative quantity that its activity is masked. Conversely, the synergistic effect of multiple metabolites within an extract can elicit an inhibitory effect in bioassays. When these metabolites are then separated in an attempt to isolate a pure metabolite, the observed bioactivity may be lost.<sup>234</sup> Li, *et al.* used bioactivity-guided fractionation of an extract from the cyanobacterium *Derbsia* sp.. After isolating the suspected bioactive metabolite, pogoamide A, they discovered that the pure metabolite did not show inhibition in their calcium oscillation assay.<sup>155</sup> For these reasons, fractionation of crude extracts is an important part of the natural product and drug discovery process. This is achieved using a variety of

separation and chromatographic techniques, such as liquid-liquid extraction (LLE), solid phase extraction (SPE), vacuum liquid chromatography (VLC), and pressurised liquid chromatography (low – LPLC, medium – MPLC, high -HPLC, ultra-high – UHPLC).<sup>149</sup>

### 5.1.2 Aims and Objectives

The impact of 405 nm light on microalgal strains was assessed by monitoring growth, stress to the Photosystem II machinery, and comparative metabolomics methodology. Four strains, each belonging to a different phylum, were assessed to compare trends in growth and metabolite production across taxonomic boundaries. It was not expected that there would be a mutual response by all four strains, but perhaps specific metabolites would be affected by the narrowband wavelength of light. It was hypothesised that discovery of high value metabolites, such as anti-microbial metabolites, could offset the high cost required to cultivate microalgae under 405 nm which has the additional benefit of reduced contamination.

Objective 1: To evaluate the effect of narrowband 405 nm LED illumination on the growth of *Nannochloropsis oculata* CCAP 849/1, *Dunaliella primolecta* CCAP 11/34, *Phaeodactylum tricornutum* CCAP 1055/15, and *Porphyridium cruentum* UTEX 161.

- Compare growth of strains under 405 nm and white LED illumination.
- Determine growth rates under both light conditions.
- Measure quantum efficiency of Photosystem II under both light conditions.

Objective 2: To investigate whether narrowband 405 nm LED elicits the production of antimicrobial metabolites.

- Analyse metabolite extracts using multivariate statistics and molecular networking.
- Fractionate extracts to increase the relative concentration of individual metabolites.
- Test antimicrobial activity of metabolite extracts and fractions.

## 5.2 Results

### 5.2.1 Effect of 405 nm on Growth and Photosynthetic Efficiency

Four strains of microalgae were grown in triplicate in MicroPharos™ photobioreactors under white and 405 nm illumination. The average starting concentration for each strain was  $1.9 \times 10^6$  cells/mL for *Nannochloropsis oculata*,  $4.5 \times 10^4$  cells/mL for *Dunaliella primolecta*,  $3.8 \times 10^5$  cells/mL for *Phaeodactylum tricornutum*, and  $5.3 \times 10^4$  cells/mL for *Porphyridium cruentum*. The growth curves showed great variation amongst the four strains with a lag phase of 1-9 days followed by a linear phase lasting from 10-27 days. Overall culturing times also varied from 14 days for *N. oculata* to 31 days for *D. primolecta*.

*N. oculata* did not show any significant changes in growth when cultured under white and 405 nm light (**Figure 5.1, Figure 5.5**), although growth rate and final cell concentration were both lower for 405 nm cultures. Even though the growth curves ended at a similar cell concentration, there is a clear difference in the steepness of the linear portion of the curve, which is confirmed by the reduced specific growth rate of  $0.24 \text{ day}^{-1}$  under 405 nm light compared to  $0.34 \text{ day}^{-1}$  under white light (**Figure 5.5, Appendix Table A4**). The growth curves and growth rates for *P. tricornutum* (**Figure 5.3**) were very similar to that of *N. oculata*. Both strains had a short lag time that was not observable in the growth curves and reached stationary phase at day 14 and day 15, respectively. The shape of both sets of curves were very similar to one another, except for the steepness of the curves, which resulted in specific growth rates of  $0.32 \text{ day}^{-1}$  under white light and  $0.30 \text{ day}^{-1}$  under 405 nm light (**Figure 5.5, Appendix Table A4**). *P. tricornutum* also had the most consistent growth across all three replicates with a standard error of the mean (SEM) of 0.003 for cultures grown under white light and 0.008 for those grown under 405 nm light (**Appendix Table A4**). This certainly was not the case for *D. primolecta* and *P. cruentum* which showed fluctuations throughout the period of growth and amongst replicates. *D. primolecta* (**Figure 5.2**) under 405 nm light did not begin to grow until after day nine, suggesting that the strain had to adapt to utilise this wavelength of light. Meanwhile, the cell concentration of *P. cruentum* under 405 nm light did not increase at all during the culturing period. Cell counts for *D. primolecta* were inconsistent throughout the culturing period which could only be attributed to sampling variation as cells sunk to

the bottom of the reactor and had to be manually agitated before samples were taken. However, the overall trend of reduced growth under 405 nm light is still clear. In fact, *D. primolecta* showed a 50% reduction in growth under 405 nm light compared to white light. The red microalga (Rhodophyte) *P. cruentum* did not grow at all under 405 nm illumination (**Figure 5.4**). However, this may be due to low light intensity rather than the wavelength of light. Cultures were inoculated at a starting concentration of  $5.3 \times 10^4$  cells/mL and light input was kept low at 5 mA ( $13.3 \mu\text{mol photons/m}^2/\text{s}$  for white light and  $3.8 \mu\text{mol photons/m}^2/\text{s}$  for 405 nm light). When grown at higher light intensities, cultures aggregated and sunk to the bottom of the photobioreactor and adjusting the culture medium and pH did not reduce this phenomenon. It was then postulated that light intensity was causing photodamage. Cultures under low intensity white light grew well to a maximum density of  $1.4\text{-}1.9 \times 10^6$  cells/mL but did not grow under the low intensity 405 nm light. There were large inconsistencies in cell counts throughout the culturing period which may be due to the aggregation of cells caused by the excretion of exopolysaccharides, although this was only observable in a couple of instances when cells were viewed under the microscope. There was also a variation in when cultures reached stationary phase from day 19 for replicate one, day 18 for replicate two, and day 21 for replicate three. A possible explanation for this is the relative age of the stock cultured used to inoculate the photobioreactors. *P. cruentum* stock cultures grew very slowly and so the same stock culture was used to inoculate each replicate of the photobioreactor. This meant that the culture used to inoculate replicate three was older than the culture used to inoculate replicate one. The comparative age of the stock culture may account for the longer period required for it to reach stationary phase.

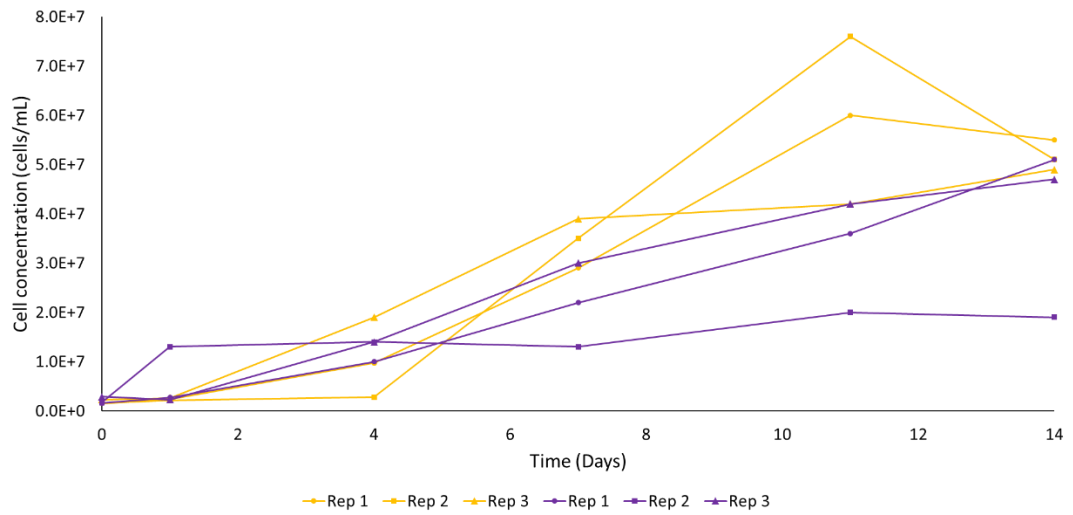


**Figure 5.1** Growth curves for *Nannochloropsis oculata* CCAP 849/1 grown in triplicate under white LED illumination (yellow) and 405 nm LED illumination (purple) in 1 L MicroPharos™ Photobioreactors. Replicates are indicated by the shape of datapoints (replicate 1, circles; replicate 2, squares; replicate 3, triangles).

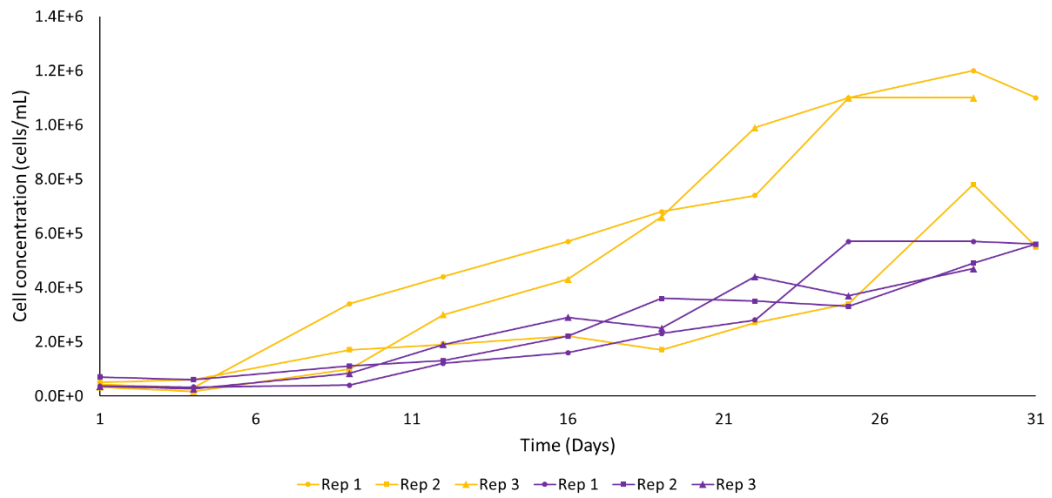


**Figure 5.2** Growth curves for *Dunaliella primolecta* CCAP 11/34 grown in triplicate under white LED illumination (yellow) and 405 nm LED illumination (purple) in 1 L MicroPharos™ Photobioreactors. Replicates are indicated by the shape of datapoints (replicate 1, circles; replicate 2, squares; replicate 3, triangles).



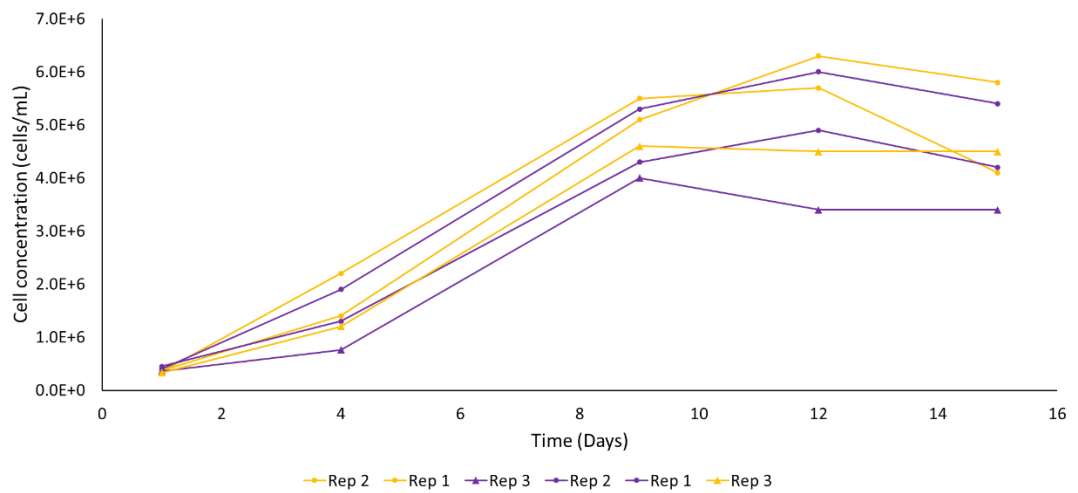


**Figure 5.3** Growth curves for *Phaeodactylum tricornutum* CCAP 1055/15 grown in triplicate under white LED illumination (yellow) and 405 nm LED illumination (purple) in 1 L MicroPharos™ Photobioreactors. Replicates are indicated by the shape of datapoints (replicate 1, circles; replicate 2, squares; replicate 3, triangles).

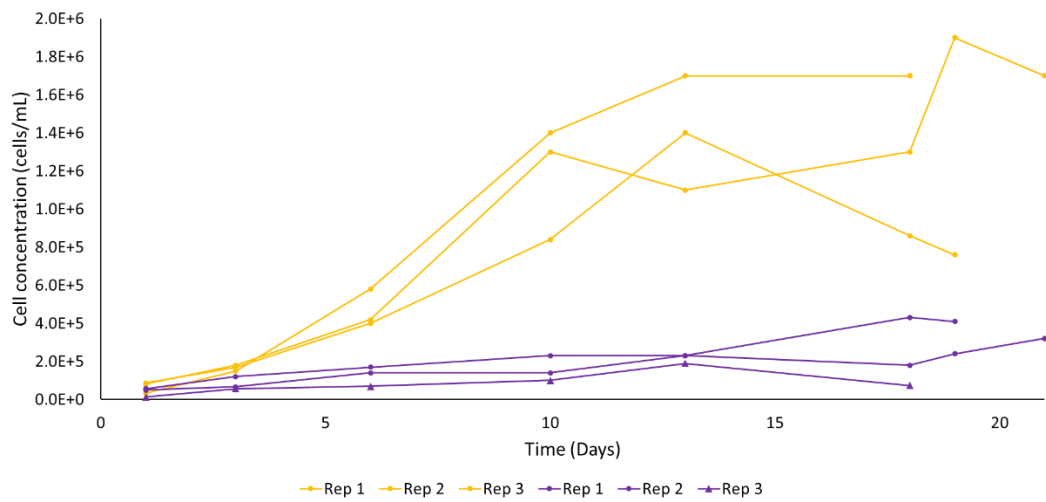


**Figure 5.4** Growth curves for *Porphyridium cruentum* UTEX 161 grown in triplicate under white LED illumination (yellow) and 405 nm LED illumination (purple) in 1 L MicroPharos Photobioreactors. Replicates are indicated by the shape of datapoints (replicate 1, circles; replicate 2, squares; replicate 3, triangles).

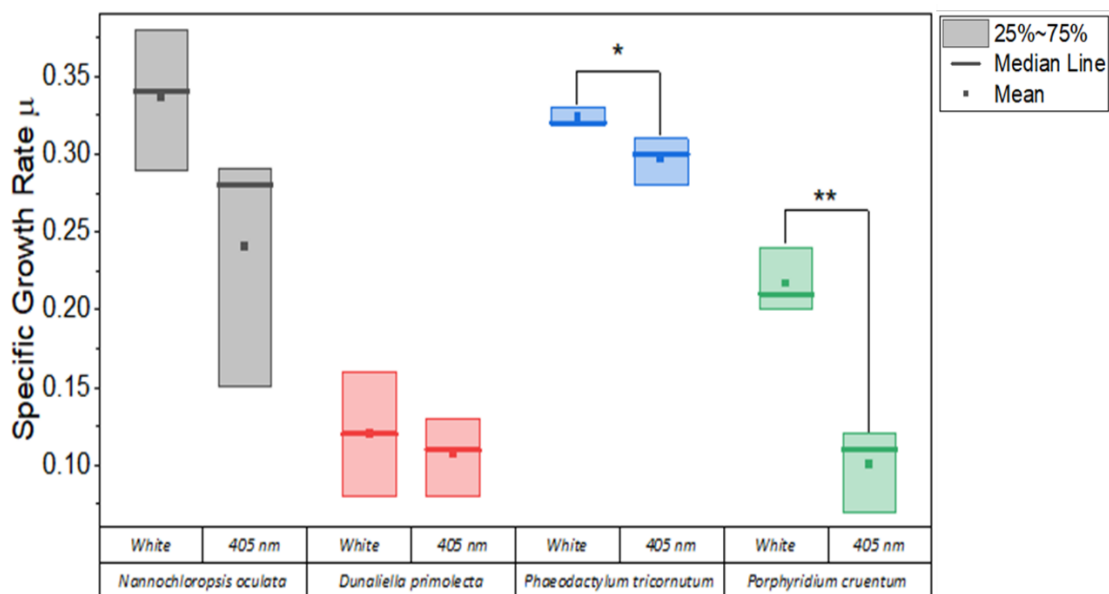


**Figure 5.5** Boxplots showing the specific growth rates of *Nannochloropsis oculata* (grey), *Dunaliella primolecta* (red), *Phaeodactylum tricornutum* (blue) and *Porphyridium cruentum* (green) grown in triplicate under white and 405 nm LED illumination. Coloured boxes show 25-75 percentile, the bold line represents the median value, and the bold square represents the mean value. *P*-values are represented as \* ( $\leq 0.05$ ), \*\* ( $\leq 0.01$ ), or \*\*\* ( $\leq 0.005$ ).

Whilst growth and visual monitoring are methods of measuring health within the culture, fluorometry offers a more detailed insight into the cells' ability to perform photosynthesis, a critical process in autotrophic organisms.  $F_v/F_m$  (and  $F_v'/F_m'$ ) values of healthy microalgal cells typically vary between 0.5-0.8 but this depends on depth, temperature, and other abiotic factors.<sup>249, 250, 251</sup> Most importantly, in this study, is how the  $F_v'/F_m'$  values between white LED and 405 nm LED compare to one another.  $F_v'/F_m'$  were measured for each strain after seven days of culturing (**Table 5.2**). This was done at the same time to avoid diurnal fluctuations in photosynthetic activity. Interestingly, the  $F_v'/F_m'$  values in all cases are higher for the 405 nm cultures compared to the white light control. Although the growth of *P. cruentum* and *P. tricornutum* was significantly reduced under 405 nm light, the  $F_v/F_m$  values increased by 10% and 5%, respectively. For *D. primolecta*, the growth curves were similar for both 405 nm and white light with final cell concentrations of  $5.6 \times 10^5$  and  $8.25 \times 10^5$  cells/mL, respectively. This corroborated well with  $F_v'/F_m'$  which showed a 2% increase between 405 nm and white light. Whilst growth and fluorometry measurements give information on cultures health, growth looks at the overall population, whilst fluorometry focuses on the health of individual cells within the culture. Light intensity was maintained at a low level (5-10 mA, 15-30  $\mu\text{mol}/\text{m}^2/\text{s}$  PPFD for white LED and 4-8  $\mu\text{mol}/\text{m}^2/\text{s}$  for 405 nm LED) throughout culturing which may also contribute to the low level of light stress experienced by each of the strains.

**Table 5. 2** Average Fv'/Fm' values for *Nannochloropsis oculata*, *Dunaliella primolecta*, *Phaeodactylum tricornutum*, and *Porphyridium cruentum* grown in triplicate under white and 405 nm LED illumination. Measured using a Fast Repetition Rate fluorometer (Chelsea Technologies) with 450, 530, and 624 nm excitation wavelengths.

<b>Strain</b>	<b>White LED</b>	<b>405 nm LED</b>	<b>p-value</b>
<i>Phaeodactylum tricornutum</i> CCAP 1055/15	0.551± 0.003	0.581± 0.001	5.2x10 <sup>-5</sup>
<i>Dunaliella primolecta</i> CCAP 11/34	0.562± 0.004	0.571± 0.007	0.13
<i>Porphyridium cruentum</i> UTEX 161	0.513± 0.0006	0.570± 0.002	1.37x10 <sup>-6</sup>
<i>Nannochloropsis oculata</i> CCAP 849/1	0.495± 0.007	0.531± 0.002	7.4x10 <sup>-4</sup>

### 5.2.2 Fractionation and Bioactivity Screening of Extracts

Metabolite extracts mass of a minimum of 20 mg was required in order to fractionate extracts using SPE. Only *Phaeodactylum tricornutum* and *Nannochloropsis oculata* were of sufficient extract mass for fractionation (**Figure 5.6**). Four metabolite fractions were produced for each extract; water (discarded), acetonitrile, methanol, and ethyl acetate. As expected, the least polar ethyl acetate fraction had the greatest mass of metabolites (2.5-5 mg). However, for both *P. tricornutum* and *N. oculata*, the white light fractions had a greater metabolite mass (3.1 mg and 5 mg for white light, and 2.5 mg and 3.5 mg for 405 nm light, respectively). Conversely, the acetonitrile metabolite fractions originating from 405 nm light extracts had a greater mass which may indicate that 405 nm light stimulated the production of more polar metabolites in both strains. The crude extracts from all four strains, as well as the fractions from *P. tricornutum* and *N. oculata* were screened for antimicrobial activity at 50 µg/mL. The extracts and fractions were tested against *Bacillus subtilis*, *Escherichia coli*, *Staphylococcus aureus*, *Klebsiella pneumoniae*, *Acinetobacter baumannii*, *Pseudomonas aeruginosa*, *Enterococcus faecalis*, *Candida albican*, and *Rhizopus oryzae*. No inhibitory activity was observed for the extracts or fractions tested at these concentrations.

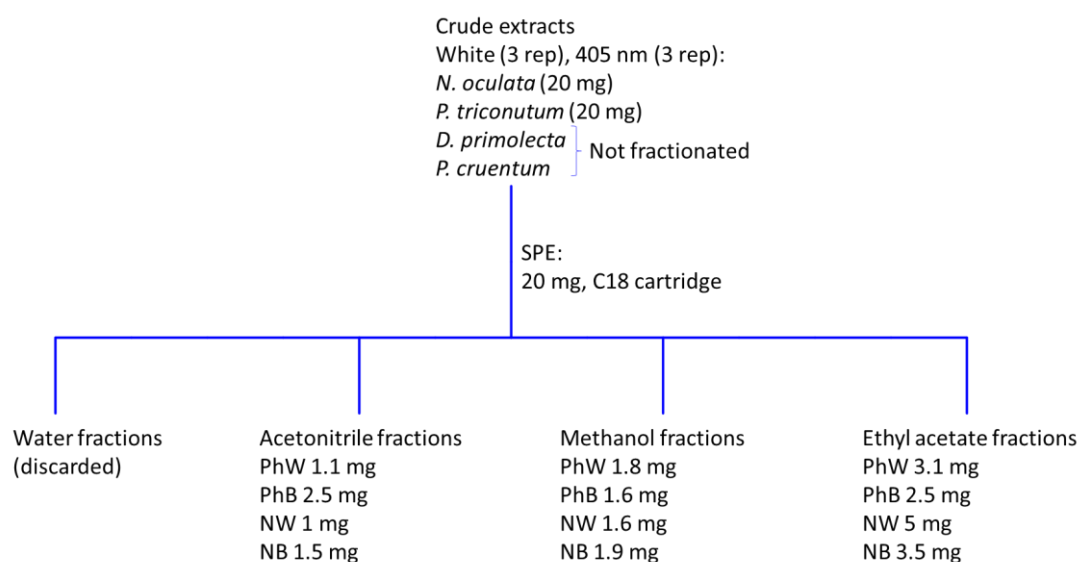


**Figure 5.6** Masses of metabolite fractions produced using SPE. Each strain had 3 crude metabolite extracts from white LED cultures and 3 crude metabolite extracts from 405 nm LED cultures and the average mass of metabolite fractions are given (PhW = *P. tricornutum* white light, PhB = *P. tricornutum* 405 nm light, NW = *N. oculata* white light, NB = *N. oculata* 405 nm light). Only metabolite extracts from *N. oculata* and *P. tricornutum* were fractionated using SPE.

### 5.2.3 Chemical Analysis of Extracts from White and 405 nm LED Light

LC-MS/MS data was generated for the crude extracts from all four strains and analysed using multivariate statistics and GNPS classical molecular networking. The PCA (**Figure 5.7**) shows good repeatability amongst replicates as each set of replicates cluster closely together in the scores plot. The only exception is replicate three from *P. tricornutum* 405 nm light which has a chemical profile similar to that of the f/2 medium which suggests insufficient extraction of metabolites, although there is no obvious reason why this may have occurred. Generally, each strain occupies a distinct area of chemical space which further supports the argument that there is no core microalgal metabolome, as discussed in **chapter 3**. There is, however, overlap between the 95% confidence limits of the chemical profiles for the diatom *P. tricornutum* and the Rhodophyte *P. cruentum*. This is surprising as our previous analysis showed that diatoms and Rhodophytes had distinct chemical profiles (**Chapter 3.2.3**). However, neither *Phaeodactylum* nor *Porphyridium* strains were included in that analysis which illustrates the need for large datasets when exploring metabolomic trends across taxonomic boundaries. The chemical profile of *N. oculata* extracts diverge from the other species, however this variation is mostly along the principal component 2 (PC2) axis which only accounts for 7.7% of the variation between samples. In this instance, the loadings plot (**Figure 5.7 (B)**) is not particularly informative as it shows the distribution of metabolites across species rather than across conditions. However, classical molecular networking was used to gain greater insight into the effect of 405 nm light on metabolite production in these four strains.



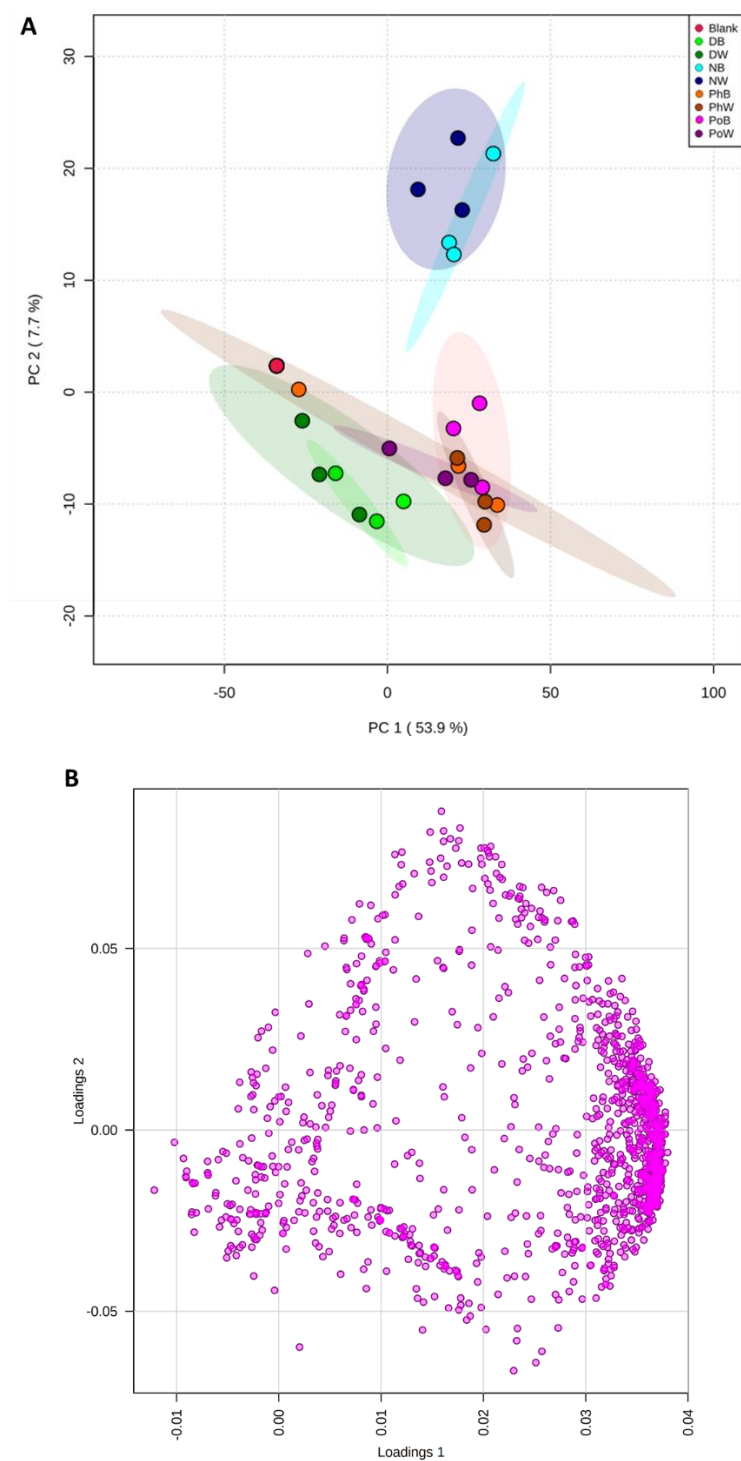


**Figure 5.7** Principal Component Analysis (PCA) of four strains grown under white and 405 nm light. **(A)** Scores plot: blank = media control, red; DB = *D. primolecta* 405 nm light, light green; DW = *D. primolecta* white light, dark green; NB = *N. oculata* 405 nm light, cyan; NW = *N. oculata* white light, navy; PhB = *P. tricornutum* 405 nm light, orange; PhW = *P. tricornutum* white light, brown; PoB = *P. cruentum* 405 nm light, pink; PoW = *P. cruentum* white light, purple. **(B)** Loadings plot showing distribution of metabolites across samples.

A total of 3252 features were detected in the molecular network (**Figure 5.8**) with 2.4% constituting metabolites from the f/2 medium control and only 3.1% (100 features) shared between all strains grown under both conditions. Overall, *P. tricornutum* (diatom) had the highest number of metabolites with a total of 2550 features detected. This was closely followed by *N. oculata* (Ochrophyte) with 2349 features, *P. cruentum* (Rhodophyte) with 1934 features, and finally *D. primolecta* (Chlorophyte) with 1139. This agrees well with our previous analysis as diatoms and Ochrophytes had more metabolites detected compared to Rhodophytes and Chlorophytes.<sup>252</sup>

Denoting white LED light as the control, it was considered that metabolites found in extracts from cultures grown under white LED light and not in the 405 nm light condition were absent due to the light stress. The effect of the 405 nm light condition was considered to be the absence of metabolites only found in white LED conditions plus the presence of metabolites only found in the 405 nm LED condition. In that respect, *N. oculata* was most affected from culturing under 405 nm light, despite the similarity in growth across both conditions. A staggering 24.6% of metabolites produced by *N. oculata* were affected by light stress with the production of 363 (15.5%) metabolites (**Figure 5.9**) decreased to the point of no detection and 216 (9.1%) metabolites only detected when the strain was grown under 405 nm light. It was expected that growth under 405 nm light would alter the metabolism of *N. oculata* however, it was also hypothesised that this light stress would dysregulate the production of certain classes of metabolites. This is based on the biosynthetic machinery affected as a result of the narrowband wavelength of light used for growth. Whilst this is supported in some cases by the presence or absence of multiple metabolites belonging to the same molecular family, the effect on metabolite production is more widespread than initially anticipated. The example given in **Figure 5.10 (A)** shows a molecular family where nine of the metabolites (with a range of 394.257-573.451  $m/z$ ) were only detected when *N. oculata* was grown under 405 nm light. These metabolites, along with one other metabolite (425.251  $m/z$ ) only found in the white light condition, are all closely related structurally as indicated by the thickness of the edges connecting the nodes (edge thickness is correlated to the cosine score of similarity). This suggests that 405 nm light has a more nuanced effect rather

than suppressing or triggering entire metabolic pathways. This is further evidenced in **Figure 5.10 (C)** where some metabolites from *P. tricornutum* in the cluster are specific to 405 nm samples and others are specific to white light samples. One such cluster contains four metabolites (352.846, 338.921, 414.878, and 456.105  $m/z$ ) only detected in 405 nm samples and three more metabolites (281.108, 340.933, and 400.828  $m/z$ ) that are connected by thick edges, indicating a high level of structural similarity (cosine  $\geq 0.7$ ). Interestingly, an opposite trend can be observed for *D. primolecta* and *P. cruentum*. Here, the metabolites detected in white light extracts are mostly found in molecular families that do not contain metabolites specific to 405 nm samples. In fact, one cluster containing four high molecular weight metabolites (951.567-2834.45  $m/z$ , **Figure 5.10 (D)**) from *P. cruentum* were only detected in white light samples.

Looking at the overall distribution of metabolites across species and conditions (

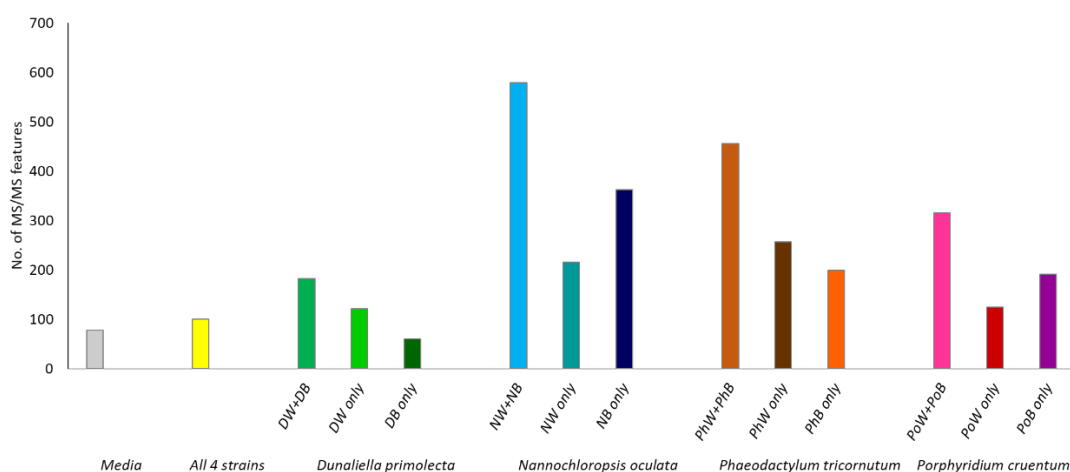


**Figure 5.9)** it can be concluded that 405 nm light affects the metabolism of each strain differently. This is expected as each strain has a varied light-harvesting pigment composition. For *D. primolecta*, *P. tricornutum*, and *N. oculata*, a similar percentage of metabolites were only found in white light samples (10.7%, 10.2%, and 9.2%, respectively). This was considerably lower at 6.5% for *P. cruentum* samples. Growth under 405 nm light resulted in extracts with a higher number of metabolites for *N. oculata* (363, 15.4%) and *P. cruentum* (191, 9.1%) when compared to metabolites only detected in white light samples. The opposite is true for *D. primolecta* where only 5.3% of metabolites are specific to 405 nm samples and *P. tricornutum* with 7.8%.

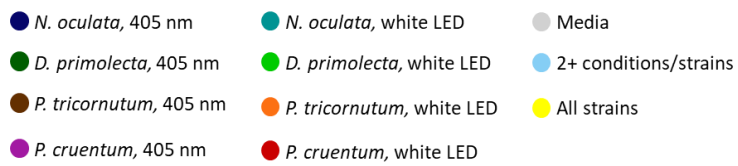
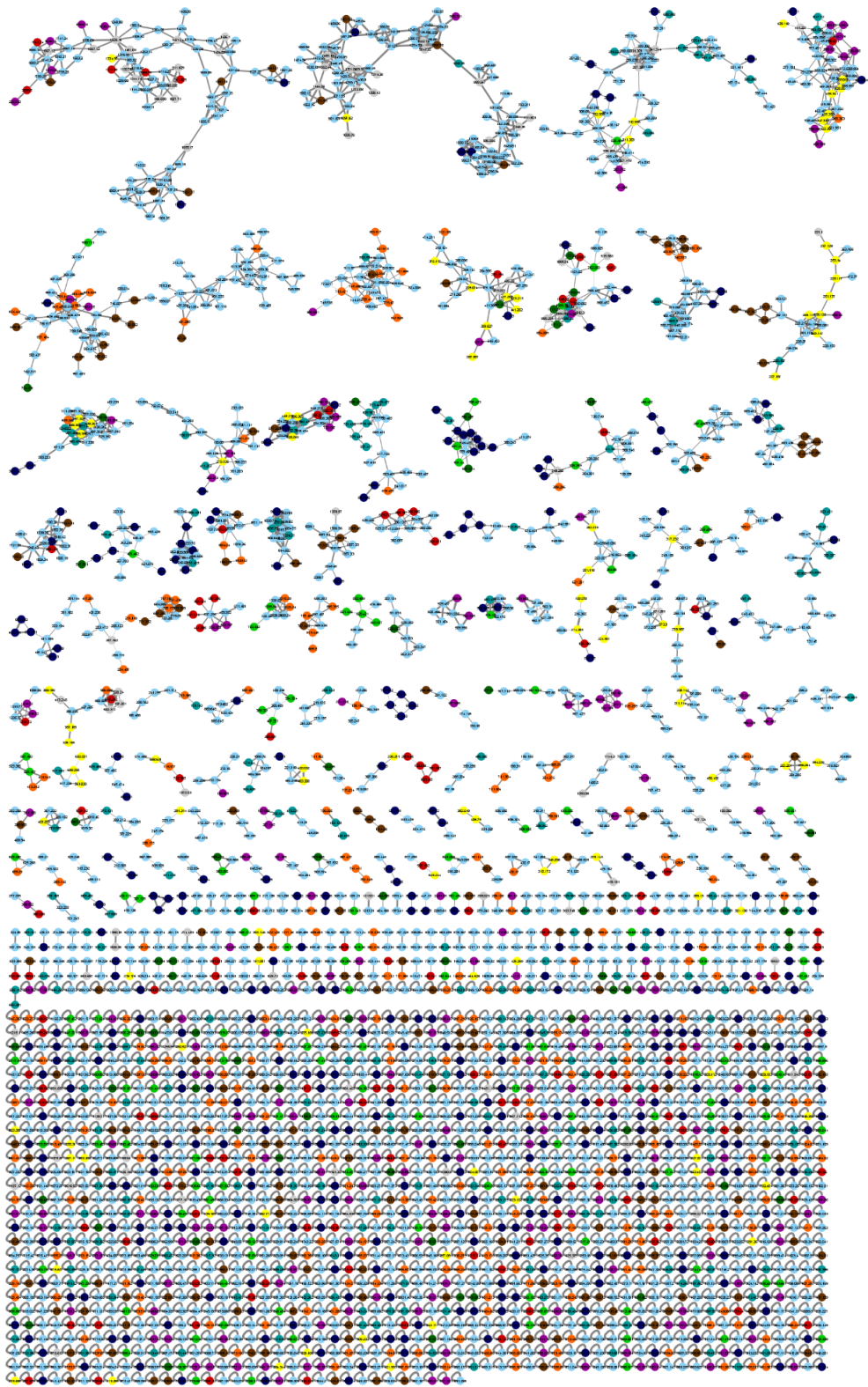


**Figure 5.8** Classical Molecular Network of four strains grown under white LED and 405 nm light conditions; *Nannochloropsis oculata* (405 nm, navy; white LED, blue), *Dunaliella primolecta* (405 nm dark green; white LED, green), *Phaeodactylum tricornerutum* (405 nm, brown; white LED, orange), and *Porphyridium cruentum* (405 nm, purple; white LED, red). Features from f/2 medium and solvents blanks are depicted in grey, features shared across multiple strains are in light blue, and features shared across all four strains are in yellow.

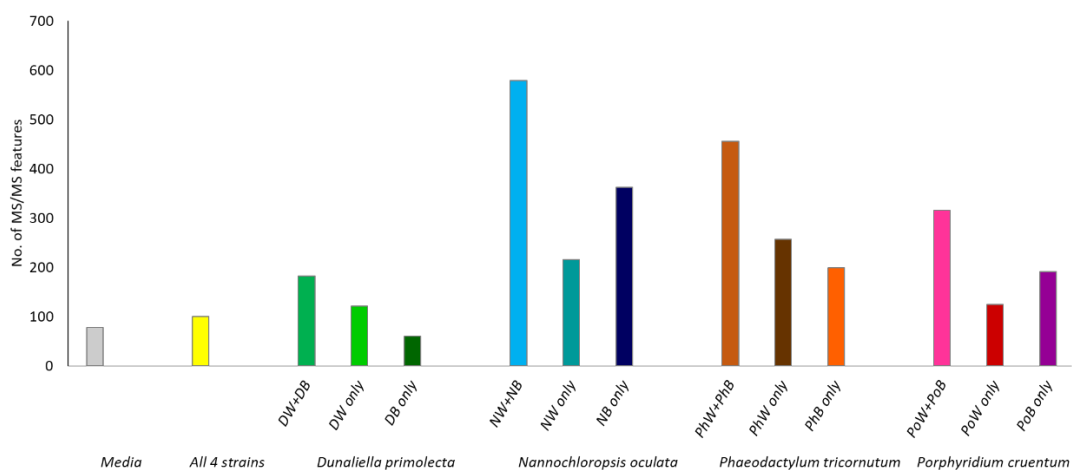


**Figure 5.9** Bar chart illustrating the distribution of metabolites across all conditions.

Features detected in f/2 medium and solvent controls are grey whilst features depicted in yellow are shared across all strains. Each cluster thereafter represents features detected only from that strain (DW+DB, NW+NB, PhW+PhB, PoW+PoB), features only detected from the white LED condition (DW, NW, PhW, PoW), and features only detected in the 405 nm light condition (DB, NB, PhB, PoB).

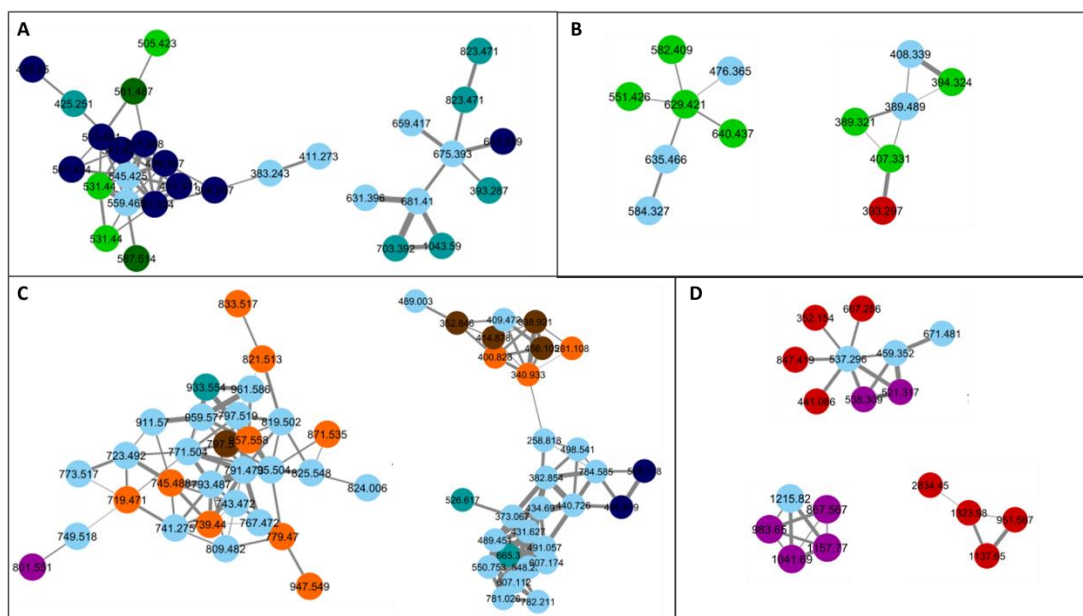


**Figure 5.10** Examples of multiple metabolites from a molecular family affected by growth under 405 nm light for **(A)** *Nannochloropsis oculata*, **(B)** *Dunaliella primolecta*, **(C)** *Phaeodactylum tricornutum*, and **(D)** *Porphyridium cruentum*. Colour scheme is the same as Figure 5.8.

## 5.3 Discussion

### 5.3.1 Effect of 405 nm Illumination on Microalgal Growth

Overall, the four strains of microalgae did not grow as well under 405 nm light compared with white LED illumination, but the extent of the light stress varied considerably from one strain to another. Ge, *et al.*, reported that maximum dry weight for *Chlorella vulgaris* was achieved under red light (231.74 mg/L) compared to white light (210.53 mg/L) and blue light (96.67 mg/L).<sup>253</sup> Another study found that a combination of blue and red light was required to achieve maximum growth for *Chlorella* sp.<sup>254</sup> Furthermore, an in-depth analysis by Baer, *et al.*, demonstrated that light conditions must be optimised for each individual strain to achieve maximum growth. For example, a maximum biomass of 312 mg/L/d for *Porphyridium purpureum* was achieved with the light regimen of 40:40:20 of red:green:blue illumination with growth decreasing as blue light increased beyond 20%. This is in good agreement with our findings as *P. cruentum* did not grow at all under 405 nm illumination. This strain specificity could be due to pigment composition and/or genomic properties of the strain. For example, the main pigments found in *Nannochloropsis* spp. are chlorophyll a,  $\beta$ -carotene, and violaxanthin.<sup>255</sup> Although most carotenoids absorb light in the 400-500 nm range, violaxanthin in particular has an absorption peak at 417 nm which may be why *N. oculata* can grow well under narrowband 405 nm light. In addition, genomic analysis of the closely related *N. oceanica* CCMP1779 shows at least 19 light harvesting complex (LHC) proteins belonging to three different subfamilies; fucoxanthin-chlorophyll protein-like LHC, red algal-like LHC, and stress-responsive LHC.<sup>256</sup> A number of orthologs of blue light sensing proteins similar to the cryptochrome photolyase family protein 1 (CPF1) found in diatoms, were also found in the *N. oceanica* genome.<sup>256</sup> This protein family may also explain why the growth curves of *Phaeodactylum tricorutum* were similar under 405 nm and white light, as the PtCPF1 protein plays a role in blue light-regulated gene expression and ultraviolet DNA damage.<sup>257</sup> The variation in light intensity, light quality, and photoperiod used in individual studies makes comparing literature on this topic incredibly difficult. Many studies report the effect of “blue” or “red” light without specifying the wavelength ranges used which is important to include as blue light spans from 380-500 nm and microalgal strains respond differently to wavelengths



within this range. This is demonstrated by comparing the results of this study to that of Han, *et al.* where it was reported that growth of *D. salina* under blue light (450 nm) decreased by 25% when compared to white light.<sup>258</sup> However, in our study, *D. primolecta* showed a 50% reduction in growth under 405 nm light compared to white light. The primary pigments found in *Dunaliella* spp. are chlorophyll *a* and *b*,  $\beta$ -carotene, and lutein, all of which have an absorption peak between 423–474 nm which explains why cultures could grow more efficiently under 450 nm than 405 nm illumination.

### 5.3.2 Antimicrobial Screening of Extracts and Fractions

Under the conditions tested in this study, neither growth under 405 nm light nor fractionation elicited the production of antimicrobial metabolites. This is a frustrating result as there is a plethora of literature reporting antibacterial and antifungal activity from microalgal cultures. One such example, from McGee, *et al.*, screened 80 microalgal extracts and their fractions against two Gram positive bacteria, two Gram negative bacteria, and *Candida albicans* with 27% of fractions showing activity against at least one pathogen.<sup>90</sup> Notably, only 6% of ethyl acetate fractions showed any activity, with 66% of diethyl ether fractions and 28% of methanolic fractions reported as active. They observed a trend that methanolic fractions tended to demonstrate Gram positive bacterial inhibition whilst non-polar diethyl ether fractions showed Gram positive antibacterial and anticandidal activity. McGee, *et al.*, then chose three promising strains (*Chlorococcum* sp., *Stauroneis* sp., and *Prymnesium* sp.) and studied the effect of different light regimens on their bioactivity and concluded that culturing under blue LED light yielded significantly more bioactivity compared to growth under red and white light. This comparison shows the importance in carefully designing extraction protocols based on the research question at hand. For this thesis, extracting chemical diversity was the main objective. However, if drug discovery or evaluating bioactivity was the primary objective, solvents such as diethyl ether or methanol would be more appropriate to use. This could be achieved by producing large amounts of biomass followed by sequential extractions using solvents of increasing polarity and screening these crude extracts in the same manner above. This would provide a relatively high throughput method of testing microalgal metabolite extracts for antimicrobial activity. The above process of fractionation and

eventual purification of metabolites could greatly help efforts to discover new antimicrobial metabolites.

### 5.3.3 Effect of 405 nm Light on Metabolite Production

Results from the statistical analysis and molecular networking agreed well with our previously conducted research on the chemical diversity of microalgae belonging to different phyla.<sup>252</sup> In that analysis, Haptophytes were the most chemical rich clade followed by diatoms, Ochrophytes, Chlorophytes, and Rhodophytes. In this study, the diatom *Phaeodactylum tricoratum* had the greatest number of LC-MS/MS features followed by the Ochrophyte *Nannochloropsis oculata*, the Rhodophyte *Porphyridium cruentum*, and finally the Chlorophyte *Dunaliella primolecta*. It also supported the argument that there is no shared or core metabolome between microalgae, with only 100 out of 3252 features shared between all four strains. This must be considered with the caveat that ethyl acetate is not particularly efficient at extracting polar carotenoids and that these metabolites are often shared by phylogenetically related microalgae.<sup>193</sup> It is difficult to postulate the classes of metabolites or putative identification of metabolites without purifying and characterising metabolites through NMR or comparing LC-MS and LC-MS/MS data to known standards. 405 nm light has a large effect on metabolite production as 16-25% of metabolites extracted were either exclusively found in the 405 nm samples or absent in this condition compared with the white light control. Most of the changes were the result of metabolite production being switched off (i.e., in control but not in 405 nm) and these tended to belong to molecular families suggesting that growth under 405 nm light is suppressing specific metabolic pathways. Blue light has been shown to increase haematocyst germination in *Haematococcus pluvialis*<sup>259</sup> whilst the sexual life cycle of *Chlamydomonas reinhardtii* was impaired when the gene *Phot* that encodes blue light sensing protein, phototropin, was disrupted using interference RNA.<sup>260</sup> These are some examples of how blue light may negatively affect the reproduction and growth of microalgal strains but specific evidence of blue light suppressing particular pathways and metabolite production could not be found. When conducting research into the effect of a particular stress on the growth and production of metabolites from an organism, it is important to note that these two things may have a negative correlation. As seen for *P. cruentum*, growth was significantly reduced under 405 nm light, however metabolite production increased by

9.9%. This was also observed in **chapter 4** where reduced growth was often coupled with increased metabolite production. It should be carefully considered whether the advantage of higher metabolite production compensates for the lower biomass yield, or if strategies can be employed to maximise both. A common approach to maximise both is to use light switching where certain light parameters are used to produce maximum biomass before switching to a different light regimen that is optimised for metabolite production. Xi, *et al.*, demonstrated this by cultivating *Haematococcus pluvialis* under red light for six days before switching to blue light which saw a 50% increase in astaxanthin production compared to just growing *H. pluvialis* under red light.<sup>134</sup>

## 6. General Discussion and Future Work

---

### 6.1 General Discussion

Algae (encompassing cyanobacteria, eukaryotic microalgae, and seaweeds) are a polyphyletic group of organisms with members in all kingdoms except Animalia. They comprise 15 phyla and 54 classes, and it is estimated that there are 72,000 extant species of microalgae alone.<sup>38</sup> The biological diversity between different phyla and classes has led some to dub algae as a “false taxon.” Classification of these organisms is further stunted by the fact that molecular approaches (using 18S rRNA, ITS-2, rbcL, or COX-1 genes) often fail to distinguish between higher taxonomic levels (i.e., genus or species).<sup>44</sup> Despite this confusion in classifying microalgae, they are of great interest in applied sciences, particularly biotechnology. Furthermore, it is postulated that the biological diversity of these organisms should result in chemical diversity in the metabolites they produce. This hypothesis was tested in this body of work by examining the chemical profiles of 20 microalgae: seven Chlorophytes, six Haptophytes, four diatoms, two Ochrophytes, and one Rhodophyte, resulting in distinct chemical profiles for each phylum. To capture chemical diversity within a single extract, four different solvent systems were compared using GNPS molecular networking and an extraction method using HP-20 diaionic resin and ethyl acetate was optimised. Haptophytes represented the phylum with the greatest number of metabolites (average of 370 per strain) and thus a rich source of chemistry. We then challenged the traditional taxonomic classification of species by comparing the chemical profiles of multiple strains of *Dunaliella tertiolecta* (4), *Chrysothila carterae* (3), and *Prymnesium parvum* (3) from both freshwater and marine environments. Strains isolated from similar environments had a higher similitude in their chemical profiles than those from different environments, leading to the conclusion that chemotyping strains may be more useful in applied research than traditional taxonomic classifications. This is supported by recent work from Riba, *et al.*, in which 133 colonies of the cyanobacterium *Nostoc*-like strains were classified into four chemotypes based on the peptides they produced.<sup>261</sup> Chemotypes have also been reported for collections of the seaweed *Plocamium cartilagineum* which were

classified as  $\alpha$  and  $\beta$  groups based on the presence of enzymes required to introduce bromine atoms into monoterpene synthesis.<sup>262</sup>

Genome sequencing of bacteria and other microorganisms has revealed that they often have a higher biosynthetic potential than the number of metabolites detected when these organisms are grown under standard laboratory conditions.<sup>160</sup> With this in mind, three strains of marine microalgae – *Dunaliella primolecta*, *Nannochloropsis oculata*, and *Phaeodactylum tricornutum* – were selected for a systematic comparative metabolomics study using the OSMAC approach to elicit metabolite production. Comparing varying levels of nitrate, salinity, NaCl, and pH, salinity was found to have the most profound effect with 22.8% of metabolites across all three strains only produced in response to salinity stress. However, this increase in metabolite production was coupled with a decrease in growth and thus smaller biomass and extract mass. Additionally, this approach is untargeted and thus labour-intensive in terms of the number of experiments and data analysis required. A major bottleneck in this research is the lack of metabolites from microalgae that have been isolated and characterised by the research community. The 2020 Marine Natural Products report detailed the discovery of 1554 new metabolites from marine organisms in 2018.<sup>263</sup> From this, one arsenolipid was discovered from the microalga *Dunaliella tertiolecta*, nine metabolites from dinoflagellates, and 66 from cyanobacteria. This is compared to 240 bacterial, 144 from mangrove-associated fungi, and 617 from other marine fungi. The rate of discovery of metabolites from microalgae is dismally low when the chemical diversity and range of bioactivities from microalgal extracts are considered. Additionally, spectral information on metabolites that have been discovered from algal sources are hidden behind paywalls in libraries like MarinLit,<sup>264</sup> and AntiBase.<sup>265</sup> The recent release of the open-access Natural Products Atlas (2020)<sup>161</sup> could potentially resolve this side of this bottleneck as developers are working to integrate this database into the GNPS ecosystem. Unfortunately, this database currently only contains natural products isolated from cyanobacteria although it is hoped this will expand to eukaryotic microalgae in future versions.

Understanding the biological and chemical diversity, and how to elicit this chemistry could be vital for solving some of the major global crises threatening our health and environment. During the SARS-CoV-2 pandemic, which had killed almost 4.5 million

people as of September 2021 ([www.ourworldindata.org](http://www.ourworldindata.org)), there was concern over the presence of SARS-CoV-2 in wastewater, and treated wastewater.<sup>266, 267</sup> Phycoremediation – the use of algae to remove contaminants from waste – has seen great traction in recent years as it can be used to recycle phosphorous, remove heavy metals, and even remove viruses from water. In particular, the extremophile *Galderia sulphuraria* has been reported to remove high amounts of noroviruses, coliphages, and enteroviruses from wastewater.<sup>268</sup> Recently, Gustafsson, *et al.*, developed a filter membrane using *Pithophora* sp. which can be used for point-of-use purification of drinking water.<sup>269</sup> Such academic developments into phycoremediation could help drastically reduce the transmission of waterborne viruses and protect human lives. However, this cannot be achieved without collaboration between academia, government, and industry to ensure scalability and regulation. Working with industry allows for rapid research and development from academic collaborators with a strong focus on real-life applications. For example, in our collaboration with Xanthella Ltd., they were interested in exploring the potential of 405 nm light for its antibacterial properties which can suppress contamination in large 1000 L photobioreactors. By testing this hypothesis at a small scale using academic partners, a rapid exploration into the effect of 405 nm light on the growth and metabolite production of diverse microalgae could be achieved, with relatively low cost. This collaborative approach to research has resulted in exciting breakthroughs, particularly in the area of antimicrobial resistance (AMR), another global health challenge that is expected to see death rates rise to 10 million per year by 2050.<sup>270</sup> Collaborative research between MGB-BioPharma, InnovateUK, and the University of Strathclyde (Scotland, UK) developed a new class of antibiotic for treating *Clostridium difficile* which has completed phase II clinical trials in the US and Canada.<sup>271, 272</sup> Microalgae could also play a role in the fight against AMR as numerous studies have reported antimicrobial activity,<sup>273, 90, 274</sup> including their ability to biosynthesise silver nanoparticles with antibacterial activity.<sup>275</sup> Finally, microalgae are playing a significant role, both positively and negatively, in climate change. Ocean acidification and eutrophication are leading to increased incidences of harmful algal blooms which bring with it public health concerns from paralytic shellfish poisoning and economic damage to the fishing and tourism industries.<sup>222, 196</sup> In chapter 4, we evaluated the effect of nitrate and pH on

metabolite production for non-bloom-forming microalgae, however this investigation could be expanded to include bloom-forming and toxin-producing microalgae, as well as expanding the stress types and levels to better mimic changing environmental parameters. In 2009, a fluorometric method was developed to distinguish bloom-forming species which allowed for *in situ* monitoring. However, the accuracy of this method was disrupted by noise from environmental blanks. Kelsey, *et al.*, used a combination of metabolomics and proteomics to study the allelopathic relationship between the bloom-forming and toxic *Karenia brevis* and two diatoms, *Asterionellopsis glacialis* which often co-occurs with *K. brevis* blooms and *Thalassiosira pseudomana* which is sensitive to *K. brevis* allelopathic compounds. Whilst there is great promise in this methodology, metabolomics needs to be coupled with genomic, transcriptomic, or proteomic data to give understanding into the changes in gene regulation and expression caused by varying biotic and abiotic factors. It is also important to note that these methods only provide a snapshot of a dynamic ecosystem and cannot replace *in situ* monitoring approaches.

## **6.2 Future Work**

Comparative metabolomics, and in particular molecular networking using the GNPS ecosystem has been used to evaluate the diversity of microalgae across taxonomic boundaries and the elicitation of metabolites using abiotic factors. A natural continuation to this work would be to expand the scale of each of these studies to include more strains. The concept of using chemotypes rather than species for applied research is worth consideration and a large study involving multiple strains of one species from different environments (e.g., freshwater, marine) and locations (e.g., tropics, polar) would make for a worthwhile comparison. The work presented in chapter 4 offers a starting point into exploring the chemical space of microalgae and this research could continue down several relevant pathways. Since salinity had the greatest effect on the strains used in this study, this could be further explored by using smaller increments of change in salinity levels and running a transcriptomic analysis alongside metabolomics analysis to identify at what level the stress response in these strains is triggered. The addition of HPLC-analysis would also allow quantification of carotenoids in response to salinity as hypersalinity is known to trigger carotenoid biosynthesis and these metabolites are of high value to the nutraceutical, cosmetics,

and textiles industries.<sup>186, 276</sup> Furthermore, this analysis could be coupled with bioactivity-based molecular networking to prioritise extracts with promising activity to undergo isolation and purification.<sup>234</sup> On the other hand, the OSMAC strategy could be used for environmental research using abiotic and biotic factors to understand what stresses (or combination of stresses) trigger the formation of harmful algal blooms. For example, it has been shown that decreasing salinity from oceanic to coastal levels resulted in a 14-fold increase in the production of brevetoxins by *Karenia brevis*.<sup>277</sup> Finally, continued collaboration with industry can test the scalability of lab-based discoveries and the feasibility of bringing new high-value metabolites to the market.

### **6.3 Conclusion**

This thesis has demonstrated several applications of comparative metabolomics from understanding how biological diversity translates into chemical diversity, how small changes in culturing parameters can lead to big changes in metabolite production, and how to explore the biotechnological potential of industrially relevant microorganisms. It contributes to filling a large gap in knowledge around the chemical space of microalgae that goes far beyond the production of lipids and carotenoids. Furthermore, it opens the door for continued exploration into the elicitation and identification of metabolites from these incredibly diverse microorganisms and their potential in resolving some of the greatest challenges faced by our generation.



## References

- (1) Efanje, S. M. N. Natural Products: A Continuing Source of Inspiration for the Medicinal Chemist. In *Advances in Phytomedicine*; Elsevier, 2002; Vol. 1, pp 61–69. [https://doi.org/10.1016/S1572-557X\(02\)80014-9](https://doi.org/10.1016/S1572-557X(02)80014-9).
- (2) Ji, H.; Li, X.; Zhang, H. Natural Products and Drug Discovery: Can Thousands of Years of Ancient Medical Knowledge Lead Us to New and Powerful Drug Combinations in the Fight against Cancer and Dementia? *EMBO Rep.* **2009**, *10* (3), 194–200. <https://doi.org/10.1038/embor.2009.12>.
- (3) Fatemeh Ashtiania. Tropane Alkaloids of *Atropa Belladonna* L. and *Atropa Acuminata* Royle Ex Miers Plants. *J. Med. Plants Res.* **2011**, *5* (29). <https://doi.org/10.5897/JMPR11.482>.
- (4) Choudhary, A.; Naughton, L.; Montánchez, I.; Dobson, A.; Rai, D. Current Status and Future Prospects of Marine Natural Products (MNPs) as Antimicrobials. *Mar. Drugs* **2017**, *15* (9), 272. <https://doi.org/10.3390/md15090272>.
- (5) Vane, J. R.; Botting, R. M. The Mechanism of Action of Aspirin. *Thromb. Res.* **2003**, *110* (5–6), 255–258. [https://doi.org/10.1016/S0049-3848\(03\)00379-7](https://doi.org/10.1016/S0049-3848(03)00379-7).
- (6) Jack, D. B. One Hundred Years of Aspirin. *The Lancet* **1997**, *350* (9075), 437–439. [https://doi.org/10.1016/S0140-6736\(97\)07087-6](https://doi.org/10.1016/S0140-6736(97)07087-6).
- (7) Dias, D. A.; Urban, S.; Roessner, U. A Historical Overview of Natural Products in Drug Discovery. *Metabolites* **2012**, *2* (2), 303–336. <https://doi.org/10.3390/metabo2020303>.
- (8) Moloney, M. Francis. *Irish Ethno-Botany and the Evolution of Medicine in Ireland.*; M. H. Gill.; Dublin, 1919. <https://doi.org/10.5962/bhl.title.46355>.
- (9) Blunt, J. W.; Copp, B. R.; Keyzers, R. A.; Munro, M. H. G.; Prinsep, M. R. Marine Natural Products. *Nat. Prod. Rep.* **2015**, *32* (2), 116–211. <https://doi.org/10.1039/C4NP00144C>.
- (10) Bergmann, W.; Feeney, R. J. Contributions to The Study of Marine Products. XXXII The Nucleoside of Sponges I. *J. Org. Chem.* **1951**, *16* (6), 981–987. <https://doi.org/10.1021/jo01146a023>.
- (11) Martins, A.; Vieira, H.; Gaspar, H.; Santos, S. Marketed Marine Natural Products in the Pharmaceutical and Cosmeceutical Industries: Tips for Success. *Mar. Drugs* **2014**, *12* (2), 1066–1101. <https://doi.org/10.3390/md12021066>.
- (12) Jin, W.; Williams, R. M. Synthetic Studies on Ecteinascidin 743: Asymmetric Synthesis of the Versatile Amino Acid Component. *Tetrahedron Lett.* **2003**, *44* (25), 4635–4639. [https://doi.org/10.1016/S0040-4039\(03\)01082-7](https://doi.org/10.1016/S0040-4039(03)01082-7).
- (13) Carroll, A. R.; Copp, B. R.; Davis, R. A.; Keyzers, R. A.; Prinsep, M. R. Marine Natural Products. *Nat. Prod. Rep.* **2019**, *36* (1), 122–173. <https://doi.org/10.1039/C8NP00092A>.
- (14) Feling, R. H.; Buchanan, G. O.; Mincer, T. J.; Kauffman, C. A.; Jensen, P. R.; Fenical, W. Salinosporamide A: A Highly Cytotoxic Proteasome Inhibitor from a Novel Microbial Source, a Marine Bacterium of the New Genus *Salinospora*. *Angew. Chem. Int. Ed.* **2003**, *42* (3), 355–357. <https://doi.org/10.1002/anie.200390115>.

- (15) Trimurtulu, G.; Ohtani, I.; Patterson, G. M. L.; Moore, R. E.; Corbett, T. H.; Valeriote, F. A.; Demchik, L. Total Structures of Cryptophycins, Potent Antitumor Depsipeptides from the Blue-Green Alga *Nostoc* Sp. Strain GSV 224. *J. Am. Chem. Soc.* **1994**, *116* (11), 4729–4737. <https://doi.org/10.1021/ja00090a020>.
- (16) Hamann, M. T.; Scheuer, P. J. Kahalalide F: A Bioactive Depsipeptide from the Sacoglossan Mollusk *Elysia Rufescens* and the Green Alga *Bryopsis* Sp. *J. Am. Chem. Soc.* **1993**, *115* (13), 5825–5826. <https://doi.org/10.1021/ja00066a061>.
- (17) Yang, C.; Hua, Q.; Shimizu, K. Energetics and Carbon Metabolism during Growth of Microalgal Cells under Photoautotrophic, Mixotrophic and Cyclic Light-Autotrophic/Dark-Heterotrophic Conditions. *Biochem. Eng. J.* **2000**, *6* (2), 87–102. [https://doi.org/10.1016/S1369-703X\(00\)00080-2](https://doi.org/10.1016/S1369-703X(00)00080-2).
- (18) Handbook of Marine Microalgae - 1st Edition <https://www.elsevier.com/books/handbook-of-marine-microalgae/kim/978-0-12-800776-1> (accessed 2018 -05 -03).
- (19) Garwood, R. Patterns in Palaeontology: The First 3 Billion Years of Evolution. *PALAEONTOLOGY[online]*, 2012.
- (20) Keeling, P. J. Diversity and Evolutionary History of Plastids and Their Hosts. *Am. J. Bot.* **2004**, *91* (10), 1481–1493. <https://doi.org/10.3732/ajb.91.10.1481>.
- (21) Heimann, K.; Huerlimann, R. Microalgal Classification. In *Handbook of Marine Microalgae*; Elsevier, 2015; pp 25–41. <https://doi.org/10.1016/B978-0-12-800776-1.00003-0>.
- (22) Bhattacharya, D.; Medlin, and L. Algal Phylogeny and the Origin of Land Plants. *Plant Physiol.* **1998**, *116* (1), 9–15. <https://doi.org/10.1104/pp.116.1.9>.
- (23) Goma, F.; Garcia, P. A.; Delaney, J.; Girguis, P. R.; Buie, C. R.; Edgcomb, V. P. Toward Establishing Model Organisms for Marine Protists: Successful Transfection Protocols for *Parabodo Caudatus* (Kinetoplastida: Excavata): Protist Transfection. *Environ. Microbiol.* **2017**, *19* (9), 3487–3499. <https://doi.org/10.1111/1462-2920.13830>.
- (24) Harris, E. H. *Chlamydomonas* As A Model Organism. *Annu. Rev. Plant Physiol. Plant Mol. Biol.* **2001**, *52* (1), 363–406. <https://doi.org/10.1146/annurev.arplant.52.1.363>.
- (25) Paulin, J. J.; Bussey, J. Oral Regeneration in the Ciliate *Stentor Coeruleus*: A Scanning and Transmission Electron Optical Study. *J. Protozool.* **1971**, *18* (2), 201–213. <https://doi.org/10.1111/j.1550-7408.1971.tb03308.x>.
- (26) Poulsen, N.; Berne, C.; Spain, J.; Kröger, N. Silica Immobilization of an Enzyme through Genetic Engineering of the Diatom *Thalassiosira Pseudonana*. *Angew. Chem. Int. Ed.* **2007**, *46* (11), 1843–1846. <https://doi.org/10.1002/anie.200603928>.
- (27) Miao, W.; Xiong, J.; Bowen, J.; Wang, W.; Liu, Y.; Braguinets, O.; Grigull, J.; Pearlman, R. E.; Orias, E.; Gorovsky, M. A. Microarray Analyses of Gene Expression during the *Tetrahymena Thermophila* Life Cycle. *PLoS ONE* **2009**, *4* (2), e4429. <https://doi.org/10.1371/journal.pone.0004429>.
- (28) Hedges, S. B. The Origin and Evolution of Model Organisms. *Nat. Rev. Genet.* **2002**, *3* (11), 838–849. <https://doi.org/10.1038/nrg929>.

- (29) Abou-Shanab, R. A. I.; Matter, I. A.; Kim, S.-N.; Oh, Y.-K.; Choi, J.; Jeon, B.-H. Characterization and Identification of Lipid-Producing Microalgae Species Isolated from a Freshwater Lake. *Biomass Bioenergy* **2011**, *35* (7), 3079–3085. <https://doi.org/10.1016/j.biombioe.2011.04.021>.
- (30) Geider, R.; La Roche, J. Redfield Revisited: Variability of C:N:P in Marine Microalgae and Its Biochemical Basis. *Eur. J. Phycol.* **2002**, *37* (1), 1–17. <https://doi.org/10.1017/S0967026201003456>.
- (31) Zhang, B.; Zhang, Y.; Downing, A.; Niu, Y. Distribution and Composition of Cyanobacteria and Microalgae Associated with Biological Soil Crusts in the Gurbantunggut Desert, China. *Arid Land Res. Manag.* **2011**, *25* (3), 275–293. <https://doi.org/10.1080/15324982.2011.565858>.
- (32) Aburai, N.; Ohkubo, S.; Miyashita, H.; Abe, K. Composition of Carotenoids and Identification of Aerial Microalgae Isolated from the Surface of Rocks in Mountainous Districts of Japan. *Algal Res.* **2013**, *2* (3), 237–243. <https://doi.org/10.1016/j.algal.2013.03.001>.
- (33) Post, F. J. The Microbial Ecology of the Great Salt Lake. *Microb. Ecol.* **1977**, *3* (2), 143–165. <https://doi.org/10.1007/BF02010403>.
- (34) Oren, A. Microbiological Studies in the Dead Sea: Future Challenges toward the Understanding of Life at the Limit of Salt Concentrations. *Hydrobiologia* **1999**, *405*, 1–9.
- (35) Arthern, R. J.; Vaughan, D. G.; Rankin, A. M.; Mulvaney, R.; Thomas, E. R. In Situ Measurements of Antarctic Snow Compaction Compared with Predictions of Models. *J. Geophys. Res.* **2010**, *115* (F3), F03011. <https://doi.org/10.1029/2009JF001306>.
- (36) Takagi, M.; Karseno; Yoshida, T. Effect of Salt Concentration on Intracellular Accumulation of Lipids and Triacylglyceride in Marine Microalgae *Dunaliella* Cells. *J. Biosci. Bioeng.* **2006**, *101* (3), 223–226. <https://doi.org/10.1263/jbb.101.223>.
- (37) Azua-Bustos, A.; González-Silva, C.; Arenas-Fajardo, C.; Vicuña, R. Extreme Environments as Potential Drivers of Convergent Evolution by Exaptation: The Atacama Desert Coastal Range Case. *Front. Microbiol.* **2012**, *3*. <https://doi.org/10.3389/fmicb.2012.00426>.
- (38) Guiry, M. D. How Many Species of Algae Are There? *J. Phycol.* **2012**, *48* (5), 1057–1063. <https://doi.org/10.1111/j.1529-8817.2012.01222.x>.
- (39) Guiry, M. D.; Guiry, G. M. Algaebase :: Listing the World's Algae <http://www.algaebase.org/> (accessed 2018 -06 -24).
- (40) Ragan, M. On the Delineation and Higher-Level Classification of Algae. *Eur. J. Phycol.* **1998**, *33* (1), 1–15. <https://doi.org/10.1080/09670269810001736483>.
- (41) Bittner, L.; Gobet, A.; Audic, S.; Romac, S.; Egge, E. S.; Santini, S.; Ogata, H.; Probert, I.; Edvardsen, B.; de Vargas, C. Diversity Patterns of Uncultured Haptophytes Unravelling by Pyrosequencing in Naples Bay. *Mol. Ecol.* **2013**, *22* (1), 87–101. <https://doi.org/10.1111/mec.12108>.
- (42) Janda, J. M.; Abbott, S. L. 16S rRNA Gene Sequencing for Bacterial Identification in the Diagnostic Laboratory: Pluses, Perils, and Pitfalls. *J. Clin. Microbiol.* **2007**, *45* (9), 2761–2764. <https://doi.org/10.1128/JCM.01228-07>.

- (43) Metting, F. B. Biodiversity and Application of Microalgae. *J. Ind. Microbiol. Biotechnol.* **1996**, *17* (5–6), 477–489. <https://doi.org/10.1007/BF01574779>.
- (44) Guo, L.; Sui, Z.; Zhang, S.; Ren, Y.; Liu, Y. Comparison of Potential Diatom ‘Barcode’ Genes (the 18S rRNA Gene and ITS, COI, RbcL) and Their Effectiveness in Discriminating and Determining Species Taxonomy in the Bacillariophyta. *Int. J. Syst. Evol. Microbiol.* **2015**, *65* (4), 1369–1380. <https://doi.org/10.1099/ijs.0.000076>.
- (45) Alverson, A. J.; Cannone, J. J.; Gutell, R. R.; Theriot, E. C. THE EVOLUTION OF ELONGATE SHAPE IN DIATOMS<sup>1</sup>. *J. Phycol.* **2006**, *42* (3), 655–668. <https://doi.org/10.1111/j.1529-8817.2006.00228.x>.
- (46) Sorhannus, U. Diatom Phylogenetics Inferred Based on Direct Optimization of Nuclear-Encoded SSU rRNA Sequences. *Cladistics* **2004**, *20* (5), 487–497. <https://doi.org/10.1111/j.1096-0031.2004.00034.x>.
- (47) Bedford, J.; Ostle, C.; Johns, D. G.; Atkinson, A.; Best, M.; Bresnan, E.; Machairopoulou, M.; Graves, C. A.; Devlin, M.; Milligan, A.; Pitois, S.; Mellor, A.; Tett, P.; McQuatters-Gollop, A. Lifeform Indicators Reveal Large-scale Shifts in Plankton across the North-West European Shelf. *Glob. Change Biol.* **2020**, *26* (6), 3482–3497. <https://doi.org/10.1111/gcb.15066>.
- (48) Widdicombe, C. E.; Eloire, D.; Harbour, D.; Harris, R. P.; Somerfield, P. J. Long-Term Phytoplankton Community Dynamics in the Western English Channel. *J. Plankton Res.* **2010**, *32* (5), 643–655. <https://doi.org/10.1093/plankt/fbp127>.
- (49) Gachon, C. M. M.; Day, J. G.; Campbell, C. N.; Pröschold, T.; Saxon, R. J.; Küpper, F. C. The Culture Collection of Algae and Protozoa (CCAP): A Biological Resource for Protistan Genomics. *Gene* **2007**, *406* (1–2), 51–57. <https://doi.org/10.1016/j.gene.2007.05.018>.
- (50) Chen, H.; Jiang, J.-G. Osmotic Responses of *Dunaliella* to the Changes of Salinity. *J. Cell. Physiol.* **2009**, *219* (2), 251–258. <https://doi.org/10.1002/jcp.21715>.
- (51) Lauceri, R.; Chini Zittelli, G.; Torzillo, G. A Simple Method for Rapid Purification of Phycobiliproteins from *Arthrospira Platensis* and *Porphyridium Cruentum* Biomass. *Algal Res.* **2019**, *44*, 101685. <https://doi.org/10.1016/j.algal.2019.101685>.
- (52) Zaouk, L.; Massé, A.; Bourseau, P.; Taha, S.; Rabiller-Baudry, M.; Jubeau, S.; Teychené, B.; Pruvost, J.; Jaouen, P. Filterability of Exopolysaccharides Solutions from the Red Microalga *Porphyridium Cruentum* by Tangential Filtration on a Polymeric Membrane. *Environ. Technol.* **2020**, *41* (9), 1167–1184. <https://doi.org/10.1080/09593330.2018.1523234>.
- (53) Droop, M. R. Some New Supra-Littoral Protista. *J. Mar. Biol. Assoc. U. K.* **1955**, *34* (2), 233–245. <https://doi.org/10.1017/S0025315400027612>.
- (54) Armbrust, E. V. The Genome of the Diatom *Thalassiosira Pseudonana*: Ecology, Evolution, and Metabolism. *Science* **2004**, *306* (5693), 79–86. <https://doi.org/10.1126/science.1101156>.
- (55) Borowitzka, M. A.; Volcani, B. E. THE POLYMORPHIC DIATOM PHAEODACTYLUM TRICORNUTUM: ULTRASTRUCTURE OF ITS MORPHOTYPES<sup>2</sup>. *J. Phycol.* **1978**, *14* (1), 10–21. <https://doi.org/10.1111/j.1529-8817.1978.tb00625.x>.

- (56) Yao, S.; Lyu, S.; An, Y.; Lu, J.; Gjermansen, C.; Schramm, A. Microalgae-Bacteria Symbiosis in Microalgal Growth and Biofuel Production: A Review. *J. Appl. Microbiol.* **2019**, *126* (2), 359–368. <https://doi.org/10.1111/jam.14095>.
- (57) Croft, M. T.; Lawrence, A. D.; Raux-Deery, E.; Warren, M. J.; Smith, A. G. Algae Acquire Vitamin B12 through a Symbiotic Relationship with Bacteria. *Nature* **2005**, *438* (7064), 90–93. <https://doi.org/10.1038/nature04056>.
- (58) Cho, D.-H.; Ramanan, R.; Kim, B.-H.; Lee, J.; Kim, S.; Yoo, C.; Choi, G.-G.; Oh, H.-M.; Kim, H.-S. Novel Approach for the Development of Axenic Microalgal Cultures from Environmental Samples. *J. Phycol.* **2013**, *49* (4), 802–810. <https://doi.org/10.1111/jpy.12091>.
- (59) Andersen, R. A.; America, P. S. of. *Algal Culturing Techniques*; Academic Press, 2005.
- (60) Moheimani, N. R.; Borowitzka, M. A.; Isdepsky, A.; Sing, S. F. Standard Methods for Measuring Growth of Algae and Their Composition. In *Algae for Biofuels and Energy*; Borowitzka, M. A., Moheimani, N. R., Eds.; Springer Netherlands: Dordrecht, 2013; pp 265–284. [https://doi.org/10.1007/978-94-007-5479-9\\_16](https://doi.org/10.1007/978-94-007-5479-9_16).
- (61) Jia, F.; Kacira, M.; Ogden, K. Multi-Wavelength Based Optical Density Sensor for Autonomous Monitoring of Microalgae. *Sensors* **2015**, *15* (9), 22234–22248. <https://doi.org/10.3390/s150922234>.
- (62) Griffiths, M. J.; Garcin, C.; van Hille, R. P.; Harrison, S. T. L. Interference by Pigment in the Estimation of Microalgal Biomass Concentration by Optical Density. *J. Microbiol. Methods* **2011**, *85* (2), 119–123. <https://doi.org/10.1016/j.mimet.2011.02.005>.
- (63) Zhu, C. J.; Lee, Y. K. Determination of Biomass Dry Weight of Marine Microalgae. *J. Appl. Phycol.* **1997**, *9*, 189–194.
- (64) Collier, J. L. FLOW CYTOMETRY AND THE SINGLE CELL IN PHYCOLOGY. *J. Phycol.* **2000**, *36* (4), 628–644. <https://doi.org/10.1046/j.1529-8817.2000.99215.x>.
- (65) Guzmán, H. M.; de la Jara Valido, A.; Duarte, L. C.; Presmanes, K. F. Estimate by Means of Flow Cytometry of Variation in Composition of Fatty Acids from *Tetraselmis Suecica* in Response to Culture Conditions. *Aquac. Int.* **2010**, *18* (2), 189–199. <https://doi.org/10.1007/s10499-008-9235-1>.
- (66) Khan, M. I.; Shin, J. H.; Kim, J. D. The Promising Future of Microalgae: Current Status, Challenges, and Optimization of a Sustainable and Renewable Industry for Biofuels, Feed, and Other Products. *Microb. Cell Factories* **2018**, *17* (1). <https://doi.org/10.1186/s12934-018-0879-x>.
- (67) Chen, J.; Wang, Y.; Benemann, J. R.; Zhang, X.; Hu, H.; Qin, S. Microalgal Industry in China: Challenges and Prospects. *J. Appl. Phycol.* **2016**, *28* (2), 715–725. <https://doi.org/10.1007/s10811-015-0720-4>.
- (68) Borowitzka, L. J.; Borowitzka, M. A. COMMERCIAL PRODUCTION OF (3-CAROTENE BY *DUNALIELLA SALINA* IN OPEN PONDS. *Bull. Mar. Sci.* **1990**, *47* (1), 244–252.
- (69) Ogbonda, K. H.; Aminigo, R. E.; Abu, G. O. Influence of Temperature and PH on Biomass Production and Protein Biosynthesis in a Putative *Spirulina* Sp. *Bioresour. Technol.* **2007**, *98* (11), 2207–2211. <https://doi.org/10.1016/j.biortech.2006.08.028>.

- (70) Brennan, L.; Owende, P. Biofuels from Microalgae—A Review of Technologies for Production, Processing, and Extractions of Biofuels and Co-Products. *Renew. Sustain. Energy Rev.* **2010**, *14* (2), 557–577. <https://doi.org/10.1016/j.rser.2009.10.009>.
- (71) Ugwu, C. U.; Aoyagi, H.; Uchiyama, H. Photobioreactors for Mass Cultivation of Algae. *Bioresour. Technol.* **2008**, *99* (10), 4021–4028. <https://doi.org/10.1016/j.biortech.2007.01.046>.
- (72) Gupta, P. L.; Lee, S.-M.; Choi, H.-J. A Mini Review: Photobioreactors for Large Scale Algal Cultivation. *World J. Microbiol. Biotechnol.* **2015**, *31* (9), 1409–1417. <https://doi.org/10.1007/s11274-015-1892-4>.
- (73) Richardson, J. W.; Johnson, M. D.; Zhang, X.; Zemke, P.; Chen, W.; Hu, Q. A Financial Assessment of Two Alternative Cultivation Systems and Their Contributions to Algae Biofuel Economic Viability. *Algal Res.* **2014**, *4*, 96–104. <https://doi.org/10.1016/j.algal.2013.12.003>.
- (74) Murphy, T. E. Artificial Leaf for Biofuel Production and Harvesting: Transport Phenomena and Energy Conversion, University of Texas at Austin, 2013.
- (75) Nicoletti, M. Microalgae Nutraceuticals. *Foods* **2016**, *5* (4), 54. <https://doi.org/10.3390/foods5030054>.
- (76) Ghasemi, Y.; Rasoul-Amini, S.; Naseri, A. T.; Montazeri-Najafabady, N.; Mobasher, M. A.; Dabbagh, F. Microalgae Biofuel Potentials (Review). *Appl. Biochem. Microbiol.* **2012**, *48* (2), 126–144. <https://doi.org/10.1134/S0003683812020068>.
- (77) Skjånes, K.; Rebours, C.; Lindblad, P. Potential for Green Microalgae to Produce Hydrogen, Pharmaceuticals and Other High Value Products in a Combined Process. *Crit. Rev. Biotechnol.* **2013**, *33* (2), 172–215. <https://doi.org/10.3109/07388551.2012.681625>.
- (78) Roy, S. S.; Pal, R. Microalgae in Aquaculture: A Review with Special References to Nutritional Value and Fish Dietetics. *Proc. Zool. Soc.* **2015**, *68* (1), 1–8. <https://doi.org/10.1007/s12595-013-0089-9>.
- (79) Spolaore, P.; Joannis-Cassan, C.; Duran, E.; Isambert, A. Commercial Applications of Microalgae. *J. Biosci. Bioeng.* **2006**, *101* (2), 87–96. <https://doi.org/10.1263/jbb.101.87>.
- (80) de la Jara, A.; Ruano-Rodriguez, C.; Polifrone, M.; Assunção, P.; Brito-Casillas, Y.; Wägner, A. M.; Serra-Majem, L. Impact of Dietary Arthrospira (Spirulina) Biomass Consumption on Human Health: Main Health Targets and Systematic Review. *J. Appl. Phycol.* **2018**, *30* (4), 2403–2423. <https://doi.org/10.1007/s10811-018-1468-4>.
- (81) Mühling, M.; Belay, A.; Whitton, B. A. Variation in Fatty Acid Composition of Arthrospira (Spirulina) Strains. *J. Appl. Phycol.* **2005**, *17* (2), 137–146. <https://doi.org/10.1007/s10811-005-7213-9>.
- (82) García, J. L.; de Vicente, M.; Galán, B. Microalgae, Old Sustainable Food and Fashion Nutraceuticals. *Microb. Biotechnol.* **2017**, *10* (5), 1017–1024. <https://doi.org/10.1111/1751-7915.12800>.
- (83) Analysis: UK carbon emissions in 2017 fell to levels last seen in 1890 <https://www.carbonbrief.org/analysis-uk-carbon-emissions-in-2017-fell-to-levels-last-seen-in-1890> (accessed 2018 -06 -24).

- (84) Zhang, Z.; Lohr, L.; Escalante, C.; Wetzstein, M. Food versus Fuel: What Do Prices Tell Us? *Energy Policy* **2010**, *38* (1), 445–451. <https://doi.org/10.1016/j.enpol.2009.09.034>.
- (85) van Eijck, J.; Batidzirai, B.; Faaij, A. Current and Future Economic Performance of First and Second Generation Biofuels in Developing Countries. *Appl. Energy* **2014**, *135*, 115–141. <https://doi.org/10.1016/j.apenergy.2014.08.015>.
- (86) Lee, R. A.; Lavoie, J.-M. From First- to Third-Generation Biofuels: Challenges of Producing a Commodity from a Biomass of Increasing Complexity. *Anim. Front.* **2013**, *3* (2), 6–11. <https://doi.org/10.2527/af.2013-0010>.
- (87) Teo, C. L.; Atta, M.; Bukhari, A.; Taisir, M.; Yusuf, A. M.; Idris, A. Enhancing Growth and Lipid Production of Marine Microalgae for Biodiesel Production via the Use of Different LED Wavelengths. *Bioresour. Technol.* **2014**, *162*, 38–44. <https://doi.org/10.1016/j.biortech.2014.03.113>.
- (88) Chisti, Y. Biodiesel from Microalgae. *Biotechnol. Adv.* **2007**, *25* (3), 294–306. <https://doi.org/10.1016/j.biotechadv.2007.02.001>.
- (89) López, Y.; Soto, S. M. The Usefulness of Microalgae Compounds for Preventing Biofilm Infections. *Antibiotics* **2019**, *9* (1), 9. <https://doi.org/10.3390/antibiotics9010009>.
- (90) Mc Gee, D.; Archer, L.; Smyth, T. J.; Fleming, G. T. A.; Touzet, N. Bioprospecting and LED-Based Spectral Enhancement of Antimicrobial Activity of Microalgae Isolated from the West of Ireland. *Algal Res.* **2020**, *45*, 101704. <https://doi.org/10.1016/j.algal.2019.101704>.
- (91) Huheihel, M.; Ishanu, V.; Tal, J.; Arad, S. (Malis). Activity of Porphyridium Sp. Polysaccharide against Herpes Simplex Viruses in Vitro and in Vivo. *J. Biochem. Biophys. Methods* **2002**, *50* (2–3), 189–200. [https://doi.org/10.1016/S0165-022X\(01\)00186-5](https://doi.org/10.1016/S0165-022X(01)00186-5).
- (92) Li, S.; Ji, L.; Shi, Q.; Wu, H.; Fan, J. Advances in the Production of Bioactive Substances from Marine Unicellular Microalgae Porphyridium Spp. *Bioresour. Technol.* **2019**, 122048. <https://doi.org/10.1016/j.biortech.2019.122048>.
- (93) Raposo, M. F. de J.; de Moraes, A. M. M. B.; de Moraes, R. M. S. C. Influence of Sulphate on the Composition and Antibacterial and Antiviral Properties of the Exopolysaccharide from Porphyridium Cruentum. *Life Sci.* **2014**, *101* (1–2), 56–63. <https://doi.org/10.1016/j.lfs.2014.02.013>.
- (94) Ben Amor, F.; Elleuch, F.; Ben Hlima, H.; Garnier, M.; Saint-Jean, B.; Barkallah, M.; Pichon, C.; Abdelkafi, S.; Fendri, I. Proteomic Analysis of the Chlorophyta Dunaliella New Strain AL-1 Revealed Global Changes of Metabolism during High Carotenoid Production. *Mar. Drugs* **2017**, *15* (9), 293. <https://doi.org/10.3390/md15090293>.
- (95) Adkins, Y.; Kelley, D. S. Mechanisms Underlying the Cardioprotective Effects of Omega-3 Polyunsaturated Fatty Acids. *J. Nutr. Biochem.* **2010**, *21* (9), 781–792. <https://doi.org/10.1016/j.jnutbio.2009.12.004>.
- (96) Banskota, A. H.; Stefanova, R.; Gallant, P.; McGinn, P. J. Mono- and Digalactosyldiacylglycerols: Potent Nitric Oxide Inhibitors from the Marine Microalga Nannochloropsis Granulata. *J. Appl. Phycol.* **2013**, *25* (2), 349–357. <https://doi.org/10.1007/s10811-012-9869-2>.

- (97) Kim, S. M.; Jung, Y.-J.; Kwon, O.-N.; Cha, K. H.; Um, B.-H.; Chung, D.; Pan, C.-H. A Potential Commercial Source of Fucoxanthin Extracted from the Microalga *Phaeodactylum Tricornutum*. *Appl. Biochem. Biotechnol.* **2012**, *166* (7), 1843–1855. <https://doi.org/10.1007/s12010-012-9602-2>.
- (98) Samarakoon, K. W.; Ko, J.-Y.; Lee, J.-H.; Kwon, O.-N.; Kim, S.-W.; Jeon, Y.-J. Apoptotic Anticancer Activity of a Novel Fatty Alcohol Ester Isolated from Cultured Marine Diatom, *Phaeodactylum Tricornutum*. *J. Funct. Foods* **2014**, *6*, 231–240. <https://doi.org/10.1016/j.jff.2013.10.011>.
- (99) Mondal, A.; Bose, S.; Banerjee, S.; Patra, J. K.; Malik, J.; Mandal, S. K.; Kilpatrick, K. L.; Das, G.; Kerry, R. G.; Fimognari, C.; Bishayee, A. Marine Cyanobacteria and Microalgae Metabolites—A Rich Source of Potential Anticancer Drugs. *Mar. Drugs* **2020**, *18* (9), 476. <https://doi.org/10.3390/md18090476>.
- (100) Pereira, R. B.; Evdokimov, N. M.; Lefranc, F.; Valentão, P.; Kornienko, A.; Pereira, D. M.; Andrade, P. B.; Gomes, N. G. M. Marine-Derived Anticancer Agents: Clinical Benefits, Innovative Mechanisms, and New Targets. *Mar. Drugs* **2019**, *17* (6), 329. <https://doi.org/10.3390/md17060329>.
- (101) Romano, S.; Jackson, S.; Patry, S.; Dobson, A. Extending the “One Strain Many Compounds” (OSMAC) Principle to Marine Microorganisms. *Mar. Drugs* **2018**, *16* (7), 244. <https://doi.org/10.3390/md16070244>.
- (102) Bjorn Bode, H.; Bethe, B.; Hofs, R.; Zeeck, A. Big Effects from Small Changes: Possible Ways to Explore Nature’s Chemical Diversity. *ChemBioChem* **2002**, *3* (7), 619–627.
- (103) Blin, K.; Shaw, S.; Steinke, K.; Villebro, R.; Ziemert, N.; Lee, S. Y.; Medema, M. H.; Weber, T. AntiSMASH 5.0: Updates to the Secondary Metabolite Genome Mining Pipeline. *Nucleic Acids Res.* **2019**, *47* (W1), W81–W87. <https://doi.org/10.1093/nar/gkz310>.
- (104) Skinnider, M. A.; Dejong, C. A.; Rees, P. N.; Johnston, C. W.; Li, H.; Webster, A. L. H.; Wyatt, M. A.; Magarvey, N. A. Genomes to Natural Products PRediction Informatics for Secondary Metabolomes (PRISM). *Nucleic Acids Res.* **2015**, gkv1012. <https://doi.org/10.1093/nar/gkv1012>.
- (105) Jeon, S.; Lim, J.-M.; Lee, H.-G.; Shin, S.-E.; Kang, N. K.; Park, Y.-I.; Oh, H.-M.; Jeong, W.-J.; Jeong, B.; Chang, Y. K. Current Status and Perspectives of Genome Editing Technology for Microalgae. *Biotechnol. Biofuels* **2017**, *10* (1), 267. <https://doi.org/10.1186/s13068-017-0957-z>.
- (106) Minhas, A. K.; Hodgson, P.; Barrow, C. J.; Adholeya, A. A Review on the Assessment of Stress Conditions for Simultaneous Production of Microalgal Lipids and Carotenoids. *Front. Microbiol.* **2016**, *7*. <https://doi.org/10.3389/fmicb.2016.00546>.
- (107) Scholz, B.; Küpper, F.; Vyverman, W.; Ólafsson, H.; Karsten, U. Chytridiomycosis of Marine Diatoms—The Role of Stress Physiology and Resistance in Parasite-Host Recognition and Accumulation of Defense Molecules. *Mar. Drugs* **2017**, *15* (2), 26. <https://doi.org/10.3390/md15020026>.
- (108) Solovchenko, A. E.; Khozin-Goldberg, I.; Didi-Cohen, S.; Cohen, Z.; Merzlyak, M. N. Effects of Light Intensity and Nitrogen Starvation on Growth, Total Fatty Acids and Arachidonic Acid in the Green Microalga



- Parietochloris Incisa. *J. Appl. Phycol.* **2008**, *20* (3), 245–251.  
<https://doi.org/10.1007/s10811-007-9233-0>.
- (109) Converti, A.; Casazza, A. A.; Ortiz, E. Y.; Perego, P.; Del Borghi, M. Effect of Temperature and Nitrogen Concentration on the Growth and Lipid Content of Nannochloropsis Oculata and Chlorella Vulgaris for Biodiesel Production. *Chem. Eng. Process. Process Intensif.* **2009**, *48* (6), 1146–1151.  
<https://doi.org/10.1016/j.cep.2009.03.006>.
- (110) Dammak, M.; Hadrich, B.; Miladi, R.; Barkallah, M.; Hentati, F.; Hachicha, R.; Laroche, C.; Michaud, P.; Fendri, I.; Abdelkafi, S. Effects of Nutritional Conditions on Growth and Biochemical Composition of Tetraselmis Sp. *Lipids Health Dis.* **2017**, *16* (1). <https://doi.org/10.1186/s12944-016-0378-1>.
- (111) Khozingoldberg, I.; Cohen, Z. The Effect of Phosphate Starvation on the Lipid and Fatty Acid Composition of the Fresh Water Eustigmatophyte Monodus Subterraneus. *Phytochemistry* **2006**, *67* (7), 696–701.  
<https://doi.org/10.1016/j.phytochem.2006.01.010>.
- (112) Yruela, I. Transition Metals in Plant Photosynthesis. *Metallomics* **2013**, *5*, 1090. <https://doi.org/10.1039/c3mt00086a>.
- (113) He, P.; Duncan, J.; Barber, J. Astaxanthin Accumulation in the Green Alga Haematococcus Pluvialis: Effects of Cultivation Parameters. *J. Integr. Plant Biol.* **2007**, *49* (4), 447–451. <https://doi.org/10.1111/j.1744-7909.2007.00468.x>.
- (114) Liu, Z.-Y.; Wang, G.-C.; Zhou, B.-C. Effect of Iron on Growth and Lipid Accumulation in Chlorella Vulgaris. *Bioresour. Technol.* **2008**, *99* (11), 4717–4722. <https://doi.org/10.1016/j.biortech.2007.09.073>.
- (115) Rhodes, L.; Selwood, A.; McNabb, P.; Briggs, L.; Adamson, J.; van Ginkel, R.; Laczka, O. Trace Metal Effects on the Production of Biotoxins by Microalgae. *Afr. J. Mar. Sci.* **2006**, *28* (2), 393–397.  
<https://doi.org/10.2989/18142320609504185>.
- (116) Sunda, W. G. Trace Metals and Harmful Algal Blooms. In *Ecology of Harmful Algae*; Granéli, E., Turner, J. T., Eds.; Ecological Studies; Springer Berlin Heidelberg, 2006; Vol. 189, pp 203–214. [https://doi.org/10.1007/978-3-540-32210-8\\_16](https://doi.org/10.1007/978-3-540-32210-8_16).
- (117) Turner, M. F. Nutrition of Some Marine Microalgae with Special Reference to Vitamin Requirements and Utilization of Nitrogen and Carbon Sources. *J. Mar. Biol. Assoc. U. K.* **1979**, *59* (3), 535–552.  
<https://doi.org/10.1017/S0025315400045550>.
- (118) Carlucci, A. F.; Bowes, P. M. VITAMIN PRODUCTION AND UTILIZATION BY PHYTOPLANKTON IN MIXED CULTURE. *J. Phycol.* **1970**, *6* (4), 393–400. <https://doi.org/10.1111/j.1529-8817.1970.tb02413.x>.
- (119) Carballo-Cárdenas, E. C.; Tuan, P. M.; Janssen, M.; Wijffels, R. H. Vitamin E ( $\alpha$ -Tocopherol) Production by the Marine Microalgae Dunaliella Tertiolecta and Tetraselmis Suecica in Batch Cultivation. *Biomol. Eng.* **2003**, *20* (4–6), 139–147. [https://doi.org/10.1016/S1389-0344\(03\)00040-6](https://doi.org/10.1016/S1389-0344(03)00040-6).
- (120) Durmaz, Y. Vitamin E ( $\alpha$ -Tocopherol) Production by the Marine Microalgae Nannochloropsis Oculata (Eustigmatophyceae) in Nitrogen Limitation. *Aquaculture* **2007**, *272* (1–4), 717–722.  
<https://doi.org/10.1016/j.aquaculture.2007.07.213>.

- (121) Brown, M. R.; Miller, K. A. The Ascorbic Acid Content of Eleven Species of Microalgae Used in Mariculture. *J. Appl. Phycol.* **1992**, *4* (3), 205–215. <https://doi.org/10.1007/BF02161206>.
- (122) Descolas-Gros, C.; de Billy, G. Temperature Adaptation of RuBP Carboxylase: Kinetic Properties in Marine Antarctic Diatoms. *J. Exp. Mar. Biol. Ecol.* **1987**, *108* (2), 147–158. [https://doi.org/10.1016/S0022-0981\(87\)80019-9](https://doi.org/10.1016/S0022-0981(87)80019-9).
- (123) Maxwell, D. P.; Falk, S.; Trick, C. G.; Huner, Npa. Growth at Low Temperature Mimics High-Light Acclimation in *Chlorella Vulgaris*. *Plant Physiol.* **1994**, *105* (2), 535–543. <https://doi.org/10.1104/pp.105.2.535>.
- (124) Lynch, D. V.; Thompson, G. A. Low Temperature-Induced Alterations in the Chloroplast and Microsomal Membranes of *Dunaliella Salina*. *PLANT Physiol.* **1982**, *69* (6), 1369–1375. <https://doi.org/10.1104/pp.69.6.1369>.
- (125) Khatoon, H.; Haris, N.; Banerjee, S.; Rahman, N. A.; Begum, H.; Mian, S.; Abol-Munafi, A. B.; Endut, A. Effects of Different Salinities on the Growth and Proximate Composition of *Dunaliella Sp.* Isolated from South China Sea at Different Growth Phases. *Process Saf. Environ. Prot.* **2017**, *112*, 280–287. <https://doi.org/10.1016/j.psep.2017.04.010>.
- (126) Ishika, T.; Moheimani, N. R.; Bahri, P. A.; Laird, D. W.; Blair, S.; Parlevliet, D. Halo-Adapted Microalgae for Fucoxanthin Production: Effect of Incremental Increase in Salinity. *Algal Res.* **2017**, *28*, 66–73. <https://doi.org/10.1016/j.algal.2017.10.002>.
- (127) Luangpipat, T.; Chisti, Y. Biomass and Oil Production by *Chlorella Vulgaris* and Four Other Microalgae — Effects of Salinity and Other Factors. *J. Biotechnol.* **2017**, *257*, 47–57. <https://doi.org/10.1016/j.jbiotec.2016.11.029>.
- (128) Kato, Y.; Ho, S.-H.; Vavricka, C. J.; Chang, J.-S.; Hasunuma, T.; Kondo, A. Evolutionary Engineering of Salt-Resistant *Chlamydomonas Sp.* Strains Reveals Salinity Stress-Activated Starch-to-Lipid Biosynthesis Switching. *Bioresour. Technol.* **2017**, *245*, 1484–1490. <https://doi.org/10.1016/j.biortech.2017.06.035>.
- (129) Bricaud, A.; Babin, M.; Morel, A.; Claustre, H. Variability in the Chlorophyll-Specific Absorption Coefficients of Natural Phytoplankton: Analysis and Parameterization. *J. Geophys. Res.* **1995**, *100* (C7), 13321. <https://doi.org/10.1029/95JC00463>.
- (130) Yeesang, C.; Cheirsilp, B. Effect of Nitrogen, Salt, and Iron Content in the Growth Medium and Light Intensity on Lipid Production by Microalgae Isolated from Freshwater Sources in Thailand. *Bioresour. Technol.* **2011**, *102* (3), 3034–3040. <https://doi.org/10.1016/j.biortech.2010.10.013>.
- (131) Li Yang; Kui-Shan Wen; Xiao Ruan; Ying-Xian Zhao; Feng Wei; Qiang Wang. Response of Plant Secondary Metabolites to Environmental Factors. *Molecules* **2018**, *23* (4), 762. <https://doi.org/10.3390/molecules23040762>.
- (132) Xu, Y.; Harvey, P. J. Carotenoid Production by *Dunaliella Salina* under Red Light. *Antioxidants* **2019**, *8* (5), 123. <https://doi.org/10.3390/antiox8050123>.
- (133) Madhyastha, H. K.; Sivashankari, S.; Vatsala, T. M. C-Phycocyanin from *Spirulina Fussiformis* Exposed to Blue Light Demonstrates Higher Efficacy of in Vitro Antioxidant Activity. *Biochem. Eng. J.* **2009**, *43* (2), 221–224. <https://doi.org/10.1016/j.bej.2008.11.001>.

- (134) Xi, T.; Kim, D. G.; Roh, S. W.; Choi, J.-S.; Choi, Y.-E. Enhancement of Astaxanthin Production Using *Haematococcus Pluvialis* with Novel LED Wavelength Shift Strategy. *Appl. Microbiol. Biotechnol.* **2016**, *100* (14), 6231–6238. <https://doi.org/10.1007/s00253-016-7301-6>.
- (135) McGee, D.; Archer, L.; Fleming, G. T. A.; Gillespie, E.; Touzet, N. Influence of Spectral Intensity and Quality of LED Lighting on Photoacclimation, Carbon Allocation and High-Value Pigments in Microalgae. *Photosynth. Res.* **2020**, *143* (1), 67–80. <https://doi.org/10.1007/s11120-019-00686-x>.
- (136) Murdoch, L. E.; Maclean, M.; Endarko, E.; MacGregor, S. J.; Anderson, J. G. Bactericidal Effects of 405 Nm Light Exposure Demonstrated by Inactivation of *Escherichia*, *Salmonella*, *Shigella*, *Listeria*, and *Mycobacterium* Species in Liquid Suspensions and on Exposed Surfaces. *Sci. World J.* **2012**, *2012*, 1–8. <https://doi.org/10.1100/2012/137805>.
- (137) Schulze, P. S. C.; Pereira, H. G. C.; Santos, T. F. C.; Schueler, L.; Guerra, R.; Barreira, L. A.; Perales, J. A.; Varela, J. C. S. Effect of Light Quality Supplied by Light Emitting Diodes (LEDs) on Growth and Biochemical Profiles of *Nannochloropsis Oculata* and *Tetraselmis Chuii*. *Algal Res.* **2016**, *16*, 387–398. <https://doi.org/10.1016/j.algal.2016.03.034>.
- (138) Hallenbeck, P. C.; Lazaro, C. Z.; Sagir, E. CHAPTER 1. Photosynthesis and Hydrogen from Photosynthetic Microorganisms. In *Comprehensive Series in Photochemical & Photobiological Sciences*; Seibert, M., Torzillo, G., Eds.; Royal Society of Chemistry: Cambridge, 2018; pp 1–30. <https://doi.org/10.1039/9781849737128-00001>.
- (139) Falkowski, P.; Kolber, Z. Variations in Chlorophyll Fluorescence Yields in Phytoplankton in the World Oceans. *Funct. Plant Biol.* **1995**, *22* (2), 341. <https://doi.org/10.1071/PP9950341>.
- (140) Kolber, Z. S.; Prášil, O.; Falkowski, P. G. Measurements of Variable Chlorophyll Fluorescence Using Fast Repetition Rate Techniques: Defining Methodology and Experimental Protocols. *Biochim. Biophys. Acta BBA - Bioenerg.* **1998**, *1367* (1–3), 88–106. [https://doi.org/10.1016/S0005-2728\(98\)00135-2](https://doi.org/10.1016/S0005-2728(98)00135-2).
- (141) Villareal, T. A.; Morton, S. L. Use of Cell-Specific PAM-Fluorometry to Characterize Host Shading in the Epiphytic Dinoflagellate *Gambierdiscus Toxicus*. *Mar. Ecol.* **2002**, *23* (2), 127–140. <https://doi.org/10.1046/j.1439-0485.2002.02777.x>.
- (142) Hóleton, C. L.; Nédélec, F.; Sanders, R.; Brown, L.; Moore, C. M.; Stevens, D. P.; Heywood, K. J.; Statham, P. J.; Lucas, C. H. Physiological State of Phytoplankton Communities in the Southwest Atlantic Sector of the Southern Ocean, as Measured by Fast Repetition Rate Fluorometry. *Polar Biol.* **2005**, *29* (1), 44–52. <https://doi.org/10.1007/s00300-005-0028-y>.
- (143) Zhang, F.; Su, R.; Wang, X.; Wang, L.; He, J.; Cai, M.; Luo, W.; Zheng, Z. A Fluorometric Method for the Discrimination of Harmful Algal Bloom Species Developed by Wavelet Analysis. *J. Exp. Mar. Biol. Ecol.* **2009**, *368* (1), 37–43. <https://doi.org/10.1016/j.jembe.2008.10.004>.
- (144) Yang, X.; Liu, L.; Yin, Z.; Wang, X.; Wang, S.; Ye, Z. Quantifying Photosynthetic Performance of Phytoplankton Based on Photosynthesis–Irradiance Response Models. *Environ. Sci. Eur.* **2020**, *32* (1), 24. <https://doi.org/10.1186/s12302-020-00306-9>.

- (145) Bankova, V. Natural Products Chemistry in the Third Millennium. *Chem. Cent. J.* **2007**, *1* (1), 1. <https://doi.org/10.1186/1752-153X-1-1>.
- (146) Chabner, B. A. NCI-60 Cell Line Screening: A Radical Departure in Its Time. *J. Natl. Cancer Inst.* **2016**, *108* (5), djv388. <https://doi.org/10.1093/jnci/djv388>.
- (147) Bathurst, I.; Hentschel, C. Medicines for Malaria Venture: Sustaining Antimalarial Drug Development. *Trends Parasitol.* **2006**, *22* (7), 301–307. <https://doi.org/10.1016/j.pt.2006.05.011>.
- (148) Hirata, Y.; Uemura, D. Halichondrins - Antitumor Polyether Macrolides from a Marine Sponge. *Pure Appl. Chem.* **1986**, *58* (5), 701–710. <https://doi.org/10.1351/pac198658050701>.
- (149) Bucar, F.; Wube, A.; Schmid, M. Natural Product Isolation – How to Get from Biological Material to Pure Compounds. *Nat. Prod. Rep.* **2013**, *30* (4), 525. <https://doi.org/10.1039/c3np20106f>.
- (150) Tawfike, A. F.; Viegelmann, C.; Edrada-Ebel, R. Metabolomics and Dereplication Strategies in Natural Products. In *Metabolomics Tools for Natural Product Discovery*; Roessner, U., Dias, D. A., Eds.; Humana Press: Totowa, NJ, 2013; Vol. 1055, pp 227–244. [https://doi.org/10.1007/978-1-62703-577-4\\_17](https://doi.org/10.1007/978-1-62703-577-4_17).
- (151) Shishido, T. K.; Popin, R. V.; Jokela, J.; Wahlsten, M.; Fiore, M. F.; Fewer, D. P.; Herfindal, L.; Sivonen, K. Dereplication of Natural Products with Antimicrobial and Anticancer Activity from Brazilian Cyanobacteria. *Toxins* **2019**, *12* (1), 12. <https://doi.org/10.3390/toxins12010012>.
- (152) A. Farag, M. Comparative Mass Spectrometry & Nuclear Magnetic Resonance Metabolomic Approaches for Nutraceuticals Quality Control Analysis: A Brief Review <https://www.ingentaconnect.com/content/ben/biot/2014/00000008/00000001/art00004> (accessed 2018 -07 -01).
- (153) Wang, M.; Carver, J. J.; Phelan, V. V.; Sanchez, L. M.; Garg, N.; Peng, Y.; Nguyen, D. D.; Watrous, J.; Kapon, C. A.; Luzzatto-Knaan, T.; Porto, C.; Bouslimani, A.; Melnik, A. V.; Meehan, M. J.; Liu, W.-T.; Crüsemann, M.; Boudreau, P. D.; Esquenazi, E.; Sandoval-Calderón, M.; Kersten, R. D.; Pace, L. A.; Quinn, R. A.; Duncan, K. R.; Hsu, C.-C.; Floros, D. J.; Gavilan, R. G.; Kleigrewe, K.; Northen, T.; Dutton, R. J.; Parrot, D.; Carlson, E. E.; Aigle, B.; Michelsen, C. F.; Jelsbak, L.; Sohlenkamp, C.; Pevzner, P.; Edlund, A.; McLean, J.; Piel, J.; Murphy, B. T.; Gerwick, L.; Liaw, C.-C.; Yang, Y.-L.; Humpf, H.-U.; Maansson, M.; Keyzers, R. A.; Sims, A. C.; Johnson, A. R.; Sidebottom, A. M.; Sedio, B. E.; Klitgaard, A.; Larson, C. B.; Boya P, C. A.; Torres-Mendoza, D.; Gonzalez, D. J.; Silva, D. B.; Marques, L. M.; Demarque, D. P.; Pociute, E.; O’Neill, E. C.; Briand, E.; Helfrich, E. J. N.; Granatosky, E. A.; Glukhov, E.; Ryffel, F.; Houson, H.; Mohimani, H.; Kharbush, J. J.; Zeng, Y.; Vorholt, J. A.; Kurita, K. L.; Charusanti, P.; McPhail, K. L.; Nielsen, K. F.; Vuong, L.; Elfeki, M.; Traxler, M. F.; Engene, N.; Koyama, N.; Vining, O. B.; Baric, R.; Silva, R. R.; Mascuch, S. J.; Tomasi, S.; Jenkins, S.; Macherla, V.; Hoffman, T.; Agarwal, V.; Williams, P. G.; Dai, J.; Neupane, R.; Gurr, J.; Rodríguez, A. M. C.; Lamsa, A.; Zhang, C.; Dorrestein, K.; Duggan, B. M.; Almaliti, J.; Allard, P.-M.; Phapale, P.; Nothias, L.-F.; Alexandrov, T.; Litaudon, M.;

- Wolfender, J.-L.; Kyle, J. E.; Metz, T. O.; Peryea, T.; Nguyen, D.-T.; VanLeer, D.; Shinn, P.; Jadhav, A.; Müller, R.; Waters, K. M.; Shi, W.; Liu, X.; Zhang, L.; Knight, R.; Jensen, P. R.; Palsson, B. Ø.; Pogliano, K.; Linington, R. G.; Gutiérrez, M.; Lopes, N. P.; Gerwick, W. H.; Moore, B. S.; Dorrestein, P. C.; Bandeira, N. Sharing and Community Curation of Mass Spectrometry Data with Global Natural Products Social Molecular Networking. *Nat. Biotechnol.* **2016**, *34* (8), 828–837. <https://doi.org/10.1038/nbt.3597>.
- (154) Luzzatto-Knaan, T.; Garg, N.; Wang, M.; Glukhov, E.; Peng, Y.; Ackermann, G.; Amir, A.; Duggan, B. M.; Ryazanov, S.; Gerwick, L.; Knight, R.; Alexandrov, T.; Bandeira, N.; Gerwick, W. H.; Dorrestein, P. C. Digitizing Mass Spectrometry Data to Explore the Chemical Diversity and Distribution of Marine Cyanobacteria and Algae. *eLife* **2017**, *6*, e24214. <https://doi.org/10.7554/eLife.24214>.
- (155) Li, Y.; Yu, H.-B.; Zhang, Y.; Leao, T.; Glukhov, E.; Pierce, M. L.; Zhang, C.; Kim, H.; Mao, H. H.; Fang, F.; Cottrell, G. W.; Murray, T. F.; Gerwick, L.; Guan, H.; Gerwick, W. H. Pagoamide A, a Cyclic Depsipeptide Isolated from a Cultured Marine Chlorophyte, *Derbesia* Sp., Using MS/MS-Based Molecular Networking. *J. Nat. Prod.* **2020**, *83* (3), 617–625. <https://doi.org/10.1021/acs.jnatprod.9b01019>.
- (156) Keller, L.; Siqueira-Neto, J. L.; Souza, J. M.; Eribez, K.; LaMonte, G. M.; Smith, J. E.; Gerwick, W. H. Palstimolide A: A Complex Polyhydroxy Macrolide with Antiparasitic Activity. *Molecules* **2020**, *25* (7), 1604. <https://doi.org/10.3390/molecules25071604>.
- (157) MarinLit - A database of the marine natural products literature <http://pubs.rsc.org/marinlit/> (accessed 2018 -07 -01).
- (158) AntiBase: a bioinformatics tool for Natural product databases | Chemoinformatics databases <https://omictools.com/antibase-tool> (accessed 2018 -07 -01).
- (159) Dunkel, M. SuperNatural: A Searchable Database of Available Natural Compounds. *Nucleic Acids Res.* **2006**, *34* (90001), D678–D683. <https://doi.org/10.1093/nar/gkj132>.
- (160) van der Hooft, J. J. J.; Mohimani, H.; Bauermeister, A.; Dorrestein, P. C.; Duncan, K. R.; Medema, M. H. Linking Genomics and Metabolomics to Chart Specialized Metabolic Diversity. *Chem. Soc. Rev.* **2020**, *49* (11), 3297–3314. <https://doi.org/10.1039/D0CS00162G>.
- (161) van Santen, J. A.; Jacob, G.; Singh, A. L.; Aniebok, V.; Balunas, M. J.; Bunsko, D.; Neto, F. C.; Castaño-Espriu, L.; Chang, C.; Clark, T. N.; Cleary Little, J. L.; Delgadillo, D. A.; Dorrestein, P. C.; Duncan, K. R.; Egan, J. M.; Galey, M. M.; Haeckl, F. P. J.; Hua, A.; Hughes, A. H.; Iskakova, D.; Khadilkar, A.; Lee, J.-H.; Lee, S.; LeGrow, N.; Liu, D. Y.; Macho, J. M.; McCaughey, C. S.; Medema, M. H.; Neupane, R. P.; O'Donnell, T. J.; Paula, J. S.; Sanchez, L. M.; Shaikh, A. F.; Soldatou, S.; Terlouw, B. R.; Tran, T. A.; Valentine, M.; van der Hooft, J. J. J.; Vo, D. A.; Wang, M.; Wilson, D.; Zink, K. E.; Linington, R. G. The Natural Products Atlas: An Open Access Knowledge Base for Microbial Natural Products Discovery. *ACS Cent. Sci.* **2019**, *5* (11), 1824–1833. <https://doi.org/10.1021/acscentsci.9b00806>.

- (162) Reymond, J.-L.; van Deursen, R.; Blum, L. C.; Ruddigkeit, L. Chemical Space as a Source for New Drugs. *MedChemComm* **2010**, *1* (1), 30. <https://doi.org/10.1039/c0md00020e>.
- (163) Barkia, I.; Saari, N.; Manning, S. R. Microalgae for High-Value Products Towards Human Health and Nutrition. *Mar. Drugs* **2019**, *17* (5), 304. <https://doi.org/10.3390/md17050304>.
- (164) Schneider, C. A.; Rasband, W. S.; Eliceiri, K. W. NIH Image to ImageJ: 25 Years of Image Analysis. *Nat. Methods* **2012**, *9* (7), 671–675. <https://doi.org/10.1038/nmeth.2089>.
- (165) Edgar, R. C. MUSCLE: Multiple Sequence Alignment with High Accuracy and High Throughput. *Nucleic Acids Res.* **2004**, *32* (5), 1792–1797. <https://doi.org/10.1093/nar/gkh340>.
- (166) Tamura, K.; Nei, M. Estimation of the Number of Nucleotide Substitutions in the Control Region of Mitochondrial DNA in Humans and Chimpanzees. *Mol. Biol. Evol.* **1993**. <https://doi.org/10.1093/oxfordjournals.molbev.a040023>.
- (167) Kumar, S.; Stecher, G.; Tamura, K. MEGA7: Molecular Evolutionary Genetics Analysis Version 7.0 for Bigger Datasets. *Mol. Biol. Evol.* **2016**, *33* (7), 1870–1874. <https://doi.org/10.1093/molbev/msw054>.
- (168) Kessner, D.; Chambers, M.; Burke, R.; Agus, D.; Mallick, P. ProteoWizard: Open Source Software for Rapid Proteomics Tools Development. *Bioinformatics* **2008**, *24* (21), 2534–2536. <https://doi.org/10.1093/bioinformatics/btn323>.
- (169) Pluskal, T.; Castillo, S.; Villar-Briones, A.; Orešič, M. MZmine 2: Modular Framework for Processing, Visualizing, and Analyzing Mass Spectrometry-Based Molecular Profile Data. *BMC Bioinformatics* **2010**, *11* (1), 395. <https://doi.org/10.1186/1471-2105-11-395>.
- (170) Myers, O. D.; Sumner, S. J.; Li, S.; Barnes, S.; Du, X. One Step Forward for Reducing False Positive and False Negative Compound Identifications from Mass Spectrometry Metabolomics Data: New Algorithms for Constructing Extracted Ion Chromatograms and Detecting Chromatographic Peaks. *Anal. Chem.* **2017**, *89* (17), 8696–8703. <https://doi.org/10.1021/acs.analchem.7b00947>.
- (171) Chong, J.; Wishart, D. S.; Xia, J. Using MetaboAnalyst 4.0 for Comprehensive and Integrative Metabolomics Data Analysis. *Curr. Protoc. Bioinforma.* **2019**, *68* (1). <https://doi.org/10.1002/cpbi.86>.
- (172) Shannon, P. Cytoscape: A Software Environment for Integrated Models of Biomolecular Interaction Networks. *Genome Res.* **2003**, *13* (11), 2498–2504. <https://doi.org/10.1101/gr.1239303>.
- (173) Nothias, L.-F.; Petras, D.; Schmid, R.; Dührkop, K.; Rainer, J.; Sarvepalli, A.; Protsyuk, I.; Ernst, M.; Tsugawa, H.; Fleischauer, M.; Aicheler, F.; Aksenov, A. A.; Alka, O.; Allard, P.-M.; Barsch, A.; Cachet, X.; Caraballo-Rodriguez, A. M.; Da Silva, R. R.; Dang, T.; Garg, N.; Gauglitz, J. M.; Gurevich, A.; Isaac, G.; Jarmusch, A. K.; Kameník, Z.; Kang, K. B.; Kessler, N.; Koester, I.; Korf, A.; Le Gouellec, A.; Ludwig, M.; Martin H., C.; McCall, L.-I.; McSayles, J.; Meyer, S. W.; Mohimani, H.; Morsy, M.; Moyne, O.; Neumann, S.; Neuweger, H.; Nguyen, N. H.; Nothias-Esposito, M.; Paolini, J.; Phelan, V. V.; Pluskal, T.; Quinn, R. A.; Rogers, S.; Shrestha,

- B.; Tripathi, A.; van der Hooft, J. J. J.; Vargas, F.; Weldon, K. C.; Witting, M.; Yang, H.; Zhang, Z.; Zubeil, F.; Kohlbacher, O.; Böcker, S.; Alexandrov, T.; Bandeira, N.; Wang, M.; Dorrestein, P. C. Feature-Based Molecular Networking in the GNPS Analysis Environment. *Nat. Methods* **2020**, *17* (9), 905–908. <https://doi.org/10.1038/s41592-020-0933-6>.
- (174) Wandy, J.; Zhu, Y.; van der Hooft, J. J. J.; Daly, R.; Barrett, M. P.; Rogers, S. Ms2lda.Org: Web-Based Topic Modelling for Substructure Discovery in Mass Spectrometry. *Bioinformatics* **2018**, *34* (2), 317–318. <https://doi.org/10.1093/bioinformatics/btx582>.
- (175) Ernst, M.; Kang, K. B.; Caraballo-Rodríguez, A. M.; Nothias, L.-F.; Wandy, J.; Chen, C.; Wang, M.; Rogers, S.; Medema, M. H.; Dorrestein, P. C.; van der Hooft, J. J. J. MolNetEnhancer: Enhanced Molecular Networks by Integrating Metabolome Mining and Annotation Tools. *Metabolites* **2019**, *9* (7), 144. <https://doi.org/10.3390/metabo9070144>.
- (176) Jia, F.; Kacira, M.; Ogden, K. Multi-Wavelength Based Optical Density Sensor for Autonomous Monitoring of Microalgae. *Sensors* **2015**, *15* (9), 22234–22248. <https://doi.org/10.3390/s150922234>.
- (177) Guillard, R. R. L. Culture of Phytoplankton for Feeding Marine Invertebrates. In *Culture of Marine Invertebrate Animals*; Smith, W. L., Chanley, M. H., Eds.; Springer US: Boston, MA, 1975; pp 29–60. [https://doi.org/10.1007/978-1-4615-8714-9\\_3](https://doi.org/10.1007/978-1-4615-8714-9_3).
- (178) Andersen, R. A.; Brett, R. W.; Potter, D.; Sexton, J. P. Phylogeny of the Eustigmatophyceae Based upon 18S rDNA, with Emphasis on Nannochloropsis. *Protist* **1998**, *149* (1), 61–74. [https://doi.org/10.1016/S1434-4610\(98\)70010-0](https://doi.org/10.1016/S1434-4610(98)70010-0).
- (179) Bhattacharya, D.; Medlin, and L. Algal Phylogeny and the Origin of Land Plants. *Plant Physiol.* **1998**, *116* (1), 9–15. <https://doi.org/10.1104/pp.116.1.9>.
- (180) Chen, H.; Jiang, J.-G. Osmotic Responses of *Dunaliella* to the Changes of Salinity. *J. Cell. Physiol.* **2009**, *219* (2), 251–258. <https://doi.org/10.1002/jcp.21715>.
- (181) Bernaerts, T. M. M.; Kyomugasho, C.; Van Looveren, N.; Gheysen, L.; Foubert, I.; Hendrickx, M. E.; Van Loey, A. M. Molecular and Rheological Characterization of Different Cell Wall Fractions of *Porphyridium Cruentum*. *Carbohydr. Polym.* **2018**, *195*, 542–550. <https://doi.org/10.1016/j.carbpol.2018.05.001>.
- (182) Khan, M. I.; Shin, J. H.; Kim, J. D. The Promising Future of Microalgae: Current Status, Challenges, and Optimization of a Sustainable and Renewable Industry for Biofuels, Feed, and Other Products. *Microb. Cell Factories* **2018**, *17* (1). <https://doi.org/10.1186/s12934-018-0879-x>.
- (183) Saini, R. K.; Keum, Y.-S. Carotenoid Extraction Methods: A Review of Recent Developments. *Food Chem.* **2018**, *240*, 90–103. <https://doi.org/10.1016/j.foodchem.2017.07.099>.
- (184) Grima, E. M.; Medina, A. R.; Giménez, A. G.; Sánchez Pérez, J. A.; Camacho, F. G.; García Sánchez, J. L. Comparison between Extraction of Lipids and Fatty Acids from Microalgal Biomass. *J. Am. Oil Chem. Soc.* **1994**, *71* (9), 955–959. <https://doi.org/10.1007/BF02542261>.

- (185) Lipinski, C. A.; Lombardo, F.; Dominy, B. W.; Feeney, P. J. Experimental and Computational Approaches to Estimate Solubility and Permeability in Drug Discovery and Development Settings. *Adv. Drug Deliv. Rev.* **1997**, *23* (1), 3–25. [https://doi.org/10.1016/S0169-409X\(96\)00423-1](https://doi.org/10.1016/S0169-409X(96)00423-1).
- (186) Sy, C.; Gleize, B.; Dangles, O.; Landrier, J.-F.; Veyrat, C. C.; Borel, P. Effects of Physicochemical Properties of Carotenoids on Their Bioaccessibility, Intestinal Cell Uptake, and Blood and Tissue Concentrations. *Mol. Nutr. Food Res.* **2012**, *56* (9), 1385–1397. <https://doi.org/10.1002/mnfr.201200041>.
- (187) Xia, J.; Sinelnikov, I. V.; Han, B.; Wishart, D. S. MetaboAnalyst 3.0—Making Metabolomics More Meaningful. *Nucleic Acids Res.* **2015**, *43* (W1), W251–W257. <https://doi.org/10.1093/nar/gkv380>.
- (188) Paliwal, C.; Ghosh, T.; George, B.; Pancha, I.; Maurya, R.; Chokshi, K.; Ghosh, A.; Mishra, S. Microalgal Carotenoids: Potential Nutraceutical Compounds with Chemotaxonomic Importance. *Algal Res.* **2016**, *15*, 24–31. <https://doi.org/10.1016/j.algal.2016.01.017>.
- (189) Remy, S.; Solis, D.; Silland, P.; Neyts, J.; Roussi, F.; Touboul, D.; Litaudon, M. Isolation of Phenanthrenes and Identification of Phorbol Ester Derivatives as Potential Anti-CHIKV Agents Using FBMN and NAP from *Sagotia Racemosa*. *Phytochemistry* **2019**, *167*, 112101. <https://doi.org/10.1016/j.phytochem.2019.112101>.
- (190) Dolven, J. K.; Alve, E.; Rygg, B.; Magnusson, J. Defining Past Ecological Status and in Situ Reference Conditions Using Benthic Foraminifera: A Case Study from the Oslofjord, Norway. *Ecol. Indic.* **2013**, *29*, 219–233. <https://doi.org/10.1016/j.ecolind.2012.12.031>.
- (191) You, T.; Barnett, S. M. Effect of Light Quality on Production of Extracellular Polysaccharides and Growth Rate of *Porphyridium Cruentum*. *Biochem. Eng. J.* **2004**, *19* (3), 251–258. <https://doi.org/10.1016/j.bej.2004.02.004>.
- (192) Wu, M.; Zhang, H.; Sun, W.; Li, Y.; Hu, Q.; Zhou, H.; Han, D. Metabolic Plasticity of the Starchless Mutant of *Chlorella Sorokiniana* and Mechanisms Underlying Its Enhanced Lipid Production Revealed by Comparative Metabolomics Analysis. *Algal Res.* **2019**, *42*, 101587. <https://doi.org/10.1016/j.algal.2019.101587>.
- (193) Mc Gee, D.; Archer, L.; Paskuliakova, A.; Mc Coy, G. R.; Fleming, G. T. A.; Gillespie, E.; Touzet, N. Rapid Chemotaxonomic Profiling for the Identification of High-Value Carotenoids in Microalgae. *J. Appl. Phycol.* **2018**, *30* (1), 385–399. <https://doi.org/10.1007/s10811-017-1247-7>.
- (194) Calvo, M. M.; Dado, D.; Santa-María, G. Influence of Extraction with Ethanol or Ethyl Acetate on the Yield of Lycopene,  $\beta$ -Carotene, Phytoene and Phytofluene from Tomato Peel Powder. *Eur. Food Res. Technol.* **2007**, *224* (5), 567–571. <https://doi.org/10.1007/s00217-006-0335-8>.
- (195) Granéli, E.; Edvardsen, B.; Roelke, D. L.; Hagström, J. A. The Ecophysiology and Bloom Dynamics of *Prymnesium* Spp. *Harmful Algae* **2012**, *14*, 260–270. <https://doi.org/10.1016/j.hal.2011.10.024>.
- (196) Hennon, G. M. M.; Dyhrman, S. T. Progress and Promise of Omics for Predicting the Impacts of Climate Change on Harmful Algal Blooms. *Harmful Algae* **2020**, *91*, 101587. <https://doi.org/10.1016/j.hal.2019.03.005>.



- (197) Sasso, S.; Pohnert, G.; Lohr, M.; Mittag, M.; Hertweck, C. Microalgae in the Postgenomic Era: A Blooming Reservoir for New Natural Products. *FEMS Microbiol. Rev.* **2012**, *36* (4), 761–785. <https://doi.org/10.1111/j.1574-6976.2011.00304.x>.
- (198) Bouvier, F.; Rahier, A.; Camara, B. Biogenesis, Molecular Regulation and Function of Plant Isoprenoids. *Prog. Lipid Res.* **2005**, *44* (6), 357–429. <https://doi.org/10.1016/j.plipres.2005.09.003>.
- (199) Yassaa, N.; Peeken, I.; Zöllner, E.; Bluhm, K.; Arnold, S.; Spracklen, D.; Williams, J. Evidence for Marine Production of Monoterpenes. *Environ. Chem.* **2008**, *5* (6), 391. <https://doi.org/10.1071/EN08047>.
- (200) Wichard, T.; Poulet, S. A.; Halsband-Lenk, C.; Albaina, A.; Harris, R.; Liu, D.; Pohnert, G. Survey of the Chemical Defence Potential of Diatoms: Screening of Fifty Species for  $\alpha,\beta,\gamma,\delta$ -Unsaturated Aldehydes. *J. Chem. Ecol.* **2005**, *31* (4), 949–958. <https://doi.org/10.1007/s10886-005-3615-z>.
- (201) Roach, J. S.; LeBlanc, P.; Lewis, N. I.; Munday, R.; Quilliam, M. A.; MacKinnon, S. L. Characterization of a Dispiroketal Spirolide Subclass from *Alexandrium Ostenfeldii*. *J. Nat. Prod.* **2009**, *72* (7), 1237–1240. <https://doi.org/10.1021/np800795q>.
- (202) Lin, Y.-Y.; Risk, M.; Ray, S. M.; Van Engen, D.; Clardy, J.; Golik, J.; James, J. C.; Nakanishi, K. Isolation and Structure of Brevetoxin B from the “Red Tide” Dinoflagellate *Ptychodiscus Brevis* (Gymnodinium Breve). *J. Am. Chem. Soc.* **1981**, *103* (22), 6773–6775. <https://doi.org/10.1021/ja00412a053>.
- (203) Sanchez, J. F.; Chiang, Y.-M.; Wang, C. C. C. Diversity of Polyketide Synthases Found in the *Aspergillus* and *Streptomyces* Genomes. *Mol. Pharm.* **2008**, *5* (2), 226–233. <https://doi.org/10.1021/mp700139t>.
- (204) Micallef, M. L.; D’Agostino, P. M.; Sharma, D.; Viswanathan, R.; Moffitt, M. C. Genome Mining for Natural Product Biosynthetic Gene Clusters in the Subsection V Cyanobacteria. *BMC Genomics* **2015**, *16* (1), 669. <https://doi.org/10.1186/s12864-015-1855-z>.
- (205) Osbourn, A. Secondary Metabolic Gene Clusters: Evolutionary Toolkits for Chemical Innovation. *Trends Genet.* **2010**, *26* (10), 449–457. <https://doi.org/10.1016/j.tig.2010.07.001>.
- (206) Brunson, J. K.; McKinnie, S. M. K.; Chekan, J. R.; McCrow, J. P.; Miles, Z. D.; Bertrand, E. M.; Bielinski, V. A.; Luhavaya, H.; Oborník, M.; Smith, G. J.; Hutchins, D. A.; Allen, A. E.; Moore, B. S. Biosynthesis of the Neurotoxin Domoic Acid in a Bloom-Forming Diatom. *Science* **2018**, *361* (6409), 1356–1358. <https://doi.org/10.1126/science.aau0382>.
- (207) Van Dolah, F. M.; Lidie, K. B.; Monroe, E. A.; Bhattacharya, D.; Campbell, L.; Doucette, G. J.; Kamykowski, D. The Florida Red Tide Dinoflagellate *Karenia Brevis*: New Insights into Cellular and Molecular Processes Underlying Bloom Dynamics. *Harmful Algae* **2009**, *8* (4), 562–572. <https://doi.org/10.1016/j.hal.2008.11.004>.
- (208) Nymark, M.; Sharma, A. K.; Sparstad, T.; Bones, A. M.; Winge, P. A. CRISPR/Cas9 System Adapted for Gene Editing in Marine Algae. *Sci. Rep.* **2016**, *6* (1), 24951. <https://doi.org/10.1038/srep24951>.
- (209) Poliner, E.; Pulman, J. A.; Zienkiewicz, K.; Childs, K.; Benning, C.; Farré, E. M. A Toolkit for *Nannochloropsis Oceanica* CCMP 1779 Enables Gene Stacking and Genetic Engineering of the Eicosapentaenoic Acid Pathway for

- Enhanced Long-chain Polyunsaturated Fatty Acid Production. *Plant Biotechnol. J.* **2018**, *16* (1), 298–309. <https://doi.org/10.1111/pbi.12772>.
- (210) Baier, T.; Wichmann, J.; Kruse, O.; Lauersen, K. J. Intron-Containing Algal Transgenes Mediate Efficient Recombinant Gene Expression in the Green Microalga *Chlamydomonas Reinhardtii*. *Nucleic Acids Res.* **2018**, *46* (13), 6909–6919. <https://doi.org/10.1093/nar/gky532>.
- (211) Fu, W.; Nelson, D. R.; Mystikou, A.; Daakour, S.; Salehi-Ashtiani, K. Advances in Microalgal Research and Engineering Development. *Curr. Opin. Biotechnol.* **2019**, *59*, 157–164. <https://doi.org/10.1016/j.copbio.2019.05.013>.
- (212) Xi, Y.; Kong, F.; Chi, Z. ROS Induce  $\beta$ -Carotene Biosynthesis Caused by Changes of Photosynthesis Efficiency and Energy Metabolism in *Dunaliella Salina* Under Stress Conditions. *Front. Bioeng. Biotechnol.* **2021**, *8*, 613768. <https://doi.org/10.3389/fbioe.2020.613768>.
- (213) M. U., N.; Mehar, J. G.; Mudliar, S. N.; Shekh, A. Y. Recent Advances in Microalgal Bioactives for Food, Feed, and Healthcare Products: Commercial Potential, Market Space, and Sustainability. *Compr. Rev. Food Sci. Food Saf.* **2019**, *18* (6), 1882–1897. <https://doi.org/10.1111/1541-4337.12500>.
- (214) Chen, H.; Jiang, J.-G.; Wu, G.-H. Effects of Salinity Changes on the Growth of *Dunaliella Salina* and Its Isozyme Activities of Glycerol-3-Phosphate Dehydrogenase. *J. Agric. Food Chem.* **2009**, *57* (14), 6178–6182. <https://doi.org/10.1021/jf900447r>.
- (215) Pacific Ocean | Depth, Temperature, Animals, Location, Map, & Facts <https://www.britannica.com/place/Pacific-Ocean> (accessed 2021 -08 -24).
- (216) Atlantic Ocean | Definition, Temperature, Weather, & Facts <https://www.britannica.com/place/Atlantic-Ocean> (accessed 2021 -08 -24).
- (217) Pawłowicz, R. A Model for Predicting Changes in the Electrical Conductivity, Practical Salinity, and Absolute Salinity of Seawater Due to Variations in Relative Chemical Composition. *Ocean Sci.* **2010**, *6* (1), 361–378. <https://doi.org/10.5194/os-6-361-2010>.
- (218) Morel, F. M. M.; Rueter, J. G.; Anderson, D. M.; Guillard, R. R. L. AQUIL: A CHEMICALLY DEFINED PHYTOPLANKTON CULTURE MEDIUM FOR TRACE METAL STUDIES<sup>1 2</sup>. *J. Phycol.* **1979**, *15* (2), 135–141. <https://doi.org/10.1111/j.1529-8817.1979.tb02976.x>.
- (219) Tett, P.; Droop, M. R.; Heaney, S. I. The Redfield Ratio and Phytoplankton Growth Rate. *J. Mar. Biol. Assoc. U. K.* **1985**, *65* (2), 487–504. <https://doi.org/10.1017/S0025315400050566>.
- (220) Li, J.; Zhang, J.; Huang, W.; Kong, F.; Li, Y.; Xi, M.; Zheng, Z. Comparative Bioavailability of Ammonium, Nitrate, Nitrite and Urea to Typically Harmful Cyanobacterium *Microcystis Aeruginosa*. *Mar. Pollut. Bull.* **2016**, *110* (1), 93–98. <https://doi.org/10.1016/j.marpolbul.2016.06.077>.
- (221) Chaffin, J. D.; Bridgeman, T. B.; Bade, D. L. Nitrogen Constrains the Growth of Late Summer Cyanobacterial Blooms in Lake Erie. *Adv. Microbiol.* **2013**, *03* (06), 16–26. <https://doi.org/10.4236/aim.2013.36A003>.
- (222) Smayda, T. J. Complexity in the Eutrophication–Harmful Algal Bloom Relationship, with Comment on the Importance of Grazing. *Harmful Algae* **2008**, *8* (1), 140–151. <https://doi.org/10.1016/j.hal.2008.08.018>.

- (223) Béchemin, C.; Grzebyk, D.; Hachame, F.; Hummert, C.; Maestrini, S. Effect of Different Nitrogen/Phosphorus Nutrient Ratios on the Toxin Content in *Alexandrium Minutum*. *Aquat. Microb. Ecol.* **1999**, *20*, 157–165. <https://doi.org/10.3354/ame020157>.
- (224) Falkenberg, L. J.; Bellerby, R. G. J.; Connell, S. D.; Fleming, L. E.; Maycock, B.; Russell, B. D.; Sullivan, F. J.; Dupont, S. Ocean Acidification and Human Health. *Int. J. Environ. Res. Public Health* **2020**, *17* (12), 4563. <https://doi.org/10.3390/ijerph17124563>.
- (225) Cai, W.-J.; Huang, W.-J.; Luther, G. W.; Pierrot, D.; Li, M.; Testa, J.; Xue, M.; Joesoef, A.; Mann, R.; Brodeur, J.; Xu, Y.-Y.; Chen, B.; Hussain, N.; Waldbusser, G. G.; Cornwell, J.; Kemp, W. M. Redox Reactions and Weak Buffering Capacity Lead to Acidification in the Chesapeake Bay. *Nat. Commun.* **2017**, *8* (1), 369. <https://doi.org/10.1038/s41467-017-00417-7>.
- (226) Che, Y.; Ding, L.; Qiu, J.; Ji, Y.; Li, A. Conversion and Stability of New Metabolites of Paralytic Shellfish Toxins under Different Temperature and PH Conditions. *J. Agric. Food Chem.* **2020**, *68* (5), 1427–1435. <https://doi.org/10.1021/acs.jafc.9b07063>.
- (227) Hwang, S.-W.; Choi, H. I.; Sim, S. J. Acidic Cultivation of *Haematococcus Pluvialis* for Improved Astaxanthin Production in the Presence of a Lethal Fungus. *Bioresour. Technol.* **2019**, *278*, 138–144. <https://doi.org/10.1016/j.biortech.2019.01.080>.
- (228) Polle, J. E. W.; Jin, E.; Ben-Amotz, A. The Alga *Dunaliella* Revisited: Looking Back and Moving Forward with Model and Production Organisms. *Algal Res.* **2020**, *49*, 101948. <https://doi.org/10.1016/j.algal.2020.101948>.
- (229) Horai, H.; Arita, M.; Kanaya, S.; Nihei, Y.; Ikeda, T.; Suwa, K.; Ojima, Y.; Tanaka, K.; Tanaka, S.; Aoshima, K.; Oda, Y.; Kakazu, Y.; Kusano, M.; Tohge, T.; Matsuda, F.; Sawada, Y.; Hirai, M. Y.; Nakanishi, H.; Ikeda, K.; Akimoto, N.; Maoka, T.; Takahashi, H.; Ara, T.; Sakurai, N.; Suzuki, H.; Shibata, D.; Neumann, S.; Iida, T.; Tanaka, K.; Funatsu, K.; Matsuura, F.; Soga, T.; Taguchi, R.; Saito, K.; Nishioka, T. MassBank: A Public Repository for Sharing Mass Spectral Data for Life Sciences. *J. Mass Spectrom.* **2010**, *45* (7), 703–714. <https://doi.org/10.1002/jms.1777>.
- (230) Renaud, S. M.; Parry, D. L. Microalgae for Use in Tropical Aquaculture II: Effect of Salinity on Growth, Gross Chemical Composition and Fatty Acid Composition of Three Species of Marine Microalgae. *J. Appl. Phycol.* **1994**, *6* (3), 347–356. <https://doi.org/10.1007/BF02181949>.
- (231) Liska, A. J.; Shevchenko, A.; Pick, U.; Katz, A. Enhanced Photosynthesis and Redox Energy Production Contribute to Salinity Tolerance in *Dunaliella* as Revealed by Homology-Based Proteomics. *Plant Physiol.* **2004**, *136* (1), 2806–2817. <https://doi.org/10.1104/pp.104.039438>.
- (232) Nagappan, S.; Devendran, S.; Tsai, P.-C.; Jayaraman, H.; Alagarsamy, V.; Pugazhendhi, A.; Ponnusamy, V. K. Metabolomics Integrated with Transcriptomics and Proteomics: Evaluation of Systems Reaction to Nitrogen Deficiency Stress in Microalgae. *Process Biochem.* **2020**, *91*, 1–14. <https://doi.org/10.1016/j.procbio.2019.11.027>.
- (233) Masson-Delmotte, V.; P. Zhai, A. Pirani, S.; L. Connors, C. Péan, S. Berger, N. Caud, Y. Chen, L. Goldfarb, M. I. Gomis, M. Huang, K. Leitzell, E. Lonnoy, J. B.; R. Matthews, T. K. Maycock, T. Waterfield, O. Yelekçi, R.

- Yu and B. Zhou. IPCC, 2021: Climate Change 2021: The Physical Science Basis. Cambridge University Press 2021.
- (234) Bioactivity-Based Molecular Networking for the Discovery of Drug Leads in Natural Product Bioassay-Guided Fractionation - Journal of Natural Products (ACS Publications)  
<https://pubs.acs.org/doi/full/10.1021/acs.jnatprod.7b00737> (accessed 2018 - 03 -03).
- (235) An Introduction to Photosynthesis in Aquatic Systems. In *Aquatic Photosynthesis*; Princeton University Press, 2013; pp 1–43.
- (236) McCree, K. J. Photosynthetically Active Radiation. In *Physiological Plant Ecology I*; Lange, O. L., Nobel, P. S., Osmond, C. B., Ziegler, H., Eds.; Springer Berlin Heidelberg: Berlin, Heidelberg, 1981; pp 41–55.  
[https://doi.org/10.1007/978-3-642-68090-8\\_3](https://doi.org/10.1007/978-3-642-68090-8_3).
- (237) Frigaard, N.-U.; Larsen, K. L.; Cox, R. P. Spectrochromatography of Photosynthetic Pigments as a Fingerprinting Technique for Microbial Phototrophs. *FEMS Microbiol. Ecol.* **1996**, *20* (2), 69–77.  
<https://doi.org/10.1111/j.1574-6941.1996.tb00306.x>.
- (238) Larkum, A. W.; Scaramuzzi, C.; Cox, G. C.; Hiller, R. G.; Turner, A. G. Light-Harvesting Chlorophyll c-like Pigment in Prochloron. *Proc. Natl. Acad. Sci.* **1994**, *91* (2), 679–683. <https://doi.org/10.1073/pnas.91.2.679>.
- (239) Wang, L.-J.; Fan, Y.; Parsons, R.; Hu, G.-R.; Zhang, P.-Y.; Li, F.-L. A Rapid Method for the Determination of Fucoxanthin in Diatom. *Mar. Drugs* **2018**, *16* (1), 33. <https://doi.org/10.3390/md16010033>.
- (240) Liu, L.-N.; Chen, X.-L.; Zhang, X.-Y.; Zhang, Y.-Z.; Zhou, B.-C. One-Step Chromatography Method for Efficient Separation and Purification of R-Phycoerythrin from Polysiphonia Urceolata. *J. Biotechnol.* **2005**, *116* (1), 91–100. <https://doi.org/10.1016/j.jbiotec.2004.09.017>.
- (241) Strain, H. H.; Benton, F. L.; Grandolfo, M. C.; Aitzetmüller, K.; Svec, W. A.; Katz, J. J. Heteroxanthin, Diatoxanthin and Diadinoxanthin from *Tribonema Aequale*. *Phytochemistry* **1970**, *9* (12), 2561–2565.  
[https://doi.org/10.1016/S0031-9422\(00\)85778-7](https://doi.org/10.1016/S0031-9422(00)85778-7).
- (242) Parasar, D. P.; Ramakrishnan, E.; Kabilan, S.; Kotoky, J.; Sarma, H. K. Characterization of B-Cryptoxanthin and Other Carotenoid Derivatives from *Rhodotorula Taiwanensis*, A Novel Yeast Isolated from Traditional Starter Culture of Assam. *Chem. Biodivers.* **2020**, *17* (12).  
<https://doi.org/10.1002/cbdv.202000198>.
- (243) Vadiveloo, A.; Moheimani, N. R.; Cosgrove, J. J.; Bahri, P. A.; Parlevliet, D. Effect of Different Light Spectra on the Growth and Productivity of Acclimated *Nannochloropsis* Sp. (Eustigmatophyceae). *Algal Res.* **2015**, *8*, 121–127. <https://doi.org/10.1016/j.algal.2015.02.001>.
- (244) Gupta, P. L.; Lee, S.-M.; Choi, H.-J. A Mini Review: Photobioreactors for Large Scale Algal Cultivation. *World J. Microbiol. Biotechnol.* **2015**, *31* (9), 1409–1417. <https://doi.org/10.1007/s11274-015-1892-4>.
- (245) Ugwu, C. U.; Aoyagi, H.; Uchiyama, H. Photobioreactors for Mass Cultivation of Algae. *Bioresour. Technol.* **2008**, *99* (10), 4021–4028.  
<https://doi.org/10.1016/j.biortech.2007.01.046>.
- (246) Fu, W.; Chaiboonchoe, A.; Khraiwesh, B.; Nelson, D.; Al-Khairi, D.; Mystikou, A.; Alzahmi, A.; Salehi-Ashtiani, K. Algal Cell Factories:

- Approaches, Applications, and Potentials. *Mar. Drugs* **2016**, *14* (12), 225. <https://doi.org/10.3390/md14120225>.
- (247) Behrenfeld, M. J.; Bale, A. J.; Kolber, Z. S.; Aiken, J.; Falkowski, P. G. Confirmation of Iron Limitation of Phytoplankton Photosynthesis in the Equatorial Pacific Ocean. *Nature* **1996**, *383* (6600), 508–511. <https://doi.org/10.1038/383508a0>.
- (248) Boyd, P. W.; Abraham, E. R. Iron-Mediated Changes in Phytoplankton Photosynthetic Competence during SOIREE. *Deep Sea Res. Part II Top. Stud. Oceanogr.* **2001**, *48* (11–12), 2529–2550. [https://doi.org/10.1016/S0967-0645\(01\)00007-8](https://doi.org/10.1016/S0967-0645(01)00007-8).
- (249) Dijkman, N. A.; Kromkamp, J. C. Photosynthetic Characteristics of the Phytoplankton in the Scheldt Estuary: Community and Single-Cell Fluorescence Measurements. *Eur. J. Phycol.* **2006**, *41* (4), 425–434. <https://doi.org/10.1080/09670260600937791>.
- (250) Strzepak, R. F.; Boyd, P. W.; Sunda, W. G. Photosynthetic Adaptation to Low Iron, Light, and Temperature in Southern Ocean Phytoplankton. *Proc. Natl. Acad. Sci.* **2019**, *116* (10), 4388–4393. <https://doi.org/10.1073/pnas.1810886116>.
- (251) Goto, N.; Kihira, M.; Ishida, N. Seasonal Distribution of Photosynthetically Active Phytoplankton Using Pulse Amplitude Modulated Fluorometry in the Large Monomictic Lake Biwa, Japan. *J. Plankton Res.* **2008**, *30* (10), 1169–1177. <https://doi.org/10.1093/plankt/fbn073>.
- (252) Hughes, A. H.; Magot, F.; Tawfike, A. F.; Rad-Menéndez, C.; Thomas, N.; Young, L. C.; Stucchi, L.; Caretoni, D.; Stanley, M. S.; Edrada-Ebel, R.; Duncan, K. R. Exploring the Chemical Space of Macro- and Micro-Algae Using Comparative Metabolomics. *Microorganisms* **2021**, *9* (2), 311. <https://doi.org/10.3390/microorganisms9020311>.
- (253) Ge, Z.; Zhang, H.; Zhang, Y.; Yan, C.; Zhao, Y. Purifying Synthetic High-Strength Wastewater by Microalgae *Chlorella Vulgaris* under Various Light Emitting Diode Wavelengths and Intensities. *J. Environ. Health Sci. Eng.* **2013**, *11* (1), 8. <https://doi.org/10.1186/2052-336X-11-8>.
- (254) Severes, A.; Hegde, S.; D'Souza, L.; Hegde, S. Use of Light Emitting Diodes (LEDs) for Enhanced Lipid Production in Micro-Algae Based Biofuels. *J. Photochem. Photobiol. B* **2017**, *170*, 235–240. <https://doi.org/10.1016/j.jphotobiol.2017.04.023>.
- (255) Macías-Sánchez, M. D.; Mantell, C.; Rodríguez, M.; Martínez de la Ossa, E.; Lubián, L. M.; Montero, O. Supercritical Fluid Extraction of Carotenoids and Chlorophyll a from *Nannochloropsis Gaditana*. *J. Food Eng.* **2005**, *66* (2), 245–251. <https://doi.org/10.1016/j.jfoodeng.2004.03.021>.
- (256) Vieler, A.; Wu, G.; Tsai, C.-H.; Bullard, B.; Cornish, A. J.; Harvey, C.; Reca, I.-B.; Thornburg, C.; Achawanantakun, R.; Buehl, C. J.; Campbell, M. S.; Cavalier, D.; Childs, K. L.; Clark, T. J.; Deshpande, R.; Erickson, E.; Armenia Ferguson, A.; Handee, W.; Kong, Q.; Li, X.; Liu, B.; Lundback, S.; Peng, C.; Roston, R. L.; Sanjaya; Simpson, J. P.; TerBush, A.; Warakanont, J.; Zäuner, S.; Farre, E. M.; Hegg, E. L.; Jiang, N.; Kuo, M.-H.; Lu, Y.; Niyogi, K. K.; Ohlrogge, J.; Osteryoung, K. W.; Shachar-Hill, Y.; Sears, B. B.; Sun, Y.; Takahashi, H.; Yandell, M.; Shiu, S.-H.; Benning, C. Genome, Functional Gene Annotation, and Nuclear Transformation of the Heterokont

- Oleaginous Alga *Nannochloropsis Oceanica* CCMP1779. *PLoS Genet.* **2012**, 8 (11), e1003064. <https://doi.org/10.1371/journal.pgen.1003064>.
- (257) Coesel, S.; Mangogna, M.; Ishikawa, T.; Heijde, M.; Rogato, A.; Finazzi, G.; Todo, T.; Bowler, C.; Falciatore, A. Diatom PtCPF1 Is a New Cryptochrome/Photolyase Family Member with DNA Repair and Transcription Regulation Activity. *EMBO Rep.* **2009**, 10 (6), 655–661. <https://doi.org/10.1038/embor.2009.59>.
- (258) Han, S.-I.; Kim, S.; Lee, C.; Choi, Y.-E. Blue-Red LED Wavelength Shifting Strategy for Enhancing Beta-Carotene Production from Halotolerant Microalga, *Dunaliella Salina*. *J. Microbiol.* **2019**, 57 (2), 101–106. <https://doi.org/10.1007/s12275-019-8420-4>.
- (259) Ma, R.; Thomas-Hall, S. R.; Chua, E. T.; Eltanahy, E.; Netzel, M. E.; Netzel, G.; Lu, Y.; Schenk, P. M. Blue Light Enhances Astaxanthin Biosynthesis Metabolism and Extraction Efficiency in *Haematococcus Pluvialis* by Inducing Haematocyst Germination. *Algal Res.* **2018**, 35, 215–222. <https://doi.org/10.1016/j.algal.2018.08.023>.
- (260) Huang, K.; Beck, C. F. Phototropin Is the Blue-Light Receptor That Controls Multiple Steps in the Sexual Life Cycle of the Green Alga *Chlamydomonas Reinhardtii*. *Proc. Natl. Acad. Sci.* **2003**, 100 (10), 6269–6274. <https://doi.org/10.1073/pnas.0931459100>.
- (261) Riba, M.; Kiss-Szikszai, A.; Gonda, S.; Parizsa, P.; Deák, B.; Török, P.; Valkó, O.; Felföldi, T.; Vasas, G. Chemotyping of Terrestrial Nostoc-like Isolates from Alkali Grassland Areas by Non-Targeted Peptide Analysis. *Algal Res.* **2020**, 46, 101798. <https://doi.org/10.1016/j.algal.2020.101798>.
- (262) Roviroso, J.; Moena, J.; San-Martín, A. Two Chemical Types of the Red Alga *Plocamium Cartilagineum* from Chile. *Biochem. Syst. Ecol.* **1988**, 16 (7–8), 593–595. [https://doi.org/10.1016/0305-1978\(88\)90068-3](https://doi.org/10.1016/0305-1978(88)90068-3).
- (263) Carroll, A. R.; Copp, B. R.; Davis, R. A.; Keyzers, R. A.; Prinsep, M. R. Marine Natural Products. *Nat. Prod. Rep.* **2020**, 37 (2), 175–223. <https://doi.org/10.1039/C9NP00069K>.
- (264) MarinLit - A database of the marine natural products literature <http://pubs.rsc.org/marinlit/> (accessed 2018 -07 -01).
- (265) AntiBase: a bioinformatics tool for Natural product databases | Chemoinformatics databases <https://omictools.com/antibase-tool> (accessed 2018 -07 -01).
- (266) Lodder, W.; de Roda Husman, A. M. SARS-CoV-2 in Wastewater: Potential Health Risk, but Also Data Source. *Lancet Gastroenterol. Hepatol.* **2020**, 5 (6), 533–534. [https://doi.org/10.1016/S2468-1253\(20\)30087-X](https://doi.org/10.1016/S2468-1253(20)30087-X).
- (267) Wu, F.; Zhang, J.; Xiao, A.; Gu, X.; Lee, W. L.; Armas, F.; Kauffman, K.; Hanage, W.; Matus, M.; Ghaeli, N.; Endo, N.; Duvallet, C.; Poyet, M.; Moniz, K.; Washburne, A. D.; Erickson, T. B.; Chai, P. R.; Thompson, J.; Alm, E. J. SARS-CoV-2 Titers in Wastewater Are Higher than Expected from Clinically Confirmed Cases. *mSystems* **2020**, 5 (4). <https://doi.org/10.1128/mSystems.00614-20>.
- (268) Delanka-Pedige, H. M. K.; Cheng, X.; Munasinghe-Arachchige, S. P.; Abeywardana-Arachchige, I. S. A.; Xu, J.; Nirmalakhandan, N.; Zhang, Y. Metagenomic Insights into Virus Removal Performance of an Algal-

- Based Wastewater Treatment System Utilizing *Galdieria Sulphuraria*. *Algal Res.* **2020**, *47*, 101865. <https://doi.org/10.1016/j.algal.2020.101865>.
- (269) Gustafsson, O.; Manukyan, L.; Gustafsson, S.; Tummala, G. K.; Zaman, S.; Begum, A.; Alfasane, Md. A.; Siddique-e-Rabbani, K.; Mihranyan, A. Scalable and Sustainable Total Pathogen Removal Filter Paper for Point-of-Use Drinking Water Purification in Bangladesh. *ACS Sustain. Chem. Eng.* **2019**, *7* (17), 14373–14383. <https://doi.org/10.1021/acssuschemeng.9b03905>.
- (270) O' Neill, J. Tackling Drug-Resistant Infections Globally: Final Report and Recommendations.
- (271) Suckling, C. J. The Antibacterial Drug MGB-BP3: From Discovery to Clinical Trial. **2015**, *5*, 9.
- (272) Clinical Trial Success for C.Diff Treatment Discovered at Strathclyde. (*Press Release*). May 2020.
- (273) Lauritano, C.; Andersen, J. H.; Hansen, E.; Albrigtsen, M.; Escalera, L.; Esposito, F.; Helland, K.; Hanssen, K. Ø.; Romano, G.; Ianora, A. Bioactivity Screening of Microalgae for Antioxidant, Anti-Inflammatory, Anticancer, Anti-Diabetes, and Antibacterial Activities. *Front. Mar. Sci.* **2016**, *3*. <https://doi.org/10.3389/fmars.2016.00068>.
- (274) Ördög, V.; Stirk, W. A.; Lenobel, R.; Bancířová, M.; Strnad, M.; Staden, J. van; Szigeti, J.; Németh, L. Screening Microalgae for Some Potentially Useful Agricultural and Pharmaceutical Secondary Metabolites. *J. Appl. Phycol.* **2004**, *16* (4), 309–314. <https://doi.org/10.1023/B:JAPH.0000047789.34883.aa>.
- (275) Patel, V.; Berthold, D.; Puranik, P.; Gantar, M. Screening of Cyanobacteria and Microalgae for Their Ability to Synthesize Silver Nanoparticles with Antibacterial Activity. *Biotechnol. Rep.* **2015**, *5*, 112–119. <https://doi.org/10.1016/j.btre.2014.12.001>.
- (276) Minhas, A. K.; Hodgson, P.; Barrow, C. J.; Adholeya, A. A Review on the Assessment of Stress Conditions for Simultaneous Production of Microalgal Lipids and Carotenoids. *Front. Microbiol.* **2016**, *7*. <https://doi.org/10.3389/fmicb.2016.00546>.
- (277) Errera, R. M.; Campbell, L. Osmotic Stress Triggers Toxin Production by the Dinoflagellate *Karenia Brevis*. *Proc. Natl. Acad. Sci.* **2011**, *108* (26), 10597–10601. <https://doi.org/10.1073/pnas.1104247108>.

## Appendices

### 8.1 Supplementary Information

#### 8.1.1 Supplementary Tables

**Table A1** Cell counts and absorbance values for (A) *Dunaliella primolecta*, (B) *Nannochloropsis oculata*, (C) *Phaeodactylum tricornutum*, and (D) *Porphyridium cruentum* grown in triplicate (rep 1, rep 2, rep 3) with the average and standard deviations calculated.

**A**

Day	Cell concentration (cells/mL)					OD600 Absorbance				
	Rep 1	Rep 2	Rep 3	Average	Std. Dev	Rep 1	Rep 2	Rep 3	Average	Std. Dev
0	4.00E+04	2.00E+04	2.00E+04	2.67E+04	1.15E+04	0.026	0.022	0.023	0.024	0.002
1	2.00E+04	1.20E+04	3.00E+04	2.07E+04	9.02E+03	0.029	0.022	0.024	0.025	0.004
4	6.00E+04	7.00E+04	7.00E+04	6.67E+04	5.77E+03	0.025	0.037	0.037	0.033	0.007
8	4.00E+04	6.00E+04	6.00E+04	5.33E+04	1.15E+04	0.056	0.072	0.066	0.065	0.008
11	2.40E+05	1.50E+05	2.60E+05	2.17E+05	5.86E+04	0.07	0.077	0.076	0.074	0.004
15	3.00E+05	2.70E+05	2.50E+05	2.73E+05	2.52E+04	0.141	0.149	0.163	0.151	0.011
18	1.60E+05	3.30E+05	2.20E+05	2.37E+05	8.62E+04	0.165	0.175	0.151	0.164	0.012
22	3.60E+05	4.70E+05	4.50E+05	4.27E+05	5.86E+04	0.219	0.227	0.235	0.227	0.008
25	5.30E+05	6.60E+05	7.00E+05	6.30E+05	8.89E+04	0.262	0.266	0.25	0.259	0.008
28	4.00E+05	5.40E+05	6.20E+05	5.20E+05	1.11E+05	0.248	0.256	0.273	0.259	0.013

**B**

Day	Cell concentration (cells/mL)					OD600 Absorbance				
	Rep 1	Rep 2	Rep 3	Average	Std. Dev	Rep 1	Rep 2	Rep 3	Average	Std. Dev
0	1.39E+06	1.77E+06	1.34E+06	1.50E+06	2.35E+05	0.063	0.058	0.061	0.061	0.003
1	1.28E+06	1.54E+06	1.34E+06	1.39E+06	1.36E+05	0.067	0.069	0.068	0.068	0.001
4	2.78E+06	2.25E+06	2.92E+06	2.65E+06	3.53E+05	0.115	0.122	0.113	0.117	0.005
8	5.86E+06	4.66E+06	4.10E+06	4.87E+06	8.99E+05	0.234	0.219	0.236	0.230	0.009
11	9.81E+06	1.10E+07	9.90E+06	1.02E+07	6.63E+05	0.351	0.343	0.341	0.345	0.005
15	8.50E+06	1.48E+07	1.26E+07	1.20E+07	3.20E+06	0.396	0.422	0.394	0.404	0.016
18	1.93E+07	1.93E+07	2.78E+07	2.21E+07	4.91E+06	0.498	0.522	0.515	0.512	0.012
22	2.64E+07	2.54E+07	2.98E+07	2.72E+07	2.31E+06	0.683	0.703	0.725	0.704	0.021
25	2.70E+07	2.90E+07	2.90E+07	2.83E+07	1.15E+06	0.84	0.85	0.86	0.850	0.010
28	3.20E+07	2.80E+07	3.40E+07	3.13E+07	3.06E+06	0.915	0.989	0.934	0.946	0.038



C

Day	Cell concentration (cells/mL)					OD600 Absorbance				
	Rep 1	Rep 2	Rep 3	Average	Std. Dev	Rep 1	Rep 2	Rep 3	Average	Std. Dev
0	7.70E+05	9.30E+05	7.90E+05	8.30E+05	8.72E+04	0.103	0.099	0.094	0.099	0.005
1	5.60E+05	6.60E+05	7.90E+05	6.70E+05	1.15E+05	0.115	0.119	0.109	0.114	0.005
4	1.32E+06	1.32E+06	1.93E+06	1.52E+06	3.52E+05	0.183	0.164	0.2	0.182	0.018
8	2.63E+06	2.45E+06	3.07E+06	2.72E+06	3.19E+05	0.308	0.276	0.321	0.302	0.023
11	4.36E+06	3.26E+06	4.76E+06	4.13E+06	7.77E+05	0.41	0.349	0.425	0.395	0.040
15	4.53E+06	4.05E+06	6.12E+06	4.90E+06	1.08E+06	0.505	0.41	0.513	0.476	0.057
18	5.75E+06	5.00E+06	7.65E+06	6.13E+06	1.37E+06	0.584	0.495	0.626	0.568	0.067
22	5.30E+06	3.60E+06	7.10E+06	5.33E+06	1.75E+06	0.672	0.577	0.737	0.662	0.080
25	4.20E+06	5.10E+06	5.10E+06	4.80E+06	5.20E+05	0.749	0.644	0.797	0.730	0.078
28	5.90E+06	4.70E+06	5.30E+06	5.30E+06	6.00E+05	0.795	0.712	0.849	0.785	0.069

D

Day	Cell concentration (cells/mL)					Absorbance (600 nm)				
	Rep 1	Rep 2	Rep 3	Average	Std. Dev	Rep 1	Rep 2	Rep 3	Average	Std. Dev
0	4.00E+04	5.00E+04	7.00E+04	5.33E+04	1.53E+04	0.027	0.023	0.023	0.024	0.002
1	1.00E+04	2.00E+04	4.00E+04	2.33E+04	1.53E+04	0.009	0.017	0.009	0.012	0.005
4	4.00E+04	1.00E+04	1.00E+04	2.00E+04	1.73E+04	0.001	0.012	0.002	0.005	0.006
8	1.00E+04	1.00E+04	5.00E+04	2.33E+04	2.31E+04	0.012	0.021	0.016	0.016	0.005
11	2.00E+05	3.70E+05	1.60E+05	2.43E+05	1.12E+05	0.015	0.024	0.019	0.019	0.005
15	5.20E+05	2.90E+05	2.30E+05	3.47E+05	1.53E+05	0.064	0.059	0.090	0.071	0.017
18	4.10E+05	2.40E+05	5.80E+05	4.10E+05	1.70E+05	0.057	0.094	0.130	0.094	0.037
22	9.00E+05	5.90E+05	2.10E+05	5.67E+05	3.46E+05	0.184	0.093	0.054	0.110	0.067
25	5.00E+05	5.90E+05	7.00E+05	5.97E+05	1.00E+05	0.079	0.170	0.030	0.093	0.071

**Table A2** Specific growth rates ( $\mu$ ) for *Dunaliella primolecta*, *Nannochloropsis oculata*, *Phaeodactylum tricornutum*, and *Porphyridium cruentum* grown in triplicate (rep 1, rep 2, rep 3) with the average and standard deviations calculated. Includes data for both cell counts (counts) and absorbance at 600 nm (abs).

Strain	Method	Rep 1	Rep 2	Rep 3	Mean	Median	p-value
<i>D. primolecta</i>	counts	0.111	0.129	0.113	0.118	0.113	0.01
<i>D. primolecta</i>	abs	0.094	0.083	0.083	0.087	0.083	
<i>N. oculata</i>	counts	0.094	0.098	0.114	0.102	0.098	0.01
<i>N. oculata</i>	abs	0.071	0.075	0.074	0.073	0.074	
<i>P. tricornutum</i>	counts	0.1	0.091	0.098	0.096	0.098	0.005
<i>P. tricornutum</i>	abs	0.081	0.075	0.079	0.078	0.079	
<i>P. cruentum</i>	counts	0.071	0.047	0.079	0.066	0.071	0.57
<i>P. cruentum</i>	abs	0.13	0.125	0.014	0.09	0.125	

**Table A3** Specific growth rates ( $\mu$ ) of *D. primolecta*, *N. oculata*, and *P. tricornutum* grown under stress conditions (cond.) in triplicate (rep 1, rep 2, and rep 3) with mean, median, and p-values given. Conditions are as follows: N-C, NaNO<sub>3</sub> control (8.82x10<sup>-4</sup> M); N-L, NaNO<sub>3</sub> low (8.82x10<sup>-5</sup> M); N-H, NaNO<sub>3</sub> high (8.82x10<sup>-3</sup> M); C-C, NaCl control (24 g/L); C-L, NaCl low (12 g/L); C-H, NaCl high (36 g/L); C-D, NaCl deplete (0 g/L); S-C, salinity control (43 ppt); S-L, salinity low (4.3 ppt); S-H, salinity high (86 ppt); P-C, pH control (7.6); P-L, pH low (4); P-H, pH high (10). \* p-values are based on a t-test between condition and control for each stress.

Strain	Cond.	Rep 1	Rep 2	Rep 3	Mean	Median	p-value*
<i>D. primolecta</i>	N-C	15.13	16.62	16.67	16.17	16.62	
	N-L	2.76	11.83	-6.74	2.62	2.76	0.066
	N-H	16	14.45	15.53	15.33	15.53	0.29
	C-C	5.19	4.48	5.44	5.03	5.19	
	C-L	4.23	4.6	4.19	4.34	4.23	0.09
	C-H	3.74	4.69	4.39	4.27	4.39	0.13
	C-D	2.28	1.45	1.13	1.62	1.45	0.002
	S-C	9.32	9.29	9.9	9.5	9.32	
	S-L	5.73	6.03	6.07	5.94	6.03	9.43
	S-H	8.85	8.08	8.27	8.4	8.27	0.022
	P-C	4.61	4.15	5.45	4.74	4.61	
	P-L	6.34	5.6	6.56	6.17	6.34	0.04
P-H	4.16	4.45	5.52	4.71	4.45	0.96	
<i>N. oculata</i>	N-C	9.21	12.38	12.17	11.25	12.17	
	N-L	17.39	15.98	15.17	16.18	15.98	0.015
	N-H	12.86	12.59	13.06	12.84	12.86	0.2
	C-C	13.12	14.23	16.91	14.75	14.23	
	C-L	8.83	13.67	9.85	10.78	9.85	0.1
	C-H	23.7	26.24	28.54	26.16	26.24	0.003
	C-D	9.25	7.41	8.28	8.31	8.28	0.007
	S-C	10.43	10.3	10.95	10.56	10.43	
	S-L	7.96	7.76	8.65	8.12	7.96	0.002
	S-H	12.56	13.2	11.95	12.57	12.56	0.008
	P-C	6.71	4.63	4.47	5.27	4.63	
	P-L	5.06	4.03	4.23	4.44	4.23	0.35
P-H	6.65	4.73	5.2	5.53	5.2	0.79	
<i>P. tricornutum</i>	N-C	11.78	11.2	10.14	11.04	11.2	
	N-L	-2.42	-4.22	-14.74	-7.13	-4.22	0.009
	N-H	9.37	10.59	10.17	10.04	10.17	0.17
	C-C	8.34	7.89	9.24	8.49	8.34	
	C-L	7.99	7.31	7.97	7.76	7.97	0.18
	C-H	2.99	2.03	2.46	2.49	2.46	2.4x10 <sup>-4</sup>
	C-D	7.6	6.95	7.03	7.19	7.03	0.04
	S-C	34.24	35.22	41.59	37.02	35.22	
	S-L	30.26	27.97	25.18	27.8	27.97	0.028
	S-H	34.64	31.51	30.81	32.32	31.51	0.14
	P-C	14.1	13.24	12.79	13.38	13.24	
	P-L	11.49	11.23	11.05	11.26	11.23	0.006
P-H	7.68	7.92	8.21	7.94	7.92	1.9x10 <sup>-4</sup>	

**Table A4** Specific growth rates ( $\mu$ ) of *D. primolecta*, *N. oculata*, *P. tricorutum*, and *P. cruentum* grown under white and 405 nm light conditions (cond.) in triplicate (rep 1, rep 2, and rep 3) with mean, standard error of mean (SEM), and p-values given.

<b>Strain</b>	<b>Cond</b>	<b>Rep 1</b>	<b>Rep 2</b>	<b>Rep 3</b>	<b>Mean</b>	<b>SEM</b>	<b>p-value</b>
<i>D. primolecta</i>	White	0.12	0.08	0.16	0.12	0.04	0.65
	405 nm	0.13	0.08	0.11	0.11	0.01	
<i>N. oculata</i>	White	0.34	0.38	0.29	0.34	0.03	0.137
	405 nm	0.29	0.15	0.28	0.24	0.04	
<i>P. tricorutum</i>	White	0.33	0.32	0.32	0.32	0.003	0.047
	405 nm	0.31	0.28	0.30	0.30	0.009	
<i>P. cruentum</i>	White	0.21	0.20	0.24	0.22	0.01	0.004
	405 nm	0.07	0.11	0.12	0.12	0.02	

## 8.2.2 Supplementary Figures

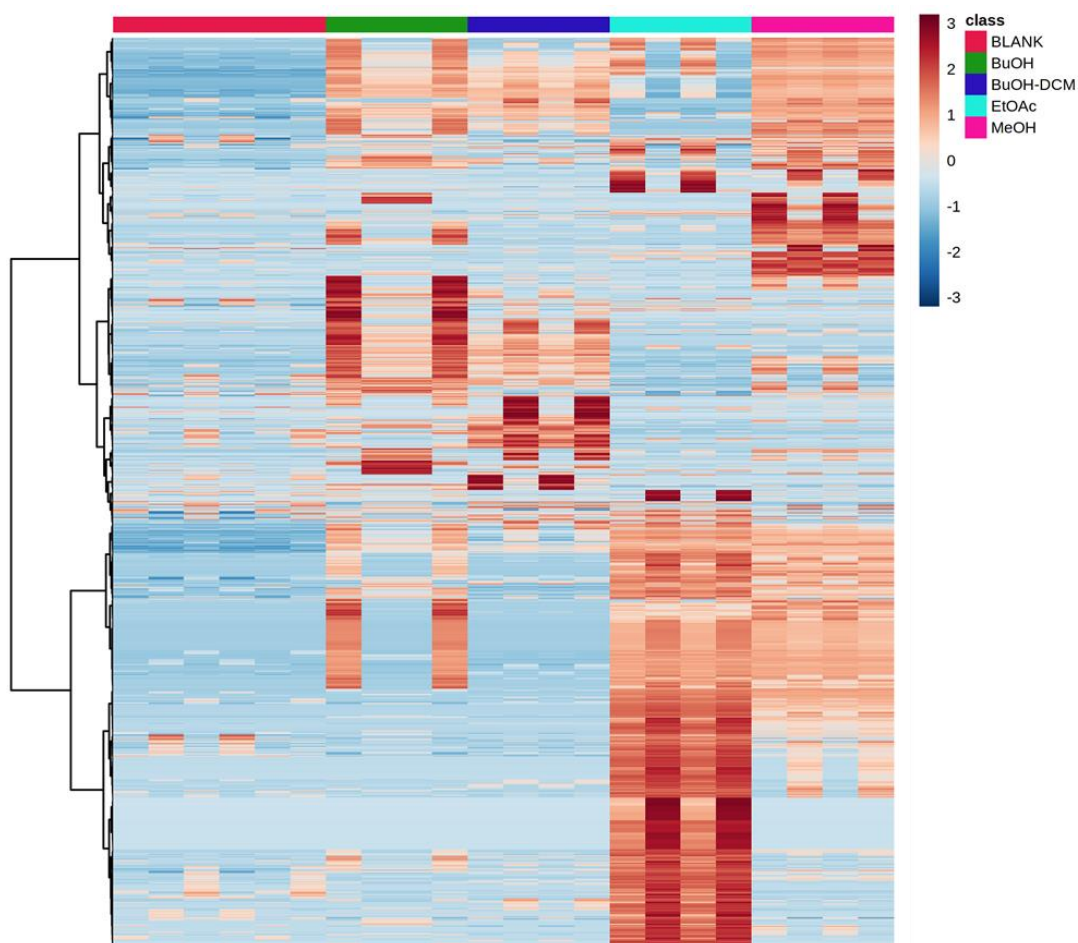


**Figure A1** Extended heatmap of all features detected when *Chlorella sorokiniana* cultures were extracted using butanol (BuOH, green), butanol:dichloromethane (BuOH:DCM, blue), ethyl acetate (EtOAc, cyan), and methanol (MeOH, pink) based on hierarchical clustering. The scale ranges from most intense (red) to least intense (blue).

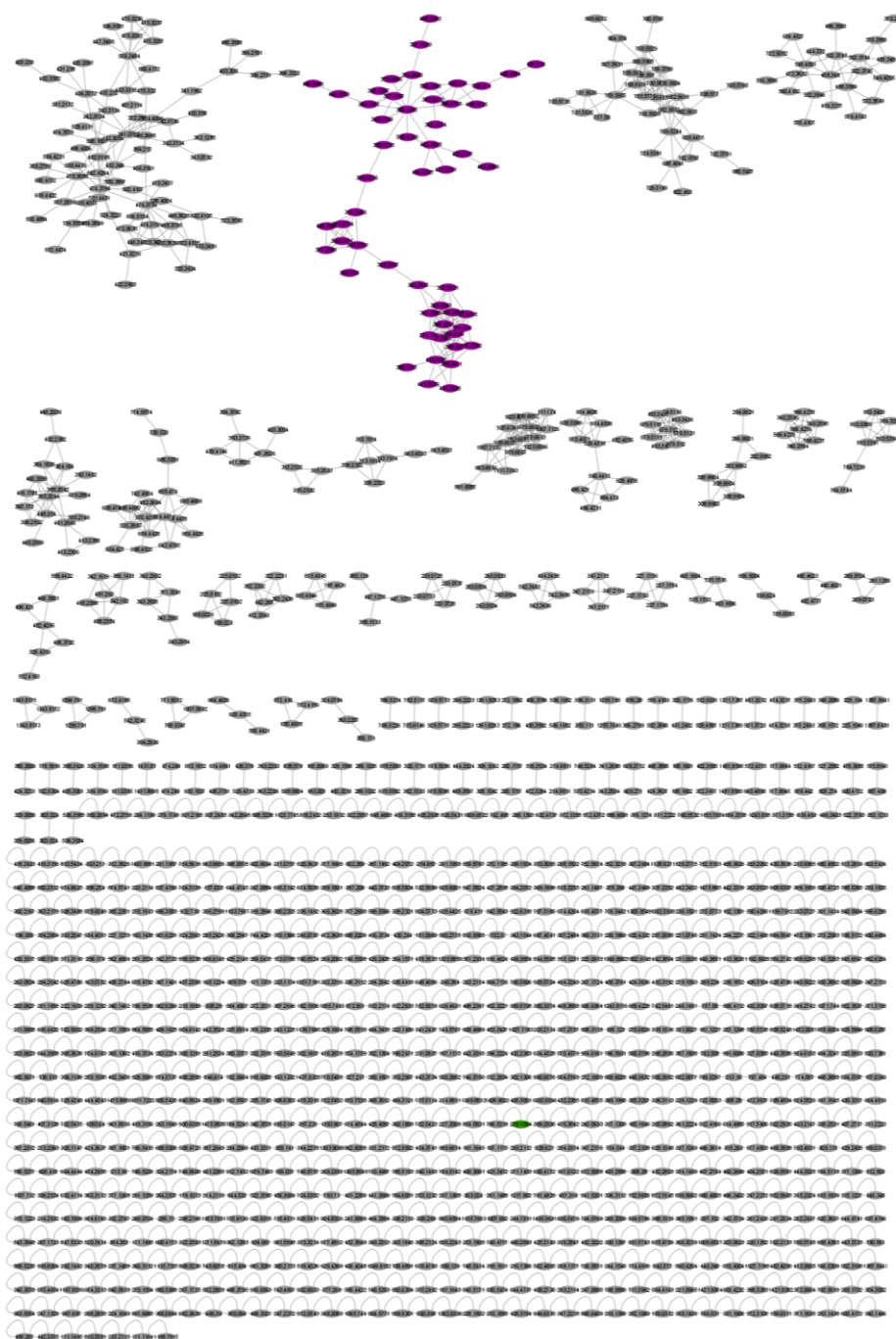


**Figure A2** MolNetEnhancer network of LC-MS/MS features detected when *Chlorella sorokiniana* cultures were extracted using different solvents (butanol, butanol:dichloromethane, ethyl acetate, and methanol). Nodes highlighted in purple represent a molecular family annotated as fatty acid esters.

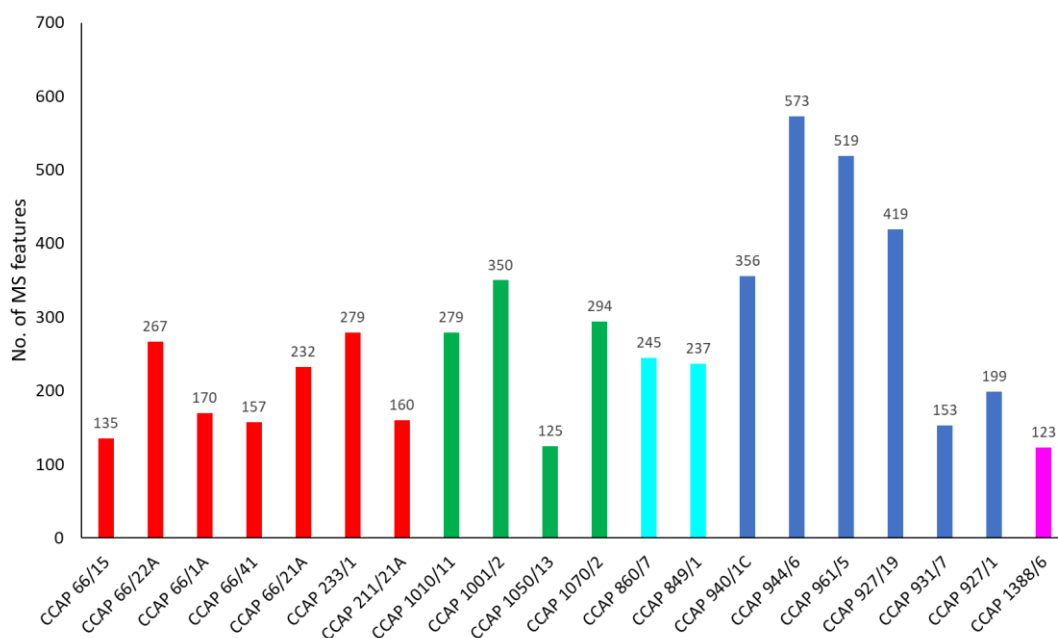


**Figure A3** Bar chart of LC-MS features detected for each strain (strain ID on x-axis) coloured according to phylum: Chlorophytes (red), diatoms (green), Haptophytes (blue), Ochrophytes (cyan), Rhodophytes (pink). Number of features are given above each bar.

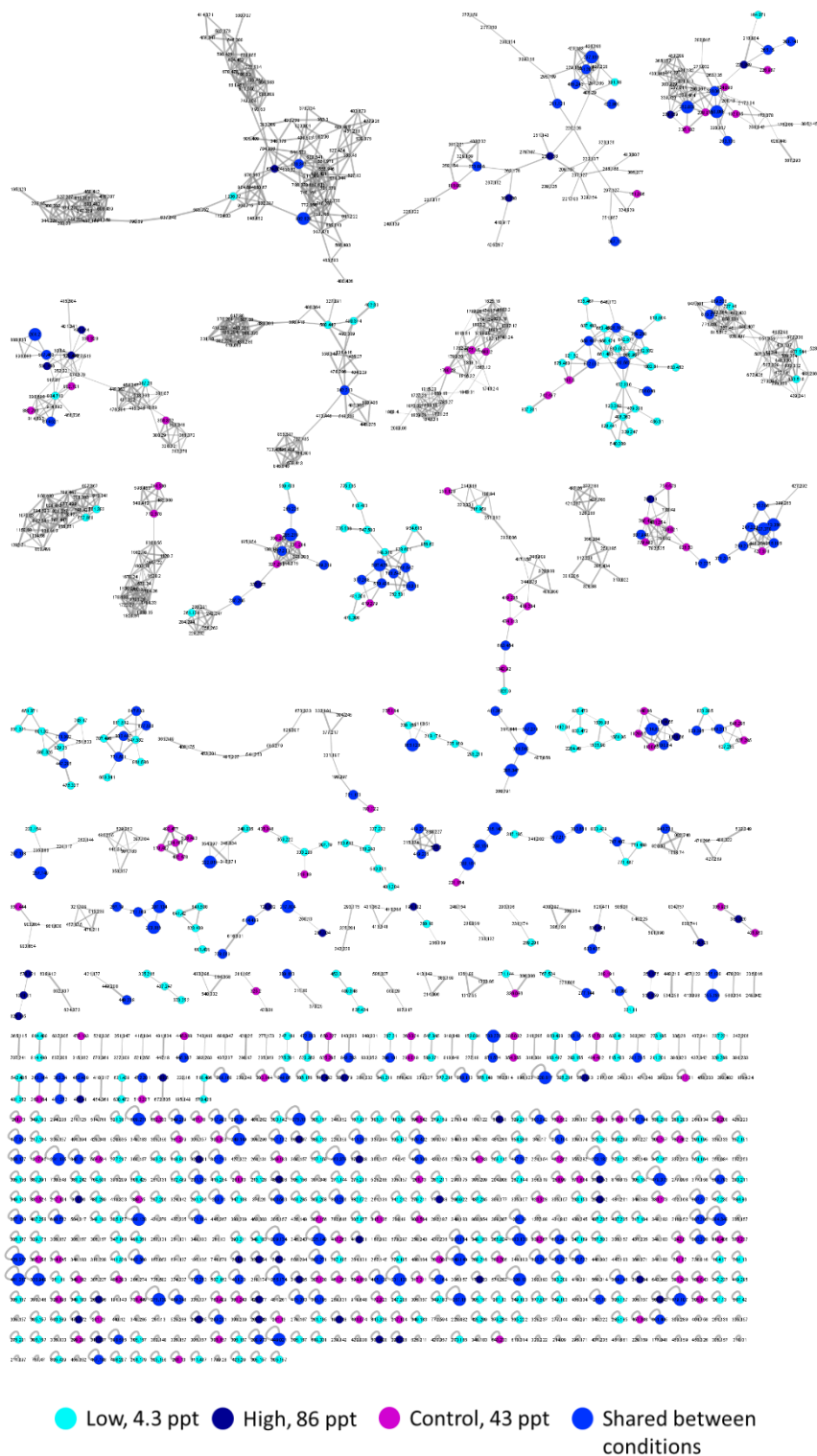
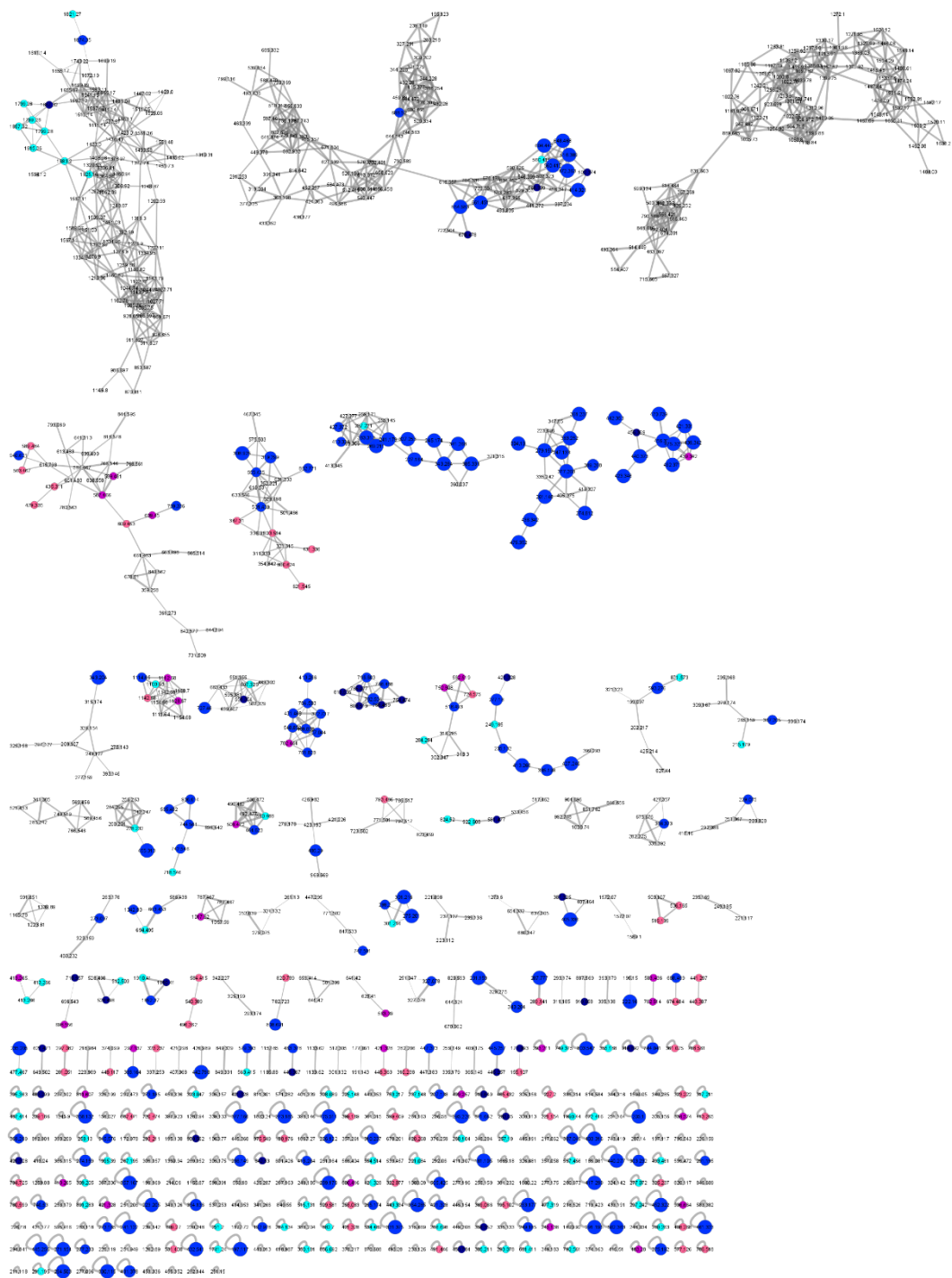


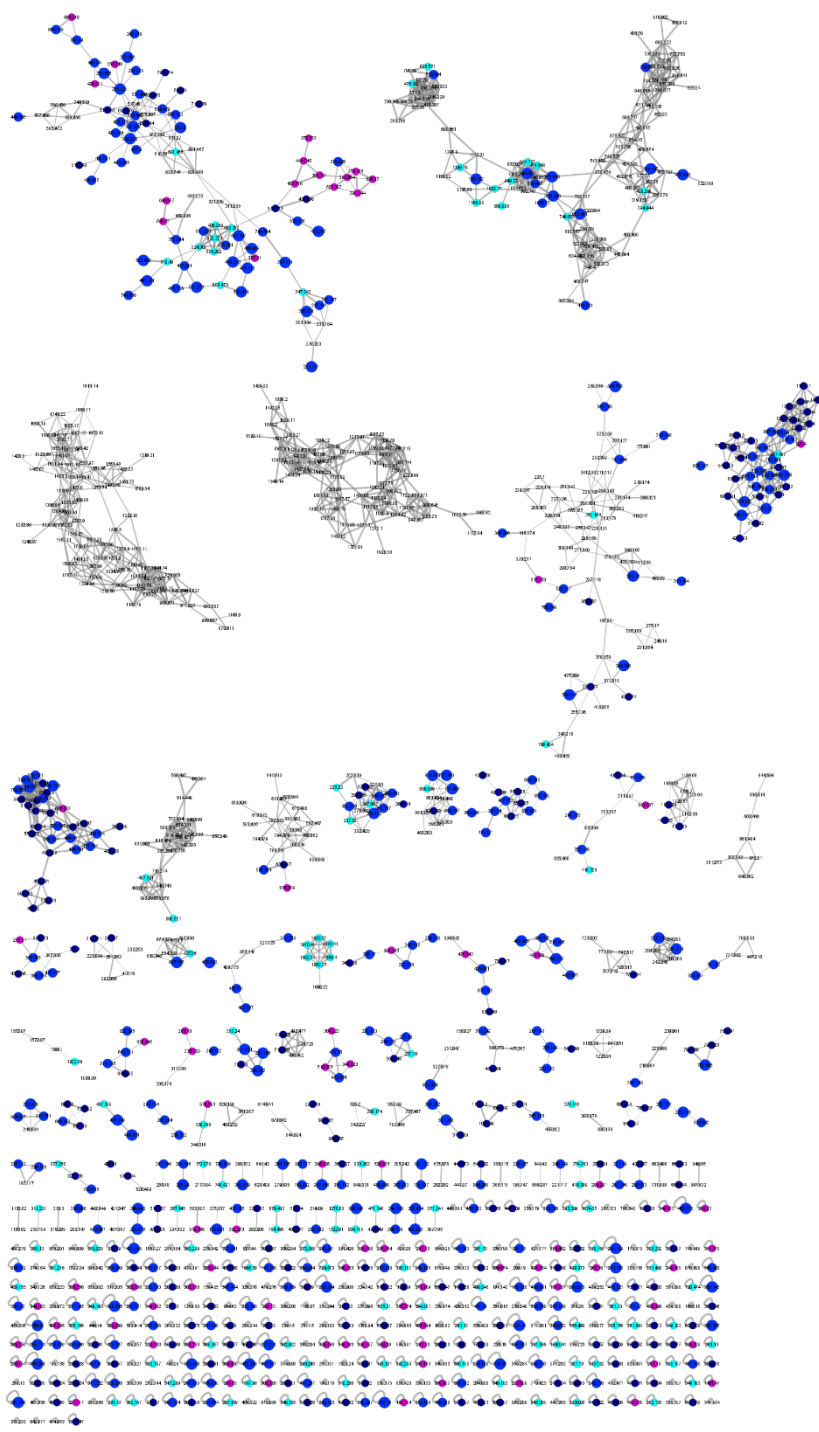
**Figure A4** GNPS classical molecular network of MS/MS features detected from extracts of *Nannochloropsis oculata* grown under varying salinity: low = 4.3 ppt Aquil, cyan; control = 43 ppt Aquil, purple; high = 86 ppt Aquil, navy). Features shared between conditions are presented as blue circles.





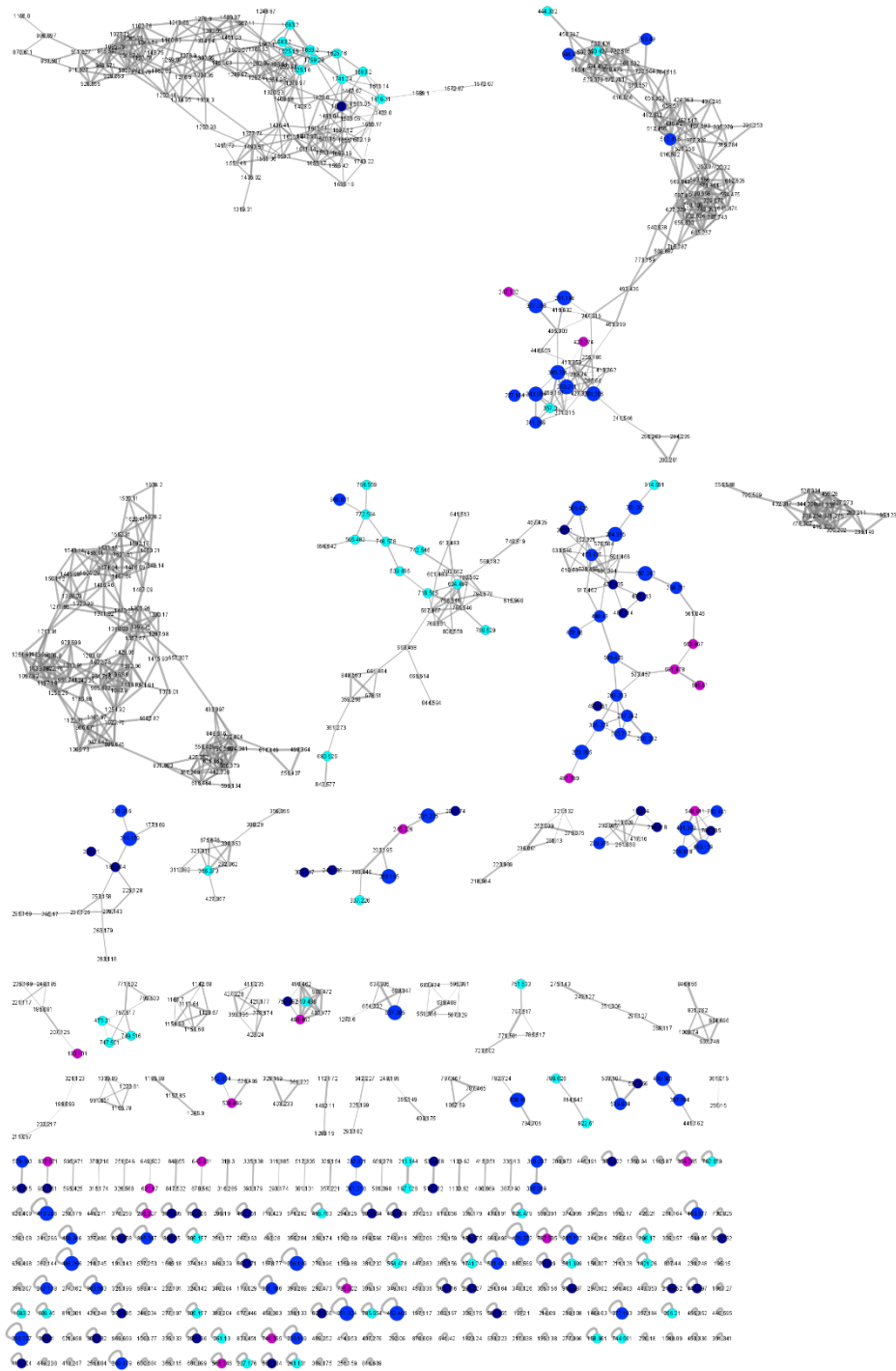
● Deplete, 0 g/L  
 ● Low, 12 g/L  
 ● Control, 24 g/L  
 ● High, 36 g/L  
 ● Shared between conditions

**Figure A5** GNPS classical molecular network of MS/MS features detected from extracts of *Nannochloropsis oculata* grown under varying NaCl concentrations: deplete = 0 g/L, pink; low = 12 g/L, cyan; control = 24 g/L, purple; high = 36 g/L, navy). Features shared between conditions are presented as blue circles.



● Low,  $8.82 \times 10^{-5}$  M   
 ● Control,  $8.82 \times 10^{-4}$  M   
 ● High,  $8.82 \times 10^{-3}$  M   
 ● Shared between conditions

**Figure A6** GNPS classical molecular network of MS/MS features detected from extracts of *Nannochloropsis oculata* grown under varying  $\text{NaNO}_3$  concentrations: low =  $8.82 \times 10^{-5}$  M, cyan; control =  $8.82 \times 10^{-4}$  M, purple; high =  $8.82 \times 10^{-3}$  M, navy). Features shared between conditions are presented as blue circles.



● Low, pH 4    
 ● Control, pH 7.6    
 ● High, pH 10    
 ● Shared between conditions

**Figure A7** GNPS classical molecular network of MS/MS features detected from extracts of *Nannochloropsis oculata* grown under varying pH: low = pH 4, cyan; control = pH 7.6, purple; high = pH 10, navy. Features shared between conditions are presented as blue circles.

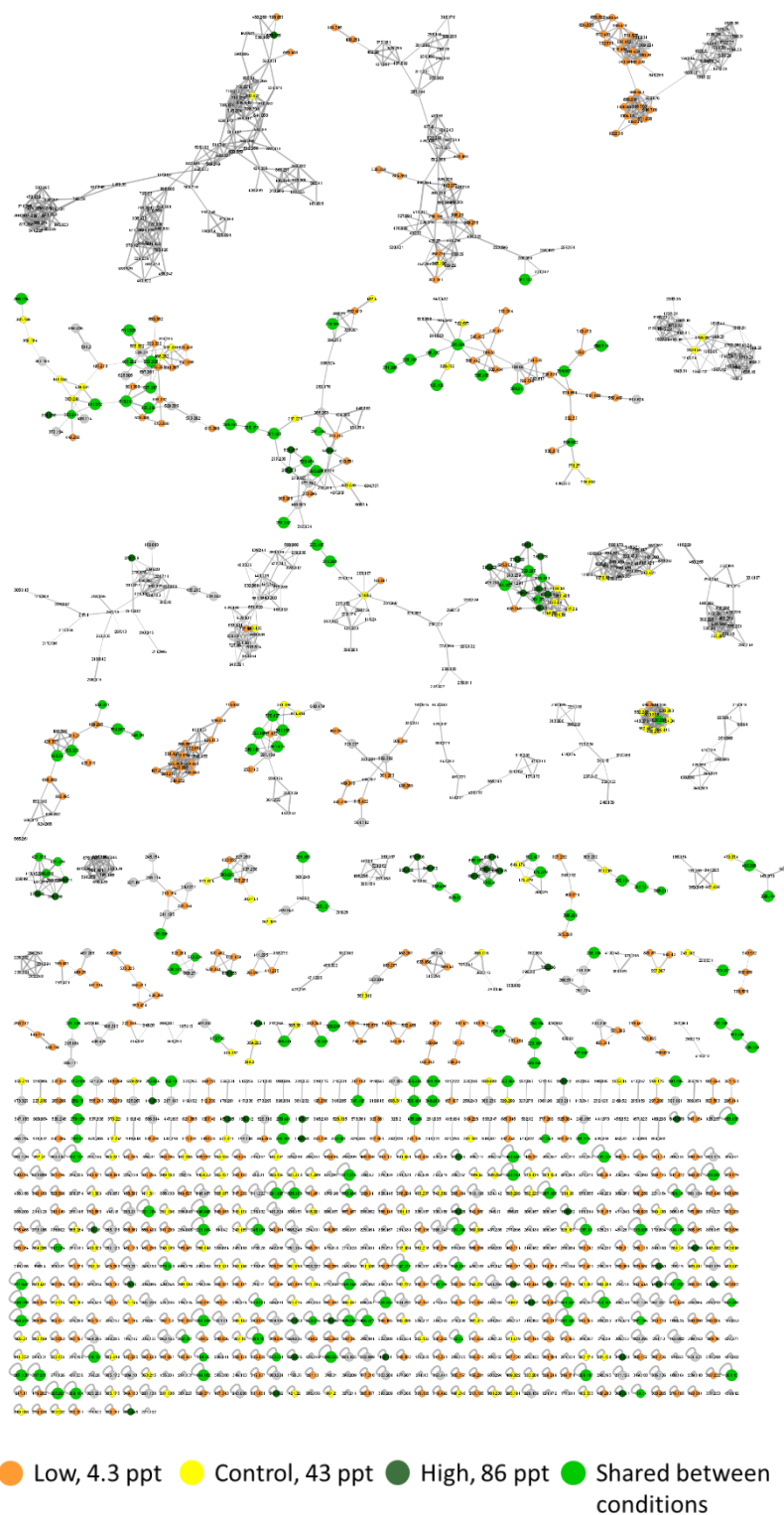


**Figure A8** GNPS classical molecular network of MS/MS features detected from extracts of *Dunaliella primolecta* grown under varying salinity: low = 4.3 ppt Aquil, orange; control = 43 ppt Aquil, yellow; high = 86 ppt Aquil, dark green). Features shared between conditions are presented as green circles.

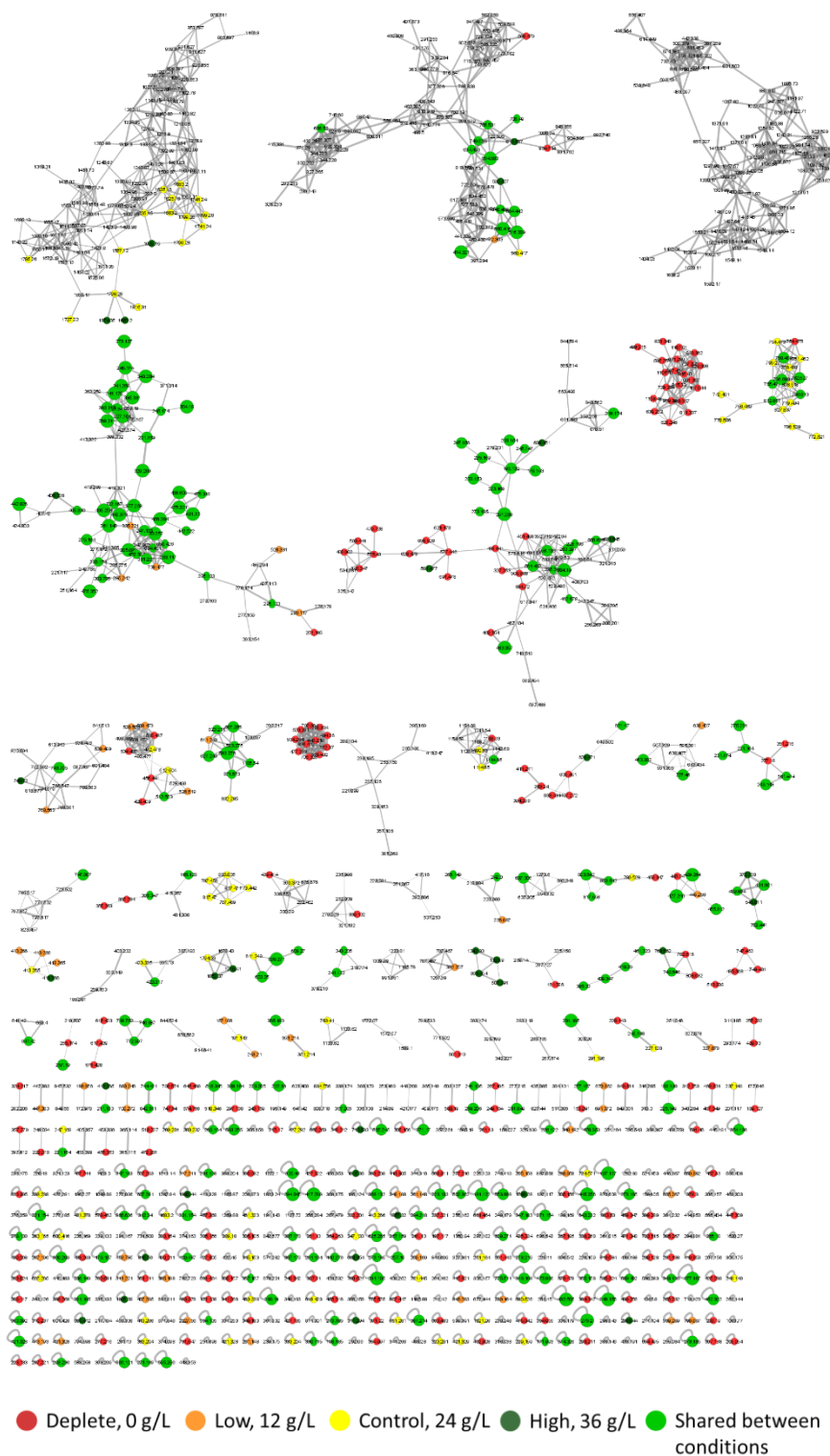


**Figure A9** GNPS classical molecular network of MS/MS features detected from extracts of *Dunaliella primolecta* grown under varying NaCl concentrations: deplete = 0 g/L, red; low = 12 g/L, orange; control = 24 g/L, yellow; high = 36 g/L, dark green). Features shared between conditions are presented as green circles.

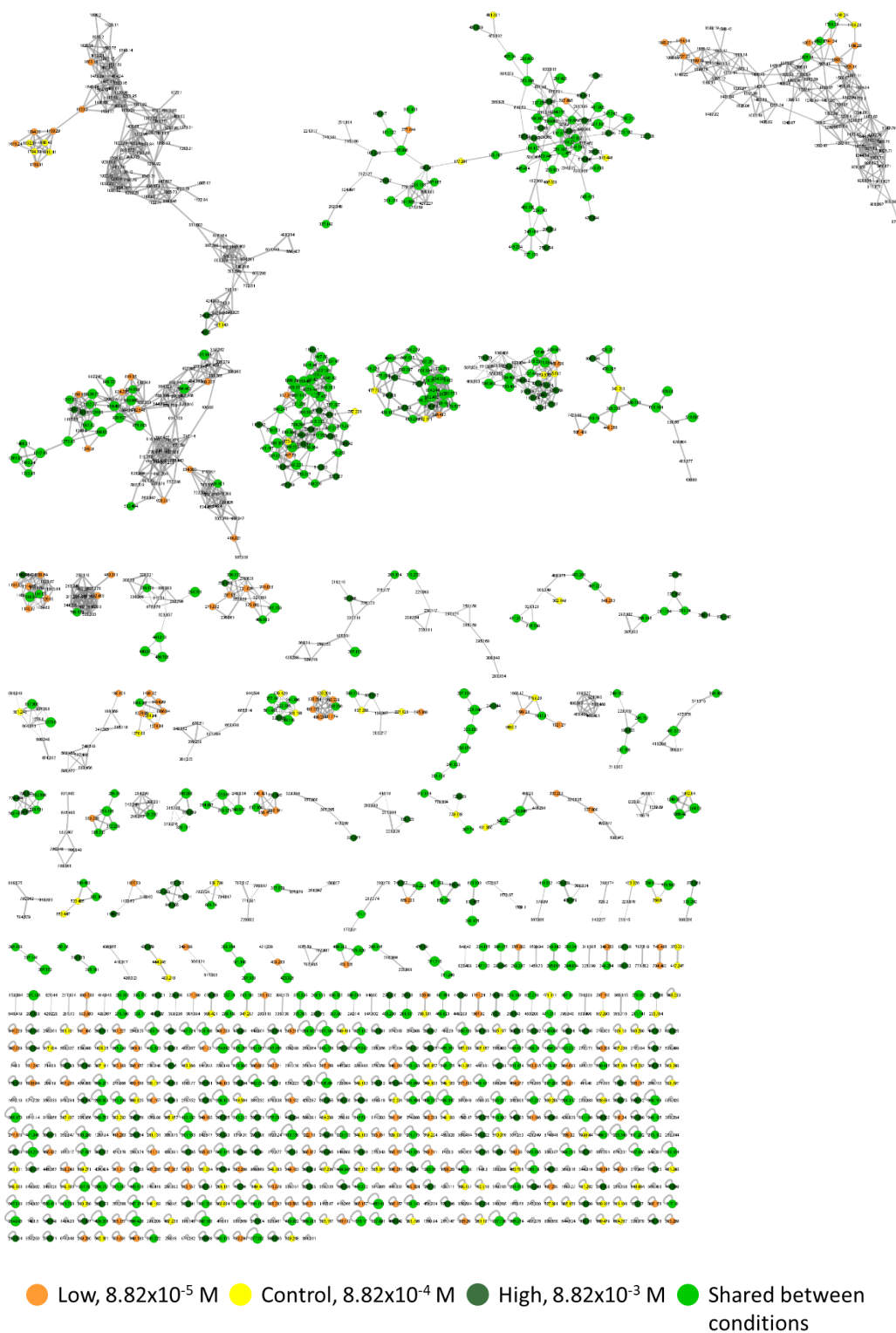


**Figure A10** GNPS classical molecular network of MS/MS features detected from extracts of *Dunaliella primolecta* grown under varying  $\text{NaNO}_3$  concentrations: low =  $8.82 \times 10^{-5}$  M, orange; control =  $8.82 \times 10^{-4}$  M, yellow; high =  $8.82 \times 10^{-3}$  M, dark green). Features shared between conditions are presented as green circles.

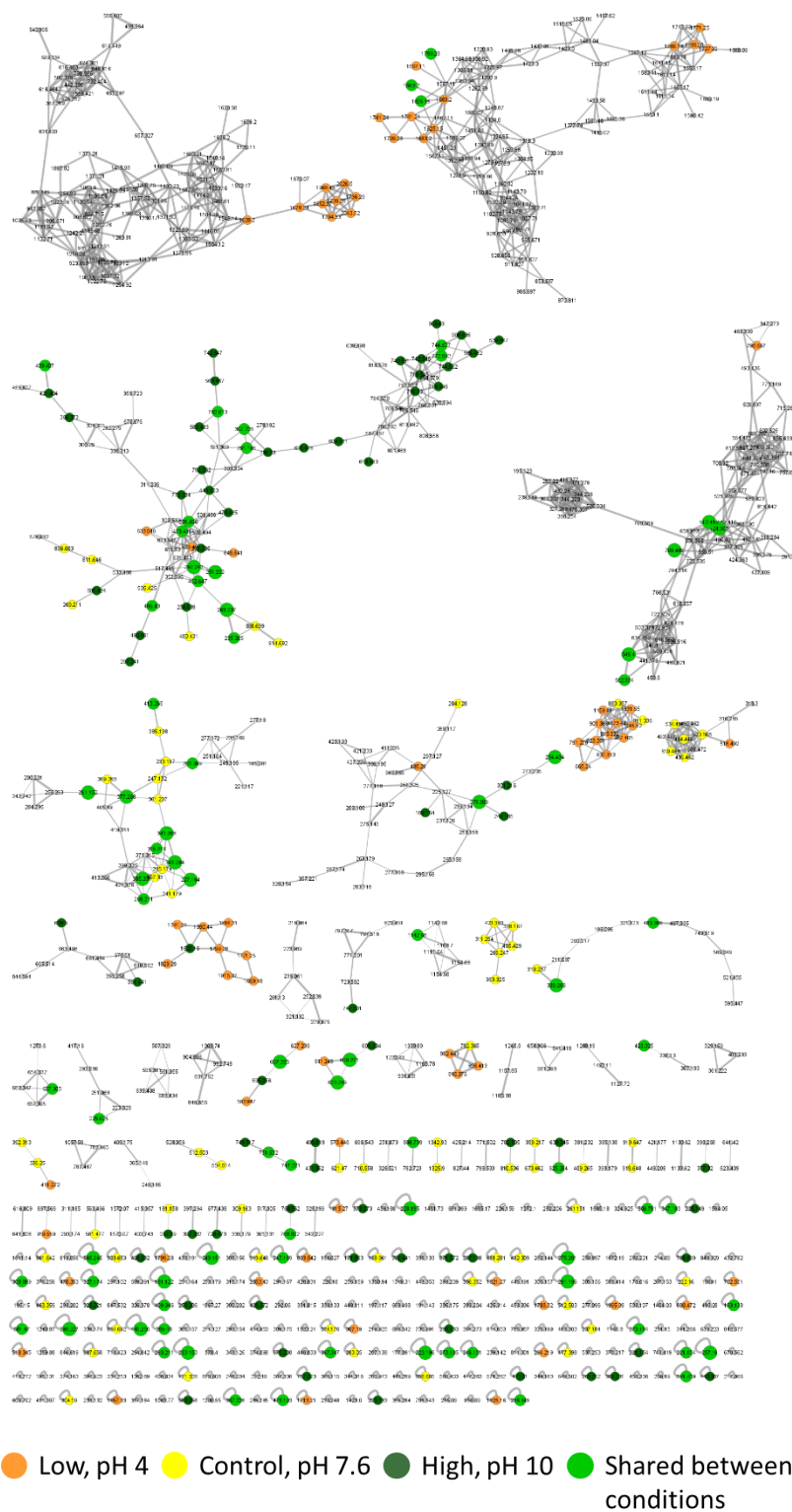
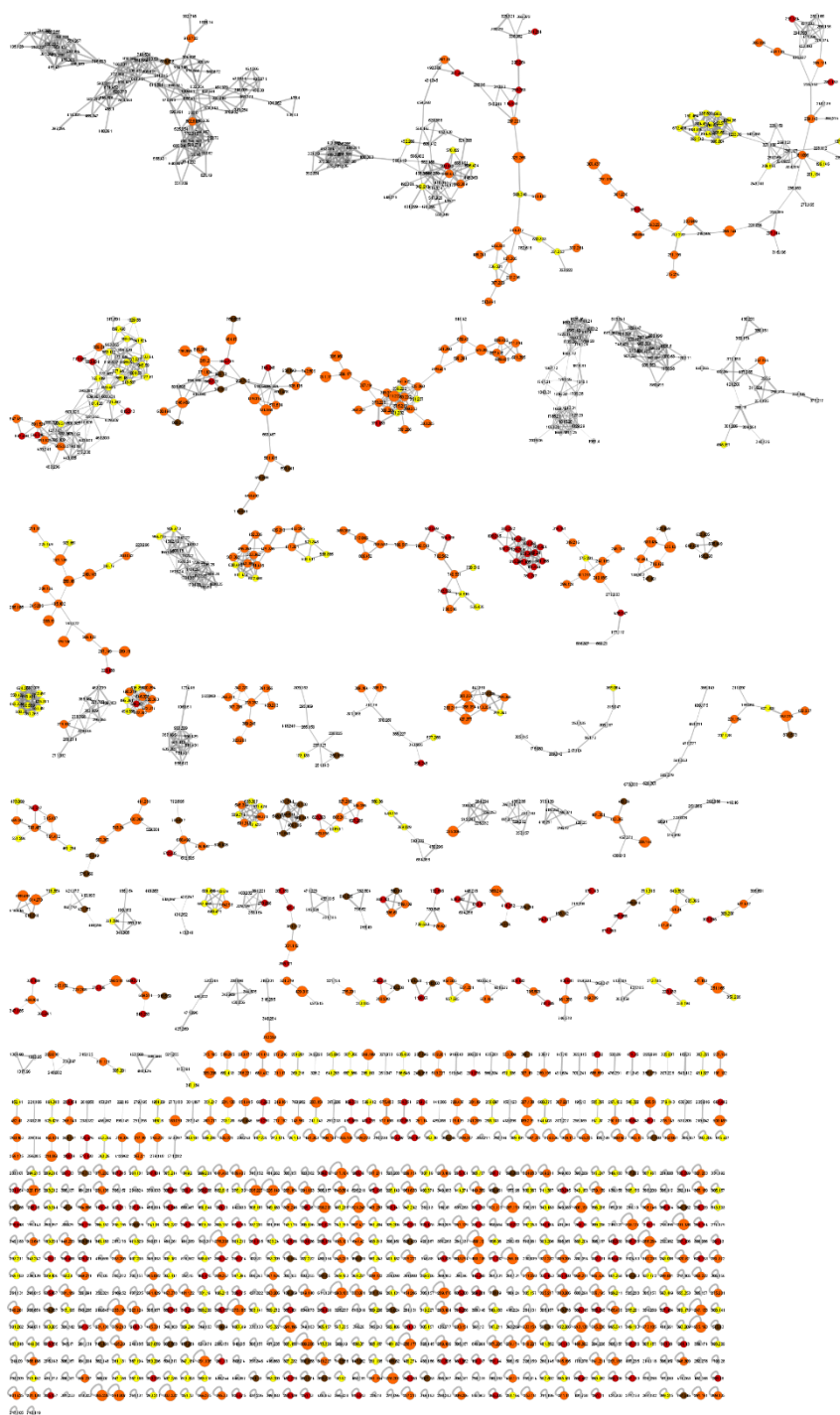


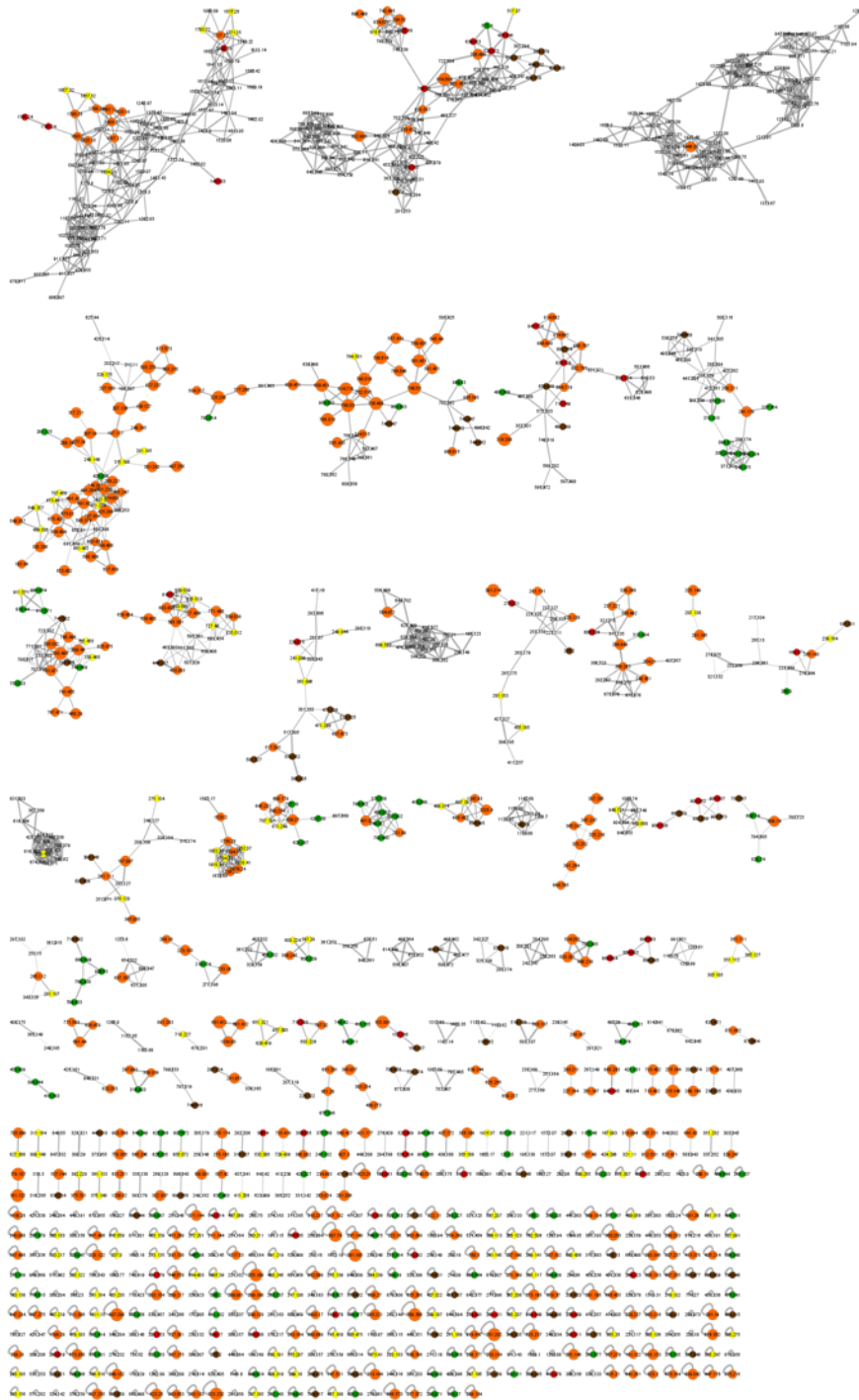
**Figure A11** GNPS classical molecular network of MS/MS features detected from extracts of *Dunaliella primolecta* grown under varying pH: low = pH 4, orange; control = pH 7.6, yellow; high = pH 10, dark green). Features shared between conditions are presented as green circles.



● Low, 4.3 ppt   
 ● Control, 43 ppt   
 ● High, 86 ppt   
 ● Shared between conditions

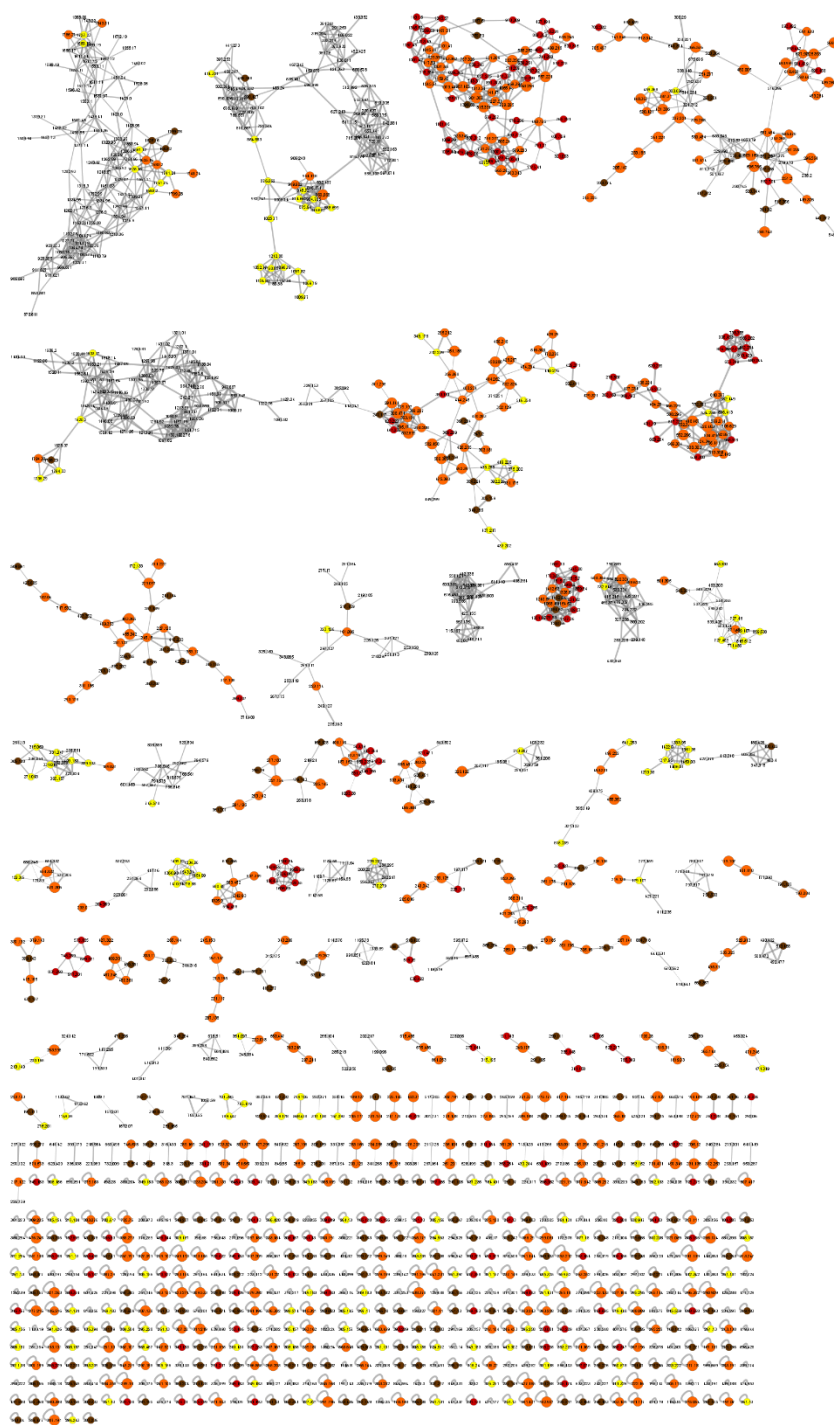
**Figure A12** GNPS classical molecular network of MS/MS features detected from extracts of *Phaeodactylum tricornutum* grown under varying salinity: low = 4.3 ppt Aquil, yellow; control = 43 ppt Aquil, red; high = 86 ppt Aquil, dark brown). Features shared between conditions are presented as orange circles.





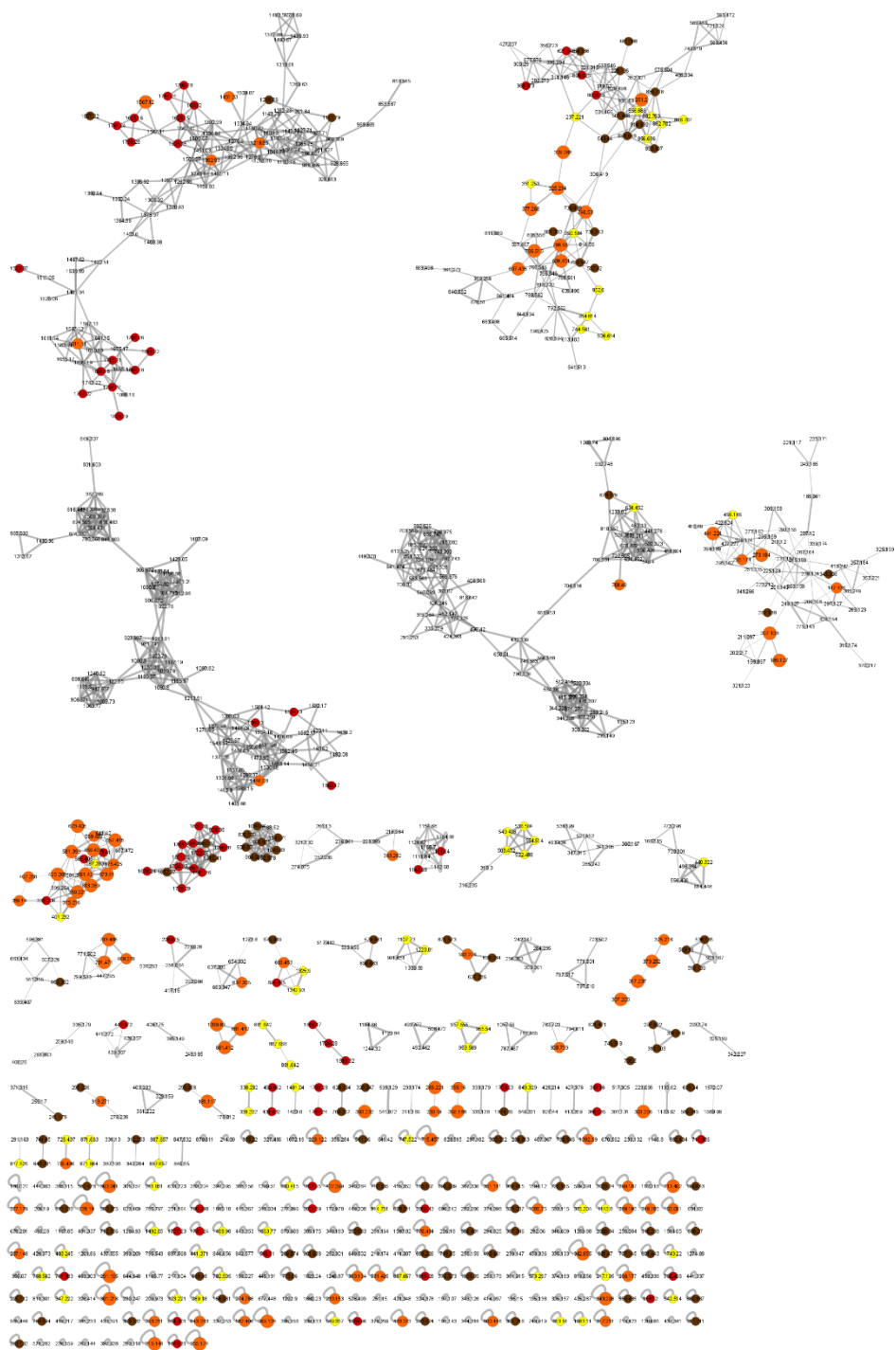
● Deplete, 0 g/L   
 ● Low, 12 g/L   
 ● Control, 24 g/L   
 ● High, 36 g/L   
 ● Shared between conditions

**Figure A13** GNPS classical molecular network of MS/MS features detected from extracts of *Phaeodactylum tricornutum* grown under varying NaCl concentrations: deplete = 0 g/L, green; low = 12 g/L, yellow; control = 24 g/L, red; high = 36 g/L, dark brown). Features shared between conditions are presented as orange circles.



● Low,  $8.82 \times 10^{-5}$  M   
 ● Control,  $8.82 \times 10^{-4}$  M   
 ● High,  $8.82 \times 10^{-3}$  M   
 ● Shared between conditions

**Figure A14** GNPS classical molecular network of MS/MS features detected from extracts of *Phaeodactylum tricornutum* grown under varying  $\text{NaNO}_3$  concentrations: low =  $8.82 \times 10^{-5}$  M, yellow; control =  $8.82 \times 10^{-4}$  M, red; high =  $8.82 \times 10^{-3}$  M, dark brown). Features shared between conditions are presented as orange circles.



● Low, pH 4 ● Control, pH 7.6 ● High, pH 10 ● Shared between conditions

**Figure A15** GNPS classical molecular network of MS/MS features detected from extracts of *Phaeodactylum tricornerutum* grown under varying pH: low = pH 4, yellow; control = pH 7.6, red; high = pH 10, dark brown). Features shared between conditions are presented as orange circles.